Moist convection within the Indian summer monsoon

Peter David Willetts

Submitted in accordance with the requirements for the degree of
Doctor of Philosophy

The University of Leeds
School of Earth and Environment
July 20, 2019

Declaration of authorship

The candidate confirms that the work submitted is his own, except where work which has formed part of jointly-authored publications has been included. The contribution of the candidate and the other authors to this work has been explicitly indicated below. The candidate confirms that appropriate credit has been given within the thesis where reference has been made to the work of others.

Some of the work contained in Chapter 4 forms part of a jointly-authored manuscript which has been published in *The Quarterly Journal of the Royal Meteorological Society*. The candidate was not the lead-author. The candidate conducted data processing and analysis of radiosonde data, and the subsequent generation of figures for the publication.

Parker DJ, Willetts P, Birch C, Turner AG, Marsham JH, Taylor CM, Kolusu S, Martin GM. 2016. The interaction of moist convection and mid-level dry air in the advance of the onset of the indian monsoon. *Quarterly Journal of the Royal Meteorological Society* **142**: 2256–2272

The calculation of localised onset regions used in Chapter 4 was performed by R. Fitzpatrick, which formed the basis of the second publication. The candidate commented on the manuscript, providing understanding on the Indian monsoon, which the lead-author was not familiar with.

Fitzpatrick RGJ, Parker DJ, Willetts PD. 2016. Assessing the level of spatial homogeneity of the agronomic Indian monsoon onset. *Geophysical Research Letters* **43**: 2016GL070 711, doi: 10.1002/2016GL070711

The work contained in Chapter 5 forms the basis of a jointly-authored manuscript which has been published in *The Quarterly Journal of the Royal Meteorological Society*. S. Webster performed the model simulations and Simon Peatman (not a co-author) provided code to compute the diurnal harmonics of rainfall. All other data processing and analysis was

conducted by the candidate. The candidate wrote the manuscript with guidance from the co-authors.

Willetts PD, Marsham JH, Birch CE, Parker DJ, Webster S, Petch J. 2017a. Moist convection and its upscale effects in simulations of the Indian monsoon with explicit and parametrized convection. *Quarterly Journal of the Royal Meteorological Society* **143**(703): 1073–1085, doi: 10.1002/qj.2991

The work presented in Chapter 6 forms the basis of a jointly-authored manuscript which is to be submitted to *The Quarterly Journal of the Royal Meteorological Society*. S. Webster and C. Birch performed the model simulations, and code to perform storm tracking was provided by Julia Crook and Thorwald Stein. All other data processing and analysis was conducted by the candidate. The candidate wrote the manuscript with input from the co-authors.

Willetts PD, Marsham JH, Birch CE, Parker DJ, Webster S, 2017. Propagation of rainfall upstream of the Western Ghats. Quarterly Journal of the Royal Meteorological Society : (in preparation)

Acknowledgements

This work has been completed as part of the CASE studentship grant NE/K006932/1; in conjunction with the UK Met Office. The sponsoring body for this work is the Natural Environment Research Council. The candidate would also like to acknowledge the support and guidance provided by the supervisors who assisted with this work; Dr. John H. Marsham, Professor Douglas J Parker, Dr. Cathryn Birch, Dr. Stuart Webster, and Dr. Jon Petch.

Abstract

The vagaries of Indian monsoon rainfall have profound consequences, but improved forecasting, on all timescales, has proved elusive. Subseasonal variability significantly influences interannual variability. However, a wide range poorly understood processes and feedbacks control the variability. Systematic model biases persist, with moist convection a dominant source of error. Cumulus scale biases can grow upscale to affect synoptic scales in two days, and the largest scales in two weeks.

The onset of the monsoon rains progresses northwards over India over about 6 weeks, the reasons for which are not well understood. This is shown, primarily using radiosonde data, to be related to a mid-level dry layer, which retreats in response to closely related thermodynamic and dynamic transitions. The dry mid-level layer does not, however, significantly control the interannual variability of the onset.

Systematic rainfall biases in models with convective parametrisations typically include a Western Equatorial Indian Ocean (WEIO) wet bias, an Indian dry bias, and too weak low-level flow into India. Explicitly representing convection, in continental-scale simulations, is shown to reduce the dry bias and alters circulation and fluxes to sustain more rainfall over northern India. WEIO rainfall is too high in convection-permitting simulations with grid-spacings above $\sim$2km, which also substantially alters the circulation.

Towards a better understanding of the high rainfall upstream of the coastal mountains on the west coast of India, the role of offshore rainfall propagation is examined. Rainfall propagation likely results through storm advection and gravity waves, and varies in response to the passage of Boreal Summer Intraseasonal Oscillations. Contrary to satellite observations, rainfall consistently propagates onshore in convection-permitting simulations.

The results demonstrate the importance of understanding scale interactions in the Indian monsoon. Improved models must capture storm-to-mesoscale processes that affect the entire monsoon.

Contents

List of Figures

List of Tables

Abbreviations

APHRODITE	**A**sian **P**recipitation **H**ighly-**R**esolved **O**bservational **D**ata **I**ntegration **T**owards **E**valuation
BSISV	**B**oreal **S**ummer **I**ntra**S**easonal **V**ariability
CAPE	**C**onvective **A**vailable **P**otential **E**nergy
CIN	**C**onvective **IN**hibition
CISK	**C**onditional **I**nstability of the **S**econd **K**ind
CMORPH	NOAA **C**PC **MORPH**ing technique
CPC	**C**limate **P**rediction **C**enter
CQE	**C**onvective **Q**uasi-**E**quilibrium
ECMWF	**E**uropean **C**entre for **M**edium-**R**ange **W**eather **F**orecasts
ENSO	**E**l **N**iño **S**outhern **O**scillation
GSMAP	**G**lobal **S**atellite **M**apping of **P**recipitation project
IGRA	**I**ntegrated **G**lobal **R**adiosonde **A**rchive
IITM	**I**ndian **I**nstitute of **T**ropical **M**eteorology
IITMHomInd	IITM **Hom**ogeneous **Ind**ian rainfall region
IMD	**I**ndian **M**eteorological **D**epartment
ISM	**I**ndian **S**ummer **M**onsoon
ISO	**I**ntra**S**easonal **O**scillation
IST	**I**ndian **S**tandard **T**ime
ITCZ	**I**nter**T**ropical **C**onvergence **Z**one
JJAS	**J**une **J**uly **A**ugust **S**eptember
LCL	**L**ifted **C**ondensation **L**evel
LFC	**L**evel of **F**ree **C**onvection
LOR	**L**ocalised **O**nset **R**egion
LPS	**L**ow-**P**ressure **S**ystem

MIDAS	**M**et **O**ffice **I**ntegrated **D**ata **A**rchive **S**ystem
MJO	**M**adden-**J**ulian **O**scillation
MSE	**M**oist-**S**tatic **E**nergy
NERC	**N**atural **E**nvironment **R**esearch **C**ouncil
NWP	**N**umerical **W**eather **P**rediction
OLR	**O**utgoing **L**ongwave **R**adiation
OSTIA	**O**perational **S**ea **S**urface **T**emperature and sea **I**ce **A**nalysis
PCC	**P**earson **C**orrelation **C**oefficient
PV	**P**otential **V**orticity
RH	**R**elative **H**umidity
RV	**R**elative **V**orticity
SLP	**S**ea-**L**evel **P**ressure
SMAG	**SMAG**orinsky turbulence scheme
SST	**S**ea **S**urface **T**emperature
TRMM	**T**ropical **R**ainfall **M**easurement **M**ission
UKV	Met Office Unified Model **U**nited **K**ingdom **V**ariable model
UTC	**C**oordinated **U**niversal **T**ime
WAM	**W**est **A**frican **M**onsoon
WEIO	**W**estern **E**quatorial **I**ndian **O**cean
WVMR	**W**ater **V**apour **M**ixing **R**atio
VHF	**V**ery **H**igh **F**requency
VMF	**V**ertically-integrated **M**oisture **F**lux

Chapter 1

Introduction

1.1 Motivation

The Indian Monsoon is the largest annual reversal in synoptic patterns of wind and rainfall in the world. Its summer rains are critical, socially and economically, to the more than one billion people of the Indian subcontinent.

Although the Indian monsoon has been studied for centuries, many of its key processes are still not fully understood. Halley (1686) proposed that the monsoon is a planetary-scale sea breeze circulation, generated as a result of differential heating between land and ocean. Although this theory is still widely regarded as the basic mechanism for monsoons (e.g. Webster *et al.*, 1998), it cannot alone explain, for example, the rapid onset of the monsoon in contrast to the steady increase in heating (e.g. Bordoni and Schneider, 2008; Boos and Emanuel, 2009), nor that India is hotter in May before the monsoon onset than in July, when the monsoon is at its strongest (Simpson, 1921).

In 1925, The Royal Commission On Agriculture In India described the Indian economy as a gamble on the monsoon. While the contribution of agriculture to the total GDP of India has fallen in modern times, to about 14%, about half of the Indian population work as farmers, of whom just over two-thirds farm for subsistence (Agriculture Census Division, 2015). Variations in rainfall greatly affect agricultural output, which has a cascading effect on the rest of the Indian people and economy, through unstable food prices. Even a bumper crop from a good rainfall year can have adverse effects, if the wrong selection of crops are

grown, by driving down the selling price of produce to a point where farmers cannot recover their costs.

Most of India receives more than 80% of its annual rainfall during the summer monsoon months of June through September (Venkateswarlu and Rao, 2013). The majority of agriculture during the summer (the kharif growing season) is rain-fed, which produces about half of India's farm output. The summer rain also replenishes surface and ground water supplies, which supply water for the largely irrigation-fed rabi growing season (October-February), which have become increasingly depleted in recent years (Rodell *et al.*, 2009), as a result of rapid economic development and population growth.

There is a high degree of spatial and temporal variability in the rains. Floods and droughts can occur contemporaneously in different regions. The Indian Space Research Organisation say that 68% of the cultivable area in India is prone to drought in varying degrees, a third of which is chronically-drought prone. Roughly one-eighth of the country is prone to flooding. The timing of the first onset of the summer rains is important in relation to the timing of crop plantation and the length of the growing season, as well as water resource management, but cyclic periods of active and break rainfall during the summer can also have significant impact.

Improving forecasting is a key factor in reducing the impact of monsoon rainfall variability. Recent investments in India in high-performance computing facilities, forecast dissemination services, and human resources have led to a service providing crop-specific advisories at district level twice a week, through multimedia channels and SMS text messaging. Where this service has been provided, farmers have been able to increase their profits by, for example, using it to manage sowing if the onset of rainfall is delayed at the start of the season, to switch to short-duration crops if a long-term delay in rainfall is forecast, to defer spraying of pesticides if rainfall is predicted, and to reduce unnecessary water use for irrigation if heavy rainfall is forecast. The Indian National Council of Applied Economic Research (NCAER), in a 2015 study, found that 93% of surveyed farmers found the forecasts to be reliable and the incremental profit associated with the service was assessed to be 25% of their net income (Maini and Basu, 2016).

After severe flooding in Pakistan in 2010, Webster *et al.* (2011), showed that in a current state-of the art medium range weather model, rainfall over Pakistan is generally highly

predictable out to 6-8 days including rainfall in the summer of 2010. If the model had been coupled to a hydrological model, they say the flooding could have been anticipated and steps taken to reduce its impact. Similarly, the rainfall that led to flooding in the north Indian state of Uttarakhand in 2013 has since then been shown to be predictable 10-12 days in advance (Joseph *et al.*, 2015), but the model missed important extratropical teleconnections that contributed to the high amounts of rainfall, which they say could be due to an inherent cold bias in the model they used.

Improving prediction of the Indian monsoon on seasonal and longer timescales is a unique challenge. In May 2002 there was no indication from any empirical or atmospheric general circulation model that all-India rainfall in June and July would be 30% below normal (19% deficit for June through September) with a similar failure in 2004, when there was a seasonal (June through September) rainfall deficit of 13% (Gadgil *et al.*, 2002, 2005). Many areas of the tropics have exhibited a high degree of predictability on these timescales due to the dominant influence of slow-varying boundary forcings, such as sea surface temperature, on variability. However, in the Indian monsoon, a large part of the interannual variability is determined by the intraseasonal variability (e.g. Palmer and Anderson, 1994), a substantial proportion of which may be unrelated to slow-varying boundary forcings, and hence unpredictable (e.g. Sperber *et al.*, 2000). Systematic biases in the representation of the Indian monsoon system remain in general-circulation model simulations, indicating that potential predictability is being missed because physical processes are not being sufficiently well represented. There is also still uncertainty over how much of the Indian monsoon variability on subseasonal timescales is unpredictable, again because of a lack of physical understanding of a wide range of processes, on a range of timescales. As convection is a fast physical process and is commonly cited as a dominant source of error in models, improving forecasts for the Indian summer monsoon, on all timescales, has been linked to a need for a better understanding of the role of deep convection in the tropics.

1.2 Aims of the thesis

The aim of this thesis is to contribute to a better physical understanding of the Indian summer monsoon, by studying some of the roles of moist convection within it.

In the monsoon onset there is still debate over, for example, how the rapid transition to the summer monsoon circulation is best explained, how the onset of the monsoon rains progresses more slowly to the northwest, taking 6 weeks on average, and what the key processes are in determining the spatial and temporal year-to-year variability of the onset. The monsoon onset has been examined in this thesis with the aim of a better understanding of the role of mid-level dry air in the progressive onset of the monsoon rains toward the northwest. This includes examining its evolution in relation to other transitions in the thermodynamics and in the large-scale circulation, and considering its role in the onset interannual variability.

The thesis also aims to improve our understanding of how the representation of moist convection can impact on the representation of the established monsoon. This is approached through the comparison of simulations that explicitly represent convection, with simulations that parametrise convection. In the first instance, how are Indian monsoon model biases related to a parametrised representation of convection? The aim is not just to compare the biases, but to use the relative biases to elicit a more complete picture of the cause and effect relationships between the biases. As convection-permitting simulations are increasingly being used for a wider range of applications, the inter-comparison of the convection-permitting simulations also aims to give some idea of how suitable certain convection-permitting model configurations might be for future simulations.

Convection centres are commonly found upstream of coastal mountain ranges in the Asian monsoon. The second highest rainfall accumulations in the Indian monsoon are upstream of the Western Ghats mountain range on the west coast of the Indian peninsula, with the highest upstream of the mountains of Myanmar, on the northeast coastline of the Bay of Bengal. The work here aims to elicit a more complete understanding of what determines the distribution of rainfall upstream of the Western Ghats by examining the role of rainfall propagation. The climatological nature of the storm propagation is characterised, and is related to local and large-scale intraseasonal variability. This provides a basis for some proposed hypotheses on the probable mechanisms for storm propagation in the region.

1.3 Thesis outline

The concepts discussed in this chapter, and other scientific background are presented in more detail in Chapter 2.

The main datasets and methods used are described in Chapter 3.

The monsoon onset is examined using a climatology of radiosonde data in Chapter 4. Some results, originally presented in Parker *et al.* (2016), that highlight the role mid-level dry air plays in the onset, are reviewed. Further work then focuses on the progression of the onset in terms of the changing circulation, and the interannual variability in the onset.

Chapter 5 presents a comparison of convection-permitting and parametrised convection simulations and observations of the Indian monsoon. The results are used to make inferences about how model biases in the representation of convection can affect the representation of the Indian monsoon system. This work was originally published in Willetts *et al.* (2017a).

Chapter 6 focuses on rainfall over the eastern Arabian Sea and west coast of India. It first compares rainfall propagation in convection-permitting simulations and satellite observations, before examining climatological patterns of rainfall propagation and their relationship to other aspects of the monsoon.

The thesis conclusions and suggestions for future work are given in Chapter 7.

Chapter 2

Scientific background

For many, the Indian monsoon is synonymous with its rainfall, brought about by moist convective processes, but to get an understanding of why the rainfall happens when and where it does, a great body of work over the years shows that it is important to consider a wide range of land, ocean and atmosphere processes and the couplings between them. This chapter aims to give a sufficiently broad background that the work presented in later chapters can be considered in this context, but without digressing too far from the main topics of the thesis. §2.1 provides a background on the physical understanding of the Indian Summer Monsoon, looking at the large-scale features of the Indian summer monsoon (§2.1.1), the monsoon onset (§2.1.2), and the variability of the monsoon (§2.1.3). §2.2 looks at the predictability of the Indian monsoon, in terms of the current state-of-the-art and some of the key areas of research. §2.3 looks at moist convection and how it is represented in models, and §2.4 concludes the chapter.

2.1 The Indian summer monsoon

The classic defining feature of monsoonal regions is the large-scale seasonal reversals in wind direction, although to many the associated change in patterns of precipitation is the more prevalent feature. The Inter-Tropical Convergence Zone (ITCZ) and its associated rainfall migrates northwards and southwards from the equator with the seasons, following the belt of maximum heating. When it is summer in the northern or southern hemisphere, the ITCZ reaches its furthest limit in that hemisphere, thus producing the annual rainy

season in monsoonal regions. Although it is termed the ITCZ here, when it is far from the equator, such as when it is over northern India, it is more accurately described as the tropical convergence zone.

The prevailing concept is that the large-scale wind reversal is a result of land-sea thermal contrast (e.g. Halley, 1686; Holton, 1992; Webster *et al.*, 1998). As a result of the lower heat capacity of land compared to ocean, the land is warmer than the ocean in the summer, and cooler than the ocean in winter. Originally formed from the study of regional monsoons circulations in isolation, such as that over India, this concept has more recently been considered in the context of a global monsoon. Rao (1966) and Sankar-Rao (1970) first referred to a global monsoon, and investigated forcings on the tropical atmosphere, in this context, in idealised models. An alternative hypothesis, originally proposed by Charney (1969), is that the migration of the ITCZ is the main driver of the global monsoon. In this theory, the monsoon is a result of an ITCZ more than 10° from the equator, which does not rely on the land-sea thermal contrast. Sikka and Gadgil (1980), in the first study of daily satellite imagery over the Indian monsoon region, showed that the cloud band in the monsoon trough (a part of the convergence zone within a monsoonal region), during an active period of the monsoon, has a similar appearance to those in other parts of the ITCZ, and that the system has the same patterns of low-level convergence, intense cyclonic vorticity above the boundary layer, and organized deep convection. Chao and Chen (2001) propose that the existence of, for example, the monsoon trough over India, or other convergence zones over land in monsoon regions, does not always require a land-sea thermal contrast. They suggest the role of land-sea contrast is more or less equivalent to a Sea Surface Temperature (SST) contrast, in determining the longitudinal location of the ITCZ, based on general circulation models simulations with monsoon region landmasses removed, and replaced with oceans that have a similar SST distribution to that which is observed in the surrounding ocean. They also find that topography is more important than land-sea thermal contrast, in replicating the Asian monsoon.

2.1.1 Large-scale features

In the boreal summer, the surface to mid-troposphere winds over India are from the south-west, and in the winter they are from the northeast (Figure). The southwesterly summer winds are connected upstream, to the west, with a cross-equatorial low-level flow that is

mostly concentrated close to the East African highlands, and is often called the Somali or Findlater jet (Findlater, 1971; Krishnamurti and Bhalme, 1976). The Somali Jet winds pick up moisture as they cross the Arabian Sea warm pool, and separate into two branches. One crosses the Western Ghats (WG), on the west coast of peninsular India, precipitating heavily as it does so, and the second branch enters the Bay of Bengal with a southerly component, before making landfall in the northeast of India, and Myanmar. In northern India, there is a low-pressure trough at sea-level, termed the monsoon trough, which forms as a result of northward migrations of the ITCZ. The upper troposphere, in the northern summer, is characterised by increasing temperature from the equator to the subtropics, with associated easterlies induced by the thermal gradient between ∼10°N and ∼20°N (Raghavan, 1973). There is a zonally-averaged cross-equatorial overturning circulation in the Indian monsoon longitudes, with ascent in the summer hemisphere subtropics, and descent in the winter hemisphere.

The highest rainfall accumulations in the Indian monsoon are over the sea, in the northern Bay of Bengal upstream of the low coastal mountains of Myanmar (the Arakan Yoma and Bilauktang mountain ranges, and in the eastern Arabian Sea upstream of the Western Ghats, a mountain range running parallel to the western coast of the Indian peninsula (Figure &). Over the subcontinent, rainfall is concentrated over the Western Ghats, along the foothills of the Himalayas and in the Ganges-Mahanadi Basin (GB) in north-east India. In addition, transient low pressure systems which form in the Bay of Bengal or northeast India, and propagate northwestward over India, which happens most often in the monsoon trough region, generate a significant fraction of the total Indian summer monsoon rainfall (e.g. Yoon and Chen, 2005). Where there are the highest rainfall accumulations over the sea, upstream of the Western Ghats and Myanmar mountain ranges, the rainfall is predominantly from large regions of precipitation, which are initiated by relatively weak convection (Houze *et al.*, 2015). Conversely, cumulonimbus systems with deep convective cores only really form over land, and in the summer monsoon season they, along with convective systems containing wide convective core structures, preferentially form in the foothills of the Himalayas (Romatschke *et al.*, 2010). Although the rainfall amounts along the foothills of the Himalayas are lower than in the Arabian Sea and Bay of Bengal centres, they are coincident with the maxima in upper tropospheric heating and pressure (Figure).

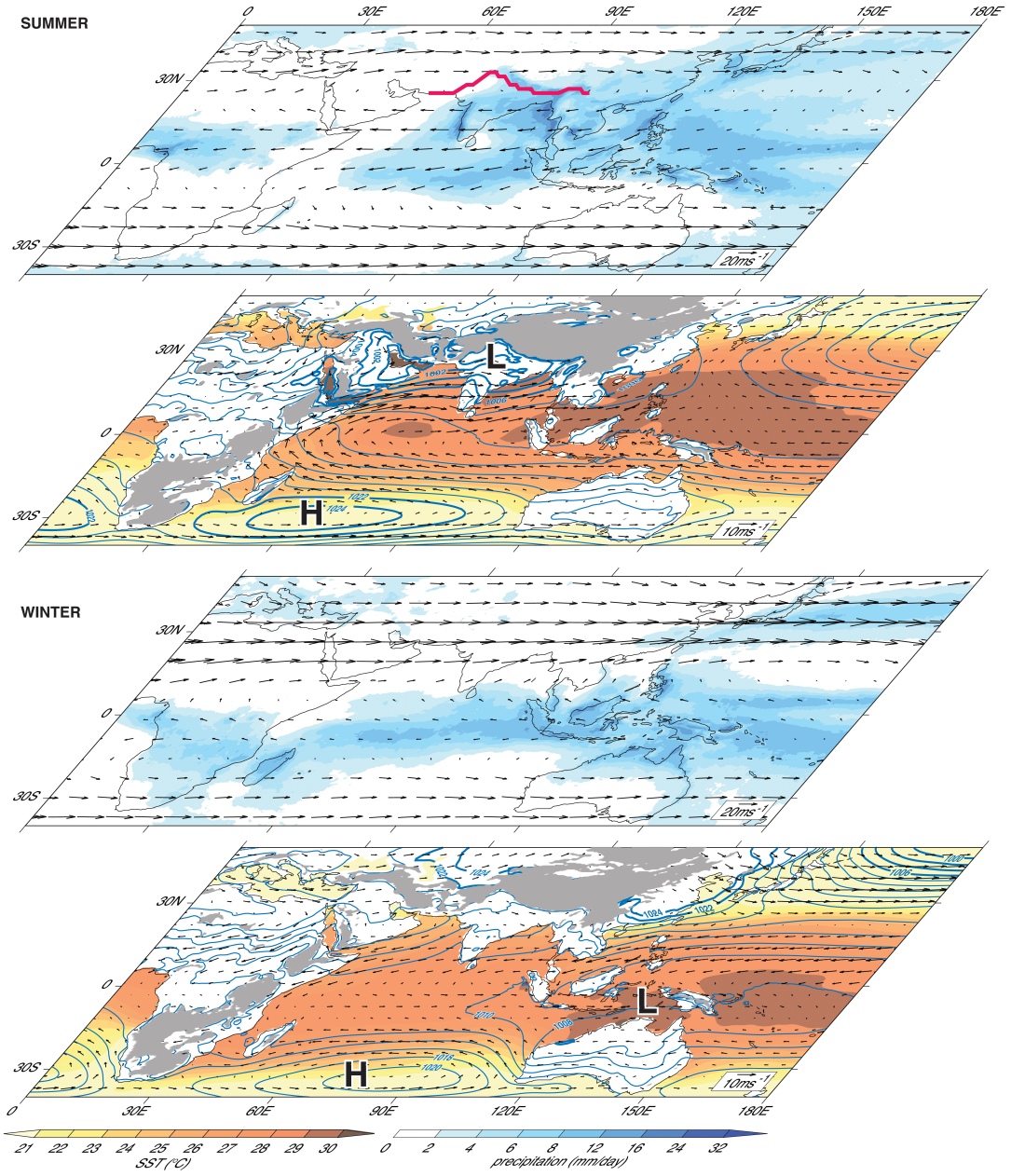

FIGURE : Schematic of boreal summer (June-September) and winter (December-February) atmospheric conditions in the South Asian monsoon region. The summer and winter panels depict the Asian and Australian monsoons, respectively. In each case, the lower panels show: orography (>1,000 m, shaded grey); SSTs from the Hadley Centre Sea Ice and Sea Surface Temperature data set for 1979-2010 (shaded yellow/orange); sea-level pressure for 1979-2010 (blue contours, interval 2 hPa) and lower tropospheric (850 hPa) winds from the European Centre for Medium Range Weather Forecasts Interim Reanalysis. 'H' and 'L' refer to the monsoon highs and lows, respectively, in the both summer and winter. Reproduced from Turner and Annamalai (2012)

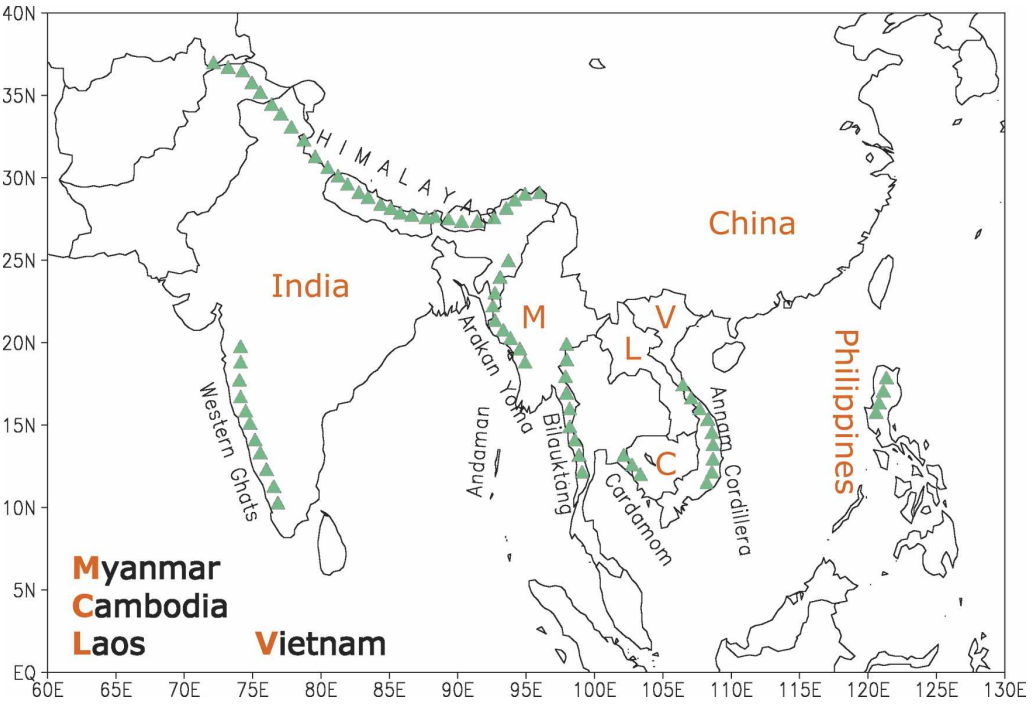

FIGURE : Asian tropical mountain ranges. Reproduced from Xie *et al.* (2006)

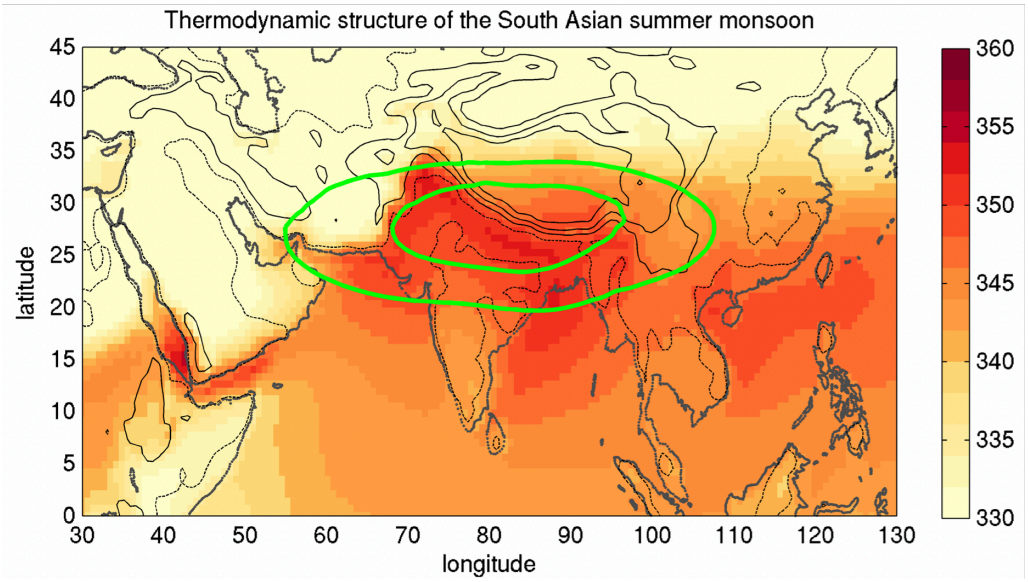

FIGURE : ERA-Interim June-August climatological mean (1979-2012) thermodynamic structure of the South Asian monsoon. Shading shows moist static energy about 40 hPa above the surface, represented in K by dividing by the specific heat of dry air at constant pressure. Green contours show 200-400 hPa average temperature (the 245.5 and 246.5 K isotherms). Dotted black line is the 300 m topographic contour and solid black lines are topographic contours starting at 1.5 km with a 1.5 km interval. Reproduced from Boos (2015).

2.1.1.1 The role of the Tibetan Plateau

In the framework of land-sea thermal contrast as the main driver of monsoon circulation, the Tibetan Plateau, as an elevated heating source, has commonly been thought of as the main driver of the Indian summer monsoon (Flohn, 1968; Yanai and Wu, 2006). At a mean height of greater than 5km above sea level, and a size of about one-quarter of Chinese territories, the Tibetan Plateau acts as a massive, elevated source of ground surface sensible heat in summer (Yeh *et al.*, 1957). The plateau directly heats the middle and upper troposphere, which has less than half the mass of the atmosphere at sea level, and so more effectively heats the air above the plateau than at lower levels (Ye, 1981). Flohn (1957, 1960) originally suggested that this elevated heating is responsible for the reversal of the meridional temperature and pressure gradients in the middle and upper troposphere, between the equator and the subtropics, which ultimately leads to the establishment of the boreal summer monsoon circulation. As a result, the mid-troposphere westerly jet stream shifts from the south side to the north side of the Plateau in early summer, and the upper troposphere warm-core anticyclone moves north from its wintertime location over the Bay of Bengal in spring/early Summer to a summertime position over the plateau (Figure), where it is called the Tibetan anticyclone (Raghavan, 1973).

On the discovery that latent heating from the condensation and precipitation of water south of the plateau, over northern India and the Bay of Bengal, was the dominant diabatic heat source of the South Asian monsoon, it was suggested that sensible heating over the Tibetan plateau was causing the latent heat source to the south through a heat pump effect (Flohn, 1968). Warm ascending air over the Tibetan and, to a lesser extent, the Iranian plateau, primarily due to surface sensible heating, leads to cyclonic circulation of lower tropospheric air, which converges towards and rises over the plateaux, producing moist convection and hence latent heating over northern India. The latent heating, as a result of convergence, drives the large-scale atmospheric flow in the Indian monsoon.

Recent work has challenged the theory that the Tibetan plateau, as an elevated heat source, is important in strengthening the Indian monsoon circulation, and that convergence in the lower troposphere and the associated heating from moist convection is the mechanism driving the large-scale circulation (e.g. Boos and Kuang, 2010; Molnar *et al.*, 2010; Boos and Hurley, 2013). The Tibetan plateau sensible heat pump theory, which still has its

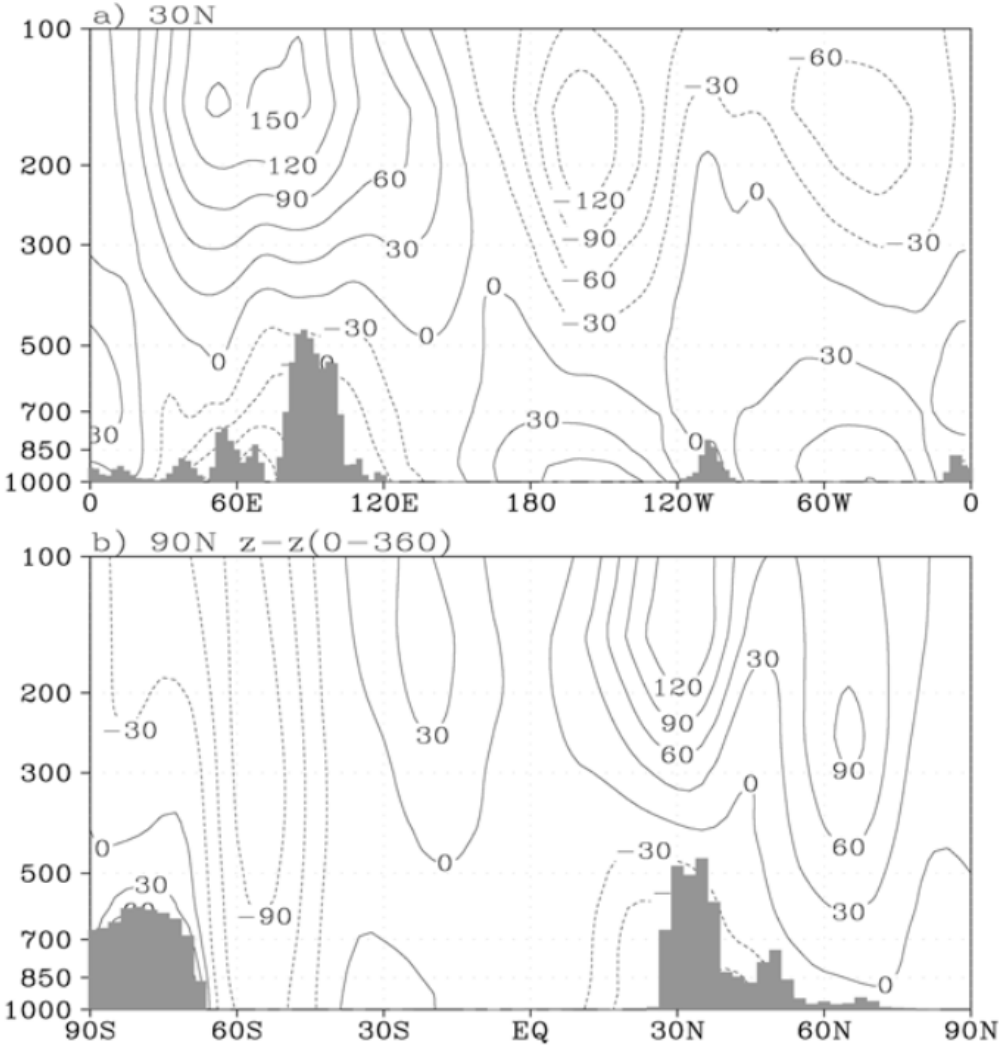

FIGURE : 1980-1997 July mean cross sections of geopotential height deviation from the corresponding zonal mean (a) along 30°N and (b) along 90°E (in units of geopotential meter(gpm)). From Yanai and Wu (2006)

proponents (e.g. Wu *et al.*, 2007; Yanai and Wu, 2006; Wu *et al.*, 2012) is described, by some of its detractors (e.g. Boos, 2015), as relying on a positive feedback mechanism between moisture convergence and precipitation, known as Conditional Instability of the Second Kind (CISK). CISK was originally formulated in theories of tropical cyclones (e.g. Charney and Eliassen, 1964; Kuo, 1965), and relies on an assumed relationship between heating and the production of kinetic energy, but it apparently does not account for the necessary positive correlation between heating and temperature fluctuations for disturbance energy to be produced (Emanuel *et al.*, 1994).

In the last couple of decades, convective quasi-equilibrium has come to dominate theories

on the relationship of deep convection to the large-scale environment, while moisture-convergence closures, based on CISK theories are now rarely used. Under a quasi radiative-convective equilibrium model for monsoon dynamics (Emanuel, 1995), which has been found to be consistent with observations of all monsoon regions except the North and South American monsoons (Nie *et al.*, 2010), the monsoon circulation is correlated with and includes low-level moisture convergence, but deep precipitating convection becomes an internal variable that keeps the free-tropospheric temperature maximum of the thermally direct monsoon circulation in approximate equilibrium with the maximum in moist static energy of air below cloud base (h_b). In this framework, it is the sensible and latent surface heat fluxes, in the region of the free-tropospheric heating maximum, which are important in establishing the monsoon flow.

In the case of the Indian monsoon, Boos and Emanuel (2009) and Boos and Kuang (2010) found that the free tropospheric temperature maximum lies just south of the Himalayas, over northern India, and not over Tibet as was commonly assumed, and is approximately collocated with the subcloud maximum in equivalent potential temperature, consistent with a convective quasi-equilibrium framework. In addition, in modelling studies Chakraborty *et al.* (2006) and Boos and Kuang (2010) show that the role the orography plays is in insulating the maximum in h_b from cold extratropical air, and that the Tibetan plateau as an elevated heat source is not important to the Indian monsoon circulation. The findings of Ma *et al.* (2014) confirmed this, and that the surface heat fluxes in the region of the free-tropospheric temperature maximum exerted the most influence on monsoon strength. However, they also found that removing orography increased the h_b needed to maintain convective quasi-equilibrium, apparently by allowing dry air into the monsoon free-troposphere, which can then be entrained into convecting plumes. This effect of removing orography was greater than that of removing surface heat fluxes and shows, similar to previous studies (e.g. Derbyshire *et al.*, 2004; Holloway and Neelin, 2009), how variations in free-tropospheric humidity may lead to an environment where strict convective quasi-equilibrium (where CAPE is only determined by h_b and free tropospheric temperature) does not adequately represent moist convection. Boos (2015) note that the minimum in h_b in the Indian monsoon region is over the western deserts of Pakistan, Afghanistan and Iran, so it is hot, dry air that the orography insulates the monsoon convection from, rather than cold, dry air from extratropical oceans. The importance of dry desert air intrusions in determining the

space-time evolution of the monsoon onset and the intraseasonal variability are discussed in §2.1.2 and §2.1.3.1.

2.1.1.2 Zonal and meridional overturning circulation

Across the tropical and subtropical regions, there is a persistent overturning of the atmosphere, which varies by season, in line with the annual cycle of solar heating. In the equinox seasons, there is a zonally-averaged pattern of almost symmetric cells about the equator, with ascent near the equator, and descent in the subtropics. In the solsticial seasons, rising motion in the summer hemisphere is, to some extent, compensated by subsidence in the winter hemisphere. There is also a significant zonal component to the tropical overturning circulation, as a result of asymmetries in the location of heating (Gill, 1980). Coastlines and orography localise heat sources so that most of the meridional circulation is within the regional monsoon circulations, and precipitating ascent in one zonal region, such as the Indian subcontinent, can lead to adiabatic subsidence in others (Krishnamurti, 1971; Rodwell and Hoskins, 1996).

Two types of meridional overturning circulation have been identified. There is a deep, moist baroclinic circulation, and a shallow dry circulation, which Trenberth *et al.* (2000) say account for 60% and 20% of the annual cycle variance in the divergent mass circulation. Gadgil (2003) note that the vertical structure of the deep moist circulation corresponds to the deep convection associated with the ocean ITCZ or the north Indian monsoon trough, and that of the shallow circulation corresponds to a heat low type structure, like the low in the northwestern regions of the Indian monsoon, and the pre-onset heat low over northern India.

Monsoon circulations are commonly thought of as being described by the deep first-baroclinic mode, with convergence in the lower and middle troposphere, and divergence in the upper troposphere. Shallow circulations have now been identified in the lower and middle troposphere in nearly all monsoon regions. They can be hard to identify in the global zonal mean, but as a localised phenomenon, their magnitude can be comparable to that of the deep circulation (Zhang *et al.*, 2008). The ascent in shallow meridional circulations in monsoon regions has been found to typically occur over desert regions northward of the region of deep, moist ascent (e.g. Nie *et al.*, 2010), and to flow southward in the middle

troposphere, between 800-500hPa (Zhang *et al.*, 2008; Kawamura *et al.*, 2002) Cool, moist air is transported northward in the lower part of the circulation, across the precipitation maximum of the deep ascent, which produces, by the horizontal advection, near-surface cooling and moistening north of the precipitation maximum. There is an associated southward transport of hot, dry air in the upper part of the circulation, which warms and drys the lower to middle troposphere over the precipitation maximum. The near-surface moistening and mid-level drying through advection in shallow meridional overturning circulations has been argued to affect the onset and subseasonal variability of monsoons, and also the seasonal mean precipitation (Zhai and Boos (2017), and references therein), which will be discussed further in sections 2.1.2 and 2.1.3.1.

2.1.1.3 Low-level cross-equatorial flow

Of particular relevance to the Indian monsoon circulation is the low-level south to north cross-equatorial jet flow that follows the east coast of Africa (Findlater, 1969). It accounts for nearly 65% of the total mean low-level cross-equatorial transport, which balances the north to south cross-equatorial transport in the upper troposphere, in 5% of the equatorial circumference, or $\sim$85 X 10^9 kg s^{-1} within the jet according to one study (Rodwell and Hoskins, 1995).

The low-level jet winds are deflected northwards and flow over the arid low lands on the east coast of Africa; Then, at about 10°N, north-eastwards into the Arabian Sea (where it may be called the Somali Jet, or East African Low Level Jet), as they are deflected by the Somali highlands. The jet occurs at 1-1.5 km above the sea surface, with wind speeds of 25-50 ms^{-1}. It has a core width of 200-400 km, a 1 km depth, and is located about 200km east of the East African Highlands (Findlater, 1977). Several modelling studies (Anderson, 1976; Bannon, 1982) suggest that the winds are deflected by the Mascarene High, a belt of low-level divergence (located above the small islands of Mauritius in the southern Indian Ocean, east of Madagascar) towards the convergence of the monsoon trough in Northern India. Rodwell and Hoskins (1995) show, with a primitive equation model, that land-sea surface friction contrasts (particularly as it flows over East Africa), diabatic heating over the southern Indian Ocean and Africa, and increased mixing over Africa, as modifiers of material potential vorticity (PV), are important for the establishment of the jet. PV modification is shown to be essential in establishing the irreversible cross-equatorial flow of the jet, by

overcoming the effects of the Earth's rotation. Particles that experience insufficient PV modification recirculate back into the Southern Hemisphere. The strength of the jet is particularly sensitive to changes in heating over the southern Indian ocean

2.1.1.4 The monsoon trough

The monsoon trough is a low pressure belt which begins in northwestern India and Pakistan, and extends across the Gangetic plains of northern India into and to the east of the Bay of Bengal (Ramage, 1971). The trough is made up of a well-marked low in the northwest of the subcontinent and the boreal summer tropical convergence zone that extends southwest into the Bay of Bengal. The low in the northwest is typically described as a heat low, and is associated with dry shallow convection (2-3 km ascent), whereas the ascent further east is throughout the lower troposphere, as a result of moist instability. In contrast to a heat low, which would be mainly formed by sensible heating at the surface, Bollasina and Nigam (2011) observe that the northwestern low is deepest in July rather than May, after the onset of the monsoon and its rains have cooled the land-surface and sensible heating is reduced, and also that the low is centred over the vegetated Indus river plain, and not desert. They suggest that, regionally, the influence of the Hindu-Kush mountain range to the west is more important than the land surface heating in establishing the presence of the low, and that it is the onset of deep convection to the east that deepens the low from May through to July.

The location and intensity of the monsoon trough exert a major influence on rainfall activity in north-central India. A large fraction of the rainfall in the monsoon trough region comes from transient low-pressure systems superposed on the mean flow, the most intense of which are called monsoon depressions (e.g. Yoon and Chen, 2005), that generally form in the Bay of Bengal and propagate northwestward, against the mean low-level flow. Keshavamurty and Awade (1970) find that the kinetic energy of the mean monsoon trough is maintained by the pressure gradient of the large-scale circulation, and is not a statistical result of transient perturbations.

2.1.2 Monsoon onset

As the sun's midday zenith moves north in the boreal summer, the different heat capacities of earth and water mean that land regions heat up more quickly than the surrounding oceans. A surface heat low forms over northern India in late May, and as a result the meridional temperature and pressure gradient reverses in the lower troposphere towards the equator. The meridional temperature gradient in the middle and upper troposphere reverses; The associated baroclinic wind is consistent with the upper-level tropical easterly jet stream (Koteswaram, 1958) and the low-level westerly monsoon winds (Findlater, 1969; Krishnamurti and Bhalme, 1976). The southerly low-level cross-equatorial flow begins to develop in April over the ocean east of Africa, which focuses into the zonal cross-equatorial jet near the East African Highlands (Krishnamurti and Bhalme, 1976) in May. Following the meridional peak in insolation, the ITCZ moves north in April and May from its position just south of the equator, to a mean Boreal summer position of 20°N on the Indian subcontinent (where it is referred to as the monsoon trough).

2.1.2.1 Large-scale onset

In relation to the seasonal cycle of insolation, the fundamental forcing of the monsoon, the onset involves rapid dynamic and thermodynamic changes. Just prior to the onset of the monsoon rains over India, there is a rapid intensification of the southwesterly low-level jet winds that cross the Arabian Sea (Boos and Emanuel, 2009), and are the major moisture source of the Indian monsoon, as well as a rapid intensification of the upper-level easterly jet (Raju *et al.*, 2005). Yanai *et al.* (1992) describe an 'explosive' expansion of warm air over the Tibetan Plateau in the late spring and early summer of 1979. There is a similarly rapid change in the large-scale meridional overturning circulation from the zonally-averaged equinox pattern of two cells almost symmetric about the equator, to a single cross-equatorial cell (Bordoni and Schneider, 2008) which rises in the summer hemisphere, and descends in the winter hemisphere (Figure). At the same time as the abrupt onset of the summer monsoon circulation, there is a marked increase in heat and moisture flux convergence, and deep convection over the off-equatorial Arabian Sea, Indian peninsula, and Bay of Bengal, with further intensification as the onset progresses (Raju *et al.*, 2005).

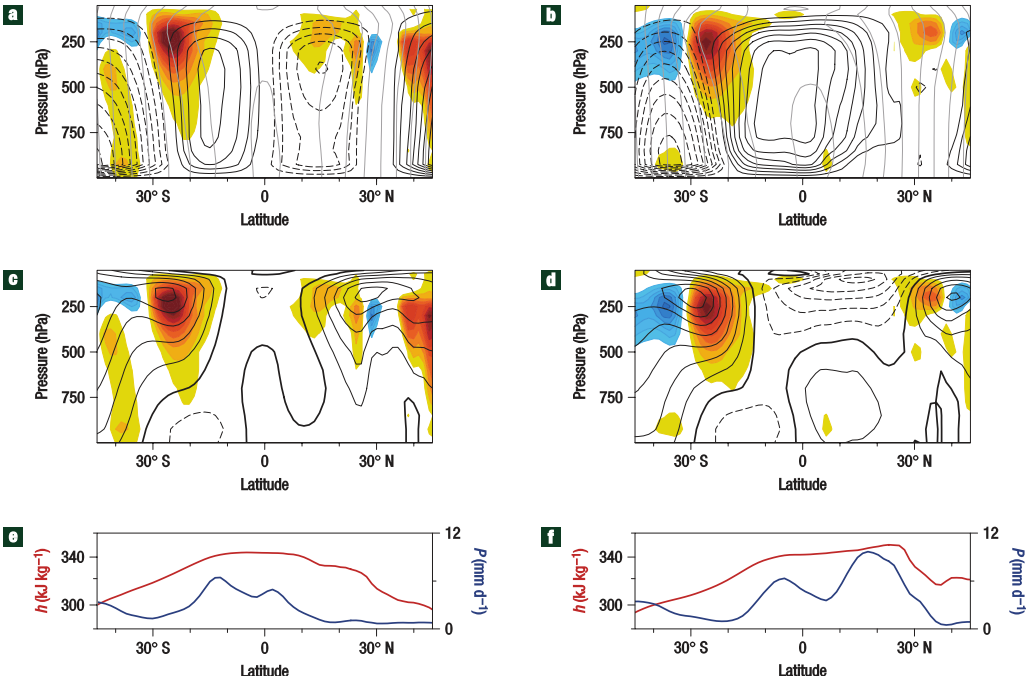

FIGURE : Zonal and temporal-mean circulation in the Asian monsoon sector at two 20-day periods before (left panels, Julian Day 81-100) and after (right panels, Julian Day 161-180) monsoon onset. (a),(b), Streamfunction of meridional overturning circulation (black contours, contour interval $50\text{x}10^9$ kg s^{-1}, with solid contours for anticlockwise rotation and dashed contours for clockwise rotation), angular momentum per unit mass (grey contours, contour interval $\Omega\, a^2/15$ with Earth's rotation rate Ω and radius a) and transient eddy momentum flux divergence $div([\overline{u'v'}])cos\phi$, with horizontal velocity vector $v = (u, v)$ (colour contours, contour interval $0.6\text{x}10^{-5}$ m s^{-2} in (a) and $1.2\text{x}10^{-5}$ m s^{-2} in (b), with red tones for positive and blue tones for negative values). Here, $(\cdot)$ denotes a temporal mean over the 20-day period and over all years of data, primes denote deviations from this mean and $[\cdot]$ denotes a zonal mean over the monsoon sector. (c),(d), Zonal wind (black contours, contour interval 6 m s^{-1}) and eddy momentum flux divergence (colour contours) as in (a),(b). (e),(f), Precipitation P (blue) and near-surface (850 hPa) Moist Static Energy h (red). Except for precipitation, all quantities are obtained from the ERA-40 reanalysis and are averaged over the years 1981-2000. In the latitude zones of the tropical overturning circulation, the horizontal eddy momentum flux divergence shown in the figure is the dominant term balancing the Coriolis force on the mean meridional flow and the mean meridional momentum advection in the zonal momentum budget; other terms, such as the stationary eddy momentum flux divergence and the zonal geopotential gradient across the monsoon sector, are smaller. Reproduced from Bordoni and Schneider (2008).

The traditional theory to explain the rapid onset of the southeast Asian monsoon in May, and the Indian monsoon in June are respectively related to a rapid increase in heating over the eastern and western parts of the Plateau, and associated reversals of the meridional temperature gradient in the mid and upper troposphere (He *et al.*, 1987; Yanai *et al.*, 1992). Other theories which attempt to explain the abrupt monsoon onset de-emphasise the importance of land-surface heating, particularly over the Tibetan Plateau, Boos and Emanuel (2009), considering the rapid onset in a convective quasi-equilibrium framework, favour a wind-evaporation feedback (Numaguti, 1995; Boos and Emanuel, 2008) in the oceanic regions where there are simultaneous large increases in low-level wind, surface enthalpy fluxes and deep ascent as the main mechanism by which the southwesterly monsoon winds rapidly increase over the Arabian Sea.

Bordoni and Schneider (2008); Schneider and Bordoni (2008) demonstrate, using an aqua-planet general circulation model, how the effect of large-scale extratropical eddies in the upper troposphere affect the strength of the vertical overturning circulation, and may produce an abrupt monsoon onset in the absence of land-surface forcings. It is the transition from a non-angular momentum conserving circulation to a momentum conserving that they say determines the rapid onset, which happens when the absolute vorticity in the upper troposphere becomes close to zero. Upper troposphere large-scale extratropical eddies can easily penetrate into the subtropics when there are upper-level westerlies, which keeps the absolute vorticity relatively high. The upper-level easterlies that develop in spring and summer over India, shield the subtropics from the eddies, and so the absolute vorticity reduce.

The most prevalent method of defining the onset date requires a sustained period of heavy rainfall over Kerala (Ananthakrishnan *et al.*, 1967), which is also used by the Indian Meteorological Department, but with a subjective analysis of the evolution of the large-scale circulation. Other onset indices are based on circulation changes over the Arabian Sea (Moron and Robertson (2014) provide a brief review). As defined by these methods, the mean onset date, for the start of the onset in southern Indian, is between 29 May and June 5.

After the first onset of rain on the southernmost west coast of India, which is associated with the abrupt transition to the summer monsoon circulation, the northwestward progression of the rains takes 6 weeks on average to reach the Pakistan border. The Indian Meteorological

Department climatological mean onset isochrones (Figure), which are an effective measure of the progression of the northern limit of monsoon rains (Parker *et al.*, 2016), show the onset beginning on 1 June in Kerala. Two weeks later, by 15 June, the monsoon rains have begun over the entire extent of the western peninsula coast of India, and have progressed northwestward from the Bay of Bengal over the southeastern part of the monsoon trough region. It is another month (15 July) until the onset occurs over the northwestern desert and semi-arid regions of India and Pakistan. The curvature of the IMD onset isochrones (Figure), which becomes sharper from 31 May to 15 June follows the pattern of strengthening low-level monsoon circulation, as the ITCZ shifts northward, and the monsoon trough becomes established over India (Sikka and Gadgil, 1980).

The northwestward progression of the monsoon onset happens against the time-mean low-level monsoon flow (westerly) and mid-level (northwesterly) flow and moisture advection (Figure). Mid-level dry air, that is advected over India by the northwesterly winds, forms a wedge that deepens toward the northwest. Parker *et al.* (2016) propose that, as a result, the conditions for the onset of deep convection are more favourable to the south. Following the abrupt transition to the summertime monsoon circulation, moisture advection from the Arabian Sea increases, and the mid-level dry air is eroded by moistening from below, progressively allowing the onset of deep convection towards the northwest. Some of the work originally presented in Parker *et al.* (2016) is presented in Chapter 4

2.1.2.2 Local onsets

Regional-scale measures of onset, may not give an effective measure of the onset on smaller scales. This is true both for the climatological local onset dates, and the interannual variability of the local onset dates. The local onset of rainfall can be of great importance in, for example, the sowing of crops. If the local onset can be related to larger-scale predictable drivers, it may be predictable. A level of spatial coherence in the local onset indicates regions where the local onset is significantly determined by larger-scale variability. The level of spatial coherence in the local onset will depend on the definition of the onset, and the definition of spatial coherence.

The onset at local scales is less well documented than the first onset of the monsoon and its mean progression. Two recent studies assess the spatial coherence of local onsets in the

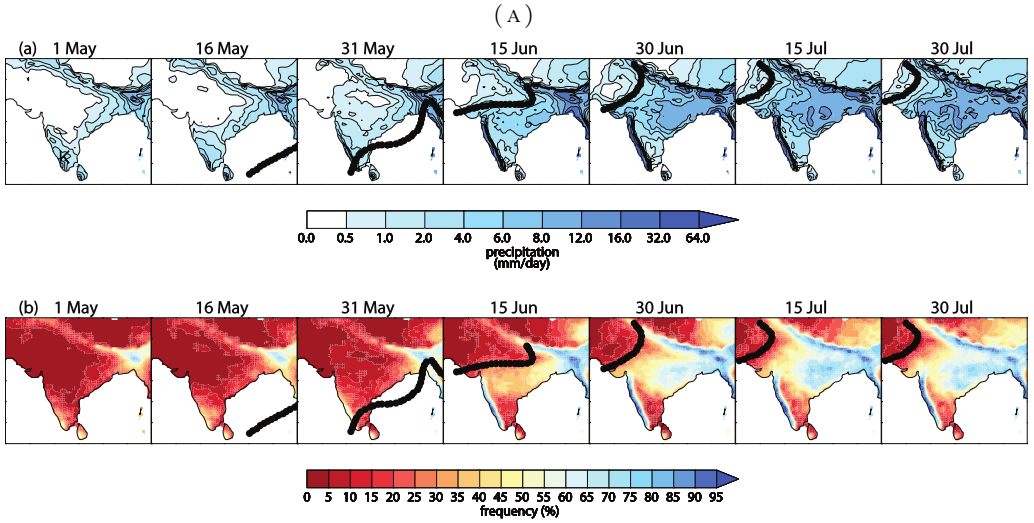

FIGURE : Statistics of rainfall over India during the monsoon onset from the APHRODITE 0.5° gridded gauge-based dataset, averaged over 1951-2007, with each panel labelled with the middle day of its 5-day period. Climatological isochrones of monsoon progression as defined by the Indian Meteorological Department (IMD) are also shown by the thick black lines; the closest in time in each panel (the five chosen isochrones being 25 May, 1 June, 15 June, 1 July and 15 July). (a) Mean rainfall (mm day^{-1}) and (b) mean frequency of rainfall occurrence, expressed as a percentage. The IMD standard rainy day threshold of 2.5 mm is used to define rainfall occurrence. The state of Kerala is indicated in (a) with a letter 'K'. Reproduced from Parker *et al.* (2016).

Indian monsoon (Moron and Robertson, 2014; Fitzpatrick *et al.*, 2016). Both use 'agronomic' definitions of local onset (see Marteau *et al.* (2009) for a review), where the local onset date is determined by four criteria:

1. the amount of rainfall received during an initial wet spell
2. the amount of rainfall received during any dry spell following the initial wet spell
3. the duration of the initial wet spell
4. the length of any dry spell following the wet spell

These criteria are designed to ensure sufficient soil moisture for planting and growing periods, to avoid crop failure. The dry spell criteria are designed to ensure against taking short pre-onset rainfall spells as the onset. In Fitzpatrick *et al.* (2016), the local onset date is taken as the first rainy day (with at least 1 mm of precipitation) of two consecutive rainy days (with total precipitation greater than 20 mm) and no 7 day dry spell with less than 5 mm of rainfall in the next 20 days. The definition in Moron and Robertson (2014) is very slightly different, with an initial wet spell defined as 1 or 2 consecutive days where the total

rainfall is at least 20 mm, and all other criteria the same. These criteria are not designed to capture the onset in drier regions, such as in the northwest semi-arid and desert regions of the Indian subcontinent.

The mean local onset over the Western Ghats and monsoon trough region is found to be robust, and therefore potentially predictable (Moron and Robertson, 2014). The two studies come to different conclusions, however, about the spatial coherence of the onset interannual variability(Moron and Robertson, 2014; Fitzpatrick *et al.*, 2016). Moron and Robertson (2014) find at best moderate spatial coherence over India. The Localised Onset Region method of Fitzpatrick *et al.* (2016) finds large regions with significant spatial coherence over the Western Ghats region, the Bay of Bengal, and the monsoon trough region. The studies use different rainfall datasets and different measures of spatial coherence. Moron and Robertson (2014) use a 1° gridded rainfall dataset (Rajeevan *et al.*, 2006) based on rain gauge measurements (1901-2004), and Fitzpatrick *et al.* (2016) use the 0.25 TRMM 3B42 satellite rainfall retrieval product (1998-2014). Clearly the satellite product covers a much shorter time period, but how well the different products capture local rainfall variability is unclear.

The estimate of local onset spatial coherence in Moron and Robertson (2014) is a conditional probability, based on counting the number of times the local onset dates at each gridpoint co-occur within 5 days of the date at the surrounding eight gridpoints. The level of spatial coherence in Fitzpatrick *et al.* (2016) is assessed based on the size of areas with a certain level of homogeneity in the local onset dates. LORs are found where the percentage of gridpoints with suitably similar onset dates exceeds a threshold. The onset dates are suitably similar if their correlation with the LOR median onset dates exceeds a certain confidence level. The disagreement between the two studies may perhaps, therefore, be explained by the LOR method being less sensitive to the correlation of onset dates between adjacent gridpoints. The LORs are used in Chapter 4 (where their calculation is described in further detail), in the work that examines the interannual variability of the onset.

2.1.3 Variability of the monsoon

The spatial and temporal variability of Indian monsoon rainfall is much more complex than can be explained by theories for the establishment of the cross-equatorial monsoon

circulation, which rely on slow varying forcings such as the land-sea temperature gradient, or the influence of the Himalayas. Rainfall variability on a wide range of timescales, as a result of processes both internal and external to the Indian monsoon system, is significant in determining the long-term interannual variability.

2.1.3.1 Intraseasonal variability

The most commonly discussed aspects of the intraseasonal variability in the Indian summer monsoon, with their important socio-economic effects in terms of timings and amount of rainfall, are the monsoon onset and active/break cycles of convection. There are predominant modes of intraseasonal variability on timescales of 10-20 and 30-60 days. The 30-60 day mode is strong during the onset phase of the monsoon, in June, and less coherent in the established phase in July and August, while the 10-20 days mode is strong during the established phase (Annamalai and Slingo, 2001).

Climatologically, the Indian Meteorological Department have determined the monsoon onset to occur over Kerala (the most southern state in India), on 1 June, and by 15 July in northwestern India, but the relative and absolute onset timings, as well as the strength are highly variable from year-to-year. From mid-May to mid-June, the phase of the 30-60 day mode of variability, which manifests as northward and eastward propagating convective anomalies from the equatorial Indian Ocean, modulates the effect of the growing insolation over the northern hemisphere, and determines the timing of the onset (Flatau *et al.*, 2001). By mid-June the large-scale pressure gradient is sufficiently large that onset will occur regardless of the phase of the intraseasonal oscillation. Fieux and Stommel (1977) identified, from shipping reports of wind strength in the Arabian Sea, single, multiple and gradual onsets. The single onsets manifest as a rapid onset in the low-level monsoon winds, while the gradual onsets are when westerly winds begin to develop earlier than usual, in early May, when the large-scale cross-equatorial pressure gradient is still relatively weak. Multiple onsets are when westerly winds begin to develop, followed by a wind reversal, before another onset of westerly winds. In the case of multiple onsets, convection and circulation patterns develop in the Indian monsoon region in early May, in relation to an intraseasonal oscillation, when the pressure gradient is too weak to support the full onset of the summer monsoon system. These so-called 'bogus' onsets have been associated with subsequent heat-wave

conditions over India, and a delayed onset of the monsoon, which happened, for example, in 1995, 2002, and 2003 (Flatau *et al.*, 2001, 2003)

There are typically three to four active periods during the May to September season (Webster *et al.*, 1998), when there is a peak in rainfall over the continent. During these periods, it is typical for the monsoon westerly winds, which vary significantly in strength during the season, to have speeds of >10 m s^{-1} and to extend across to the northwestern Pacific Ocean. During the break parts of the active break cycle, rainfall is at a minimum over much of India, but is enhanced over the far north and south. The cycle is non-periodic, and the active and break parts can be several day or weeks long.

About four weeks is the longest the tropical convergence zone over India can survive without interaction with or reestablishement by an oceanic tropical convergence zone (Sikka and Gadgil, 1980). These continental and oceanic convergence zones, over northern India and the equatorial Indian Ocean, are the two preferred locations of convection within the Indian summer monsoon. The establishment and maintenance of the monsoon trough over India has been described as being a result of successive northward propagations of the tropical convergence zone from the Indian Ocean at intervals of 2-6 weeks (Gadgil, 2003). These northward propagating events form the dominant 30-60 day mode of variability (Yasunari, 1980) in the Asian summer monsoon which essentially captures the active/break cycles of convection and circulation in the Indian monsoon (Annamalai *et al.*, 1999). Annamalai and Slingo (2001) estimate that the 30-60 day mode of variability accounts for about 2/3 of the total subseasonal variability, while the 10-20 day mode (Krishnamurti and Bhalme, 1976; Krishnamurti and Ardanuy, 1980) accounts for about 1/4, and is comprised of westward propagating events (Figure). In active periods, associated with the 30-60 day northward propagating events, convection is significantly enhanced in a band across the Indian subcontinent, Bay of Bengal, and equatorial west Pacific, and suppressed significantly over the equatorial Indian Ocean and north-west Pacific (Annamalai and Slingo, 2001). The large-scale cross-equatorial Hadley and east-west circulations are also greatly affected. The 10-20 day mode exhibits a more regional effect; It simultaneously modulates convection in the continental and oceanic tropical convergence zones, with enhancement in one and suppression in the other. Krishnamurti and Bhalme (1976) also describe a dominant mode on a time scale of 2-6 days, associated with local instabilities and local transient disturbances.

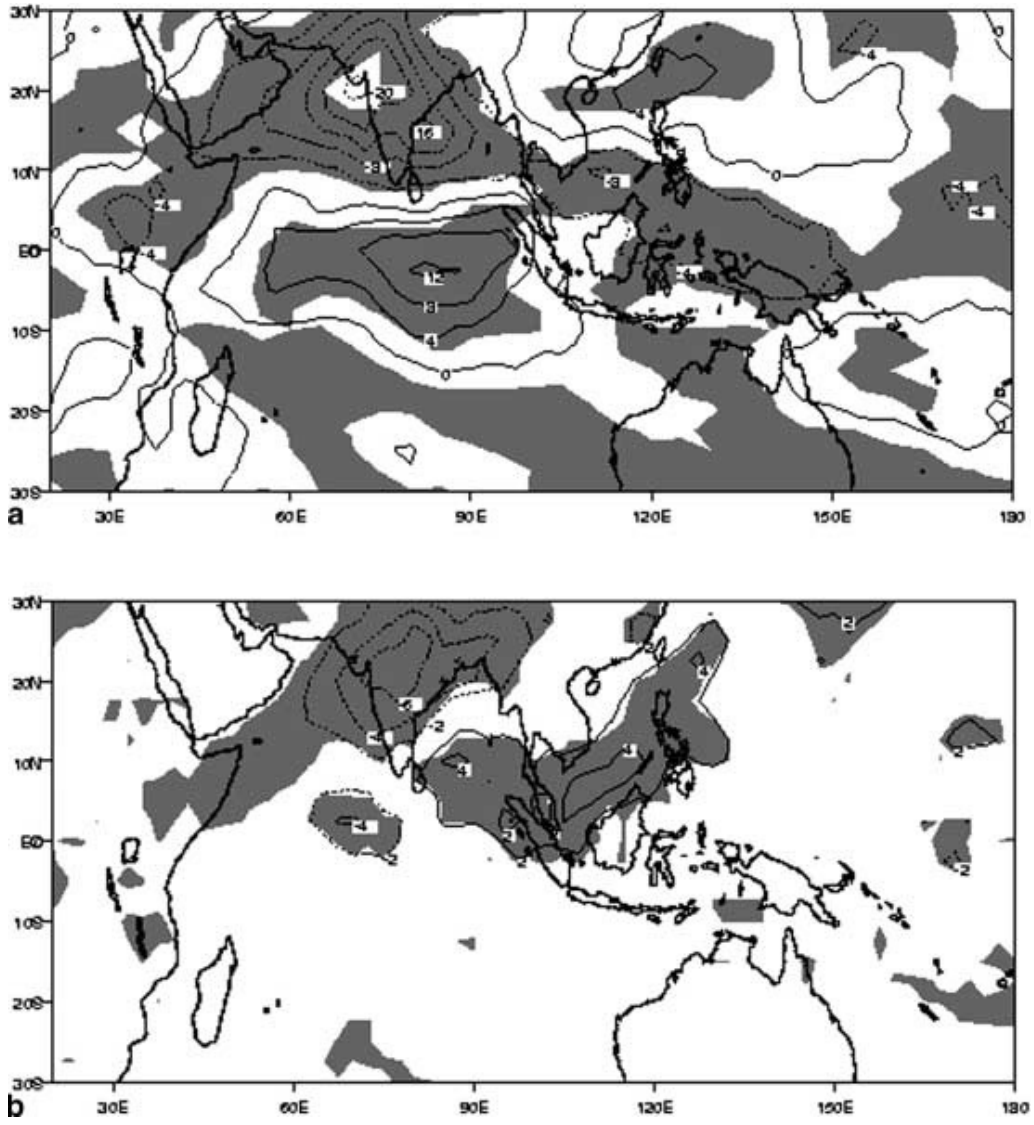

FIGURE : Composites of active minus break days of OLR for the dominant (a) 40-day (30-60 days), and (b) 15-day (10-20 day) modes of intraseasonal variability in filtered daily All-India rainfall. The contour interval for (a) is 4 W m^{-2} and (b) is 2 W m^{-2}. Shaded area indicates regions significant at 5% level. Reproduced from (Annamalai and Slingo, 2001).

The 30-60 day timescale of the northward propagating events is similar to the timescale of eastward propagating Madden-Julian Oscillations (MJO). The MJO is most often associated with eastward propagation of envelopes of large-scale convective systems, which is the predominant pattern in the boreal winter and spring, when the strongest MJO events occur. During the boreal summer monsoon season, when convection over landmasses in the Indian monsoon longitudes places the convective heating far from the equator, the MJO is typically weaker and has a more complex character (Madden, 1986). This includes a northward movement of convection, which begins in the central equatorial Indian Ocean

and ends in northern India, which is found, most of the time, to be related to a concurrent eastward movement of convection into the western Pacific Ocean (Lawrence and Webster, 2001), resulting in an apparent northeastward propagation of convective anomalies. The northeastward propagation is due, at least in part, to favourable vertical easterly wind shear and the shedding of Rossby waves over this domain during boreal summer (Lau and Peng, 1990; Wang and Xie, 1997; Annamalai and Sperber, 2005).

2.1.3.2 Synoptic-scale activity: Monsoon depressions and other low-pressure systems

Monsoon depressions are broad cyclonic circulations that generate over the warm waters of the Bay of Bengal and normally propagate northwestward along the monsoon trough/ITCZ region (Figure). 6 form every year, on average, and they typically last for 4-5 days. The Indian Meteorological Department define monsoon depressions as having surface winds between 8.5-16.5 m s^{-1}. Systems with lower wind speeds may be termed a low-pressure system, or a well-marked low, and those with higher wind speeds a cyclonic storm. Yoon and Chen (2005) estimate that 45-55% of Indian Summer rainfall is from monsoon depressions.

During an active phase of the active-weak monsoon cycle (Annamalai and Slingo, 2001), which is associated with a strengthening of the ITCZ, the frequency of monsoon depression formation increases as a function of the speed with which convective instability grows in the Bay of Bengal. There is often a partial overlapping of these systems in an active period, whereas none form during a break period (Yasunari, 1979). Monsoon depressions propagate westward against the synoptic flow, and underneath the Tibetan high at about 300 hPa (Chen and Yoon, 2000).

Synoptic variability in the Bay of Bengal can also affect the onset space-time variation. For example, in 2014 the strengthening of the Arabian Sea monsoon winds was aided by the formation of cyclonic storm Nanauk. In addition, MJO activity over the maritime continent led to the development of deep convection in the northern Bay of Bengal, and a low-pressure area which formed as a result over coastal Bangladesh aided the advance of the monsoon onset in the northeast of India (Pai and Bhan, 2015).

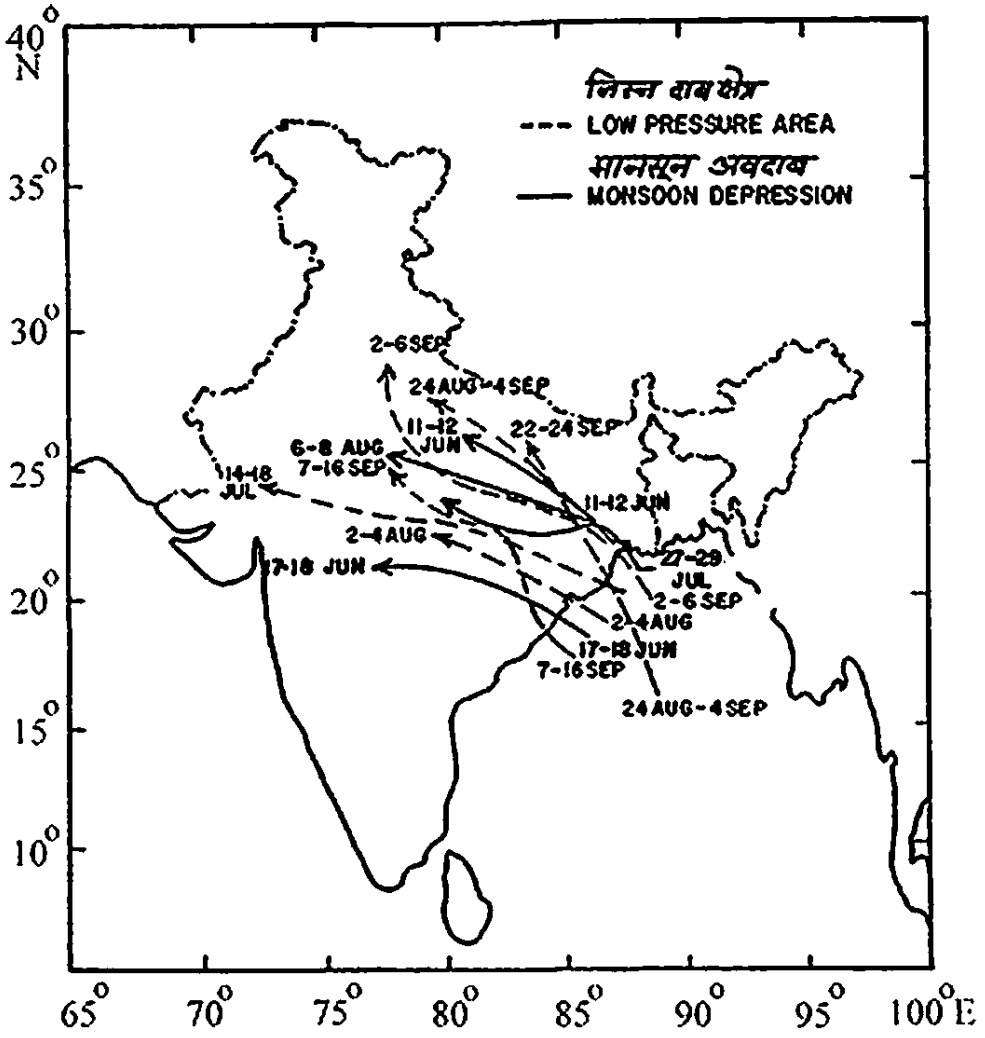

FIGURE : Paths of low pressure systems during the summer monsoon season of 1999. Reproduced from Gadgil (2003)

2.1.3.3 Interannual variability

In terms of the potential for improved prediction on seasonal and longer timescales, Palmer (1994) raised the question of whether the seasonal variability in the Indian monsoon was dominated by essentially chaotic processes, with the interannual variability determined by the number of active and break periods in a season, or whether the statistics of active/break cycles were more controlled by slow-varying (and hence, predictable) external forcings. The Palmer (1994) study, and subsequent work such as Webster *et al.* (1998) and Sperber *et al.* (2000) suggest that boundary forcings such as SST do bias the system towards more active or break periods, although part of the internal variability is still chaotic.

On timescales greater than a year, SST anomalies related to the El Niño Southern Oscillation

(ENSO) are the dominant external forcing of monsoon variability (Turner and Annamalai, 2012). Interannual variability of the monsoon has been found to occur on three major timescales. These are quasi-biennial, multi-year (3-7 years), and interdecadal.

The quasi-biennial oscillation, where there is a tendency for a relatively strong Indian monsoon to be followed by a relatively weak one, or vice versa, is strongly related to a 2-3 year oscillation in SST anomalies in the Pacific (Yasunari, 1990) and Indian (e.g. Loschnigg *et al.*, 2003) Oceans. As such, biennial variations in the Indian monsoon system are related to similar oscillations in ENSO, but questions remain over whether biennial oscillations in the Indian Ocean (the Indian Ocean dipole) that are independent of ENSO (Saji *et al.*, 1999) may also play a role.

Oscillations on timescales of 3-7 years also exhibit a clear relationship to ENSO (Webster *et al.*, 1998). In the year following anomalously warm Pacific Ocean SSTs (El Niño), all-India rainfall is often below average, and following anomalously cool Pacific Ocean SSTs (La Niña), all-India rainfall is often above average (Figure). There are, however, many years where this pattern does not prevail.

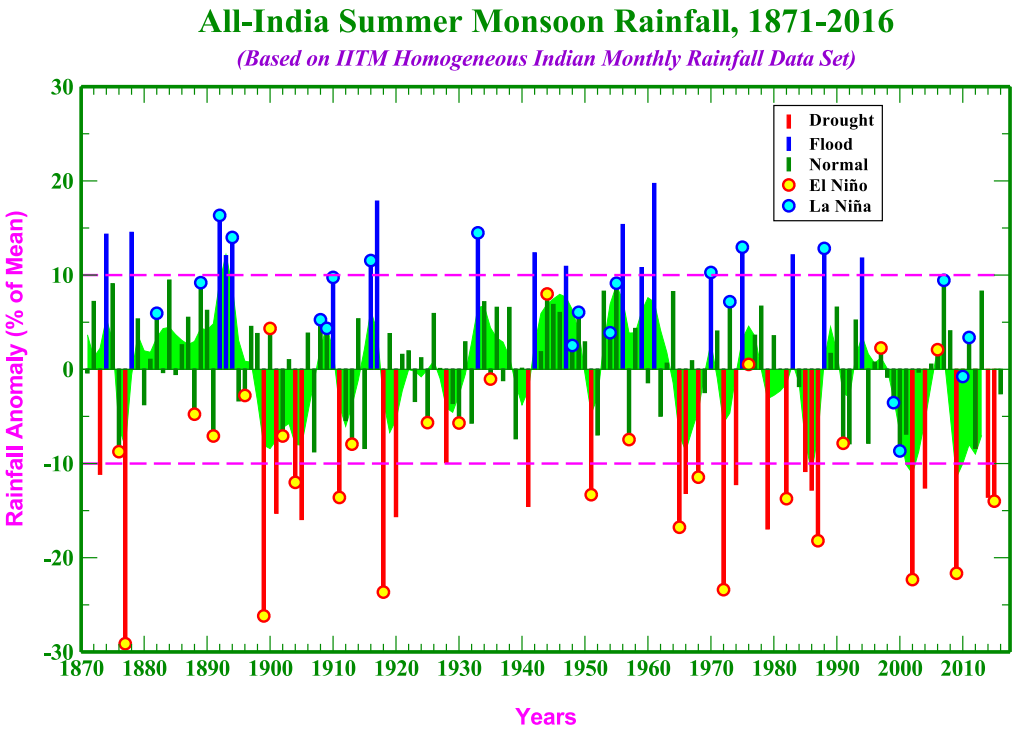

FIGURE : Time series evolution of yearly all-India summer monsoon rainfall anomalies, expressed as percent departures from its long-term mean (1871-2016). Reproduced from Indian Institute of Tropical Meteorology, Pune, India.

Interdecadal variability, where rainfall is above or below average for periods of about 3 decades (Figure) in the monsoon, has been shown to be related to interdecadal climate variability in the Pacific Ocean (e.g. Joshi and Kucharski, 2017) and the Atlantic Ocean (e.g. Ghosh *et al.*, 2012) Observations suggest that, in recent decades, there may also have been a change in the nature of the relationship to El Niño (e.g. Kumar *et al.*, 1999).

2.1.3.4 Spatial variability

There is considerable spatial structure to rainfall variablity in the Indian monsoon (Parthasarathy, 1995), on intraseasonal timescales, and also interannual, decadal and longer (e.g. Goswami *et al.*, 2006).

The two highest regions of rainfall in the Indian monsoon are upstream of relatively low coastal mountain ranges (Figure) on the west coast of the Indian peninsula (the Western Ghats), and on the Myanmar coast in the north Bay of Bengal (Xie *et al.*, 2006); A phenomenon which has not yet been fully explained (e.g. Grossman and Durran, 1984; Smith, 1985), and will be discussed further in Chapter 6. Hoyos and Webster (2007) find that the

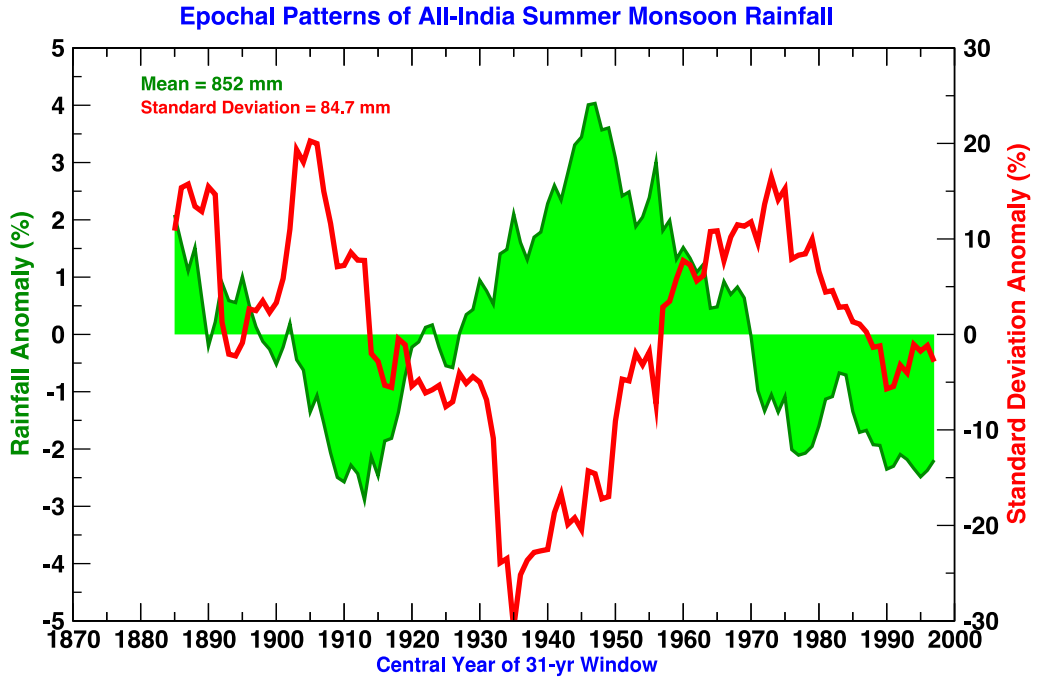

FIGURE : Time series evolution of 31-year rolling mean of all-India summer monsoon rainfall mean and standard deviation anomalies, expressed as percent departures from its long-term mean (1871-2016). Reproduced from Indian Institute of Tropical Meteorology, Pune, India.

interaction of northward propagating intraseasonal oscillations with these coastal mountains is important in explaining the rainfall maxima upstream of these coastal mountains. There is also a narrow rainband that follows the south side of the steep orography of the Himalayas. Global climate models, typically do not capture the effects of these mountain ranges (Christensen *et al.*, 2007; Kripalani *et al.*, 2007), most likely due to their coarse resolution, which cannot properly represent regional forcings such as steep orography (Rupa Kumar *et al.*, 2006).

There is a significant effect of narrow mountain ranges on the distribution of rainfall across the tropics. As well as the Western Ghats and the Myanmar coastal mountain ranges (Araka Yoma in the northern bay and Daiwna-Bilauktaung in the southern bay), there are the mountains of the Philippines, which anchor the convection in the South China Sea, there is a convection centre on the coast of Cambodia at the foothills of the Cardamom Hills, and also one on the west slope of the Annam Cordillera range on the border between Laos and Vietnam (Figure). In one experiment where, in a regional atmospheric model (Wang *et al.*, 2003), diabatic heating is imposed in narrow bands where convection is anchored by the northern Myanmar coastal mountains, the Annam Cordillera, and the mountains of the Philippines, there is a non-local effect with enhance precipitation over the eastern Arabian Sea, and over the entire Bay of Bengal, and a relative cyclonic circulation is induced over the Indian longitudes (Xie *et al.*, 2006).

Over land, the two highest regions of Indian summer monsoon rainfall are the Western Ghats, and the Ganges-Mahanadi Basin (GB) in north-east India (Figure). They both have strong mean and variance, and account for 90% of the interannual variance in all-India rainfall, but their variances are uncorrelated (Vecchi and Harrison, 2004). The rainfall variability in the monsoon trough, where much of the rainfall comes from transient disturbances, is highly correlated with all-India summer monsoon rainfall (Gadgil *et al.*, 2003), and as such, an improved prediction of variability in this region should also project onto the larger-scale predictability.

2.2 Predicting the Indian monsoon

The first attempts to predict interannual variations of the summer monsoon were based on relatively slow-varying pre-season indicators such as snowfall in the Himalayas (Blanford,

1884) and the pressure gradient between the Indian and Pacific Oceans (Walker, 1924). Much later, it was proposed (Charney and Shukla, 1981; Palmer and Anderson, 1994), and then shown, (Shukla, 1998) that in certain parts of the tropics, the atmosphere is strongly dependent on slow-varying boundary forcings, such as SST. This was in contrast to the view of the atmosphere, that emerged following the advent of numerical weather simulation, as a chaotic system (Lorenz, 1963) where skill in predicting the weather is limited to only a few days, as a result of non-linear sensitivity to errors in the initial conditions and in model formulations. In practice, the level of predictability in the tropics, on timescales longer than a few days, is higher than in the extratropics, but in certain regions potentially chaotic processes also play a significant role, Indian monsoon rainfall being 'a prime example' (Branković and Palmer, 2000).

Empirical/statistical models, beginning with Walker (1924) have had a certain degree of success in seasonal and long-range prediction of, for example, all-India summer monsoon rainfall (e.g. Chaudhuri *et al.*, 2016), and references therein), particularly when the boundary forcings are strong (such as during intense El Niño and La Niña periods). However, Gadgil *et al.* (2005) found that the forecast skill based on statistical methods had not improved since the 1930s. Successfully simulating seasonal and climate variability using dynamical models has proved more elusive. While there are observed relationships between slow-varying boundary forcings (the strongest of which is SST) and the tropical atmosphere, physically representing the necessary range of local, regional and global teleconnections remains a significant challenge. To develop a model that can successfully represent the monsoon to the level required by its intended application, these interactions need to be sufficiently well understood, observations used in determining initial conditions for simulations must give a sufficiently accurate representation of the earth system, and models must give a sufficient representation of the necessary physical processes.

Models with prescribed SSTs have shown little improvement in representing interannual variations of Asian-Australian monsoon rainfall over land (e.g. Zhou *et al.*, 2009), while models with ocean-atmosphere coupling exhibit large systematic biases, many of which are common among among the models (e.g. Bollasina and Nigam, 2009). Key areas of research include improving model representations of convection, improving understanding of air-sea interactions and land surface processes, as well as the effect of orography on dynamical and thermodynamical processes.

Atmosphere-only and coupled general-circulation models (GCMs) typically exhibit a systematic wet bias over the equatorial Indian Ocean, and a dry bias over central India, which has not changed significantly as a result of model development between the Coupled Model Intercomparison Project CMIP3 assessment (Meehl *et al.*, 2007) and CMIP5 assessment (Sperber *et al.*, 2013). Indian monsoon rainfall onset is systematically late, by about 10 days, in most CMIP5 climate models (Sperber *et al.*, 2013), which would not be remedied by just reducing the continental dry bias (Sperber and Annamalai, 2014). Higher resolution regional climate models (RCMs), which are able to represent regional forcings, feedbacks, and processes, improve the representation of rainfall in the Indian summer monsoon, particularly over regions of steep orography such as the Himalayas and Western Ghats (Rupa Kumar *et al.*, 2006), and have been found to give a realistic timing of the monsoon onset, although the withdrawal is less well simulated (Lucas-Picher *et al.*, 2011). However, Lucas-Picher *et al.* (2011) show significant differences in the representation of the Indian Monsoon by a number of RCMs forced with lateral boundary conditions from the 45-year European Centre for Medium-Range Weather Forecasts (ECMWF) Re-Analysis (ERA-40) for the period 1981-2000, highlighting that they fail to properly represent important feedbacks and processes, even when biases introduced by the driving model are reduced.

Boreal Summer Intraseasonal Variability (BSISV), predominantly in the form of the 30-60 day intraseasonal oscillations which exhibit northward as well as eastward propagation in the Asian tropics (as described in §2.1.3.1), projects strongly onto the interannual variability of the Indian monsoon (e.g. Goswami and Ajaya Mohan, 2001). On weather timescales, it also modulates the frequency of occurrence of synoptic systems events such as low-pressure systems, monsoon depressions and tropical cyclones (Maloney and Hartmann, 2001; Goswami *et al.*, 2003; Bessafi and Wheeler, 2006). As a result of the BSISV, it is still unclear how predictable the Indian monsoon may be on seasonal and longer timescales (Turner and Slingo, 2011). An important question for the prospect of improved prediction of the Indian monsoon, on seasonal and longer timescales, is whether this intraseasonal variability is essentially chaotic, or whether the slow-varying forcings dominate in determining the statistics of the intraseasonal variability. Sperber *et al.* (2000) find that the statistics of intraseasonal variability is more determined by slow-varying forcings, and thus predictable, although a significant subset of subseasonal variability is determined by the internal chaotic variability, which would limit predictability. Sperber and Annamalai (2008) propose, on the assumption that the mean-state determines the occurrence of the transient activity that

some of the processes a model must capture to give a physically correct representation of the boreal summer intraseasonal oscillations are the eastward propagation of equatorial intraseasonal convective anomalies, capturing the three main centres of precipitation over the central-equatorial Indian Ocean near India, the Bay of Bengal and the tropical west Pacific, and climatological easterly wind shear over the region to capture the effect of Rossby waves. In an assessment of the CMIP5 model historical simulations, more models simulate the northward propagating component of the BSISV than the CMIP3 models, and the models that give a reasonable representation of the intraseasonal oscillations are those with better representations of the intraseasonal SST and its coupling to convection over the equatorial Indian Ocean and eastward propagating equatorial convective anomalies east of 100°E (Sabeerali *et al.*, 2013).

The most significant source of seasonal predictability for the Indian summer monsoon is ENSO (e.g. Shukla and Paolino, 1983), but also known to be important is the effect of seesawing SSTs in the Indian Ocean, which is called the Indian Ocean Dipole (e.g. Johnson *et al.*, 2016). While there is useful skill in predicting regionally averaged ENSO SST indices at lead times of 6-12 months, models struggle to represent the spatial pattern of SST anomalies, which has a major impact on their ability to represent teleconnections to the monsoon (e.g. Turner *et al.*, 2005). In the case of Indian Ocean SST teleconnections to the monsoon, Bollasina and Nigam (2009) find a wide range of misrepresentation of local and non-local air-sea interactions in the Indian Ocean in coupled general circulation model simulations performed for the Intergovernmental Panel on Climate Change Fourth Assessment Report.

The effect of snow cover in the Himalayas (from the original hypothesis of Blanford, 1884) and north/west Eurasia have been investigated in a number of observational and modelling studies, with inconclusive findings (Fasullo, 2004) for a review), in terms of the physical processes by which the monsoon summer is influenced, and the region from where snow cover has the most impact. The suggestion from relatively recent studies is that snow cover over the Himalayan and Tibetan Plateau region can influence the monsoon through a so-called Blanford-type mechanism involving reduced surface sensible heat and longwave fluxes, which reduces heating of the troposphere over the Tibetan Plateau and consequently a reduced meridional tropospheric temperature gradient (Senan *et al.*, 2016; Turner and Slingo, 2011).

The representation of the land-surface in models has received less attention than SST. Soil moisture and vegetation reduce the Bowen ratio, and surface roughness and albedo influence the boundary layer state. Such surface heterogeneities can influence precipitation and circulation on a range of time and space scales (e.g. Goessling and Reick, 2011). Webster (1983) show how representing soil moisture could be important in recreating the northward propagation of convection, such as that seen in the BSISV. In atmospheric general circulation model simulations with 'perpetual' May insolation and SST (held fixed at their respective monthly mean values), precipitation and circulation evolve considerably, as a result of soil moisture interacting with circulation(Bollasina and Ming, 2013). The model produces a slow northwestward migration of the monsoon, which is comprised of large-scale 35-50 day coupled oscillations of soil moisture, precipitation and circulation, consistent with the observations of Krishnamurti *et al.* (2012) and the conceptual model of Parker *et al.* (2016).

As described in §2.1.3.4, the low coastal mountains of the Western Ghats and the Myanmar coast serve as anchor points, where rainfall is concentrated upstream of them over the sea. Rainfall also tends to be concentrated along the foothills of the Himalayas. The east African highlands play an important role in determining the location and intensity of the cross-equatorial flow (Hoskins and Rodwell, 1995; Slingo *et al.*, 2005). Improved representation of the effects of orography has come about as a result of increasing spatial resolution in models, with steep orography becoming better resolved. The CMIP5 historical simulations have a better multi-model mean than those of CMIP3, in terms of the spatial pattern correlation with observations, with more realistic rainfall amounts adjacent to the Western Ghats, and the foothills of the Himalayas, which may be due to their higher horizontal resolution (Sperber *et al.*, 2013). Lucas-Picher *et al.* (2011) note that the pattern of precipitation upstream of the Western Ghats is closer to that of the observational datasets in the 4 regional climate models studied than in the ERA-40 reanalysis, and that they also capture well the relatively high amount of precipitation in central India, and on the Myanmar coast.

2.3 Moist convection, and its representation in models

Moist convection occurs in narrow, saturated updrafts, with associated narrow, nearly saturated downdrafts driven by precipitation and a wider area of unsaturated subsidence surrounding the clouds. It is the result of conditional instability, where the atmosphere is

unstable with respect to moist adiabatic parcel displacements, but stable with respect to dry adiabatic displacements. Moist convection can organise into convective systems on a range of scales, which include thunderstorms, squall lines and mesoscale convective systems. The horizontal and vertical scales of moist convective updrafts are comparable and range in scale from several hundred metres for shallow convection to several kilometres for deep convection. Moist convection is a crucial element of weather and climate around the globe. It contributes to the transport of heat, moisture, aerosols and trace gases, and in the tropics is the primary source of precipitation. Deep convection can lead to extreme rainfall events, and dangerous weather such as flash flooding and high winds. By perturbation of the upper troposphere and the vertical transport of heat, deep convection can generate planetary (Rossby) waves, which have an affect on the global weather and climate.

While a typical thunderstorm cell is on the order of 10 km in all three directions, and individual cumulonimbus clouds can be explicitly resolved at grid-spacings of about 1 km, it is widely held that a minimum resolution of 100 m is needed to properly resolve deep moist convection (Bryan *et al.*, 2003a; Petch *et al.*, 2002). As a comparison, the Met Office Unified Model (MetUM) runs at grid-spacings of ∼17-33km for global weather modelling, and ∼140-280 km for global climate.

The representation of convection is a dominant source of error in global models (Jung *et al.*, 2010; Sherwood *et al.*, 2014), and there is evidence that the errors are primarily due to physical processes that occur on a short enough timescale (within the first few days, often the first 24 hours) to affect both weather and climate models (Murphy *et al.*, 2004; Rodwell and Palmer, 2007). Improvements to convective parametrisation schemes, based on weather models, should also lead to improvements in climate models. It is expected that in the next 10 years, accounting for increases in computing power, global models of weather and climate will run at grid-spacings ranging from several kilometres, to about 100 km (Holloway *et al.*, 2012b). As such, it is expected that convective parametrisation will be a necessity for the foreseeable future, when the combination of complexity, timescale, domain size and model ensemble size require it.

It can be difficult to identify the source of errors in climate models, due to feedbacks and compensating errors. The MetUM has been designed to be "seamless", and as such, can be configured for use across a range of timescales. Weather models allow the model output to be

compared with observations to identify short-timescale sources of error in parametrisations that, when corrected, lead to improvements on all timescales (Martin *et al.*, 2010).

2.3.1 Convective parametrisation

When a process is too small-scale, or complex, to be explicitly represented in a model, it is parametrised. Assumptions are made about these processes, by setting parameters, to simplify their representation in numerical models. Parameters are tuned, often unrealistically, to provide estimates of specific important processes.

Almost all convection parametrisations are based on the assumption of convective quasi-equilibrium, introduced by Arakawa and Schubert (1974). The thermodynamic adjustment of the atmosphere by convection is assumed to be almost in equilibrium with the large-scale non-convective elements of the circulation. The time adjustment of the thermodynamic profile to other forcings is assumed to be nearly instantaneous compared with the slowly varying large-scale circulation. As in Arakawa and Schubert (1974), most convection parametrisations represent an ensemble of non-interacting convective plumes in terms of mass flux. The mass flux for an individual plume is given by

$$M_i = \rho \sigma_i w_i$$

where ρ is density, σ_i is fractional area covered by plume, and w_i is the vertical updraft velocity of the plume

The plume ensemble can be represented spectrally (e.g. Arakawa and Schubert, 1974) or, more commonly, as a single entraining-detraining 'bulk' plume (e.g. Yanai *et al.*, 1973).

With increasing spatial and temporal resolution, where the assumptions made in determining the vertical mass flux ($w << w_i$ and $\sigma_i << 1$) become invalid, or the forcing varies rapidly enough (Davies *et al.*, 2013), the equilibrium assumption begins to break down. In certain areas, such as the tropical ocean, equilibrium convection is commonly a good approximation, where the generation of CAPE by large-scale processes is balanced by convection. However, in continental areas where convection can more often be inhibited by the presence of a capping inversion, and precipitation does not peak until late afternoon (Yang and Slingo, 2001), models with parametrised convection tend to peak too early, following the diurnal cycle of insolation (Guichard *et al.*, 2004).

2.3.2 Errors in parametrised models

Convective parametrisation schemes typically produce too many light rain events, too few heavy rain events, and have a diurnal cycle of continental precipitation that peaks too early in the day (Betts and Jakob, 2002; Randall *et al.*, 2003; Guichard *et al.*, 2004; Stephens *et al.*, 2010; Dirmeyer *et al.*, 2012). The intensity and frequency of precipitation influences cloud formation and associated radiative effects, aerosol effects on the radiation balance, latent heating in the atmosphere, and surface hydrological processes (Stephens *et al.*, 2010). Ground heating of the lower atmosphere due to insolation, which increases the lower-tropospheric instability, is an important control on the diurnal cycle of summertime convection and precipitation. The diurnal cycle associated with this large and well-defined solar forcing is a fundamental mode of variability in the atmosphere, and as such has been suggested to be an important test for the correctness of any model (Yang and Slingo, 2001). In addition, mesoscale circulations such as land-sea breezes, katabatic-anabatic winds, or mountain valley winds can modulate the precipitation regime and produce a diurnal cycle with distinct regional variations.

2.3.3 Convection-permitting models

In the convection-permitting simulations used here, where convection is entirely explicitly resolved, the highest resolution simulations have a grid-spacing of 2.2 km, which would generally be considered suitable for operational purposes, but not high enough to properly resolve deep convection. Model configurations with small enough grid-spacings to allow convection to be explicitly resolved are known to give, compared to simulations with convective parametrisations, a more realistic diurnal cycle of precipitation in the tropics, with rainfall typically peaking over land in the late afternoon (Guichard *et al.*, 2004; Dirmeyer *et al.*, 2012), and give a better rainfall intensity distribution, but overestimate the amount (Weisman *et al.*, 1997; Holloway *et al.*, 2012b). For the West African monsoon, when run over large domains for many days, convection permitting simulations have been shown to be much better on the continental scale, due largely to their improved representations of triggering, organisation and the diurnal cycle of precipitation (Marsham *et al.*, 2013; Birch *et al.*, 2014).

While convection-permitting models with grid spacings of 1-4 km have been found to more realistically simulate the physics of larger convective systems, such as thunderstorms, mesoscale convective systems, and squall lines (Weisman *et al.*, 1997; Romero *et al.*, 2001; Speer and Leslie, 2002), that does not necessarily lead to a significant improvement in point-specific forecasting (Done *et al.*, 2004). As resolution increases, errors from initial conditions and model processes, although smaller, grow more rapidly (Lorenz, 1969). During convective events small-scale predictability limitations, comparable to observational uncertainties, may be critical even at scales over 100 km (e.g. Romero *et al.*, 2001). Zhang *et al.* (2003), using 3.3 km simulations of a 2 day snowstorm, showed that errors are initially in the timing and position of individual convective cells, and subsequently have an effect on larger-scale aspects such as the the position of the surface low and the distribution of precipitation. Nonetheless, Roberts and Lean (2008), in a comparison of 12, 4, and 1 km MetUM simulations of 10 days when convection occurred, find that the 1 km simulation provides a better forecast of rainfall distribution and high accumulations on scales of $>$15 km, although the forecast skill at grid-scale is low.

2.4 Conclusions

The aims of the thesis, were outlined in §1.2. The main topics of the thesis are the monsoon onset, the relationship of moist convection with the large-scale monsoon circulation, and rainfall propagation over the Arabian Sea, upstream of the Western Ghats.

In the monsoon onset, the reversal of the meridional temperature gradient, associated with seasonal changes in heating, establishes the monsoon low-level southwesterlies and upper-level easterlies, as a result of the thermal wind relationship. There are also more rapid changes that happen around the time of onset, typically in late May or early June, for which a number of theories exist, such as rapid changes in heating over the Tibetan plateau, wind-induced surface heat exchange, and the effect of large-scale extratropical eddies in the upper troposphere on the overturning circulation. After the first rapid transition, the onset of the monsoon rains takes a further 6 weeks on average to reach the northwestern parts of the region, which happens against the mean low-level monsoon circulation, and has recently been proposed to be a result of the interaction of moist convection with mid-level dry air (Parker *et al.*, 2016). Chapter 4 presents some of the results from Parker *et al.* (2016) and

also looks further at the dynamical changes that take place during the onset, and also the interannual variability of the onset.

In simulations with parametrised convection schemes, the typical biases in the Indian summer monsoon are dry bias over India, a wet bias over the equatorial Indian Ocean. Models with parametrised convection schemes, such as the one used here typically produce too much light rain, too little heavy rain, and have a diurnal cycle of rainfall over land that peaks too early, in the early afternoon, following the diurnal cycle of solar heating. An explicit representation of rainfall generally gives a much better representation of the diurnal cycle of rainfall over land in the tropics, peaking in the late afternoon, and a more realistic distribution of rainfall intensities, but tends to overestimate rainfall amounts. Chapter 5 uses model simulations with and without parametrised convection schemes to assess how systematic model biases are related to the representation of convection. Given these differences in the representation of moist convection and rainfall, the work examines how the large-scale monsoon could be altered. Of particular relevance is how this alters the representation of the monsoon trough, which forms part of the monsoon circulation, and where convergence and relatively heavy rainfall are collocated, how this alters the land-sea temperature contrast and so the circulation, and how different rainfall over the equatorial Indian Ocean could also alter the circulation.

The rainfall amounts upstream of the Western Ghats, on the west coast of India, are the second highest within the Indian summer monsoon, after the rainfall amounts over the Bay of Bengal, upstream of the coastal mountains of Myanmar. The coastal mountain ranges interact with northward propagating monsoon intraseasonal oscillations, providing an important control on the temporal and spatial variability of rainfall. Chapter 6 looks at rainfall propagation upstream of the Western Ghats.

Collectively, these studies shed light on the role of deep convection in the large-scale onset and circulation, and the role of circulation in the variability of convection.

Chapter 3

Data

This chapter describes the Met Office Unified Model (MetUM) simulations, ERA-Interim reanalysis (Dee *et al.*, 2011), satellite rainfall retrievals, and radiosonde data that are used across the thesis. Further details of data and methodology are given as appropriate in later chapters.

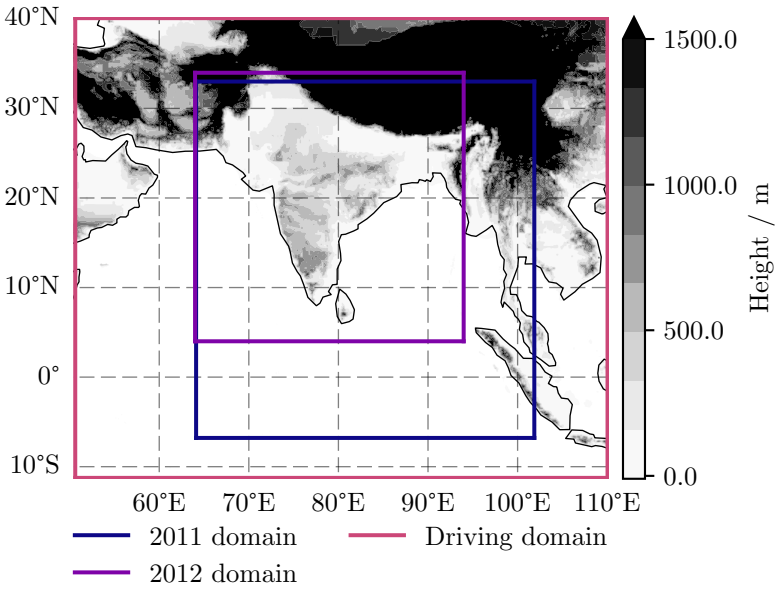

FIGURE : Region of interest, and MetUM model simulation domains. Shading shows orographic height (m).

3.1 Met Office Unified Model simulations

All simulations use the UK Met Office Unified Model (MetUM). The fully compressible non-hydrostatic deep-atmosphere equations of motion are solved using a semi-implicit, semi-Lagrangian scheme (Davies *et al.*, 2005). It uses a staggered Arakawa C-grid in the horizontal and a terrain-following hybrid-height Charney-Phillips vertical grid. There are a comprehensive set of parametrisations for processes too complex or small-scale to be physically represented, such as surface exchange (Essery *et al.*, 2001), boundary layer mixing (Lock *et al.*, 2000), mixed-phase cloud microphysics (Wilson and Ballard, 1999), and an optional mass flux convective parametrisation scheme (Gregory and Rowntree, 1990).

The MetUM simulations used here come from 2 separate modelling experiments, both of which include regional domain high-resolution convection-permitting simulations, and also parametrised convection simulations (at a range of grid-spacings) over the Indian monsoon region. There are simulations for 18 August to 9 September 2011 (21-days), and for 15 May to 15 July 2012. The domain size is bigger for the 2011 period (Figure) and, as the western boundaries are the same and there is a small difference in the location of the northern boundary, the smaller 2012 simulation does not have the same extent to the south over the equatorial Indian Ocean and to the east over southeast Asia. In order to reduce data volume, both the 2011 and 2012 simulations are nested directly within a limited area simulation ('Driving', domains in Figure), which has the same horizontal unrotated grid as the operational MetUM global model (∼24 km grid-spacing), and is reinitialised every 6 hours with Met Office operational analyses for the 2011 simulations and with ECMWF analysis for the 2012 simulations The simulations are free-running, and receive hourly local boundary conditions, which are provided by Driving, and Sea Surface Temperatures (SSTs) are prescribed and are updated daily from OSTIA analyses (Donlon *et al.*, 2012).

The 2011 simulations (Table a) are a suite of regional MetUM simulations of a 21 day period starting 18 August 2011 00:00 UTC, which was the most anomalously wet period (giving the best signal-to-noise ratio) of the 2011 Indian summer monsoon. They were run as part of the Earth system Model Bias Reduction and assessing Abrupt Climate project (EMBRACE; a collaboration between nineteen European partners, with the goal of improving Earth System Models). There are 2.2, 4, 8, and 12 km grid spacing simulations that treat convection explicitly, with no convective parametrisation and a 3D Smagorinsky

TABLE A: 2011 model run configurations. Domains are Free-Running (FR), and Driving as shown in Figure . LAM stands for Limited Area Model, SMAG is Smagorinsky scheme, 1DBL is 1-D Boundary Layer, and conv param is Convection Parametrised.

Grid-spacing	Domain	Timestep	Vertical Levels and Lid	Conv. Scheme	Referred to as
2.2 km	FR	10s	118, 78 km	Explicit 3D SMAG	2.2E
4 km	FR	10s	118, 78 km	Explicit 3D SMAG	4E
8 km	FR	10s	118 78 km	Explicit 3D SMAG	8E
8 km	FR	300s	70, 80 km	1DBL + CP	8P
12 km	FR	10s	118, 78 km	Explicit 3D SMAG	12E
12 km	FR	300s	70, 80 km	1DBL + CP	12P
24 km	FR	600s	70, 80 km	1DBL + CP	24P
120 km	FR	1200s	70, 80 km	1DBL + CP	120P
24 km	D	600s	70, 80 km	1DBL + CP	Driving

TABLE B: 2012 model run configurations. Domains are free-running (FR), and Driving as shown in Figure . LAM stands for Limited Area Model, SMAG is Smagorinsky scheme, 1DBL is 1-D Boundary Layer, and conv param is Convection Parametrised.

Grid-spacing	Domain	Timestep	Vertical levels	Conv. scheme	Referred to as
2.2 km	FR	300s	118, 78 km	Explicit 3D SMAG	2.2E
10 km	FR	300s	70, 80 km	1DBL + conv param	10P

scheme for sub-grid mixing. The simulations were originally run at the Met Office to examine the stratospheric gravity wave field above deep tropical convection (Bushell *et al.*, 2015). While grid-spacings of 8 and 12 km would normally be considered too coarse to model without a convective parametrisation, the overlap in grid-spacings allows the effects of the representation of convection to be isolated from those due to grid-spacing (as in Marsham *et al.* (2013) for the West African monsoon). Simulations with parametrised convection at grid-spacings of 8, 12, 24 (comparable with many global numerical weather prediction models), and 120 km (comparable with many climate models) use the MetUM Global

Atmosphere 4.0 (Walters *et al.*, 2014) configuration, with a 1-D boundary layer scheme for the sub-grid mixing. All of these simulations have a rotated-pole horizontal grid. The convection-permitting simulations are configured as per the operational MetUM variable grid-spacing NWP model configuration (UKV) (Cullen, 1993), but with the differences listed in Table c. The simulations are nested directly within the MetUM N512L70 (∼24 km horizontal grid-spacing) global model, which is reinitialised every 6 hours with Met Office operational analyses, and provides hourly local boundary conditions for the free-running simulations. SSTs are prescribed and are updated daily from OSTIA analyses (Donlon *et al.*, 2012).

The 2012 simulations (Table b) again form part of a suite of MetUM (version 8.5, with the newer ENDGame Dynamical core) simulations, and a 2.2 km convection-permitting simulation and a 10 km parametrised convection simulation are used here. The simulations, which run from 15 May to 15 July 2012, were designed, in part, to assess model biases in the Indian monsoon onset, and 2012 was selected as it is considered to be close to an average monsoon onset, based on climatology. In contrast to the 2011 simulations, these are performed on an unrotated grid. In standard model configurations, soil moisture properties vary spatially and, as they are poorly constrained by observations, can produce unrealistic gradients in soil moisture and evaporative fraction, which influences storm initiation. So,

TABLE C: Model configuration differences between models that handle convection explicitly (2.2E, 4E, 8E, 12E), and the Met Office variable grid-spacing NWP model (UKV). α's are scaling factor for reduced off-centering of semi-lagrangian advection (see Webster *et al.* (2008)) for further details. θ is potential temperature, LBC is local boundary condition.

	2.2E, 4E, 8E, 12E	UKV
Timestep (s)	10	50
Dynamics	α's=4*0.6+ fully 3D θ advection	α's=0.7, 1, 0.7, 1, non-interp θ advection
Sub-grid mixing	3D Smagorinsky	2D Smagorinsky + 1D boundary layer
Vertical Levels	118, 78 km lid	L70, 40 km lid
Sponge (on W)	yes (from 40 km and increases upwards in strength)	no
RHcrit (%)	99 at all levels	91 to 80
Radiation calls	Every 5 mins	Every 15 mins
Frictional heating	yes	no
Qtidy moisture conservation	yes	no
Smagorinsky diffusion of Qcl, Qcf	yes	no
LBC rim width	12 and 24 points	8 points

for the 2012 simulations, the standard global configuration MetUM model is initialised with homogeneous soil property values and run for 10 years to obtain soil moisture values for May 2012, which are used to initialise the 2012 'onset' simulations.

3.2 Reanalysis

Reanalysis, as opposed to analyses from operational forecasting systems, is entirely produced with the same data assimilation system and so is not affected by changes in method. The coverage of the global atmospheric circulation that reanalysis data provide is multivariate, spatially complete, and coherent. Reanalysis must be consistent with observations and also consistent with the laws of physics, and as such it is widely considered to be representative of the available observations and also to provide a best estimate of unobserved parameters.

The reanalysis used here is the ECMWF ERA-Interim dataset (Dee *et al.*, 2011). ERA-Interim comprises global atmospheric reanalysis for the data-rich period from 1979 to present, with four analyses per day, at 00, 06, 12 and 18 UTC and two 10-day forecasts per day, initialized from analyses at 00 and 12 UTC. The data assimilation system used to produce ERA-Interim is based on a 2006 version of the Integrated Forecast System (Cy31r2). The system includes a 4-dimensional variational analysis (4D-Var) with a 12-hour analysis window. The atmospheric model uses a T255 spherical-harmonic representation for the basic dynamical fields, and is coupled to an ocean-wave model. Surface and other grid-point fields are on a reduced gaussian grid which is approximately uniform at 79 km on 60 vertical levels from the surface up to 0.1 hPa.

3.3 Satellite rainfall retrievals

Three main satellite rainfall retrieval products are used for comparison with the model simulations, and to provide some estimate of bias among them The Tropical Rainfall Measuring Mission (TRMM) 3B42 (version 7) rainfall product (Huffman *et al.*, 2007) combines precipitation estimates from multiple satellites, and is bias-corrected with rain-gauge data. It has a 0.25° by 0.25° spatial grid, and is 3 hourly. It combines precipitation estimates from existing low orbiter microwave rainfall retrieval algorithms with spatial propagation information from infrared satellite data,

CMORPH (CPC MORPHING technique), is a satellite rainfall retrieval product which uses existing rainfall retrieval algorithms for passive microwave sensors on low orbit satellites to obtain precipitation estimates, and geostationary infrared satellite data to propagate the precipitation features between microwave estimates, which are then adjusted with daily rain-gauge analysis (Joyce *et al.*, 2004; Xie *et al.*, 2013). The data are made available on an 8 km horizontal grid and at 30-minute intervals. However, the 8 km grid is obtained from interpolation from the grid-spacing of the microwave rainfall retrieval algorithms, which is more on the order of 12 x 15 km. The rainfall estimates between microwave scans come from time-weighted interpolation of microwave-derived features that have been propagated from the previous and post microwave scans. Over land, the passive microwave algorithms are not sensitive to liquid water and precipitation where they rely on ice crystal scattering extinction at the higher frequencies to derive surface rainrates ((McCollum and Ferraro, 2003; Huffman *et al.*, 2007)).

The Global Satellite Mapping of Precipitation (GSMaP) product (Mega *et al.*, 2014), has a grid-spacing of 0.1 degree and 1 hour, and uses an algorithm to combine microwave radiometer and infrared data from multiple satellites, which is then adjusted with daily rain-gauge analysis. One notable difference between these products is the use of global analysis (Japan Meteorological Agency) data, which includes precipitation profiles, in the GSMAP algorithm, while TRMM and CMORPH do not use general circulation model data in their algorithms.

Assessing the performance of TRMM 3B42 and GSMAP satellite rainfall products over India, Prakash *et al.* (2015b) find that while they are capable of representing large-scale spatial features and capture interannual variability, there are region-specific biases, and significant biases in rainfall amount over India ($\pm$20%). Xin-Xin *et al.* (2015) find good agreement in the diurnal cycle of rainfall in TRMM and CMORPH products over most of the study domain except, notably, the Tibetan Plateau. In a comparison of a number of satellite rainfall retrievals products, including CMORPH and TMPA 3B42, with a quality-controlled gridded rain-gauge dataset over India developed by the India Meteorological Department, Prakash *et al.* (2014) find that all the satellite rainfall products give a significantly lower estimate of the all-India seasonal (June to September) rainfall, but that all have a high probability of detection and low false-alarm ratio. Comparing biases in TRMM 3B42 versions 6 and 7, Prakash *et al.* (2015a) find an overall improvement of 5-10% in V7 over high rainfall

regions on the west coast of India and in the northeast and central regions of the country, but there are still large biases in central India regions where monsoon low pressure systems are common.

3.4 Radiosonde data

The radiosonde data are from the Integrated Global Radiosonde Archive (IGRA, Durre *et al.* (2006)). IGRA provides quality controlled soundings from 1500 globally distributed stations. The quality control procedures check for proper station identification, eliminate duplicate levels within soundings, and select one sounding for every station, date, and time. Algorithms check for format problems, physically implausible values, internal inconsistencies among variables, runs of values across soundings and levels, climatological outliers, and temporal and vertical inconsistencies in temperature. Measurements identified as erroneous are set to missing, avoiding potential complications associated with interpreting flag data. Observations include pressure, temperature, geopotential height, dewpoint depression, wind direction, and wind speed at standard, surface, tropopause, and significant levels.

IGRA was used here because of the project's particular attention to record integrity. While IGRA incorporates fewer stations and has less spatial coverage prior to 1970 than other global-scale datasets, it tends to exhibit a higher level of completeness and integrity. Furthermore, its procedures avoid certain inconsistencies and deficiencies found in other datasets by focusing on being able to identify reliable data records, to detect the most significant and most common types of errors, and to preserve local phenomena.

Chapter 4

A radiosonde climatology of the Indian monsoon onset

4.1 Introduction

The onset of the Indian monsoon is a greatly anticipated event, and year-to-year variations in its timings and intensity have profound consequences, through their impacts to agriculture and water resource replenishment, for the people of the Indian subcontinent. There is, however, no universally accepted physical explanation for the first rapid onset, which typically happens in May, and also for the subsequent progression of the onset of the rains towards the northwest of India and Pakistan, which typically takes 6 weeks and happens against the mean low-level flow and advection of moisture (§ 2.1.2).

This chapter explores a new conceptual model of the progressive onset of the monsoon rains, originally published in Parker *et al.* (2016), which emphasises the role of mid-level dry air. The author conducted the original radiosonde data analysis published in Parker *et al.* (2016): This analysis is here extended to inspect the dynamical fields and their interannual variability in much more detail. In particular, the chapter has two objectives;

- In the climatological mean onset, the work examines in further detail the dynamical changes that accompany the thermodynamic changes examined in Parker *et al.* (2016). The dynamical changes include the weakening of the dry mid-level northwesterly winds, the developing low-level southwesterly flow and associated change from upper-level

westerly to easterly flow, and the development of the monsoon trough circulation. An outstanding question is whether the mid-level northwesterly flow weakens as a result of processes internal to the Indian monsoon, like the onset of deep convection, or as a result of larger-scale external changes.

- In the interannual variability of the onset, the work examines whether there is more pre-onset mid-level drying by the northwesterly winds in years with a later onset, consistent with the hypothesis of Parker *et al.* (2016).

The next section briefly reviews the hypothesis of Parker *et al.* (2016) and is followed by more background for the two further objectives.

4.1.1 The role of mid-level dry air in the climatological mean onset, and some open questions

Parker *et al.* (2016) emphasises the role of mid-level dry air in controlling the progression of the onset of deep convection towards the northwest. The hypothesis presented in Parker *et al.* (2016) is as follows. Prior to, and during the onset, a layer of dry air over-runs the monsoon flow and inhibits rainfall. The midlevel dry intrusion is deeper towards the northwest and shallower towards the southeast because, as the dry air is advected towards the southeast from the northwest, shallow cumulus and congestus clouds moisten the dry layer from below. The onset of deep convection happens first in the south because the dry layer is shallowest there. Increasing moisture advection by the strengthening monsoon circulation allows the progressive erosion of the dry layer towards the northwest by shallow-cumulus moistening, and the northwesterly flow weakens to the south of the northern limit of the rains due to momentum mixing by deep convection and the intensification of the monsoon trough.

In Parker *et al.* (2016), the analysis of the changing dynamics that accompany the monsoon onset is focused on establishing that the onset proceeds from the south to the north primarily as a result of the influence of mid-level dry air on moist convection, and not as a result of the progression of a frontal air-mass boundary, as proposed in Sawyer (1947). It is argued, in Parker *et al.* (2016), that the temporal mean winds and back-trajectories show that mid-level northwesterlies are always moving relatively rapidly through the transition zone around the northern limit of the rains, compared to the speed that the northern limit moves

towards the northwest. If the northern limit of the rains was instead associated with the progression of an air-mass front, then the winds would be expected to indicate a boundary, with winds flowing along the front, and not perpendicular to it.

Parker *et al.* (2016) noted that from the thermodynamic observations alone it is not easy to establish the extent to which the erosion of the dry intrusion during the onset period is caused by strengthening soil moisture and moist convection internal to the monsoon, or by weakening dry advection in the mid-level dry intrusion driven by circulation changes external to the monsoon. Therefore, as an extension to the work in Parker *et al.* (2016), the work here further examines how the kinematics and dynamics of the onset could interact with the thermodynamic changes that allow the onset to progress to the northwest. In Parker *et al.* (2016), the winds were examined around 3 dates in the climatological mean onset (31 May, 15 June and 15 July), so there is scope for further insight based on an analysis of the wind fields at higher temporal resolutions, which is presented here.

A question outlined for further analysis in Parker *et al.* (2016), is how the mid-level northwesterlies weaken; How much the weakening is a result of forcing by cloud thermodynamics or larger-scale circulation changes. If cloud thermodynamics play an important role in the weakening of the northwesterlies, then the development of the monsoon trough circulation and the associated moist convection might be expected to exert significant control on the weakening of the northwesterlies. In terms of large-scale interactions, the weakening of the mid-level northwesterlies as the onset progresses is known, at least in part, to be related to the development of the Tibetan anticyclone and the transition from upper-level westerly to easterly thermal winds over the monsoon region. Here, in addressing Objective I, the work here will analyse these circulation changes in greater detail.

4.1.2 Interannual variability

Parker *et al.* (2016) argued that if mid-level dry air slows the onset of the summer rains, it might be intuitive to expect drier mid-levels in years with a more inhibited onset. The results showed how years with an earlier onset at one location in central India (Nagpur), the mid-level air over India before the onset is more likely to have passed over oceanic regions and from lower altitudes, while in later onset years, the air is more likely to have descended from the dry desert regions in the northwest. This suggests that the moisture content of the

mid-level air over India should be lower in years with a later onset because of the path it has taken. However, this analysis in Parker *et al.* (2016) was relatively superficial. Here, in addressing Objective II, the aim is to examine, using different measures of onset, whether the interannual variability of mid-level dry air in the pre-onset period is related to the timing of onset, as proposed in Parker *et al.* (2016).

4.2 Methods

As in Parker *et al.* (2016), observations are prioritised in the analysis. This is because the hypotheses and aims addressed here concern fine balances between convection and its drivers, and these processes are poorly handled in models.

4.2.1 Radiosonde data

The radiosonde data used here comes from the Integrated Global Radiosonde Archive (IGRA, Durre *et al.* (2006)), which is described in § 3.4. Mean profiles at Visakhapatnam, Nagpur, Aurangabad, Jodhpur, Lucknow, and Kandahar (Figure) are computed for the years 1971-2014 at all stations except Aurangabad, where it is for 1979-2014 and Kanadahar, where regular soundings only become available from 2007 onwards. The measured variables of pressure, temperature, dewpoint temperature, wind direction, wind speed and geopotential height are interpolated onto 200 vertical levels (between 1080 and 50 hPa) using simple linear interpolation, before any calculation of other parameters and averaging. Launches at all times are included in the averaging.

Northwest to southeast sections (using station data from all the stations except Lucknow, and so approximately along the dashed line in Figure) are shown for key dates around the time of the monsoon onset (31 May, 15 June, 15 July), which are 5-day averages. The orientation of the section was selected to be approximately perpendicular to the climatological monsoon onset isochrones. For the Indian stations, the numbers of soundings used at each station in the pentads is a minimum of 225 and a maximum of 406, and at Kandahar, the 1 June pentad is the minimum with 72 soundings.

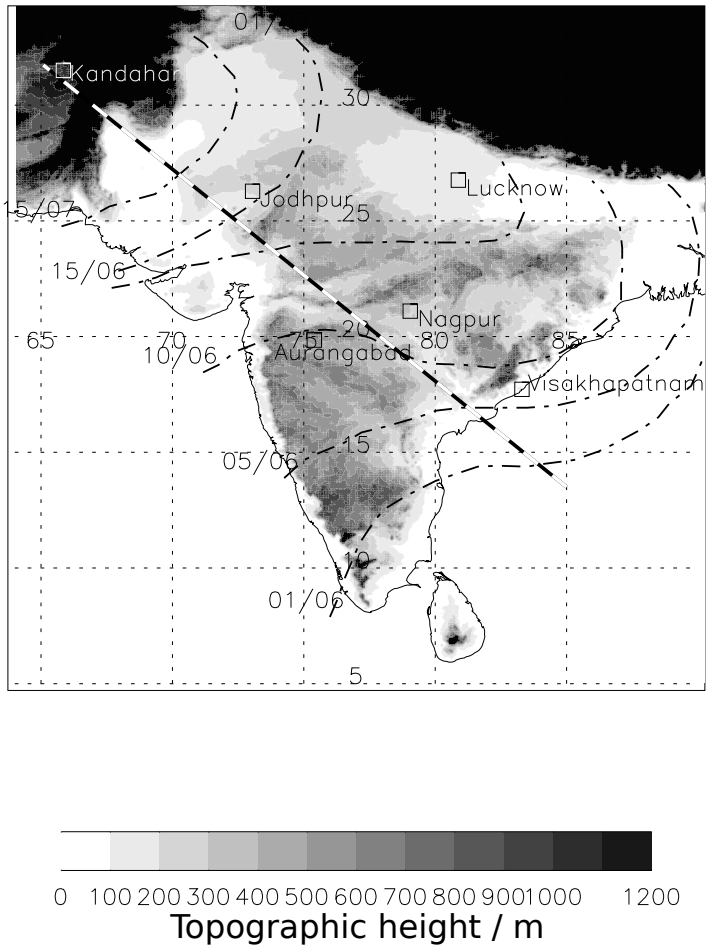

FIGURE : Map of the study region, with topographic height contoured in metres. Locations of radiosonde stations used in the analysis are labelled, and the line (dashed) show the axis for the creation of vertical cross-sections from the radiosonde data. Climatological monsoon progression isochrones (day/month) are also shown. Reproduced from Parker *et al.* (2016).

Mean time-pressure vertical sections at Nagpur and Lucknow are composited relative to the yearly onset date declared by the Indian Meteorological Department (IMD) at those locations. The dates available are from 1991-2015 at Nagpur, and 1996-2015 at Lucknow.

As a measure of the evolution of the buoyancy at Nagpur and Lucknow, throughout the profile the virtual potential temperature of a lifted parcel ($\theta_{v(par)}$) is compared to that of the environment ($\theta_{v(env)}$). The parcel properties are calculated from the composite daily mean, relative to the yearly IMD onset dates, of the thermodynamic properties of the 50-500 m layer above the surface, from which the parcel ascent profile is calculated using dry-adiabatic (below the LCL) and pseudo-adiabatic (above the LCL) lapse rates. The lifted parcel and environment profiles of virtual potential temperature are calculated using

the formula:

$$\Theta_v = \Theta \frac{\mathrm{w} + \epsilon}{\epsilon\,(1 + \mathrm{w})} \tag{4.1}$$

where w is the water vapour mixing ratio and ϵ is the ratio of dry air constant and vapour constant and as given in Markowski and Richardson (2011, p. 13).

4.2.2 Measures of onset

Different measures of onset are used here and in Parker *et al.* (2016), in order to composite radiosonde data relative to onset at Nagpur and Lucknow, and to examine the interannual variability of the onset.

The onset can, over different parts of India in any year, be early or late, fast or slow, and exhibit multiple transitions. The spatial and temporal complexity of the onset complicates efforts to determine a measure of the onset interannual variability that is suitable for a particular purpose. All the measures of onset interannual variability used here and in Parker *et al.* (2016) give a measure of the onset for regions of central and northern India. From the IMD defined climatological onset isochrones (Figure), the onset moves through this region between 10 and 15 June, after the onset has moved north along the west coast of the Indian peninsula and in the Bay of Bengal, and when the onset progresses inland and towards the northwest from the northern Bay of Bengal.

To define early and late years Parker *et al.* (2016) use yearly IMD onset dates at Nagpur, in central India. The IMD pick their onset dates based on an analysis of regional rainfall amounts and the state of the large-scale circulation. As such, the IMD method is partly subjective and, further to that, the circumstances in each year that led the IMD to declare the onset date at Nagpur are not known.

With regard to the interannual variability of the onset, during the preparation of Parker *et al.* (2016), a number of methods of categorising the yearly onset characteristics were considered, including how early or late the IMD onsets dates were at Kerala, Nagpur and Lucknow, and the amount of time between them for fast and slow onsets, as well as an examination of the yearly spatial pattern of the IMD onset isochrones. It was decided, for the publication, based on northwest to southeast radiosonde composite sections of different years, that these methods of categorising the onset variability did not give a clear indication of a sufficient

method of defining the interannual variability, in the context of further understanding the role of the dry intrusions in the timing of the onset.

The work here uses two methods to characterise the onset interannual variability, which are objective and are based solely on rainfall estimates over large areas determined to exhibit homogeneous onsets of rainfall. The IMD do not only use rainfall estimates to determine onset because in certain regions, most notably in Kerala where onset is first declared, such methods can fail due to, for example, the spatial and temporal complexity of local rainfall patterns and the occurrence of bogus onsets (e.g. Flatau *et al.*, 2001). The methods used here use rainfall estimates from regions in central and northern India (which Nagpur lies within) objectively identified as having spatially and temporally homogeneous rainfall patterns over a large enough area (Parthasarathy, 1995; Fitzpatrick *et al.*, 2016) that issues like these do not unduly influence the characterisation of onset from rainfall estimates alone.

Fitzpatrick *et al.* (2016) identifies, using the TRMM 3B42 rainfall retrievals (1 April to 31 July 1998-2104), regions in the Indian monsoon where the interannual variability of the local rainfall onset exhibits a certain degree of homogeneity (see § 2.1.2.2 for some background information). An interannual Localised Onset Region (LOR) is a region where at least ncrit% of grid cells share similar interannual variability in the rainfall onset above a certain confidence level (x). The local onset date at every grid cell is defined based on an agronomic definition of onset (Marteau *et al.*, 2009). The local onset date is taken as the first of two consecutive rainy days with at least 1 mm of precipitation, where the total precipitation is greater than 20 mm, and which is not followed by a 7-day dry period (less than 5 mm rainfall) in the next 20-days. The LORS used here come from taking ncrit% as 80% and x as the 95% confidence interval.

The LOR method used in Fitzpatrick *et al.* (2016) is restricted to either square or rectangular LORs, but this method can be extended to allow for nonregular-shaped LORs. The reasoning behind this is to keep the alogrithm relatively simple so that it is repeatable and practical for dependent stakeholders. For each grid cell, the algorithm assesses the largest possible spatial scale (with a minimum accepted size of a 3-by-3 grid box) where at least ncrit% of all grid cells show, at the x confidence level, correlation between their onset date time series and the median onset date time series of the LOR.

In the Indian monsoon, the 3 regions with LORs are over the Arabian Sea and Western Ghats, over the Bay of Bengal and further east, and over north central India (Figure). In order to consider the interannual variability in the monsoon onset from the northwest Bay of Bengal towards the northwest, a subset of the LORs is taken from over northern central India, from within the bounding box in Figure . Over north central India, there are 2 distinct areas with different size and variance of the largest LORs, with a region of larger size/smaller variance to the northeast, and a region of smaller size/larger variance to the southwest (the outlined region of relatively smaller size/larger variance in Figure). Inspection of the onset dates for the LORs covering this outlined region indicates that the large variance in this region comes mostly from years where any rainfall onset is too weak to pass the threshold test.

The average onset dates of LORs larger than 160,000 km ^{2}, within the bounding box in Figure give the interannual variability of the onset date. Years of early and late onset are taken as years outside the lower and upper 25th percentiles of these onset dates respectively.

The second way of defining the onset interannual variability uses mean June rainfall in a large region covering northwestern and central parts of India (Figure). The region has been

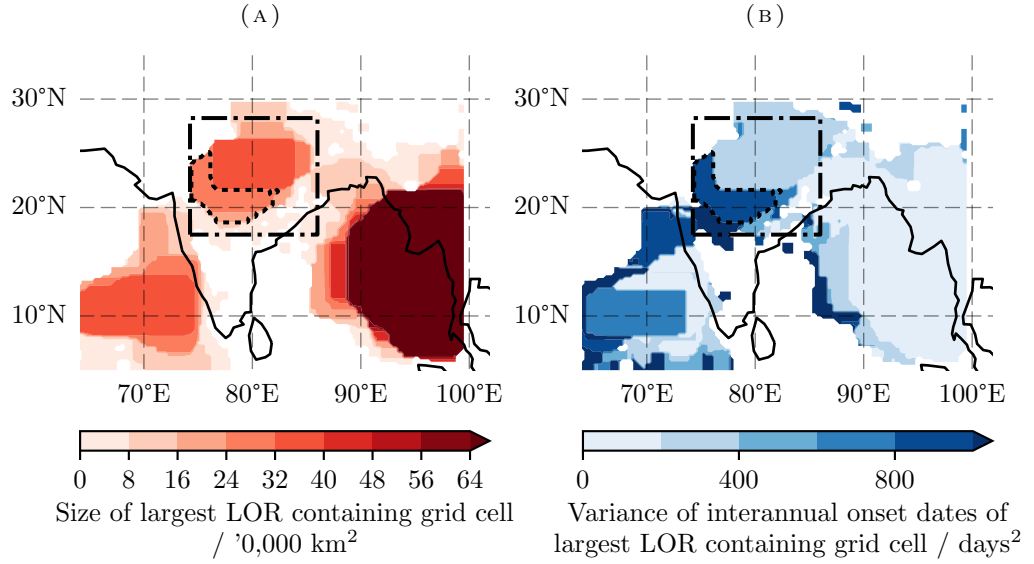

FIGURE : Size and variance, at each grid-point, of the largest bounding Localised Onset Region (LOR), where the LORs are where 80% (ncrit%) of grid-points exhibit homogeneity in rainfall onset date above the 95% confidence interval. The dot-dashed box shows the region where the LOR onset dates are averaged from, to obtain yearly onset dates, from which early and late onset years (Table a) The dotted line indicates a region described in the text. The LORs are calculated using TRMM 3B42 rainfall retrievals for the years 1998-2014.

chosen based on the coherence of its rainfall variability and the association of the rainfall variability with regional/global circulation parameters (Parthasarathy *et al.*, 1993). The June rainfall estimates for this 'Homogeneous Indian Monsoon' (HIM) region come from a monthly rainfall time series, provided by the Indian Institute of Tropical Meteorology, that is based on rain gauges measurements. Years outside the upper and lower 25th percentiles of June rainfall define years with high or low June rainfall.

Table a shows the years of early and late onset selected using the LORs and years with high or low June rainfall selected using the HIM June rainfall estimates. The LORs are calculated using TRMM satellite rainfall retrievals from 1998 to 2014, and the years 1979 to 2014 (because of ERA-Interim data availability) from the HIM series are used in determining years to composite. Comparing the early LOR onset years with high June rainfall years and

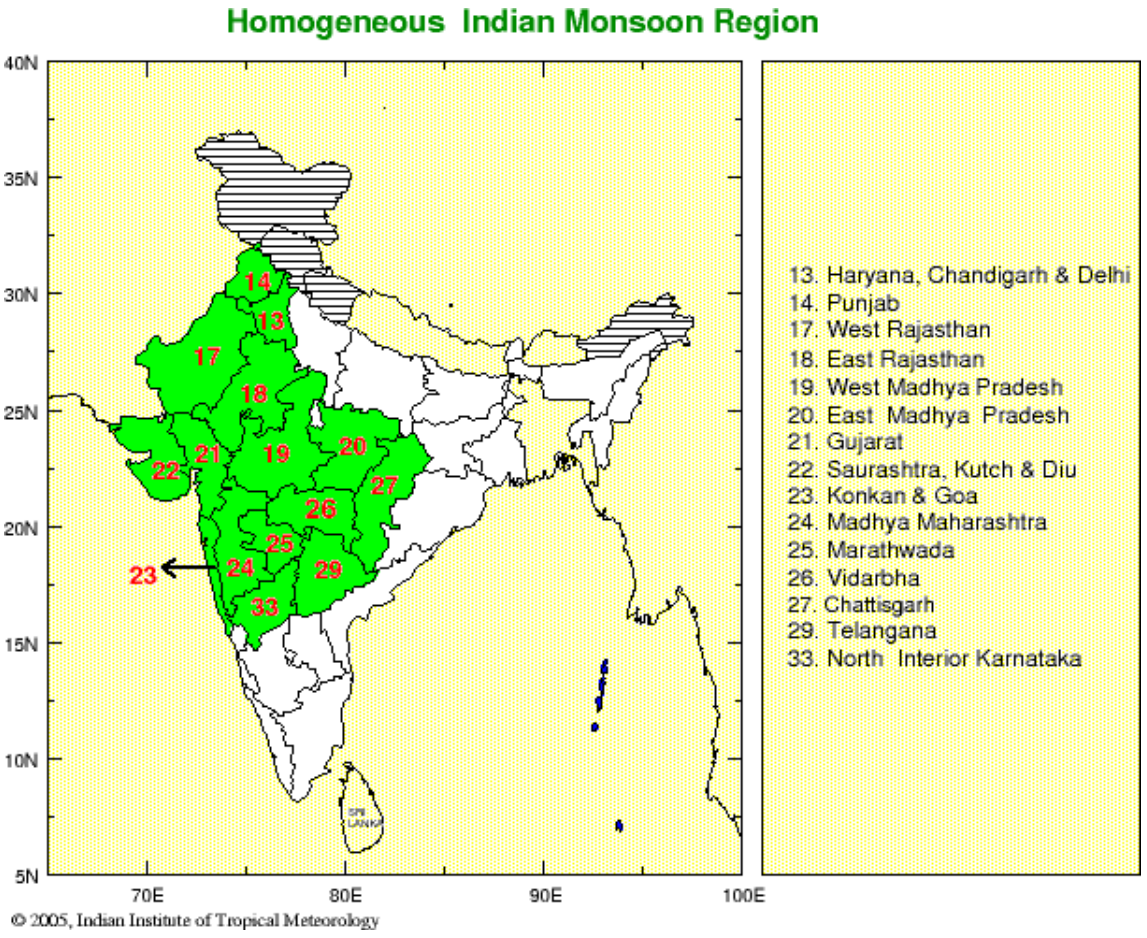

FIGURE : The 'homogeneous Indian monsoon rainfall region' as defined by the Indian Institute of Tropical Meteorology (shortened to IITMHomInd here), is shown in green. The region exhibits coherence in its rainfall variability, which is associated with regional/global circulation parameters (Parthasarathy *et al.*, 1993). Reproduced from Indian Institute of Tropical Meteorology.

the late LOR onset years with low June rainfall years, in both 3 out of 4 of the LOR onset years are also included in the corresponding June rainfall years, which shows a correlation between the date of onset and the amount of rainfall in the region.

Early minus late onset northwest to southeast sections are shown using both radiosonde data and ERA-Interim reanalysis because of the degree of variability in the number of radiosonde soundings going in to each pentad-mean (Table b), where the potential effect of quality issues with the data from individual radiosonde soundings increases as the number of soundings decreases. The ERA-Interim datasets provides higher frequency, more consistent sampling than the radiosonde data, but with the caveat that it is an analysis not direct observations. The numbers of soundings in Table b show, for the Indian stations (i.e excluding Kandahar), a higher number of soundings in general in early LOR onset compared to late LOR onset years, and also in high June HIM rainfall years compared to low years, which may reflect a greater need on the part of the IMD, for more soundings in years where the onset is more vigorous. Radiosonde soundings from Indian stations are not assimilated into ERA-Interim, and while it is not clear how this will affect biases in ERA-Interim, it does mean that the 2 datasets are independent of each other. Comparing the similarities or differences between them therefore adds robustness to analysis of whether features identified are climatologically important in the interseasonal variability of onset.

Method	Early or high rainfall years	Late or low rainfall years
LORs	**2001**, 2003, **2011**, **2013**	1999, **2009**, **2012**, **2014**
June rainfall in homogeneous Indian monsoon rainfall region	1980, 1986, 1990, 1994, 2001, 2002, 2008, 2011, 2013	1982, 1984, 1987, 1992, 1995, 2009, 2010, 2012, 2014

TABLE A: Years outside the upper and lower quartiles of mean LOR onset date for LORs within the bounding box in Figure (late/early onset years respectively) and of June rainfall in the homogeneous Indian monsoon region in Figure (high/low rainfall years respectively). Bold years are in both high rainfall and early onset years, or in both low rainfall and late onset years. LOR years are selected from the years 1998-2014, and June rainfall years are selected from 1979-2014.

Station	Early LOR	Late LOR	High June	Low June
Kandahar	10/19/20	21/14/13	13/24/25	29/33/18
Jodhpur	29/29/22	16/19/12	56/53/46	37/40/44
Aurangabad	19/14/20	14/9/8	38/32/31	25/25/21
Nagpur	35/31/37	17/12/19	61/60/59	37/34/50
Visakhapatnam	30/40/39	18/16/14	50/64/60	43/33/28

TABLE B: Number of radiosonde soundings in pre/mid/post onset pentad periods (beginning 31 May/15 June/15 July) at stations in northwest to southeast sections (Figure) for early/late LOR onset years and high/low June rainfall years. Soundings come from the onset years given in Table a.

4.3 Results

4.3.1 Thermodynamic perspective on the onset

Originally presented in Parker *et al.* (2016), Figure b shows northwest to southeast sections of some thermodynamic properties, derived from radiosonde soundings, for dates around the onset.

There is a general increase in the low-level Water Vapour Mixing Ratio (WVMR) towards the northwest as the onset progresses (Figure b(a),(b),(c)). The wedge of low-level high water vapour-mixing ratio (WVMR) that extends inland from the southeast around 31 May (Figure b(a)) deepens by 15 June (Figure b(b)). By 15 July (Figure b(c)), the high WVMR monsoon layer has become much less wedge-like, and the column moisture is much more similar at all the stations from Jodhpur to the coast.

The onset of deep convection towards the northwest is closely related to the relative humidity (RH) along the section (Figure b(d),(e),(c)); when the RH is low, cumulus convection is suppressed through the entrainment of dry air. Around 31 May, the contours of RH near the coast show higher RH at the surface confined close to the coast, and a mid-level (700-500 hPa, around the freezing level) extension inland of the moister air from the coast, which is partly from the detrainment of moisture from cumulus clouds, but also possibly from the partial detrainment of remote cumulonimbus storms. By 15 June (Figure b(e)), from Jodhpur to the coast the contours of RH up to the freezing level are close to vertical and near the surface there is a wedge of high RH with a similar gradient to that of the WVMR. After onset, around 15 July (Figure b(f)), there is an RH maximum over central India (>80% at Aurangabad, and Nagpur) between 900 and 650 hPa, and also in the wedge of

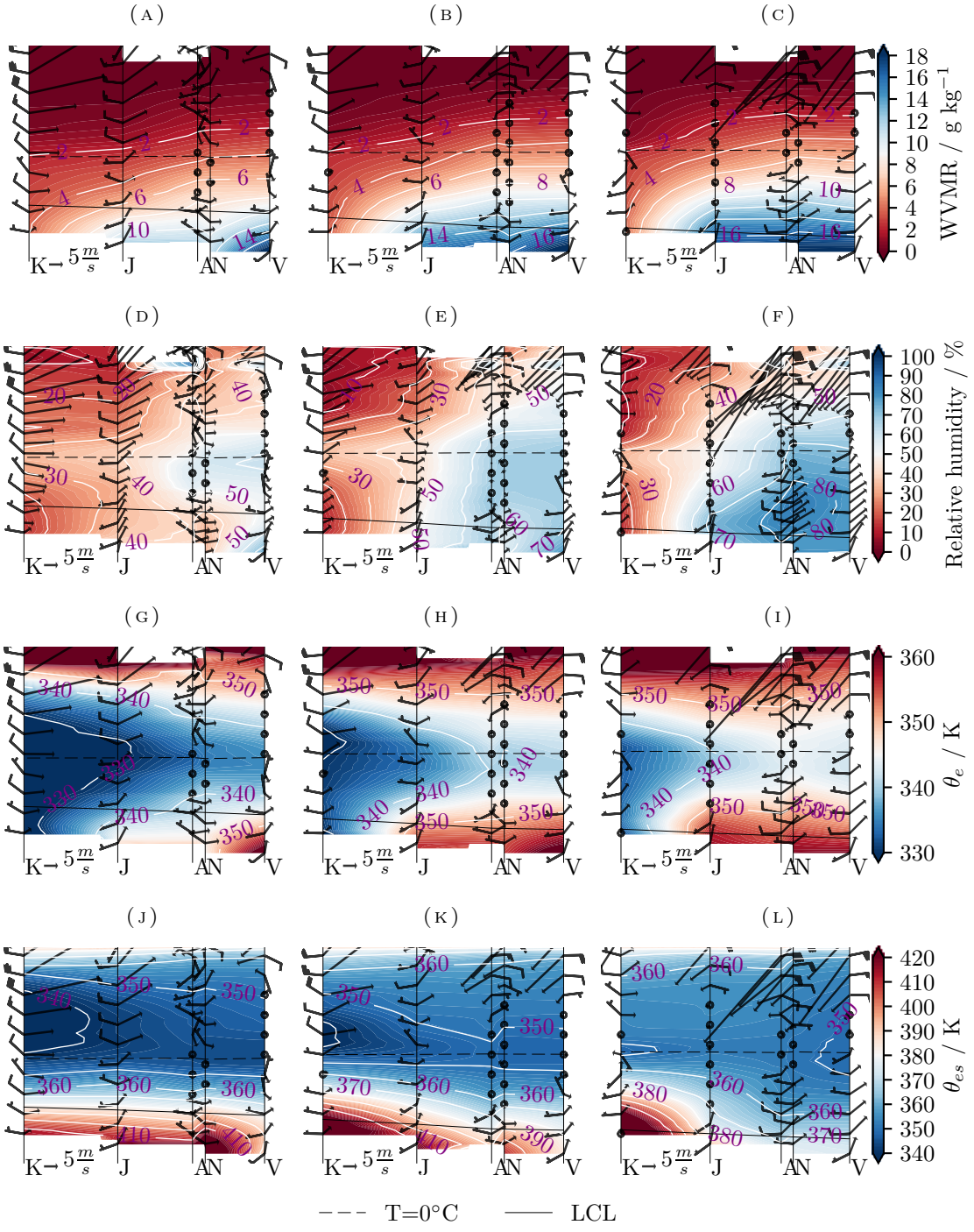

FIGURE B: Northwest to southeast sections of mean atmospheric thermodynamics and winds from radiosonde data in the period 1971-2014, for 5-day periods centred on (a),(d),(g),(j) 1 June, (b),(e),(h),(k) 15 June and (c),(f),(i),(l) 15 July. Vertical lines show the locations of the radiosonde stations, labelled as 'V'=Visakhapatnam, 'N'=Nagpur, 'A'=Aurangabad, 'J'=Jodhpur and 'K'=Kandahar (station locations are marked on Figure). The panels show (a)-(c) water vapour mixing ratio (g kg^{-1}), (d)-(f) relative humidity (%), (g)-(i) θ_e (K), and (j)-(l) θ_{es} (K). On each panel the winds are shown in two forms: wind vanes and feathers indicate the horizontal winds relative to geographical coordinates, while the vectors show the horizontal winds relative to the section orientation shown on Figure , with a horizontal vector representing flow parallel to the section. The solid line marks the LCL and the dotted line marks the T=0°C level.

low-level RH. At Aurangabad and Nagpur, the low-level pattern of low RH prior to onset, and high mid-level RH after onset are closely related to the winds, with the layer of dry pre-onset air linked to the dry northwesterly winds, and the post-onset RH maximum linked to the moist southwesterly monsoon flow.

The mid-level dry air, which is advected from the northwest, forms a wedge of low entropy (θ_e) air, which extends down to the coast prior to onset and retreats as the monsoon onset progresses (Figure b(g),(h),(i)). There is a mid-level minimum in θ_e at around 600-500 hPa, which is slightly above the freezing level prior to onset (Figure b(g)), and below during and after onset (Figure b(h),(i)). The RH is slightly higher around the freezing level, indicating it is the temperature profile that determines the height of the θ_e minimum. There is a layer of high low-level θ_e, which is highest to the southeast and deepens and flattens through the onset, but its slope is different to that of the WVMR. The general pattern is one of increasing θ_e at all stations through the onset.

The saturated equivalent potential temperature (θ_{es}) is a function of temperature and pressure only, and is homeomorphic with temperature at a given pressure level. A θ_{es} decrease with height indicates a lapse rate between the moist and dry adiabatic lapse rates, and so conditional instability. A shallower gradient of θ_{es} decreasing upward indicates a profile closer to pseudoadiabatic. Prior to onset, the highest low-level temperatures (and so highest θ_{es}; Figure b(j)) are over central India (Jodhpur, Aurangabad, and Nagpur), and are nearly constant in the lowest ∼50 hPa. Above this low-level near-pseudoadiabatic layer at these stations, there is a strong negative θ_{es} gradient up to ∼600 hPa (below the freezing level), where there is low dry static stability ($d\theta/dz$) associated with the well-mixed air in the dry intrusion and, above the freezing level up to ∼200 hPa, θ_{es} is again nearly constant and so close to pseudoadiabatic. As the onset progresses, low-level cooling (below ∼800 hPa) begins at the central Indian stations and progresses to the southeast (Figure b(k),(l)), bringing the profile below the freezing level closer to pseudoadiabatic. The cooling will likely be due to a combination of strengthening cool advection from the west, convective downdraughts, increased cloud cover, and increasing soil moisture and vegetation cover which will reduce the surface sensible heat flux (Parker *et al.*, 2016). At the same time as the low-levels cool, the low-level RH and θ_e increases. In the mid-levels, there is large-scale warming along the section through the onset.

The low-level cooling and mid-level warming bring the profile closer to pseudoadiabatic as the onset progresses. In the mid-levels, warming acts to reduce CAPE, while the low-level cooling reduces CIN. The increasing low-level θ_e reduces CIN, and increases CAPE. As such, there is a combined effect of the low-level cooling and moistening that reduces CIN, but the mid-level warming and low-level increase in θ_e give opposite effects in terms of CAPE. In addition, the general RH increase with time reduces the tendency for drier air to inhibit the development of convective clouds.

The role of dry and moist advection is clearly one important factor in the thermodynamic balance (along with surface and convective fluxes). Addressing Objective I, the wind fields are examined in more detail in the next section.

4.3.2 Analysis of the thermodynamic onset at high temporal resolution

The northwest to southeast sections in Figures b give snapshots of the evolving spatial structure of thermodynamic fields as the onset of the monsoon progresses. In Parker *et al.* (2016), the onset is also examined through the evolution of thermodynamic fields at one station (Nagpur), which are composited relative to the yearly IMD onset date (panels from Figure 8 in Parker *et al.* (2016) are reproduced in Figure b(a),(c),(e),(g)). The analysis is extended here, by also considering the evolution of the same thermodynamic fields at Lucknow (Figure b(b),(d),(f),(h)). Lucknow (26.9°N, 81°E) is north-northeast of Nagpur (21.2°N, 79.8°E) so, for example, after the monsoon trough is established, it is climatologically in the returning southeasterly flow, whereas Nagpur is in the westerly part of the flow (Figure b).

The mean IMD onset date at Lucknow is one week later than at Nagpur (23 June compared to 16 June). How this might relate to differences in the evolution of the thermodynamic profile, in particular with regard to the erosion of the mid-level dry layer, is a pertinent question. No further hypothesis are proposed in this respect. However, the differences in the thermodynamics of the onset between Nagpur and Lucknow may give some indication of whether differences in the evolution of the mid-level dry layer, or the low-level thermodynamics characteristics might play a significant role.

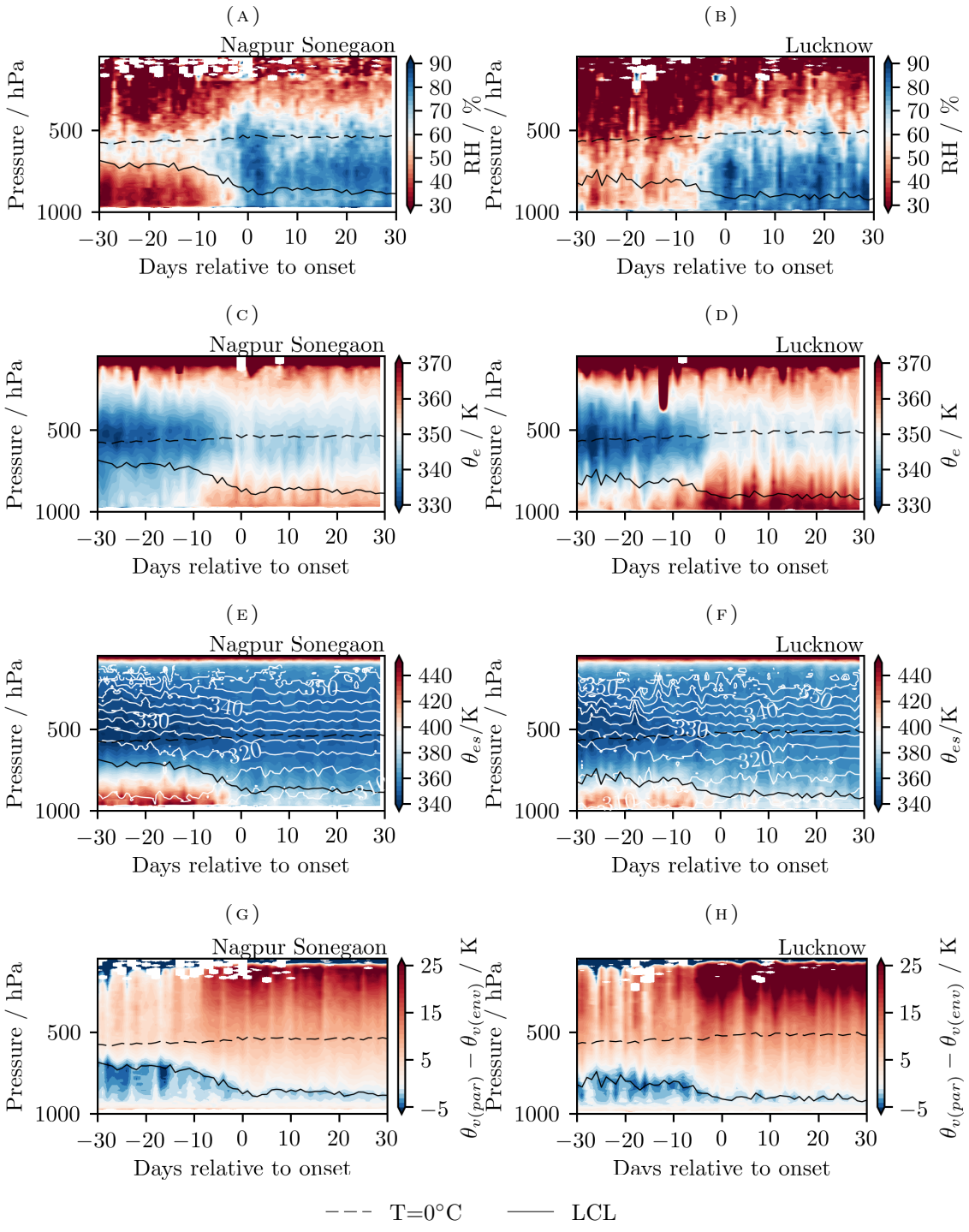

FIGURE B: Time-pressure sections for Nagpur (a),(c),(e),(g) and Lucknow (b),(d),(f),(h) showing (a),(b) relative humidity, (c),(d) θ_e, (e),(f) θ_{es} with virtual potential temperature θ_v over plotted (contours) and (g),(h) buoyancy of lifted boundary-layer parcels ($\theta_{v(par)} - \theta_{v(env)}$). All panels show LCL (solid line) and level of T=0°C (dotted line). The profiles are composite means for days relative to the Indian Meteorological Department onset date (day 0 in the time axis) in each year for the years 1991-2015 at Nagpur, and 1996-2015 at Lucknow. Over these periods, the mean arrival of the northern limit at Nagpur is 16 June, and at Lucknow is 23 June.

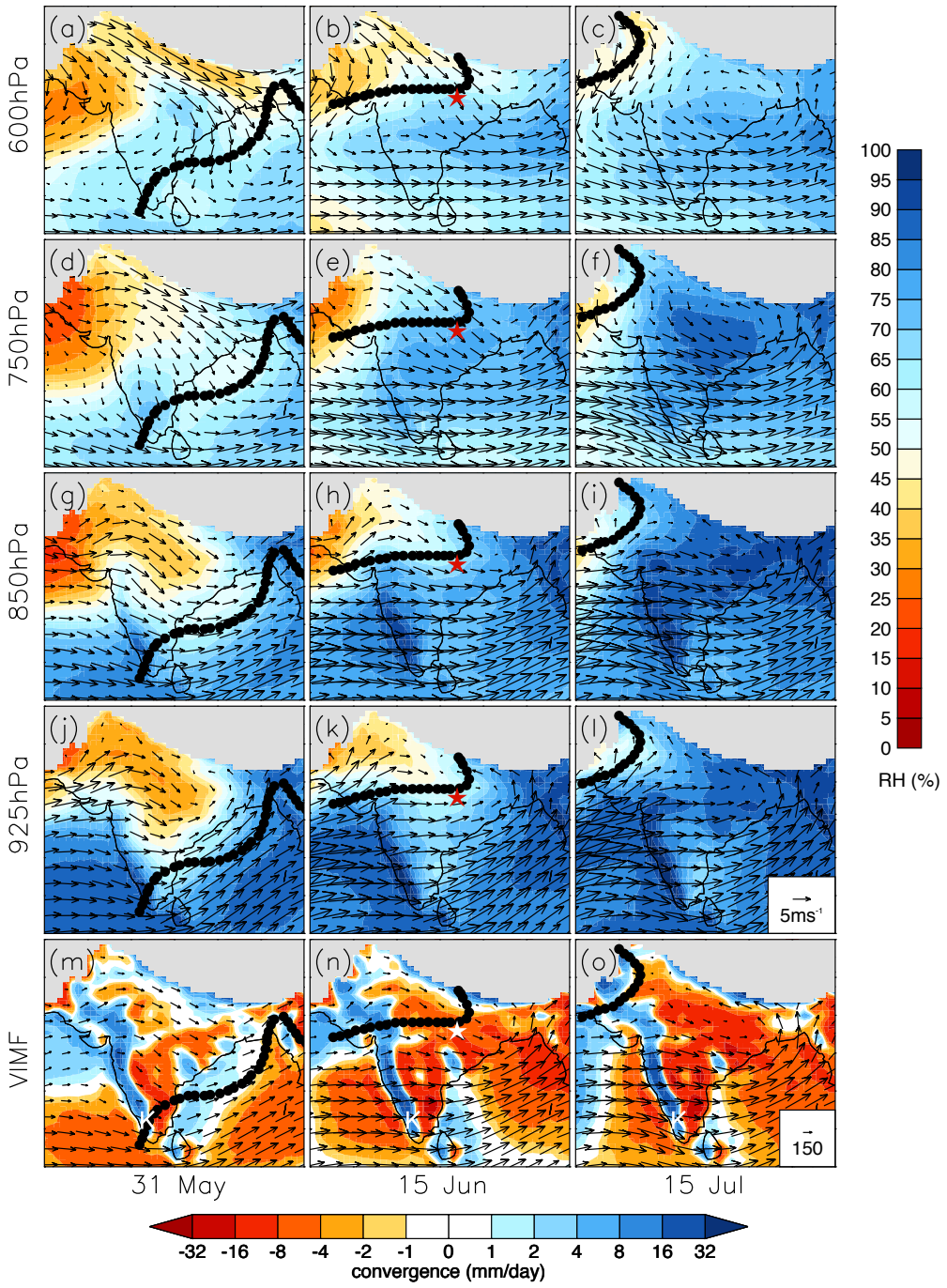

FIGURE B: Mean relative humidity (shading, %) and horizontal winds (vectors, m s^{-1}) from ERA-Interim reanalysis averaged over 5-day periods centred on (a), (d), (g), (j), (m) 31 May (around first onset; left), (b), (e), (h), (k), (n) 15 June (mid-onset; centre) and (c), (f), (i), (l), (o) 15 July (full monsoon; right column), over the years 1979–2014. The fields are shown on levels (a), (b), (c) 600 hPa (top row), (d), (e), (f) 750 hPa, (g), (h), (i) 850 hPa and (j), (k), (l) 925 hPa. The lower row (m), (n), (o) shows vertically-integrated moisture flux (VMF) vectors (kg m^{-1} s^{-1}; integration is performed from the surface to 100 hPa) and moisture flux convergence, scaled to represent mm day^{-1} of equivalent rainfall. The state of Kerala is indicated with a letter 'K'. The star indicates a location referred to in Parker *et al.* (2016). Regions in which the orographic height exceeds 1000 m are shaded in grey. Reproduced from Parker *et al.* (2016).

4.3.2.1 Relative humidity analysis and the cloud fields

The RH at Nagpur prior to onset (Figure b(a)) shows a mid-level cloud maximum close to the freezing level (550 hPa), which is gradually replaced by a deepening layer of higher relative humidity from about 10 days prior to onset. The top of the high RH layer, from about 8 days prior to onset ascends from the freezing level to ∼350 hPa around onset, and there is also moistening down to the surface, implying a growth of deep convective rainfall prior to the onset. At the same time the LCL drops from ∼700 hPa in the pre-onset, to ∼900 hPa around onset. There is a burst of higher RH (80- 90%) from onset or 1 or 2 days before, to about 7 days after onset, with an RH maximum between 800 and 700 hPa, after which it reduces (to 60-70% below the LCL, 70-80% above the LCL up to about 700 hPa, and 60-70% from 700 to 400 hPa).

At Lucknow, the mid and low-level RH (Figure b(b)) profile prior to onset is more constant below the freezing level than at Nagpur, because the RH is higher below the LCL, and lower above. At Lucknow there is also no cloud maximum around the freezing level prior to onset, although there may be some evidence of one at ∼700 hPa. The differences between the RH prior to onset at Nagpur and Lucknow are consistent with the north-south differences in wind and RH shown in Figure b, where at 600 hPa, the northwesterly wind and lowest RH are concentrated to the north, just south of the Himalayas, and at lower levels, the lowest RH is further south, closer to Nagpur.

The RH at Lucknow increases markedly around 8 days prior to onset, like at Nagpur. However, in-line with the higher low-level RH at Lucknow (there is also some evidence of a moister surface), the LCL is lower prior to onset, at ∼800 hPa, and dropping to ∼900 hPa around onset (similar to Nagpur).

4.3.2.2 Evolution of the dry intrusion

At Nagpur, as well as the increase in the RH of the dry layer above the LCL (45-60%), which will tend to suppress early cumulus development, to higher RH from about 5 days prior to onset, there is an increase from the low θ_e (Figure b(c)) values of the mid-level dry intrusion from 20 days prior to onset. On the same timescale, the low-level θ_e also increases, and from about 10 days prior to onset there is a relatively abrupt increase in the depth of

high low-level θ_e, to just above the LCL, at the same time as the RH increases above the freezing level (Figure b(a)), which suggests a significant deepening of convection. Similar to the burst of higher RH around onset, there is a mid-level maximum in θ_e close to onset (700 to 300 hPa).

The pattern of increasing mid-level and low-level θ_e in the 20 to 30 days prior to onset at Nagpur is similar at Lucknow (Figure b(d)). However, pre-onset the mid-level (800 to 300 hPa) values around the θ_e minimum are, as with the RH, lower, and the low-level (below 800 hPa) values are higher (also as with the RH).

4.3.2.3 Evolution of the conditional instability field

At Nagpur and Lucknow θ_{es} (Figure b(e)(f)) reduces below the LCL, from about 5 days prior to onset, and at the same time increases in the mid-levels (600 to 400 hPa). Consequently, close to onset the gradient becomes much closer to constant throughout the profile, which indicates a profile closer to pseudoadiabatic throughout the column that is more conducive to moist convection (as also seen in Figure b tephigrams). Pre-onset θ_{es} below the LCL is lower at Lucknow than at Nagpur, consistent with Nagpur being closer to the pre-onset heat low temperature maximum. This indicates that that the higher subcloud θ_e values at Lucknow are due to higher moisture content.

The contours in Figure b(e),(f) show the virtual potential temperature θ_v at Nagpur and Lucknow. At Nagpur, there is a relatively shallow gradient below 600 hPa prior to onset, where the air is dry and well-mixed, and from about 10 days prior to onset θ_v below $\sim$700 hPa reduces markedly, and there is a more gradual increase in θ_v, above $\sim$700 hPa in the 30 days prior to onset. Both these contribute to increasing $d\theta/dz$, but it is the low-level cooling which dominates. At Lucknow, the profile below $\sim$700 hPa prior to onset is more statically stable, indicating a less deep well-mixed layer.

As the temperature below 700 hPa decreases prior to onset (Figure b(e),(f)), θ_e is increasing and the LCL descends (Figure b(c),(d)), due to moistening in the boundary layer (Figure b(a),(b)). The effect of the combination of these changes with the pre-onset mid-level warming (Figure b(e),(f)(e),(f)) are reflected in the parcel buoyancy (Figure b(g),(h)). As the LCL descends prior to onset, the depth and total magnitude of the CIN layer below it reduces, and from about 8 days prior to onset, there is a clear increase in the buoyancy, in

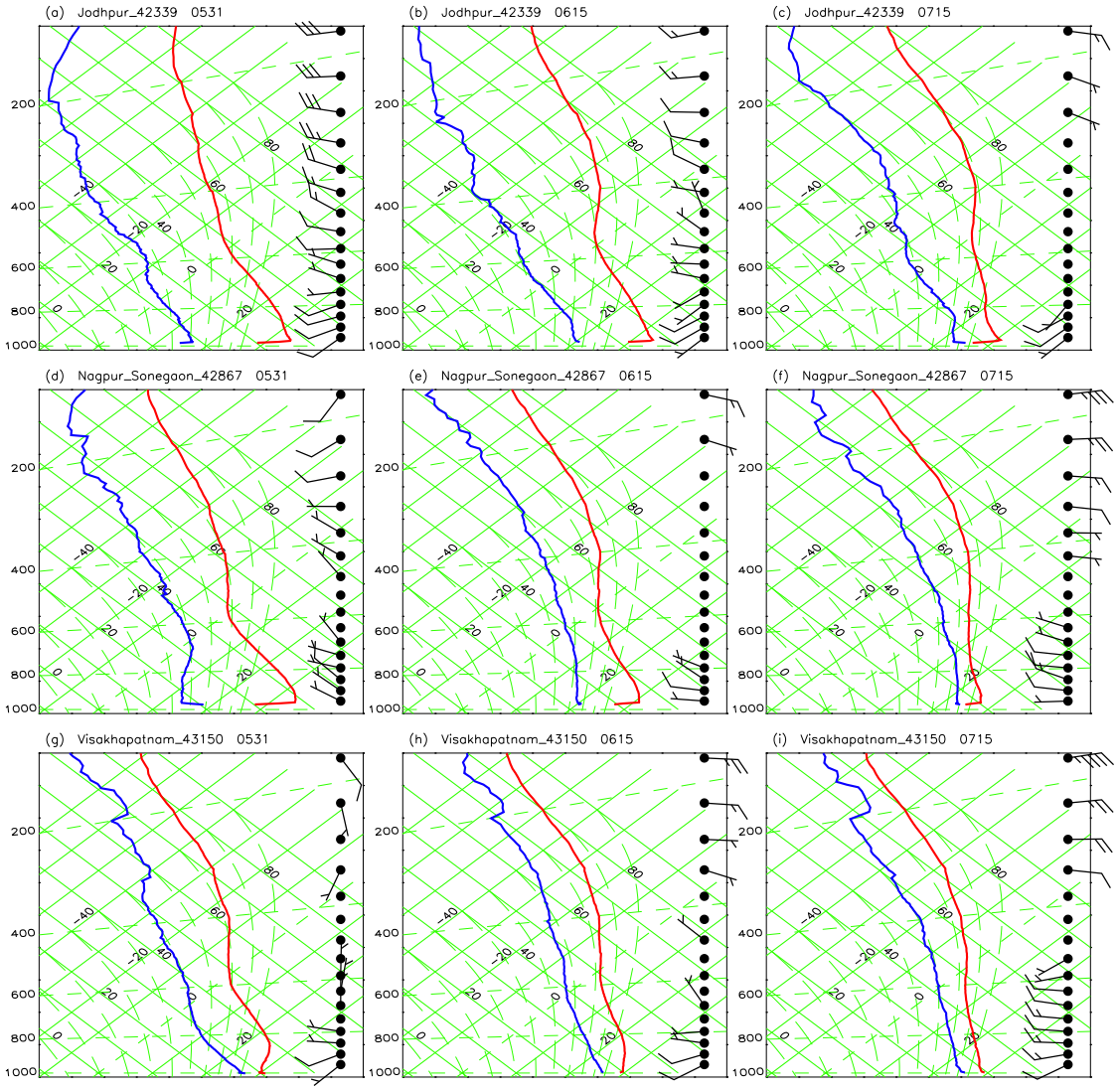

FIGURE B: Climatological mean radiosonde profiles from (top row; (a)-(c) Jodhpur, (d)-(f) Nagpur and (g)-(i) Visakhapatnam, representing a transect from the northwest to southeast of India. Temperature (red) and dew point (blue) profiles are plotted as tephigrams, for 31 May (around first onset in the far south of India); panels (a), (d), (g), 15 June (transition period); (b), (e), (h) and 15 July (around the end of onset); (c,f,i). Station locations are shown in Figure . Reproduced from Parker *et al.* (2016).

the mid and upper-levels (above 700 hPa), in line with an increase in the parcel θ_e, which has a much larger effect than that of the mid-level warming around onset, which will reduce the buoyancy there.

In conclusion, the thermodynamic data from Lucknow broadly support the conclusions of Parker *et al.* (2016) regarding the detailed thermodynamic changes associated with the onset. However, the differing locations of the 2 stations result in some notable differences. These are interpreted in relation to the the large-scale circulation, which affects the low and mid-level moisture content and the temperature below the LCL. Pre-onset at Lucknow, as a result of these differences, the LCL is lower and there are lower mid-level values of θ_e. The next subsection explores the changes in the wind fields at high temporal resolution at the two stations, providing details which were not considered by Parker *et al.* (2016).

4.3.3 Wind fields around onset

4.3.3.1 Spatial and temporal variations in the winds

When relating the changing dynamics during the onset to the thermodynamic changes described in the previous section and in Parker *et al.* (2016), the weakening of the mid-level northwesterlies that advect dry air over India is particularly pertinent. This change happens within and as part of large-scale circulation changes from the winter to summer monsoon circulation, the best known of which is probably the establishment and strengthening of the low-level summer monsoon circulation pattern over India, with westerly-southwesterly winds that cross the subcontinent from the Arabian Sea, and a returning southeasterly flow into northern India, around the monsoon trough. At the same time, upper-level westerlies over the region are gradually replaced by easterlies, as the baroclinic winds adjust to the seasonal reversal of the meridional temperature gradient in the lower and mid troposphere. There is also the reversal of the deep meridional overturning circulation (§ 2.1.1.2), which is much more abrupt. The evolution of the zonal and meridional winds along the same northwest to southeast section as shown for the thermodynamics (Figure b) and also at Nagpur (Figure b) are useful in examining the relationship between these large-scale dynamical changes and the changes that are most directly relevant to the hypothesis of mid-level dry air as a control on the progression of the onset from the north to the south.

The contours of zonal wind along the northwest to southeast section, for the pentads around onset (Figure b(a),(b),(c)), are instructive in relating the changing upper-level baroclinic jet winds to the changing winds beneath, in the mid and low levels of the troposphere. As the onset progresses, the upper-level westerly jet winds are gradually replaced by upper-level easterlies. Through the onset, as seen in these sections, the upper-level westerlies weaken and become less deep towards the northwest and the upper-level easterlies strengthen and deepen from the southeast.

Associated with the upper-level transitioning from westerly to easterly winds over India are similarly timed changes in the winds below. Between the LCL and the freezing level,

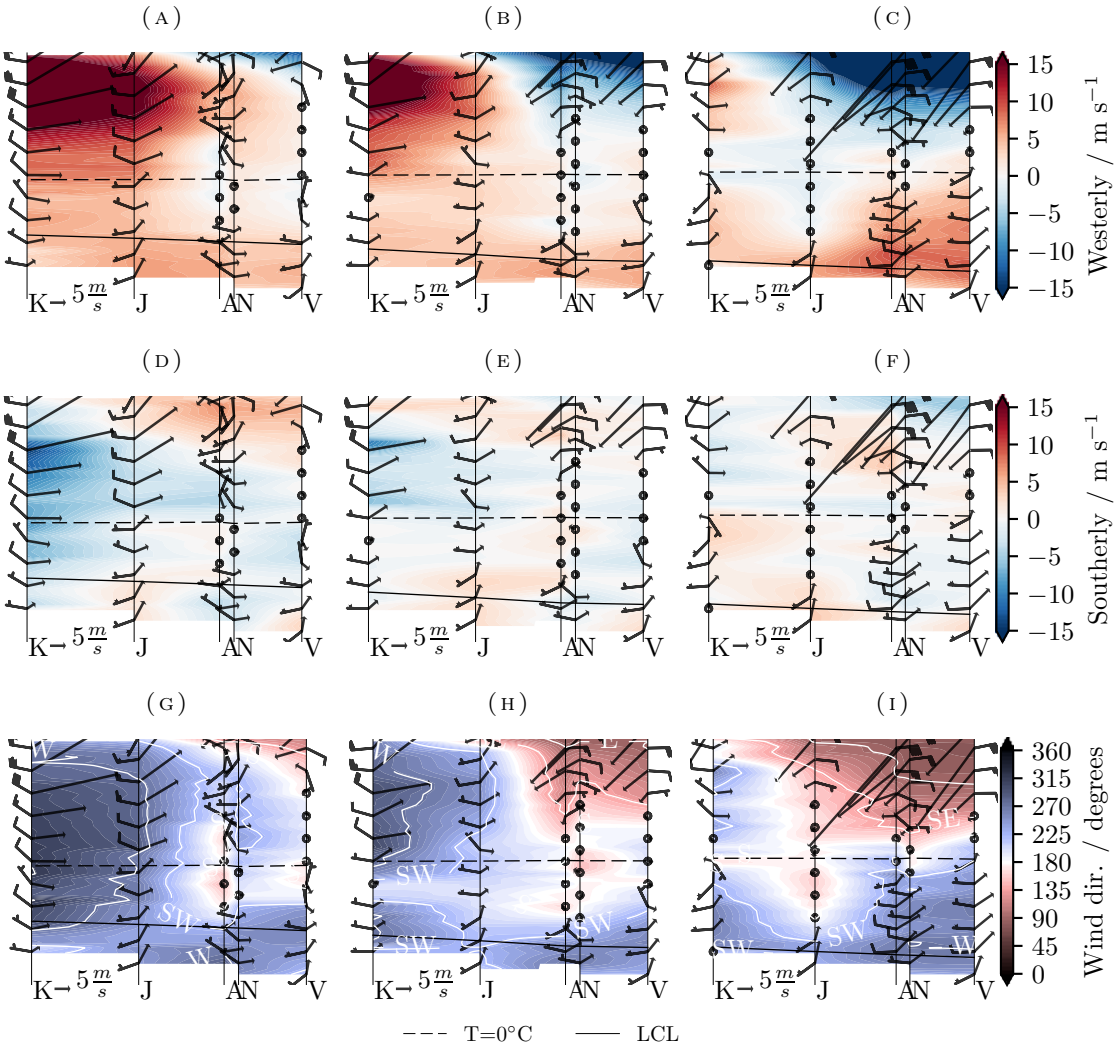

FIGURE B: As Figure b, but for (a),(b),(c) westerly wind speed (m s^{-1}), (d),(e),(f) southerly wind speed (m s^{-1}) and (g),(h),(i) compass direction wind is from (degrees). White contour lines in the wind direction panels indicate compass directions N, NE, E, SE et cetera.

more or less in line with the limit of the easterly winds above the freezing level, is a region of easterly winds which are weakly discernable at Aurangabad and Nagpur on 15 June and have moved to Jodhpur by 15 July. In the 15 July pentad, when these easterly winds below the freezing level have reached Jodhpur, westerly winds have developed to the southeast (with the strongest westerlies below 800 hPa at Aurangabad and Nagpur) which are the established low-level monsoon flow. This matches with the reanalysis winds at 600 hPa, which show, in the 31 May and 15 June pentads (Figure b(a), (b)), a change from winds with a westerly component to winds with an easterly component close to the climatological onset isochrones. As described in Parker *et al.* (2016) further to the south of the northern limit, the 600 hPa winds back again to a westerly direction, associated with the monsoon trough lying just to the south of the northern limit at this level.

In the zonal winds at Kandahar and Jodhpur, the pre-onset westerlies between ∼550 and 400 hPa are much weaker than the >15 m s^{-1} westerlies above and markedly stronger than the westerlies below the freezing level (Figure b(a)). Because this makes the westerly (Figure b(a)) and northerly (Figure b(d)) wind components more similar at these levels than at other levels, the wind direction at these levels is close to northwesterly and the wind direction turns towards westerly above and below.

The sections of wind direction (Figure b(g),(h),(i)) again show the large-scale change above the freezing level from westerlies to easterlies, and again highlight how this relates to the changing winds below. As the boundary between the winds with a westerly component to the northwest, and the wind with an easterly component to the southeast moves to the northwest during the onset, it is accompanied by mid-level (∼800-500 hPa) southeasterlies, which move to the northwest with the boundary above.

The time-pressure sections of zonal and meridional winds at Nagpur (Figure b) are shown on a longer timescale than the thermodynamic time-pressure sections (Figure b) to show some of the slower changes related to the onset. The change in the westerly wind component at Nagpur, composited relative to the yearly local IMD onset dates (Figure b(a)), shows quite clearly the changing upper-level baroclinic winds and, because of the higher temporal resolution it affords compared to the pentad mean sections, provides some additional information on the relative timings of the zonal wind changes.

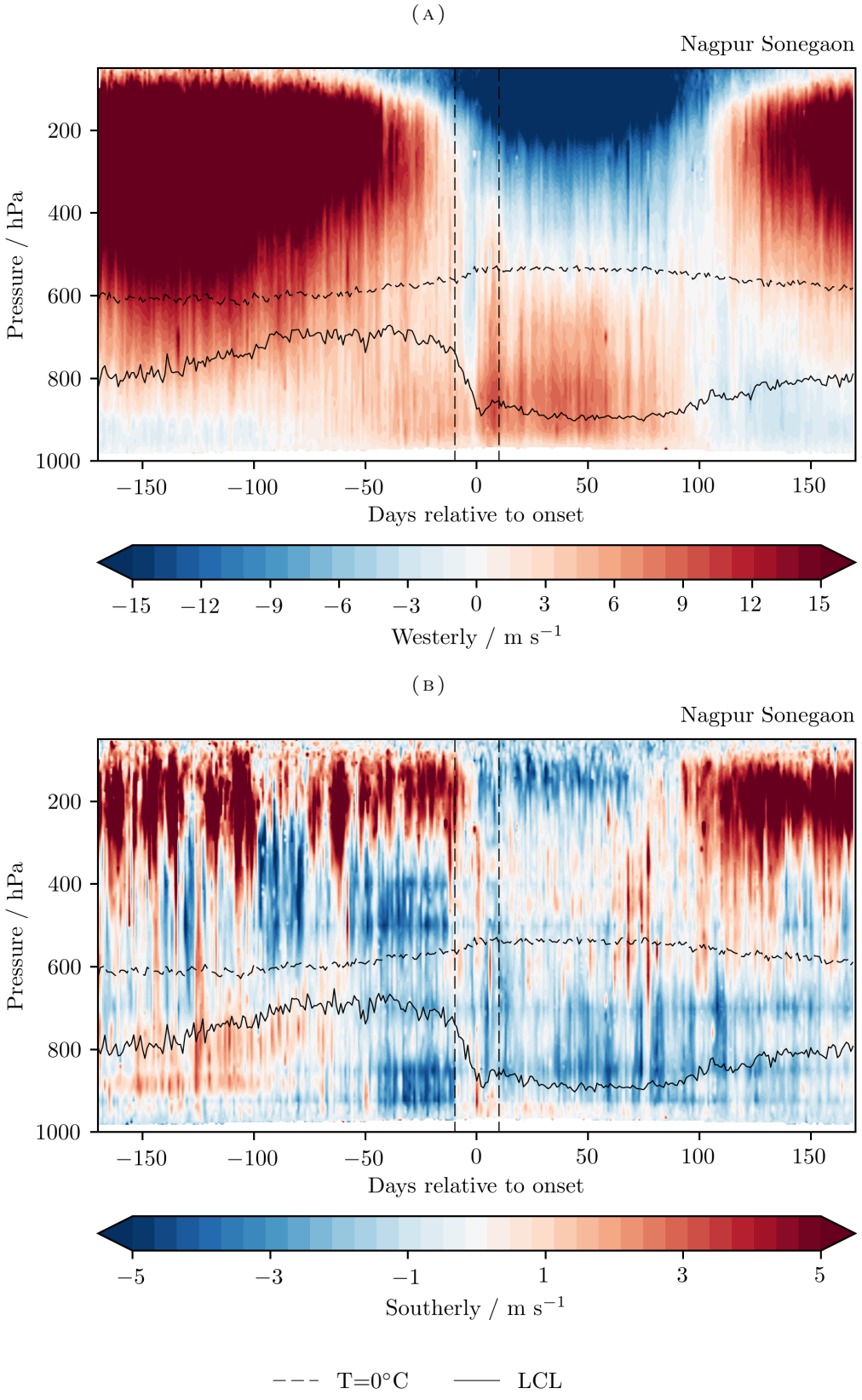

FIGURE B: As Nagpur time-pressure sections, relative to onset, of thermodynamics in Figure b (although on a longer timescale), for (a) westerly wind speed (m s^{-1}) and (b) southerly wind speed (m s^{-1}) at Nagpur.

Firstly, the longer time series of the wind time-pressure sections shows that the transition from upper-level westerly to easterly winds shown in the pentad means in Figure b(a),(b),(c) is part of a pattern of longer-term change (Figure b(a)). The depth of westerly winds >15 m s^{-1} decreases from about 120 days prior to onset (where they extend down to 600 hPa), to about 10 days prior to onset. At this time, the winds above ∼600 hPa become the summer monsoon upper-level easterlies, which strengthen and deepen above ∼300 hPa (to >15 m s^{-1}), in the 10 days before and after onset.

A particularly notable feature in the zonal winds at Nagpur is a short-lived period of easterly winds above the LCL in the ∼8 days prior to onset (<5 m s^{-1}). Given the direction and transient nature of this shift in wind direction, it appears that this is the weak south-southeasterly winds below the freezing level (∼700-600 hPa) which pass towards the northwest in the pentad mean sections along with the overlying boundary between winds with a westerly component and winds with an easterly component. Over Nagpur it is concurrent with the final transition from upper-level westerly to easterly winds.

The meridional winds along the section and at Nagpur allow us to consider how the deep meridional overturning circulation over India, and the manner in which it transitions during the onset, relates to the dynamics and thermodynamics of the mid-level dry layer. In the pentad mean northwest to southeast sections, the pre-onset meridional winds (Figure b(d),(e),(f)) show a wedge of winds with a northerly component above the freezing level (above ∼500 hPa) that becomes shallower towards the southeast, beneath southerlies that deepen towards the southeast. The time-pressure section of meridional winds at Nagpur (Figure b(b)) indicate that the overlying wedge of southerlies is the upper poleward flowing limb of the wintertime Hadley cell, most clearly evidenced by the abrupt switch around onset from southerly to northerly winds above ∼300 hPa around the time of onset.

It is well known that the deep (or first baroclinic) meridional overturning circulation transitions rapidly in monsoon regions around the time of onset (e.g. Bordoni and Schneider, 2008). The change comes about as a result of the onset of direct thermal circulation, and so indicates a thermodynamic profile conducive to deep convection. The time-pressure section of meridional winds relative to onset at Nagpur (Figure b(b)) show the timing of this change as a rapid change that takes place around the time of onset. The change is thus closely related in time to the ∼5-7 day period of winds with an easterly component above the LCL at Nagpur (Figure b(a)).

Parker *et al.* (2016) describes how the retreat of the mid-level northwesterlies, as seen in the change in wind direction at 600 hPa (Figure b(a), (b), (c)), relates to the development of the monsoon trough to the south of the northern limit and also the development of the upper-level anticyclone over Tibet and the upper-level easterly thermal winds. The analysis here further emphasises, in particular, how closely related these changes are both in time and space to each other and to the onset of deep convection. At Nagpur, the rapid reversal in the meridional overturning circulation, itself a result of the onset of deep convection, is related on the timescale of a few days, to the dying off of the mid-level northwesterlies and to the passage of the 800-600hPa winds with an easterly component that are associated with the passage of the northern limit and which precede the strengthening westerlies associated with the development of the monsoon trough. The results also highlight how the northwestward progression of the onset includes a change from upper-level westerlies to easterlies.

4.3.4 Examining the role of mid-level dry air in onset interannual variability

A logical extension to the hypothesis that mid-level dry air controls the progress of the monsoon onset towards the northwest is the hypothesis that, in the interannual variability, drier mid-level air will lead to a later onset. Parker *et al.* (2016) showed systematic differences between the origins of mid-level air at Nagpur in early and late onset years (Figure b). In early onset years the air around the time of the climatological monsoon onset was more likely to have been advected from over the Arabian Sea, while in late onset years the air was more likely to have been advected from the desert regions in the northwest. For Parker *et al.* (2016), however, the early and late onset years were picked using onset dates decided by the IMD, which are not an entirely objective measure of the onset. Here, early and late onset years have been picked using 2 objective methods, both of which are based solely on rainfall (§ 4.2.2). The differences in WVMR and relative humidity, between these early and late onset years, are examined along the northwest to southeast transect.

Prior to onset, in both the WVMR and relative humidity differences, the 4 different combinations that comes from using the LOR or HIM June rainfall method of determining onset with either radiosonde or ERA-Interim data, all show some statistically significant pattern of higher humidity in the low-levels overtopped by drier mid-levels over central

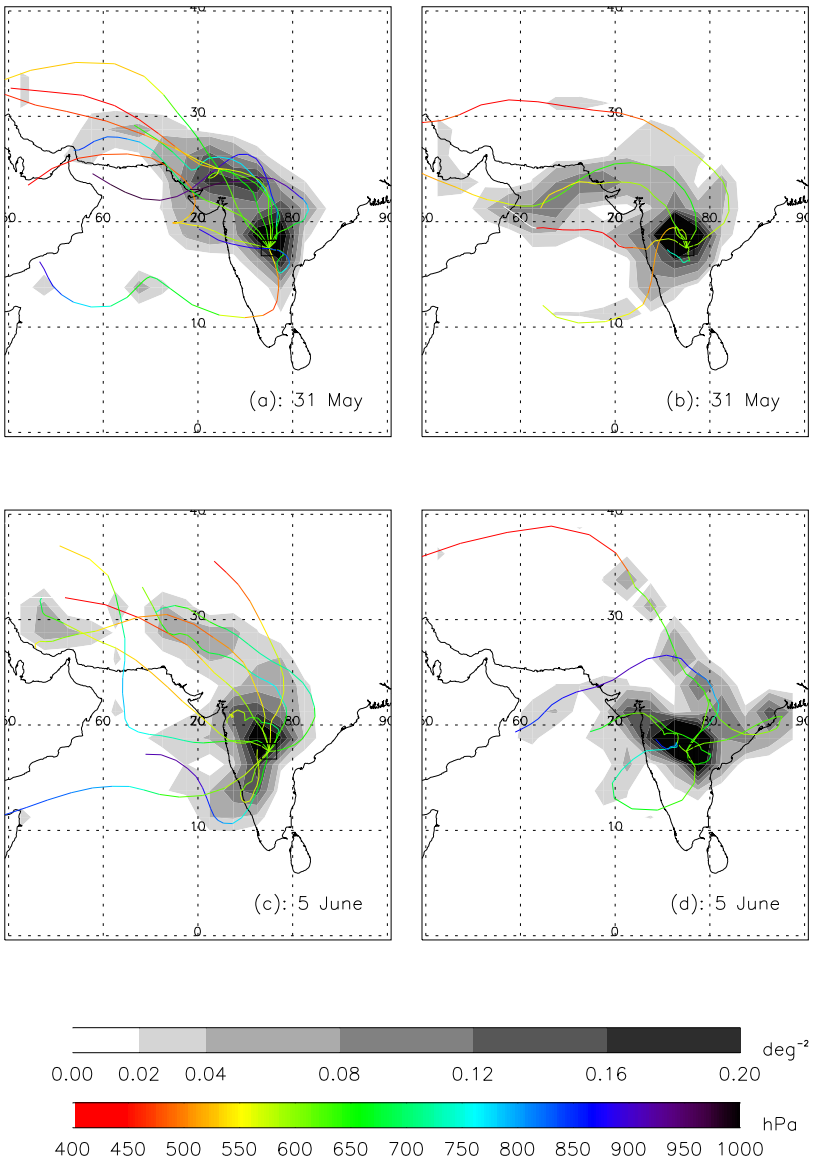

FIGURE B: Six-day back-trajectories, for the period 1981-2013, from the ECMWF operational model and ERA-15, for years of (a), (c) late onset and (b), (d) early onset at Nagpur. For each year, five back-trajectories have been launched, initialised with 0.5° spacing centred on the point marked with a square. Grey shading indicates the density of 6 hourly back-trajectory points per one-degree square, normalised by the total number of trajectories (165). The central trajectory is also plotted for each year of the sample, and coloured according to its pressure. Termination points are at 0000 UTC on (a), (b) 31 May, (c), (d) 5 June at a level of 600 hPa. Reproduced from Parker *et al.* (2016).

India (Figure b(a),(c),(e),(g)) and Figure b(a),(c),(e),(g)). By the time of onset (Figure b(b),(d),(f),(h)) and Figure b(b),(d),(f),(h)), there is a deeper layer of moister air from the surface to ∼400 hPa in the early onset years.

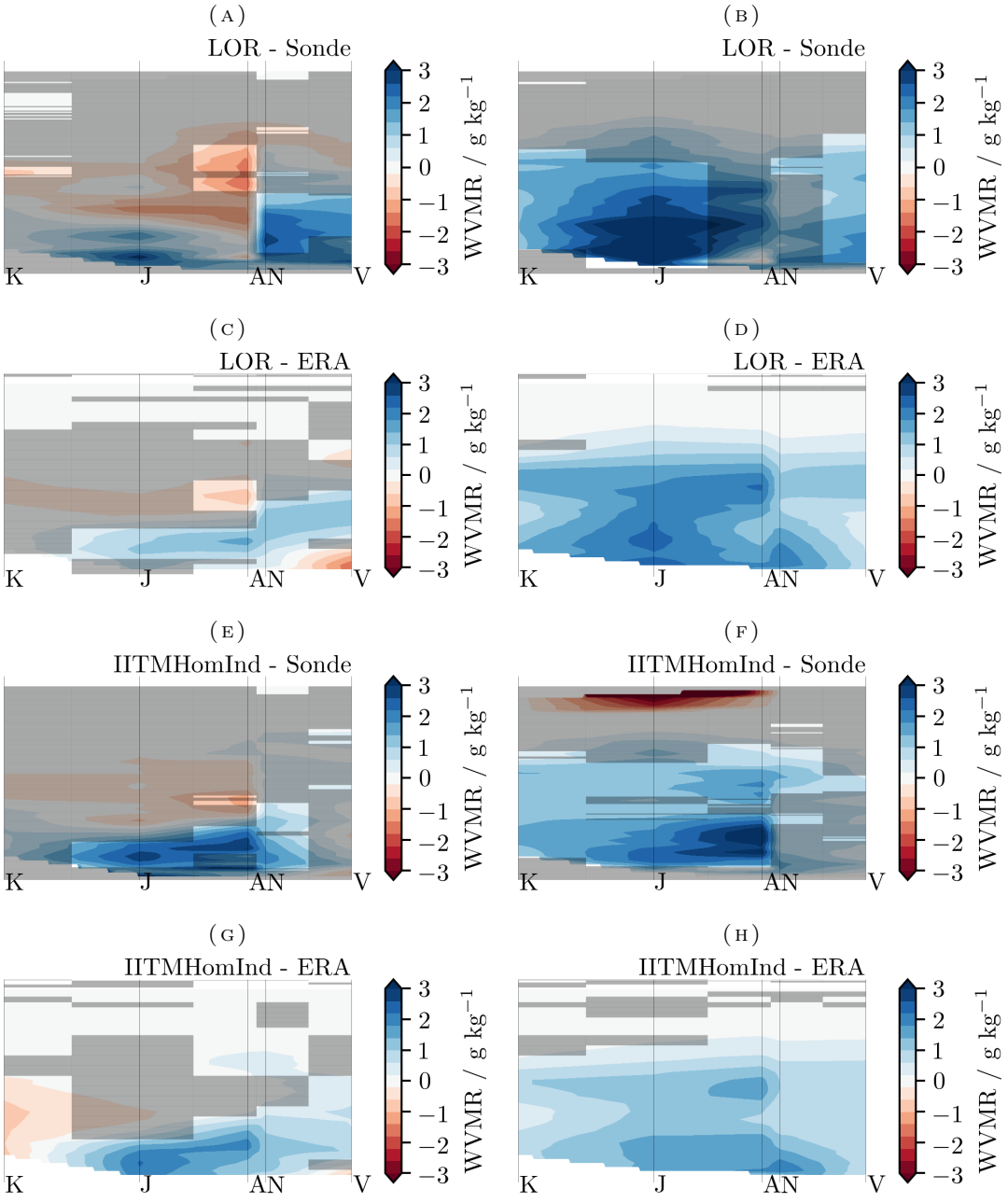

FIGURE B: Northwest to southeast composite sections of the difference in water vapour mixing ratio (g kg^{-1}) between early/late LOR onset years, and between high/low IITMHomInd June rainfall years for pre and midonset pentads (left panels are pentads centred on 31 May, right 15 June). The panels are greyed out where the differences are not statistically significant at the 95% confidence level (using the Mann-Whitney U test) (a), (b) are early minus late LOR onset years using radiosonde data. (c), (d) are early minus late LOR onset years using ERA-Interim data. (e), (f) are high minus low IITMHomInd June rainfall years using radiosonde data. (g), (h) are high minus low IITMHomInd June rainfall years using ERA-Interim data. The method for selecting years is described in § 4.2.2. Vertical lines show the locations of the radiosonde stations, labelled as 'V'=Visakhapatnam, 'N'=Nagpur, 'A'=Aurangabad, 'J'=Jodhpur and 'K'=Kandahar (station locations are marked on Figure).

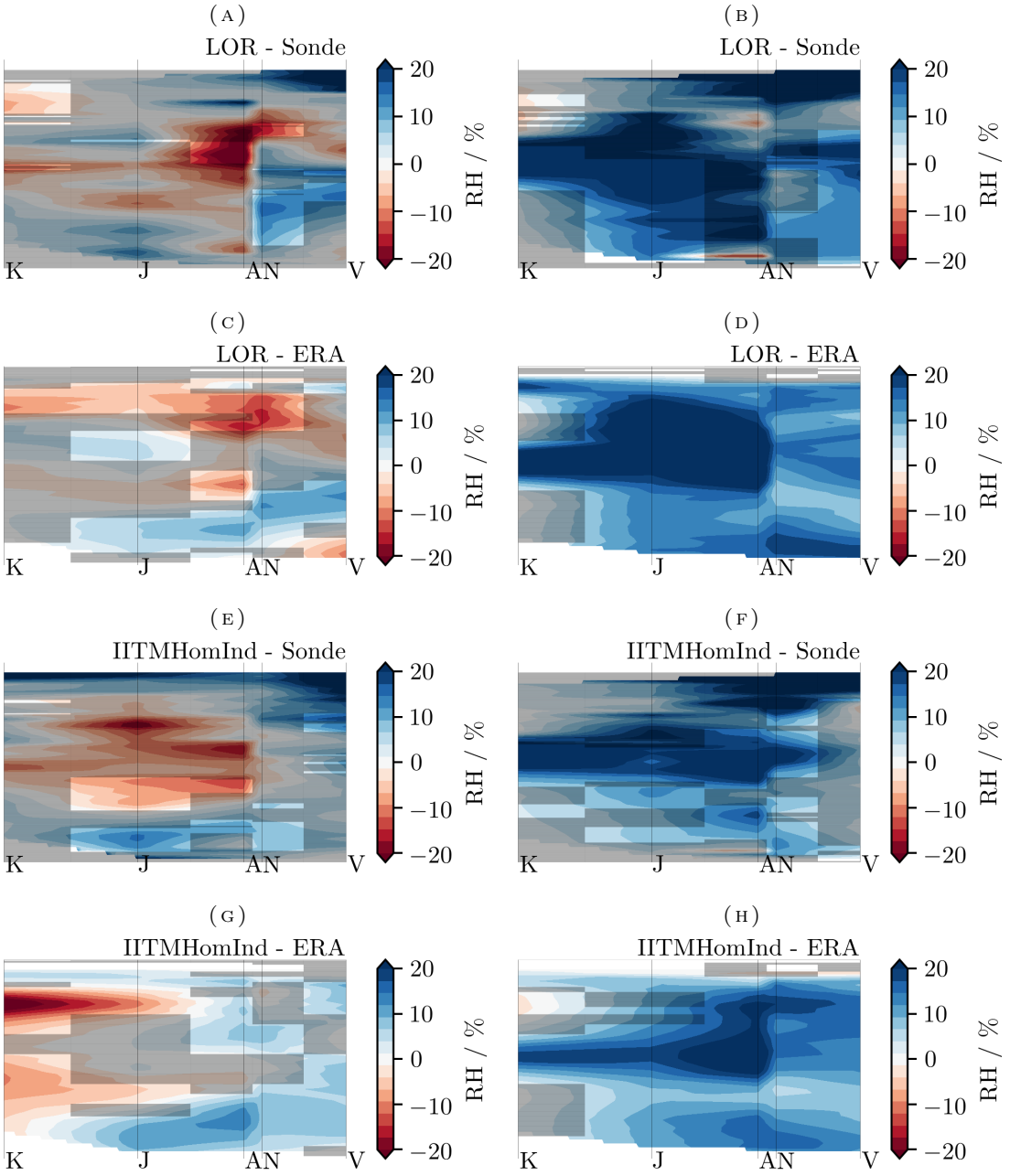

FIGURE B: As Figure b, but for relative humidity.

The onset (15 June) pentad pattern of higher WVMR and relative humidity is consistent with what would be expected from an earlier onset. However, the pre-onset differences do not support the hypothesis that mid-level dry air has a significant influence on the onset interannual variability of the onset. The pre-onset humidity differences suggest it is more likely that greater low-level moistening will lead to an earlier onset. Why the low-levels are moister in early onset years could be related to differences in, for example, the circulation and the land surface.

4.4 Conclusions

This chapter reviews and extends the analysis of Parker *et al.* (2016), which looked at the role of mid-level dry air in the monsoon onset. The further work here looks in more detail at the relationship of the dynamics of the onset to the thermodynamics, and the possible role of mid-level dry air in the interannual variability.

Parker *et al.* (2016) presented a conceptual model for how pre-onset mid-level dry air over India might be important in determining the northwestward progression of the onset of the monsoon rains over a period of about 6 weeks, which happens against the low and mid-level flow and does not follow the pattern of moisture advection. Prior to the monsoon onset, northwesterly winds form a wedge of dry air over India, above the monsoon flow, which is deepest in the northwest (Figure b(g). As the onset progresses, moistening by shallow cumulus and congestus clouds erodes the dry layer from below, bringing the atmosphere closer to pseudoadiabatic, which favours the onset of deep convection. Deep convection begins in the south because the dry layer is less deep there. As the onset of the rains progresses northwestward across India, the monsoon circulation strengthens, and so the advection of moisture from the Arabian Sea increases. This supports increasing moistening of the mid-level dry air from below, making it shallower everywhere, which progressively allows the onset of moist convection towards the northwest.

Further to Parker *et al.* (2016), the thermodynamics of the onset at Nagpur and Lucknow are compared. Parker *et al.* (2016) showed the evolution of the profile at Nagpur through the onset, and while the data from Lucknow support the the original conclusions there are some distinct differences, which are interpreted as being primarily due to Lucknow being further north than Nagpur. Before onset, because Lucknow is closer to the maximum in mid-level northwesterly flow, the pre-onset mid-level RH is lower than at Nagpur, and because of some combination of Nagpur being closer to both maximum in the low-level northwesterly flow and the low-level heat low, at Lucknow the low-level RH is higher and CIN is lower.

Parker *et al.* (2016) described how, at the same time as the northwestward march of the onset of the monsoon rains, the mid- level northwesterly winds and associated advection of dry air weaken. Further inspection of the dynamical changes shows how this weakening of the mid-level northwesterlies relates to changes in the large-scale circulation. On seasonal

timescales the wintertime upper-level westerlies weaken and, around the time of onset at Nagpur, are replaced by the the summertime upper-level easterlies, which develop and strengthen (Figure b(a)). At Nagpur there is a burst of easterly wind between the LCL and the upper-level easterlies for ∼8 days prior to onset, and at the same time a seasonal shift from northerly to southerly mid-level winds, indicating a rapid end to the northwesterly pre-onset mid-level winds. At the same time, a shift from northerly to southerly upper-level winds indicates a rapid change in the meridional overturning circulation (Figure b(b)).

With regard to the relative roles of cloud forcing and the large-scale circulation in the weakening of the northwesterlies, the strengthening of the monsoon trough circulation comes after the circulation changes that take place about 8-10 days before the onset at Nagpur. In the mid-levels, between 700 and 550 hPa (near the freezing level), there are weak south-southeasterly winds at Nagpur on 15 June (Figure b(h)), which shift to Jodhpur on 15 July (Figure b(i)). In the time-pressure sections of wind at Nagpur, this is seen as a burst of easterly winds between the LCL and the upper-level easterlies for ∼8 days prior to onset. It appears that it is only after the weak mid-level south-southeasterly winds have progressed far enough to the northwest that the monsoon trough circulation can develop.

The hypothesis that, in a certain year, drier mid-level air will delay the progression of the onset is tested. Early and late onset years are selected by 2 objective methods that use rainfall amounts in areas with spatially homogeneous variations in rainfall. Prior to onset, the differences in water vapour mixing ratio and relative humidity along the northwest to southeast section, between early and late onset years (Figures b and b), show moister low-levels (below ∼700 hPa) and drier mid-levels, in years with an earlier onset. The results shown here, therefore, do not support the hypothesis that mid-level dry air plays a role in the interannual variablity of the onset. They suggest, instead, that low-level humidity over India prior to onset plays a role in determining the year-to-year timing of the onset.

The effect that dry mid-level air can have on precipitation, particularly in the tropics, has received growing attention in recent years (e.g. Zhai and Boos, 2017). In the context of model biases, convective parametrisations typically struggle to represent the effect a mid-level dry layer can have on precipitation because they are based on the assumption that the entire troposphere should remain near to radiative-convective equilibrium. The analysis presented here shows that not only does the onset include a change from a profile that includes a mid-level dry layer to one that is close to pseudoadiabatic, but that the

the timing of this change closely relates to major dynamical changes in the large-scale circulation. Detailed analysis, using observations and high resolution model simulations, will be needed to understand the relationships between these transitions.

Chapter 5

Moist convection and its upscale effects in simulations of the Indian monsoon with explicit and parametrised convection

5.1 Introduction

While global climate models perform reasonably well on the global scale, they fail to resolve important local to regional scale processes (Karmacharya *et al.*, 2015). In the Indian monsoon, most exhibit systematic biases of too much rainfall over the equatorial Indian Ocean, too little rainfall over central India and, in the 850 hPa winds, too little cross-equatorial flow over the Western Arabian and Sea and too little flow over India and the Bay of Bengal (Sperber *et al.*, 2013). Higher resolution Regional Climate Models (RCMs), which are able to represent regional forcings, feedbacks, and processes, improve the representation of rainfall in the Indian summer monsoon, particularly over regions of steep orography such as the Himalayas and Western Ghats (Rupa Kumar *et al.*, 2006). However, Lucas-Picher *et al.* (2011) show significant differences in the representation of the Indian Monsoon by a number of RCMs forced with lateral boundary conditions from the 45-year European Centre for Medium-Range Weather Forecasts (ECMWF) Re-Analysis (ERA-40) for the

period 1981-2000, highlighting that they fail to properly represent important feedbacks and processes, even when biases introduced by the driving model are reduced.

The representation of convection, through convective parametrisation schemes, is a dominant source of error in global models (Jung *et al.*, 2010; Sherwood *et al.*, 2014). Convective parametrisation schemes typically produce too many light rain events, too few heavy rain events, and a diurnal cycle of continental precipitation that peaks too early in the day (Betts and Jakob, 2002; Randall *et al.*, 2003; Guichard *et al.*, 2004; Stephens *et al.*, 2010; Dirmeyer *et al.*, 2012). Errors develop on a short enough timescale (on the order of 1-2 days) to affect both weather and climate models (Murphy *et al.*, 2004; Rodwell and Palmer, 2007), and can have an effect on much larger scales than the convection itself. For example, cloud formation, which varies with the intensity and frequency of moist convection, affects diabatic heating, radiation fluxes, and convective transport, and near-surface rainfall and water vapour affect surface fluxes and the biosphere.

Model configurations with a high enough horizontal resolution to resolve individual clouds or cloud systems perform better in some respects, such as the diurnal cycle of precipitation in the tropics (Guichard *et al.*, 2004; Dirmeyer *et al.*, 2012), and the rainfall intensity distribution (Weisman *et al.*, 1997; Holloway *et al.*, 2012b). While increases in computing power now allow these convection-permitting model configurations to be run on continental scales and weekly timespans, it is expected that it will still be necessary to parametrise convection for the foreseeable future (Holloway *et al.*, 2012b), when the combination of complexity, timescale, domain size and model ensemble size require it.

The latest convection-permitting simulations can be used to understand the large-scale effects of biases arising from the parametrisation of convection. In a comparison of simulations of the West African monsoon with explicit and parametrised convection, improved explicit representations of convective triggering, organisation and the diurnal cycle of precipitation (Marsham *et al.*, 2013; Birch *et al.*, 2014) caused the Sahel-Sahara pressure gradient and monsoon flow to be weaker. The work here uses a suite of Met Office Unified Model (MetUM) simulations of a 3-week period of the 2011 Indian Summer Monsoon, over a domain size large enough to capture the monsoon system. Model configurations with sufficiently high horizontal resolution to permit the explicit resolution of cloud systems and temporal and spatial domain sizes large enough to allow the representation of convection to affect

the continental-scale circulation, are compared with observational data and parametrised convection model simulations of the same period.

In state-of-the-art climate models, the systematic biases of Indian monsoon rainfall and 850 hPa wind are broadly consistent with each other (Sperber *et al.*, 2013), but how they are related remains unclear. It is expected that the convection-permitting simulations will give a better representation of rainfall intensities and the diurnal cycle of rainfall compared to the parametrised convection simulations. Biases are also expected in the convection-permitting simulations, particularly as grid-spacing increases. By comparing the properties of storms within the monsoon and the monsoon circulation not only between simulations with explicit and parametrised convection, but also among the convection-permitting simulations, the aim here is to understand in detail how moist convection model biases affect the representation of the large-scale monsoon. In particular, the work examines the possible roles of latent heating, radiation and heat fluxes and land surface processes.

5.2 Data

In this chapter, the 2011 MetUM simulations, TRMM 3B42, CMORPH and GSMAP satellite rainfall retrieval datasets, and radiosonde data described in Chapter 3 are used, along with sea level pressures measured at three surface stations (Patna, Port Blair and Minicoy in Figure), as well as radiosonde sounding data from Minicoy (UK Meteorological Office, 2015; Durre *et al.*, 2006).

5.3 Results

5.3.1 Inter-comparison of modelled and observed rainfall

5.3.1.1 Mean pattern of rainfall

Figure shows the mean spatial patterns of rainfall for selected simulations and TRMM. TRMM (Figure (a)) shows regions of higher rainfall over the Himalayas, the Myanmar coast, the Bay of Bengal, the monsoon trough and the Western Ghats; all the simulations produce excessive rain over the orography of the Himalayas and the mountainous west coast

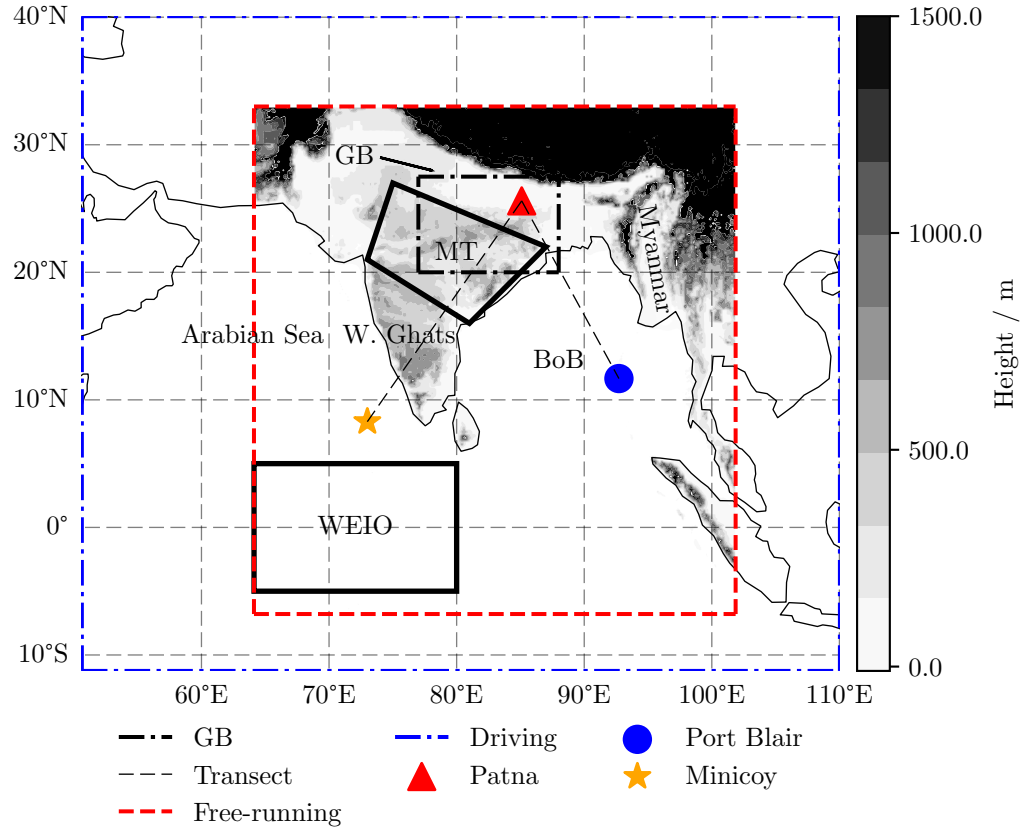

FIGURE : Simulation domains, orography (shading), ground station locations (Patna, Port Blair and Minicoy), and regions referred to in text (Arabian Sea, Western Ghats, Monsoon Trough (MT), Bay of Bengal (BoB), Ganges-Mahanadi basin (GB), and Myanmar, and part of the Western Equatorial Indian Ocean (WEIO)). The 'subcontinent' is defined here as land west of 90°E under 1500 m, and BoB as ocean east of 80°E and north of 10°N.

of Myanmar, and are too dry over the Bay of Bengal and the Western Ghats. More coarsely resolved explicit convection (Figure (c)) produces excessive rain over the equatorial Indian ocean, which is consistent with past studies (Holloway *et al.*, 2012a,b). Model performance in the monsoon trough region is discussed below.

The band of monsoon trough rainfall is further north in all the convection-permitting simulations, compared to TRMM (Figure (a)-(c)), such that there is a positive/negative dipole in the differences (Figure (e), (f)). In the parametrised simulations, the band of maximum rainfall over central India is further south (Figure (d)), in better agreement with TRMM, but there is deficient rainfall there and excess rainfall extending northwards to the Himalayas (Figure (d)), so that the dipole of rainfall difference is due to a relatively consistent spread of rainfall over central India north of 20°N, rather than a difference in the location of the rainfall maximum. Mean total rainfall amounts in the monsoon trough from 22 August to 6 September are between 242 and 250 mm for the three satellite rainfall

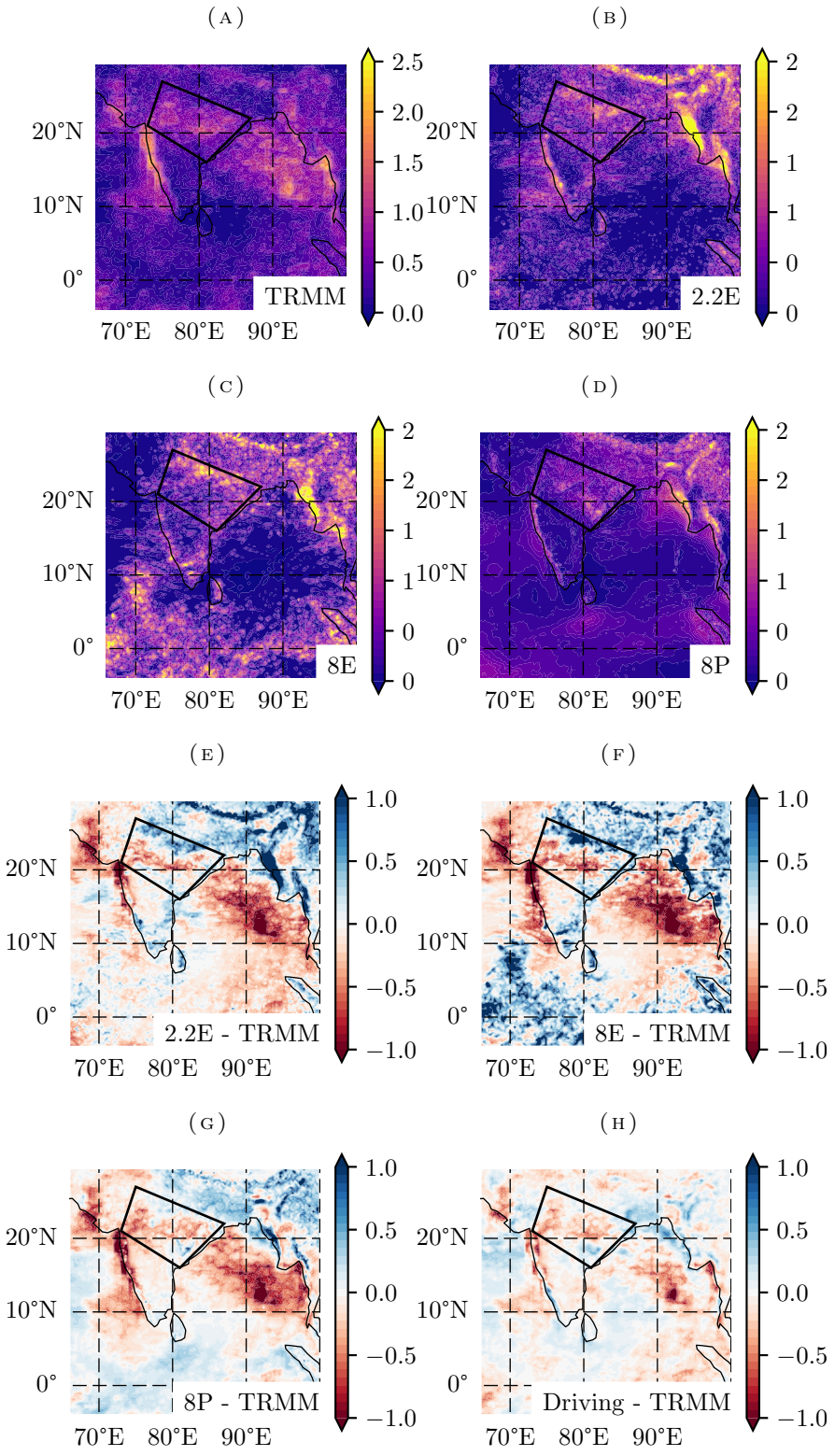

FIGURE : Mean rainfall rate and modelled rainfall rate minus TRMM (mm h^{-1}) over the 21-day period starting 18 August 2011 00:00 UTC for (a) TRMM, (b) 2.2E, (c) 8E, (d) 8P, (e) 2.2E minus TRMM, (f) 8E minus TRMM, (g) 8P minus TRMM, and (g) Driving minus TRMM. The black polygon shows the area defined as the monsoon trough. Simulations are coarse-gridded onto the TRMM grid before averaging.

retrieval products, which is relatively well captured by 2.2E, 4E, and 8E (242, 239, 237 mm respectively), although 12E produces significantly less (212 mm). The parametrised simulations produce much less in the monsoon trough, with 8P and 12P total rainfall at 175 and 174 mm respectively. A large proportion of the rainfall in the monsoon trough comes from the propagation of a Low Pressure System (LPS) northwest across India from the Bay of Bengal (discussed further in § 5.3.2), and differences in the position of the band of monsoon trough rainfall in the free-running simulations are mostly due to the path it takes.

It is not clear from these mean spatial fields of rainfall alone that, for example, 2.2E gives a better representation than 8P of this 21-day period. However, similar patterns of bias in both the convection-permitting and parametrised simulations, of deficient rainfall over the Bay of Bengal, excess rainfall over Myanmar, and deficient rainfall over the Western Ghats suggest these biases are not primarily due to a different grid spacing or representation of convection. 2 areas where the biases appear to be systematically different are in the monsoon trough region, and over the equatorial Indian Ocean. This motivates, in the next section, an analysis of some of the mean rainfall properties over land, ocean, and in the monsoon trough region.

5.3.1.2 Variability in daily rainfall, diurnal rainfall and rainfall intensity

The total rainfall, the diurnal cycle of rainfall and rainfall intensities are all much more strongly dependent on the representation of convection than on model grid spacing (Figures 3-5). Figure (a) shows that, over the subcontinent as a whole, the convection-permitting simulations consistently rain more than the satellite retrievals and the parametrised simulations, with the exception of the rainfall minimum centred around 25 August. There is a clear initial 4-day spin-up for the convection-permitting simulations over land; this presumably results from the time required for convective-scale circulations to develop and the adjustment of the large-scale state of the convection-permitting simulations to their preferred atmospheric state, from that of the MetUM operational global model, which parametrises convection. Even after this spin-up, the convection-permitting simulations tend to rain more than observed over the subcontinent (Figure (a)). Over the ocean (Figure (c), it is not clear if there is a spin-up, which may be shorter (1–2 days).

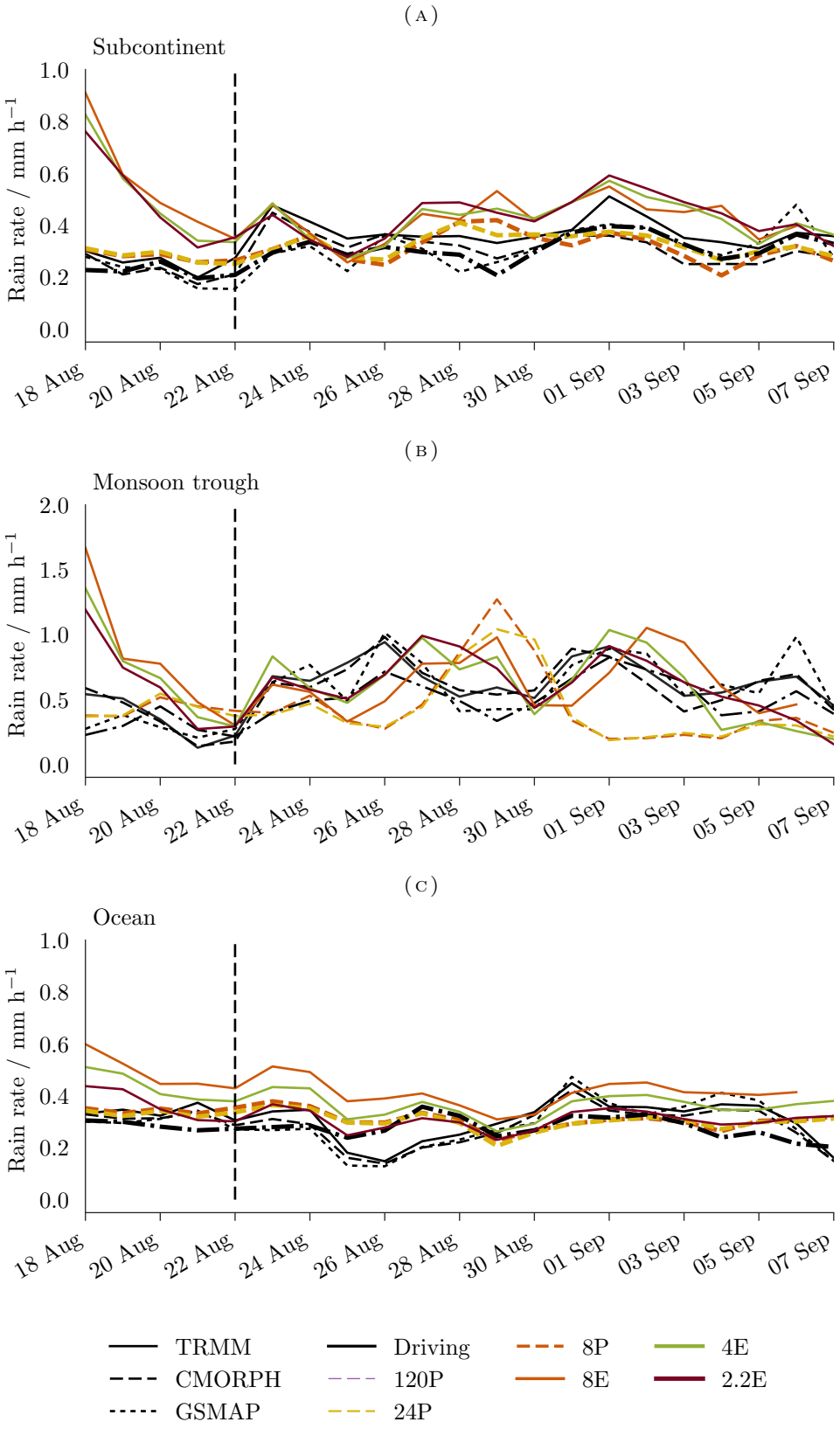

FIGURE : Daily mean rainfall rates for the 21-day simulated period over (a) the subcontinent, (b) monsoon trough, and (c) ocean, for simulations and satellite rainfall retrievals. The regions are described or shown in Figure and its caption. Vertical dashed line marks end of model 'spin-up' period.

There is a large spread in the mean satellite estimates of rainfall over the subcontinent for the period after the convection-permitting simulations spin-up period, with CMORPH closer to the parametrised free-running simulations and driving (both ∼0.3 mm h^{-1}), and TRMM closer to the convection-permitting simulations (∼0.37 and ∼0.39 mm h) respectively.

Among the free-running simulations, 2.2E, 4E and 8E capture the day-to-day variability over the subcontinent in TRMM the best, between 22 August and 7 September (after the spin-up period) with the highest Pearson Correlation Coefficients (PCC) of 0.5, 0.57, 0.46 respectively, although the PCC between TRMM and 12E is very low (0.1). Among the parametrised simulations, there is an increase of PCC with grid spacing in 8P, 12P, and 24P, which is similar to 120P (0.35, 0.36, 0.45, 0.46 respectively). This increase in correlation as grid spacing increases is an interesting result, but further investigation is beyond the scope of this article. The driving simulation, compared to TRMM, captures the day-to-day variability over the subcontinent better than the free-running simulations, with a PCC of 0.68. This is within the spread of the PCCs among the satellite rainfall retrievals (0.6–0.88), which are higher than the PCCs between all of the free-running simulations and TRMM.

In the monsoon trough, while the daily mean rainfall variability is much greater than for the whole domain (Figure (b)), the day-to-day variability in rainfall in each of the convection-permitting simulations is similar, and is distinct from the variability in the parametrised models, which are also all similar to each other. This is particularly true after ∼31 August, when the convection-permitting simulations capture the day-to-day variability in the satellite retrievals to some degree, but the rainfall drops off in the parametrised simulations and there is very little variability. Much of the variability after 31 August is associated with the propagation of a LPS northwest along the monsoon trough from the Bay of Bengal, and is discussed further in § 5.3.2

There is good correlation in the modelled daily variability of rainfall in the monsoon trough in the higher-resolution convection-permitting modes (PCC for 2.2E and 4E are 0.5 and 0.52 respectively), but lower correlation for the lower-resolution convection-permitting simulations (for 8E and 12E, PCCs are 0.05 and 0.11 respectively). This is in spite of the PCCs between 8E and 2.2E/4E being fairly high (both 0.69). The correlation with observations is negative for parametrised simulations, with PCCs between -0.2 and -0.27, while the driving simulation, as expected, has a much higher PCC at 0.83. These negative

PCCs in the parametrised simulations are, to some degree, also attributed to the propagation of the LPS northwest along the monsoon trough.

Figure shows the cumulative sum of the fractional contribution of rainfall rates to the total rain for the simulations and satellite retrievals.

A greater fraction of the total rainfall in the convection-permitting simulations and satellite observations comes from more intense rainfall, compared to the parametrised simulations, and as grid spacing decreases, the convection-permitting distribution moves closer to that of TRMM and CMORPH. The distribution is similar among the parametrised simulations, which includes the driving simulation, with the vast majority of rain coming from light

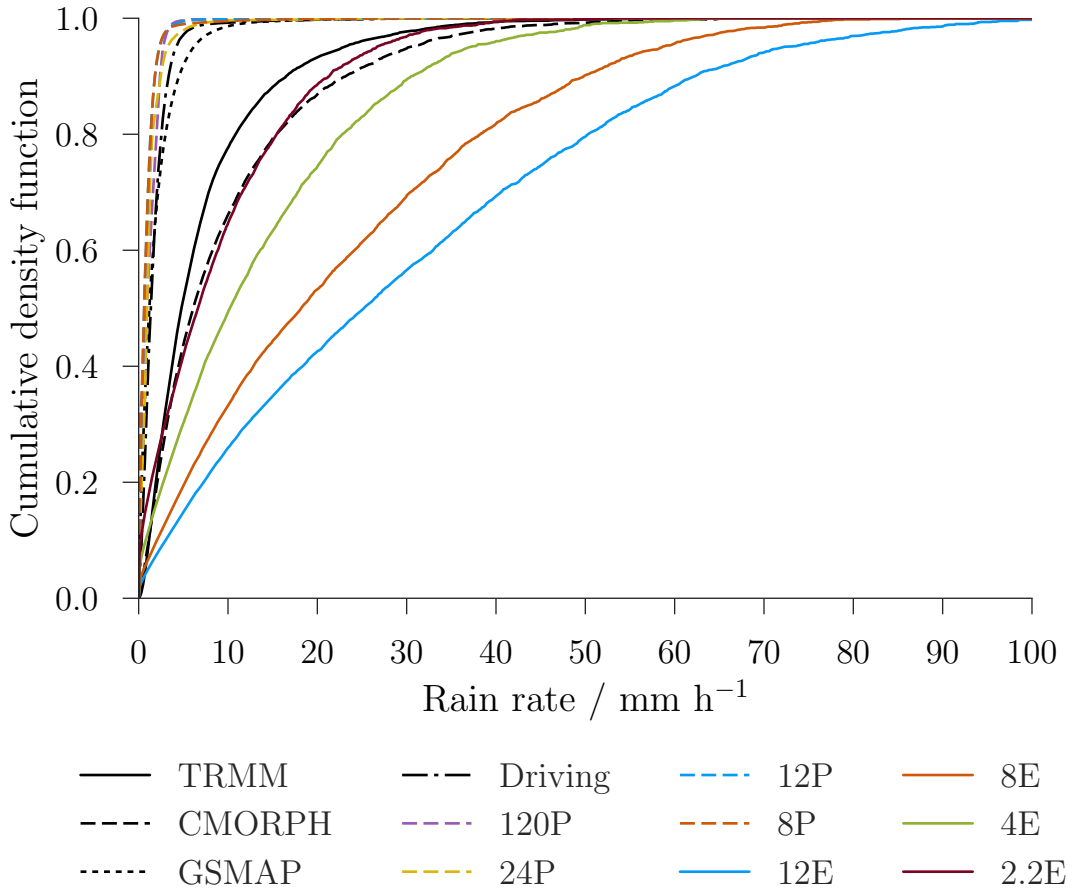

FIGURE : Cumulative sum of rainfall intensity probability distribution over the subcontinent (Figure , between 22-30 August (Figure)), for simulations and satellite rainfall retrievals. The simulations and CMORPH and GSMAP retrievals were coarse-grained to the TRMM 0.25x0.25 degree horizontal grid, and output at the three hourly TRMM time resolution, from the original hourly data for the simulations, and 30 minute data for CMORPH and GSMAP.

rain. There is a pronounced grid-spacing effect on the distribution among the convection-permitting simulations, with an increase in more intense rain as the grid spacing increases, although their total rainfall amounts are similar (Figure). About 80% of the rainfall in the parametrised (free-running and driving) simulations comes from rain rates of <3 mm h^{-1} and 95% comes from rain rates of <5 mm h^{-1}, while 70–90% (2.2E–12E) of the rainfall in the convection-permitting simulations comes from rain rates of >3 mm h^{-1} and 75 to 35% (12E–2.2E) comes from rain rates of >10 mm h^{-1}. The 2.2E distribution of rainfall intensities is a close match to CMORPH while the TRMM product has a lower proportion of the rainfall coming from rain rates between 5 mm h^{-1} and 35 mm h^{-1}. The GSMAP distribution is a close match to the parametrised simulations, and this is expected to be due to the use of model reanalysis products in its algorithm.

Consistent with past studies in other regions (Sato *et al.*, 2009; Marsham *et al.*, 2013), the phase of the diurnal cycle of rainfall over the subcontinent (Figure (a)) is much improved in the convection-permitting simulations, compared to the parametrised, although the convection-permitting simulations rain excessively during the afternoon and evening, compared to the satellite rainfall retrievals. In the convection-permitting simulations, rainfall peaks at 1500–1700 local time (India Standard Time (IST) = UTC + 5.5 h) and is at a minimum in the early morning, from 0800 to 1000 IST, in agreement with the satellite products, whereas rainfall in the parametrised convection simulations peaks too early in the morning between 0900 and 1200 IST, and is at a minimum at ∼1800 IST. There is a shift among the convection-permitting simulations to a later peak in rainfall as the grid spacing increases, consistent with many but not all past studies (Petch *et al.*, 2002; Bryan *et al.*, 2003b; Marsham *et al.*, 2013).

The mean diurnal cycles in Figure are not able to show the variety in the diurnal cycle across the land and ocean regions; this is shown in Figure , which shows the timing of the diurnal peak in rainfall across the domain. The convection-permitting simulations capture the high degree of variability seen in TRMM, whilst the parametrised show far too little variability. TRMM and 2.2E peak rainfall timings are very similar over the oceans, with a high degree of variability which is generally not captured by the parametrised simulations. Despite this, the diurnal cycle over the Bay of Bengal, with a change in peak timing here from morning to night-time from northwest to southeast as in TRMM, is still captured to some extent in the parametrised simulations.

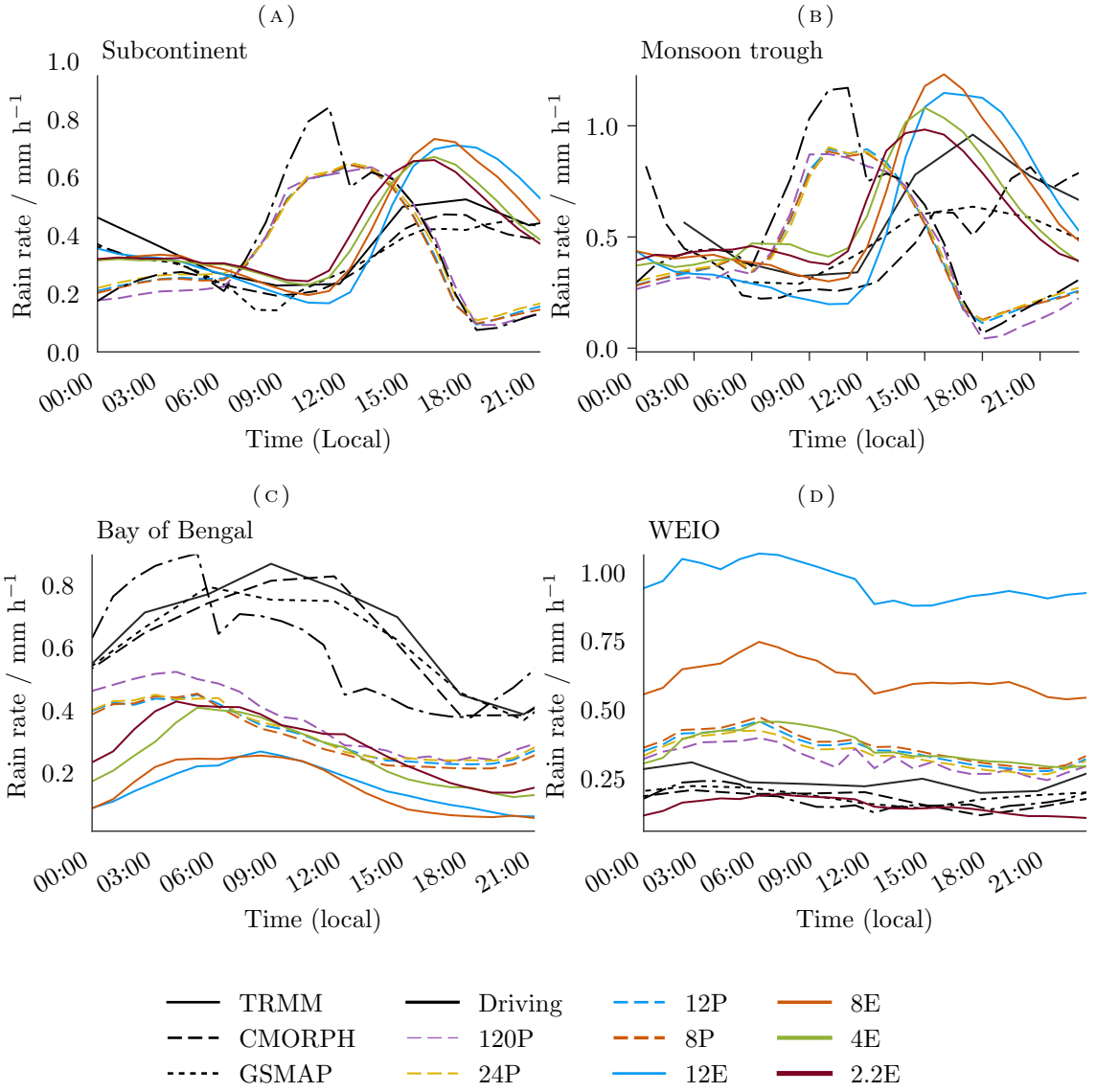

FIGURE : Mean diurnal cycle of rainfall over (a) subcontinent, (b) monsoon trough, (c) Bay of Bengal, and (d) Western Equatorial Indian Ocean (WEIO), for entire modelled period. Times are local times, which is UTC+5.5 hours, over central India (IST). See Figure for regions.

5.3.2 Interactions between convection and the monsoon

Having examined the characteristics of the modelled rainfall, this section now examines the interactions between moist convection and the monsoon flow in the simulations.

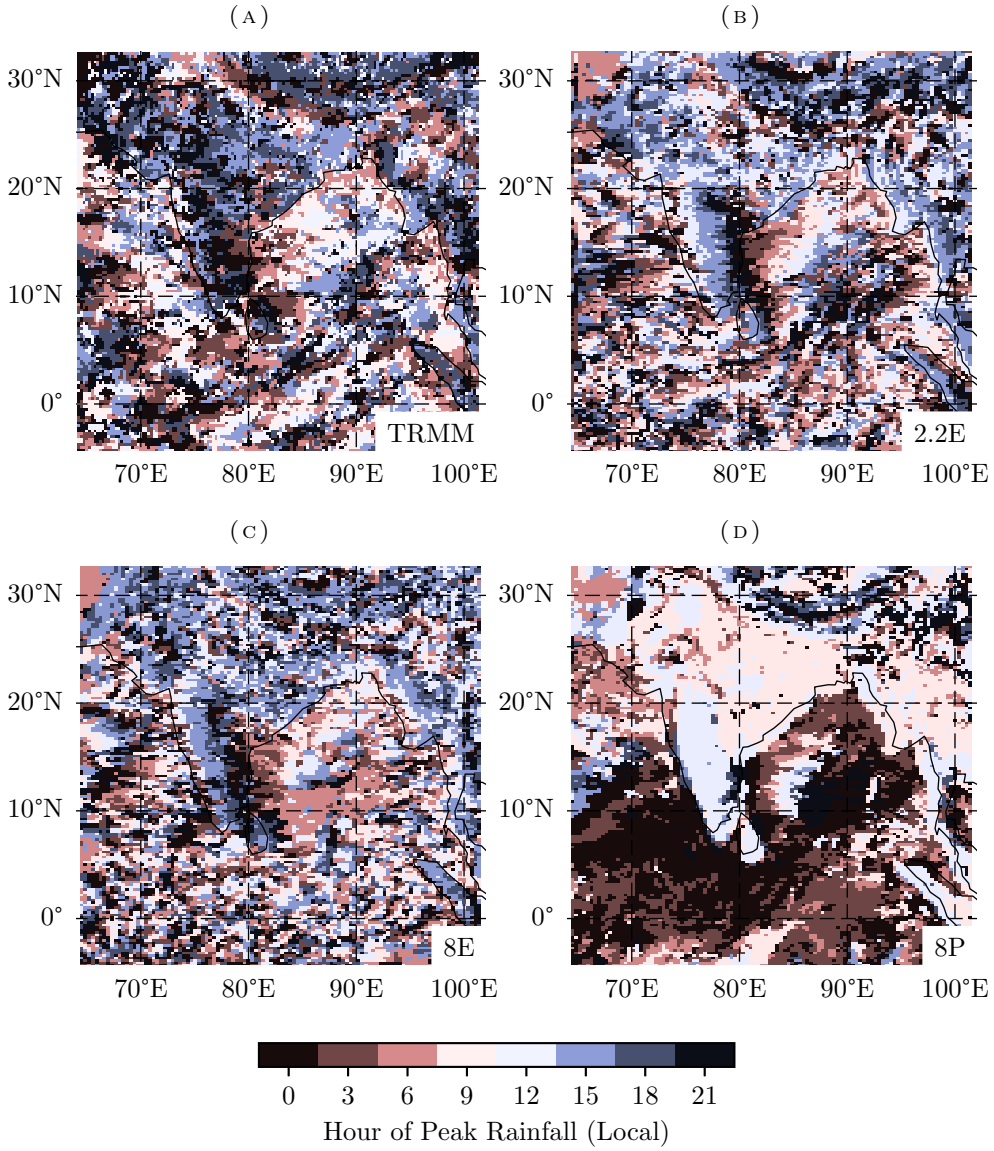

FIGURE : Mean hour of day of peak rainfall in local time (which varies with longitude, but is UTC+5.5 hours, over central India, which is IST), for EMBRACE period. Simulations coarse-grained to 24 km.

5.3.2.1 Monsoon trough

Figure shows how a change in the representation of convection produces a characteristically different monsoon trough, with a deeper trough in the convection-permitting simulations. During the first few days of spin-up, the monsoon trough is too deep in the convection-permitting simulations, but after this period they are in better agreement with driving (i.eánalyses) than the parametrised simulations. After 31 August the parametrised and convection-permitting simulations diverge significantly. After this date, the variability in

the convection-permitting simulations continues to correlate well with driving, but there is a sharp increase in pressure in the parametrised simulations. This divergence is due to the propagation of a documented LPS (Khole and Devi, 2012), northwest from the Bay of Bengal towards Pakistan, which takes less time to move through the monsoon trough in the parametrised simulations, and accounts for the lower 925 hPa geopotential heights in the parametrised simulations during 29–31 August, as well as rainfall differences in the monsoon trough (Figure (b)). Therefore the remainder of our analysis focuses on 22–30 August before the simulations diverge, due to differences in synoptic-scale weather, but after the spin-up of the convection-permitting simulations.

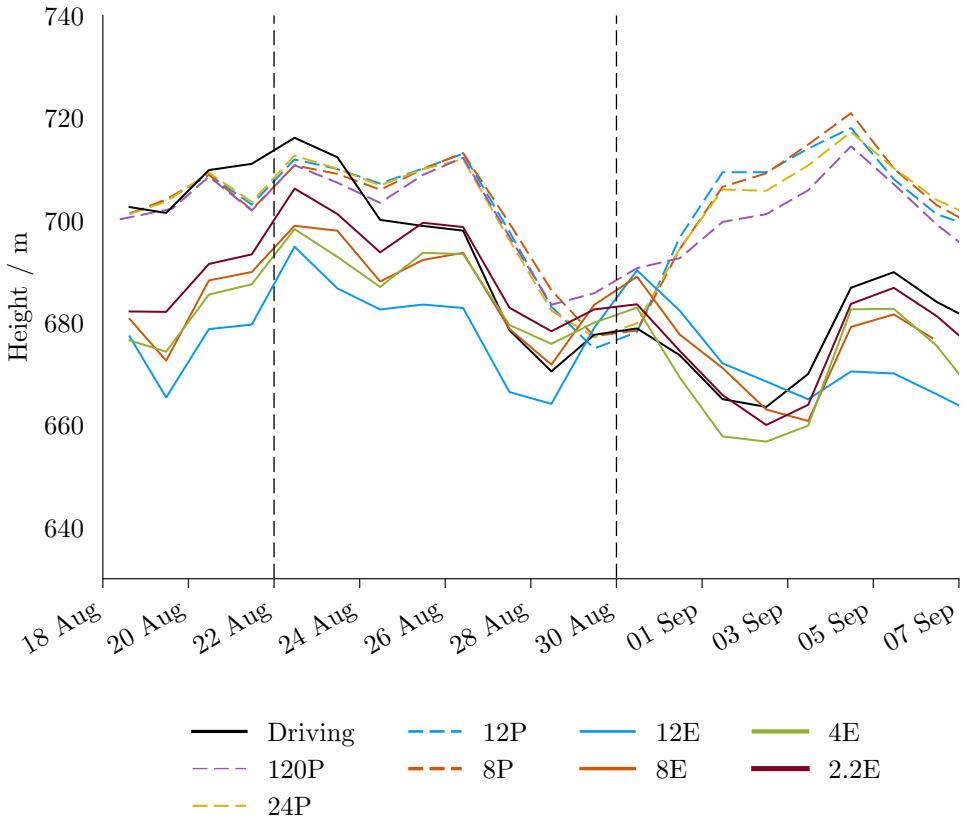

FIGURE : Daily minimum 925 hPa monsoon trough (Figure) geopotential height (m) for simulations. The vertical dashed line on 22 August shows the end of the 'spin-up period', when the convection-permitting simulations rain far too excessively over land (Figure). Around 30 August, the simulations diverge significantly in their representation of a low-pressure system (LPS) that propagates northwest along the monsoon trough, from the Bay of Bengal.

5.3.2.2 Land-sea temperature gradient

Contours in Figure show the location of the monsoon trough as a closed low in 925 hPa height over northern India in 8E, with a gradient of increasing height to the southwest over India, and marked gradients over the Arabian Sea and Bay of Bengal, which drive the onshore circulation of moist air into India. As well as deepening the monsoon trough, an explicit representation of convection also increases the land-sea temperature gradient. Colours in Figure show that 8E 925 hPa potential temperatures are, for the most part, 1–2 K higher over land and 1–2 K lower in the Bay of Bengal and Arabian Sea, compared to 8P, which will encourage ventilation of the continent by enhancing the monsoon flow. The exception to higher 8E temperatures over land is in the northwest of the domain (25°N, 70°E), which is consistent with advection of cooler oceanic air driven by changes in synoptic-scale flow between the simulations (discussed below), accelerated by the boundary effect of the adjacent highlands of Pakistan, into a region with no orography to impede the flow or cause the condensation of water vapour.

The higher 925 hPa temperatures over land are largely explained by the effect of the change in surface fluxes resulting from explicit convection shown in Figure . During the daytime, the land surface in the convection-permitting simulation receives more short-wave radiation (+20 W m^{-2} mean daily total), as a result of a later peak in clouds and convection (Figure (a), (b)). Changes in net long-wave radiation are smaller (-10 W m^{-2}), and so there is greater net surface heating in the convection-permitting simulation (+10 W m^{-2}). This actually gives increased sensible and reduced latent fluxes in 8E than in 8P (+15 and -7 W m^{-2} respectively), with a Bowen ratio greater than 1 from ∼1200 to 1500 IST in 8E, and ∼0.5 throughout the day in 8P, indicating a moister surface in 8P. This can be explained by the rainfall in the convection-permitting simulations being both more intense (Figure), and later in the day (Figure (a), (b)), resulting in decreased interception of rainfall by the vegetation canopy, greater run-off, and greater penetration into the soil (Best *et al.*, 2011), and since the rain falls after peak insolation, reduced rapid re-evaporation (Birch *et al.*, 2015). 15 W m^{-2} extra sensible heating in 8E, would correspond to ∼0.5 K extra heating for a 2 km boundary layer over 1 day, which is broadly consistent with the magnitude of the differences in 925 hPa potential temperatures in Figure .

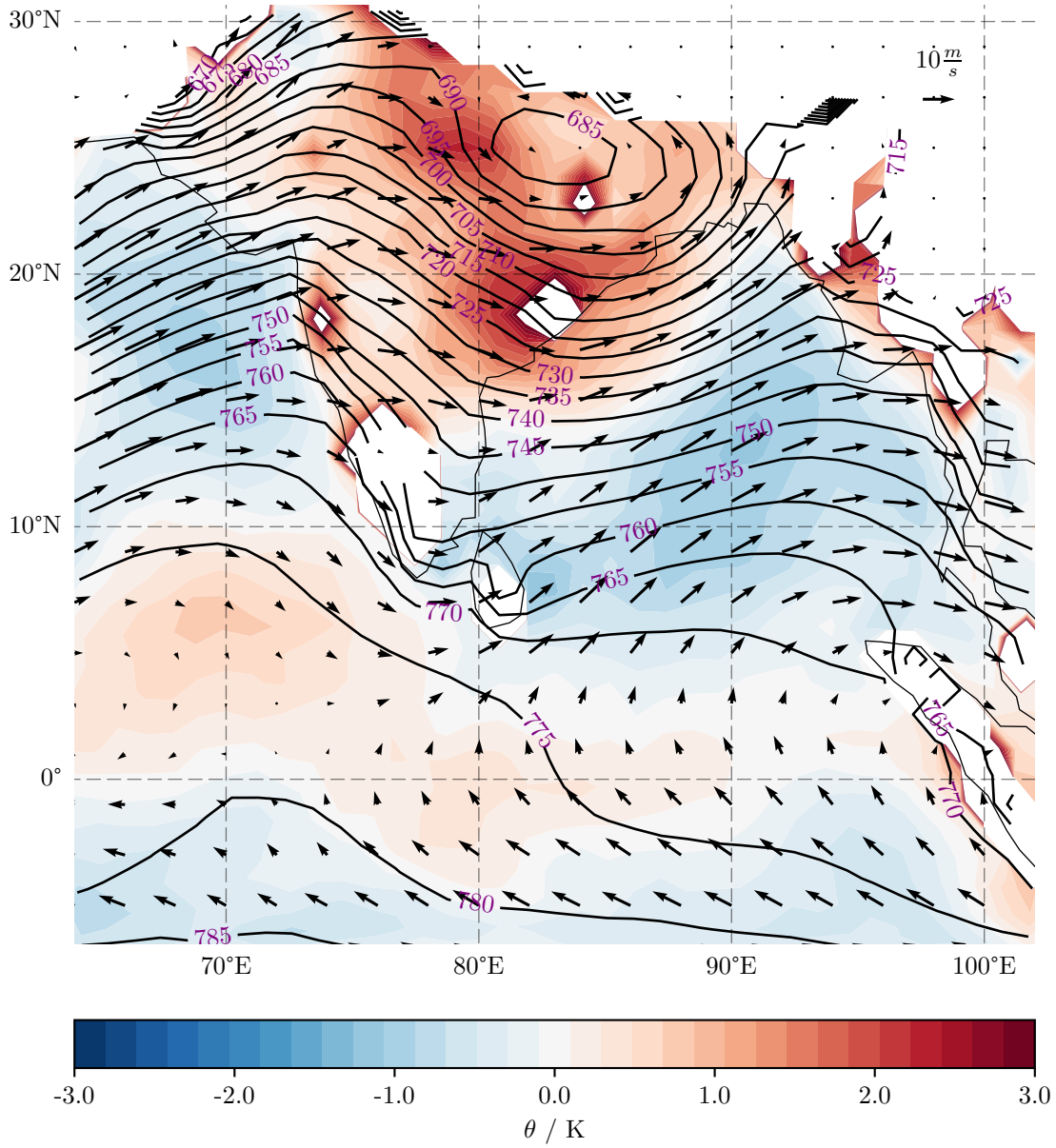

FIGURE : 8E 925 hPa geopotential height (contours) and wind vectors, and 8E minus 8P 925 hPa potential temperature (colours) between 22-30 August (Figure). Diagnostics coarse-grained to 120km grid-spacing.

Over the ocean, differences in 925 hPa air temperatures are smaller than over the land, since the SSTs are identical between the simulations, whereas land surface temperatures are free to evolve. Heavier rainfall in 8E over much of the Western Equatorial Indian Ocean (WEIO) (Figure (f), (g)), with its greater latent heat release, is spatially correlated with the 925 hPa differences in height and potential temperature.

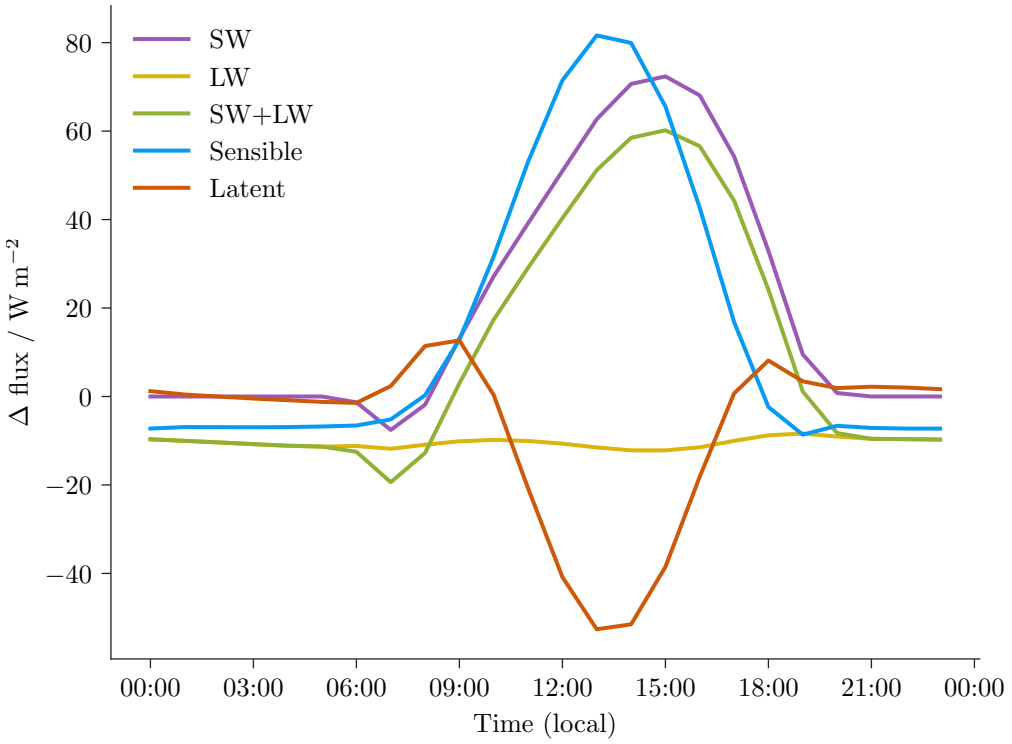

FIGURE : Diurnal cycle of 8E minus 8P surface fluxes over the subcontinent (Figure).

5.3.2.3 Effect of rainfall on circulation

Rainfall differences between the free-running simulations, over both the ocean and the subcontinent, significantly alter the mean low-level pressure distribution and flow into the subcontinent (Figure). As will be discussed, this can be seen most clearly in the region of the black box in Figure , which covers part of the Arabian Sea and the west coast of India. There is a deeper monsoon trough in 2.2E and 8E than in 8P, consistent with the greater precipitation in the convection-permitting runs (Figure (b), (c), Figure). Over northern India, differences between 2.2E, 8E and 8P (Figure (a), (b), (c)), all have positive/negative dipoles in northern India, which are related to differences in the position of the monsoon trough and rainfall within it, but these are quite localized, with the positive and negative anomalies cancelling each other in the far-field. For this reason, these differences due to the shift in location of precipitation features do not influence the differences in continental-scale gradients. Where 8E rains more than 8P at ∼24°N, 80°E, there is a relative 8E low of 16 m, whereas the relative 8P rainfall maximum at ∼20°N, 89°E corresponds to an 8P low of 2 m. In short, areas of higher rainfall in the convection-permitting simulations correspond to much larger height differences. As a result, there is a deeper monsoon trough in 2.2E

and 8E than in 8P (Figure).

Over the WEIO, 2.2E rainfall is the most realistic, compared to the observations, while 4E, 8E and 8P rain excessively (Figure (d)). Less latent heating through rainfall over the ocean in 2.2E, compared to 8E and 8P (Figure (a), (b)) corresponds to a relative high, which acts to increase the pressure gradient towards the north and onshore, leading to greater southerly flow in the Arabian Sea and onto the west coast of India. 8P rains less than 8E over the WEIO (Figure (c)) which will act to increase the land–sea pressure gradient in 8P, and favour an increase in the onshore flow, but 8E has a larger land–sea pressure gradient, as it is the pressure differences over the continent which are dominant in this case.

The differences in the modelled 925 hPa winds are largely consistent with a geostrophic response to these differences in geopotential over land and ocean, with an enhanced southerly cross-equatorial flow, in the WEIO and Arabian Sea in 2.2E, compared to 8E and 8P, and greater onshore flow in 8E than in 8P. Figure (a), (b) shows simulated and observed (radiosonde) vertical profiles of wind at Minicoy (Figure)), which is in the Indian Ocean, in the region of the largest wind differences. 2.2E is the only simulation with southerly winds below 925 hPa, and has the weakest northerlies at the jet maximum at 850 hPa. All the free-running simulations have too weak westerlies up to ∼400 hPa. It is not clear, from these simulations, what effect the domain has on the wind in the Arabian Sea. Although the enhanced southerly flow in 2.2E is actually further from the observations and analysis than 8P, the direction of the flow suggests it may be restricted by the lateral boundary conditions, and in a larger-domain simulation might give an enhanced southwesterly flow, in better agreement with analyses. The increased ageostrophic wind seen on the west coast of the Indian peninsula in Figure (c) (over land ∼18°N, 75°E) is consistent with a response to the increased land–sea contrast discussed above. However, differences in latent heating from continental rainfall are larger than the effect on surface fluxes, and are likely the dominant mechanism behind the changes in the circulation. To quantify this, in the period 22–30 August, when the convection-permitting simulations have 'spun up', and the models do not diverge due to synoptic events (Figure), 8E rains 16 mm more than 8P over the subcontinent, which corresponds to ∼47 W m^{-2} atmospheric heating from rainfall, compared to ∼16 W m^{-2} sensible heating from the surface.

Figure (a), (b), (c) shows differences between free-running simulations, while Figure (d), (e) shows differences between free-running simulations and the analysis. The differences

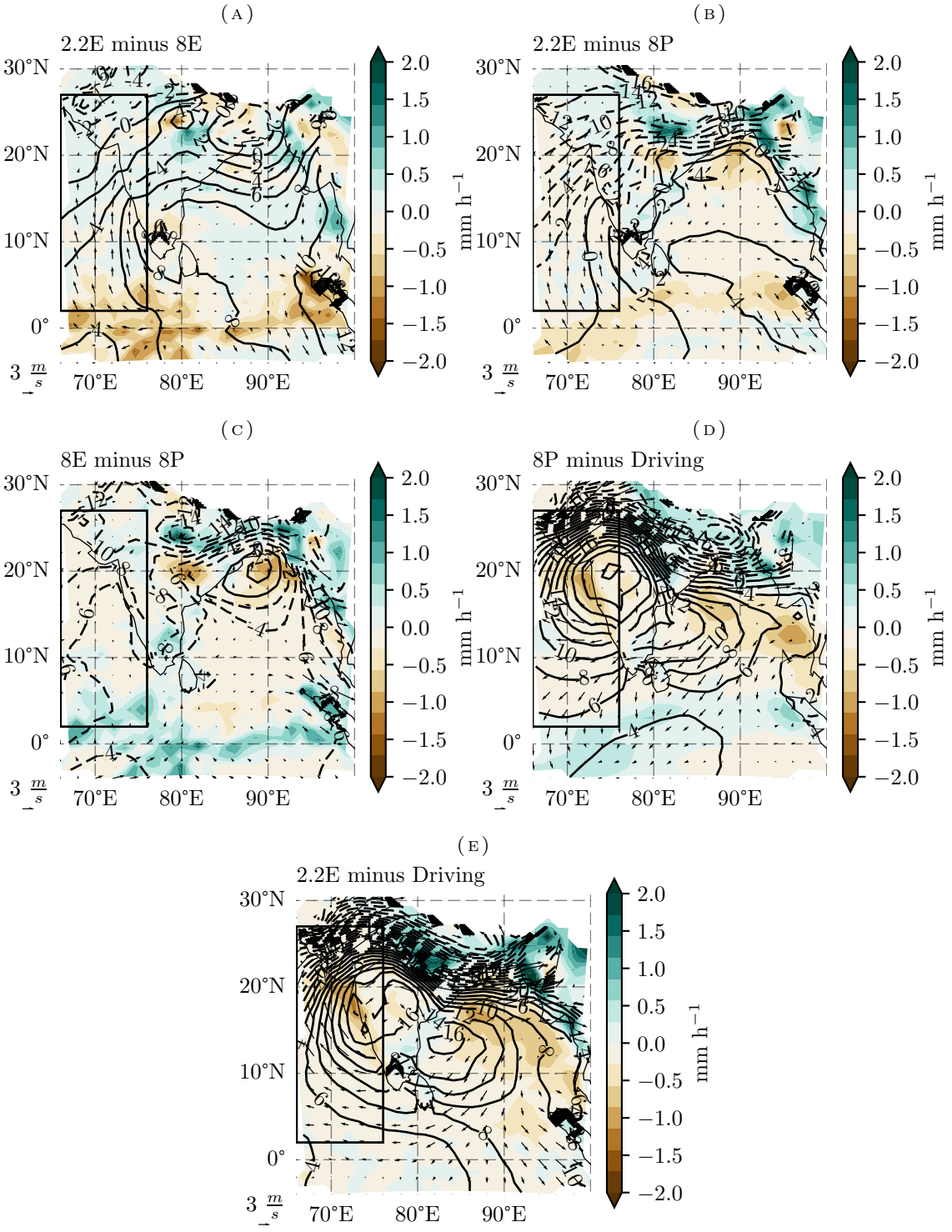

FIGURE : Simulation mean differences of 925 hPa geopotential height (contours, blue/purple contour labels for negative/positive differences), rainfall (colours), and 925 hPa wind vectors, between 22-30 August (Figure), for (a) 2.2E minus 8E, (b) 2.2E minus 8P, (c) 8E minus 8P, (d) 8P minus Driving, and (e) 2.2E minus Driving. The black box denotes an area with significant flow differences, which is discussed in the text. Diagnostics coarse-grained to 120km grid-spacing.

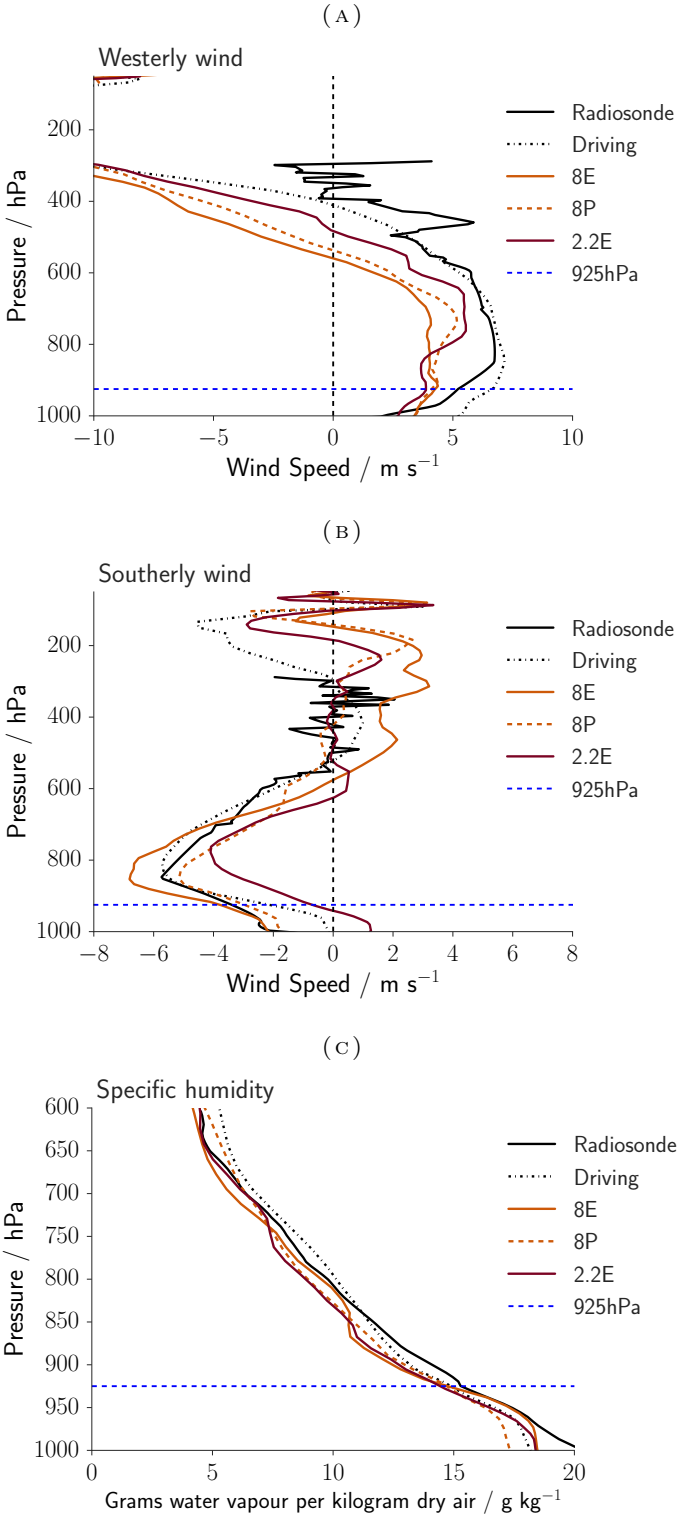

FIGURE : Mean simulated and observed vertical profiles of westerly wind, southerly wind, and specific humidity at Minicoy (Figure), between 22-30 August (Figure). Simulated means from times of actual soundings which at Minicoy is 9 soundings at 0100 UTC (0630 IST). The blue dotted line is 925 hPa, which is the pressure level of the differences in Figures and

in 925 hPa winds between 2.2E/8P and driving are relatively large, compared to the differences between, for example, 8E and 8P: Compared with driving, 8E and 8P show too strong southerlies coming onshore in from the northwest of the domain, and too weak westerlies and southwesterlies into the southern Indian peninsula and the Bay of Bengal respectively. The free-running simulations also have a northeast to southwest dipole of excess to deficient rainfall in the monsoon trough, which match with the wind differences. Although the differences between the free-running simulations and the analysis are large, they are similarly large in 2.2E and 8P, compared to the differences between them.

5.3.2.4 Effect of rainfall on moisture transport

The enhanced low-level monsoon circulation in 2.2E and 8E brings more moisture into the sub-continent, which supports the increased rainfall. Figure (c) shows simulated and observed vertical profiles of specific humidity at Minicoy. While there are large differences in the low-level flow over Minicoy (Figure), the profiles of specific humidity are very similar. As such, differences in the representation of convection and grid spacing do not, in these simulations, have a large impact on the moisture content of air advected over the Arabian Sea, and the change in the transport of moisture into the subcontinent is determined by changes in the flow, not by moisture content.

In previous work using numerical models, excess rainfall over the WEIO has been found to contribute to a dry bias over India, but the mechanisms by which the rainfall biases are reduced are different to those presented here. Bush *et al.* (2015) found that increasing the entrainment factor by 1.5 in the WEIO suppresses precipitation there which, unlike in these simulations, increases moisture in the Somali jet, and increases precipitation over the Arabian Sea and Bay of Bengal, just outside the area of increased entrainment, and over central India by a small fraction of the MetUM bias. One theory is that the meridional SST gradient in the WEIO has a large effect on the distribution of precipitation in simulations of the ISM (Bollasina and Ming, 2013). The SST gradient induces low-level wind convergence, and it is the interaction of the model parametrisation schemes with this large-scale forcing that leads to excess rainfall over the WEIO. In addition to weakening the low-level monsoon flow, Bollasina and Ming (2013) find that excess rainfall over the WEIO induces a Hadley-type circulation which has a descending branch over northeast India/Indochina which, for example, leads to a more gradual onset over India.

5.3.2.5 Effect of rainfall on diurnal cycle of surface pressure

The representation of convection not only affects the mean synoptic pattern of surface pressure (Figure), but also its diurnal cycle (Figure). The simulations are compared here to surface station data, as opposed to model analyses, which are significantly affected by their representation of convection. The diurnal cycle of MSLP at any point depends on atmospheric tides, which are global-scale periodic oscillations of the atmosphere (Woolnough *et al.*, 2004), and have a large amplitude in the Tropics (Basu, 2007). However, the effect of tides is fairly consistent across the model domain and so differences in the diurnal cycle in SLP between two points, especially those on a similar longitude, are dominated by other processes.

Figure shows the simulated and observed diurnal cycle of SLP difference between the monsoon trough and Port Blair (Bay of Bengal) and Minicoy (Arabian Sea). As the SLP for stations above sea level is derived from the measured surface pressure, differences in the magnitude of the pressure gradient are here considered less important than the relative magnitude and timings of the diurnal variation. In both Figure (a) and (b), the most negative land–sea pressure gradient is between 1500 and 1800 IST, at the time of peak rainfall over the continent, which matches well with the convection-permitting simulations, as does the least negative pressure gradient in the morning (1100 IST Port Blair gradient, 0700 IST Minicoy). The parametrised simulations differ much more from the observations: Between the monsoon trough and Port Blair, the largest pressure gradient is around 2100 IST, and between Patna and Minicoy it is around 1200 IST; these are too late and too early respectively. In the parametrised simulations, Minicoy (8.3°N, 73°E) is in a broad region where the diurnal peak in rainfall (Figure (d) is at night, whereas at Port Blair (11.6°N, 92.7°E), the peak is between 0900 and 1200, with the spatial pattern of the diurnal peak timing around Port Blair appearing to be related to the Andaman and Nicobar island chain. The daytime peak in rainfall in the parametrised simulations at Port Blair means that the diurnal cycle of rainfall there is more similar to the diurnal cycle of rainfall at Patna, giving the flatter diurnal cycle in Figure (a) compared to Figure (b).

The results are consistent with the late afternoon heating from moist convection in the monsoon trough region driving a decrease in the pressure over land in the convection-permitting simulations, and increasing the pressure gradient. The land–sea pressure gradient

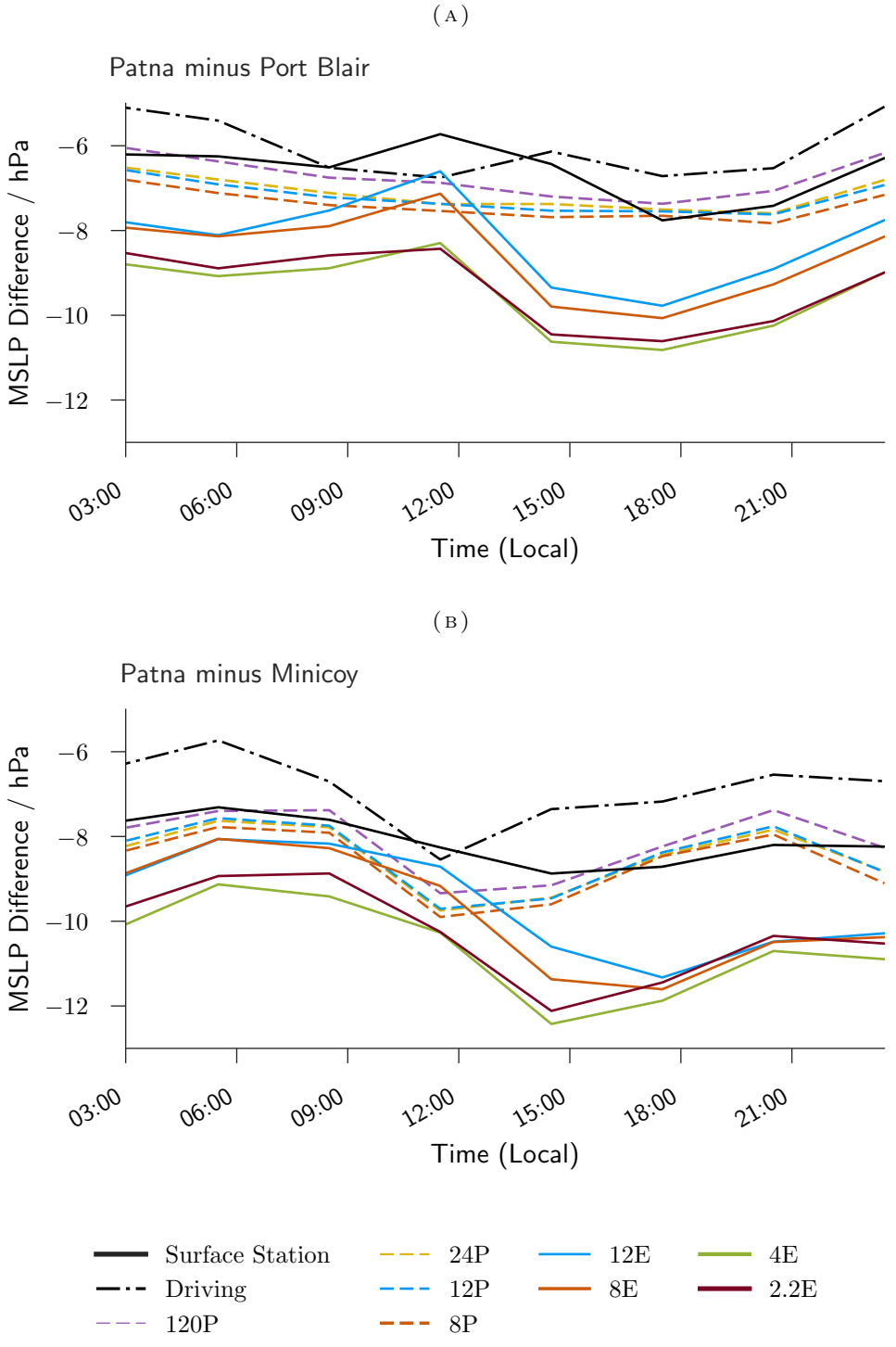

FIGURE : Diurnal cycle of mean sea-level pressure difference between (a)) central India (Patna) and Bay of Bengal (Port Blair), and (b) central India and Arabian Sea (Minicoy). See Figure for station locations. Observations are surface station data.

is then greatest at night, in agreement with the observations, when the drag effect of continental boundary-layer convection is at a minimum. It shows that the ability of the simulations to capture the diurnal cycle of convection is not only important for radiation and surface fluxes (Figure), but also for the dynamical couplings between convection and the larger-scale flows.

5.4 Conclusions

Most global climate models have a systematic dry bias over India during the Indian summer monsoon, a wet bias over the equatorial Indian Ocean and too weak monsoon flow. To investigate the role convective parametrisation plays in the development of these systematic model biases, convection-permitting simulations with grid spacings of 2.2, 4, 8 and 12 km, and convection-parametrised simulations with grid spacings of 8, 12, 24, and 120 km, are compared with model analyses and satellite and ground station observations. The combination of temporal and spatial scales large enough to capture interactions between convection and the large-scale monsoon, and the range of simulation grid-spacings and their treatment of convection allows a novel analysis of the effect of convective biases on the large-scale monsoon. The simulations are of a 3-week period during August and September 2011, with a domain that covers the subcontinent and its surrounding oceans, and captures the monsoon circulation over the subcontinent.

There is more rainfall over the subcontinent in the convection-permitting simulations, which is more intense and peaks later in the day. The 2.2E convection-permitting simulation gives the best representation of the diurnal cycle, and intensity of continental rainfall, compared to the observations. In general, the convection-permitting simulations also capture the day-to-day variability in the amount of rainfall over the continent better.

The convection-permitting simulations rain more, over the subcontinent, than the satellite rainfall retrievals and the parametrised simulations. In the monsoon trough, the convection-permitting simulations rain a similar amount to the satellite rainfall retrievals (which have a much lower spread among them than over the whole subcontinent), while the parametrised simulations rain much less. While the convection-permitting simulations rainfall may be excessive over land, the difference between them and the parametrised simulations has been used here to examine the effects of parametrised convection on the dry bias over India.

The effect of land and ocean rainfall differences between the simulations on the monsoon circulation is shown schematically in Figure . The circulation differences are attributed to differences in both latent heating and sensible heating of the atmosphere, and in the diurnal cycle Higher rainfall over the subcontinent, from more intense convection, increases the land-sea pressure gradient in the convection-permitting simulations and, consequently, the onshore advection of moisture. Higher 925 hPa temperatures over land in the convection-permitting simulations, which contribute to a larger low-level temperature gradient between land and sea, and hence enhanced onshore flow, are consistent with the higher net sensible heating at the surface. The surface heat and radiation fluxes indicate that this is due to greater surface insolation and a drier land surface. There is greater surface solar shortwave heating over land in the 8km convection-permitting simulation compared to the 8km parametrised convection simulation which, because of the later diurnal peak in rainfall, is thought to be due to reduced cloud cover during the middle of the day. Higher sensible and lower latent land surface heat fluxes in 8E compared to 8P indicate a drier surface. That it rains more and more intensely in 8E, but over the land surface the latent heat flux is lower and the sensible heat flux is higher, can be explained by the higher intensity of rainfall, because more rainfall will reach the surface, where it can be lost through run-off and penetration into the soil, rather than being intercepted by the vegetation, where it can be evaporated. As well as a larger land-sea pressure gradient in the convection-permitting simulation the diurnal cycle of the land-sea pressure gradient is also improved, as a result of the improved diurnal cycle of rainfall over land. As a result, the land-sea pressure gradient is enhanced in the late afternoon and at night, when the drag effect of boundary layer convection on the synoptic flow is reduced or nonexistent.

Rainfall over the equatorial Indian Ocean, through its effect on the onshore pressure gradient, is found to contribute to reducing low-level flow and moisture transport into the subcontinent. The 2.2 km convection-permitting simulation rains less than 8P in the Western Equatorial Indian Ocean (WEIO) and, between the convection-permitting simulations, decreasing the grid-spacing from 8 km to 2.2 km substantially reduces the rainfall over the WEIO, in better agreement with the observations. Reduced rainfall there leads to an increase in the onshore pressure gradient, and as a result there is more southerly geostrophic flow onto the Indian peninsula, from the WEIO (Figure). The observed and simulated vertical profiles of specific humidity within these large flow differences do not differ greatly, compared to the wind differences, such that it is the strength of the monsoon circulation and

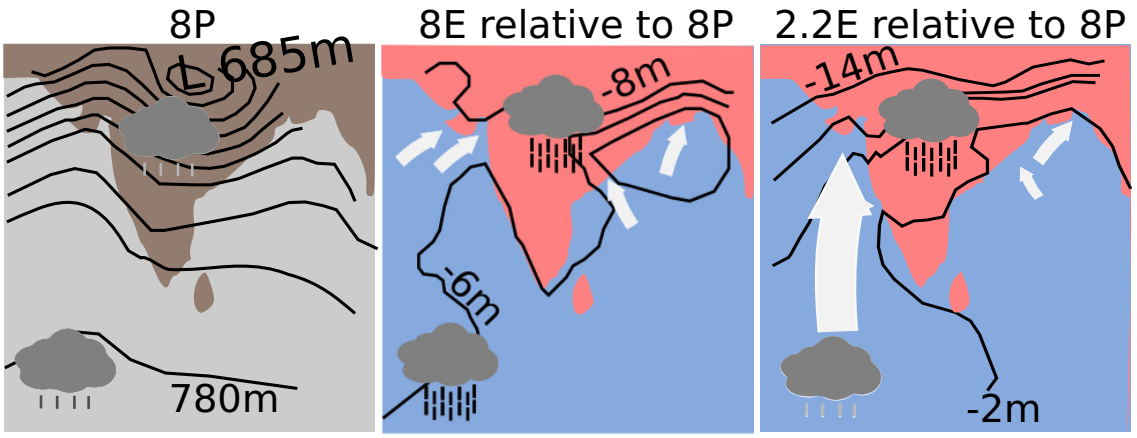

FIGURE : Schematic illustrating relative differences in rainfall (over India and the western equatorial Indian ocean) and 925 hPa height (contours), wind (arrow) and temperature, between 8P, 8E and 2.2E. The left panel shows the 8P 925 hPa mean height structure, while the middle and right panels show the respective height anomaly from 8P. Wind and rainfall are similarly relative to 8P. Darker rain represents more rainfall, with more rainfall coming from more intense events. The colour of the land and ocean in the relative panels represents the relative difference in the 925 hPa potential temperature.

not the moisture content of the flow that is important in reducing biases in the transport of moisture into the Indian subcontinent. However, it is difficult to say how the western boundary of the model domain affects these flow differences. It is possible that in a larger domain simulation, which includes the cross-equatorial Somali jet circulation, reduced rainfall over the WEIO would enhance that flow (which may also become moister) rather than the southerly flow shown here.

The monsoon trough, as seen in the 925 hPa height, is deeper in the convection-permitting simulations, in part because of their different representation of convection, but also because of how they represent the propagation of a Low Pressure System (LPS). In the first 4 days of the simulated period, when the convection-permitting simulations have very excessive rainfall as they spin-up, they have a monsoon trough which is too deep. After this, when the convection-permitting simulations are adjusted to their preferred atmospheric state, they capture the time evolution of the monsoon trough depth for the remainder of the simulated period (22 August to 7 September), whereas the monsoon trough in the parametrised simulations is generally not deep enough. The propagation of a LPS from the Bay of Bengal northwest along the monsoon trough, in the second half of the simulated period (30 August to 7 September), causes significant divergence between the convection-permitting and parametrised simulations, where the convection-permitting simulations capture the daily variability in the analysis, but the height increases significantly in the parametrised

simulations. The divergence appears to be related to differences in the speed of propagation of the LPS in the free-running simulations, with it taking less time to propagate towards the northwest in the parametrised simulations. If models that parametrise convection consistently exhibit a similar bias in the propagation of LPSs, this could contribute to a systematic dry bias in parametrised convection simulations over the subcontinent, and would also have an effect on the onshore moisture transport through a weaker land-sea pressure gradient. Further work is needed to determine if there is a systematic bias in the propagation speed of LPSs in the Indian monsoon trough, as a result of a convective parametrisation.

There are some significant biases in both the convection-permitting and parametrised convection simulations that have not been investigated here. All the simulations overestimate rainfall over the Himalayas and the orography of the Myanmar coastline, and underestimate rainfall over the WG. They also fail to capture the broad spread of rainfall over the Bay of Bengal. In some respects, the convection-permitting simulations perform worse than the parametrised simulations, particularly at coarser grid-spacings. For example, 2.2E rainfall over the Indian Ocean is comparable to TRMM, but as grid-spacing increases, rainfall in the convection-permitting simulations becomes increasingly excessive, while there is little effect due to grid-spacing in the parametrised simulations, which have rainfall amounts comparable to 4E.

The MetUM, in common with many models has had a long-standing dry bias over India during the monsoon. The results show that an explicit representation of convection affects the entire monsoon circulation, increasing rainfall in the monsoon trough region, and improving key aspects of the circulation such as the magnitude and diurnal cycle of pressure gradient from the oceans to the continent.

In conclusion, it is important for any parametrisation of convection to capture its diurnal cycle, and give an improved representation of rainfall intensities over the Indian subcontinent and the western equatorial Indian Ocean, if they are to give a realistic coupling between convection and the monsoon.

Chapter 6

Propagation of rainfall upstream of the Western Ghats

6.1 Introduction

The Western Ghats mountain range on the west coast of India acts as a barrier to the south-westerly summer monsoon winds that cross the Arabian Sea. Rainfall is concentrated upstream of the mountains and within the Indian monsoon the amount of rainfall here is the second-highest, after the rainfall in the north Bay of Bengal, which is concentrated upstream of the orography of the Myanmar coast (Figure and Xie *et al.* (2006)). Theories exist to explain the in situ enhancement of rainfall offshore, upstream of the Western Ghats (e.g. Grossman and Durran, 1984; Smith, 1985; Zhang and Smith, 2018), but none include offshore rainfall propagation. In other tropical regions, the diurnal cycle causes rainfall to propagate offshore from near the coast. Therefore, in this chapter observations and models are used to explore, for the first time, the role of offshore propagation in the observed offshore rainfall distribution.

In the Asian monsoon, latent heat release through the formation of rain interacts in significant ways with the basic monsoon flow (e.g. Webster and Chou, 1980; Willetts *et al.*, 2017a). Coastal mesoscale orography is highly effective in organising convection throughout the tropics, and understanding how it does so has important implications for improving the representation of convection-circulation interactions within the monsoon. For example,

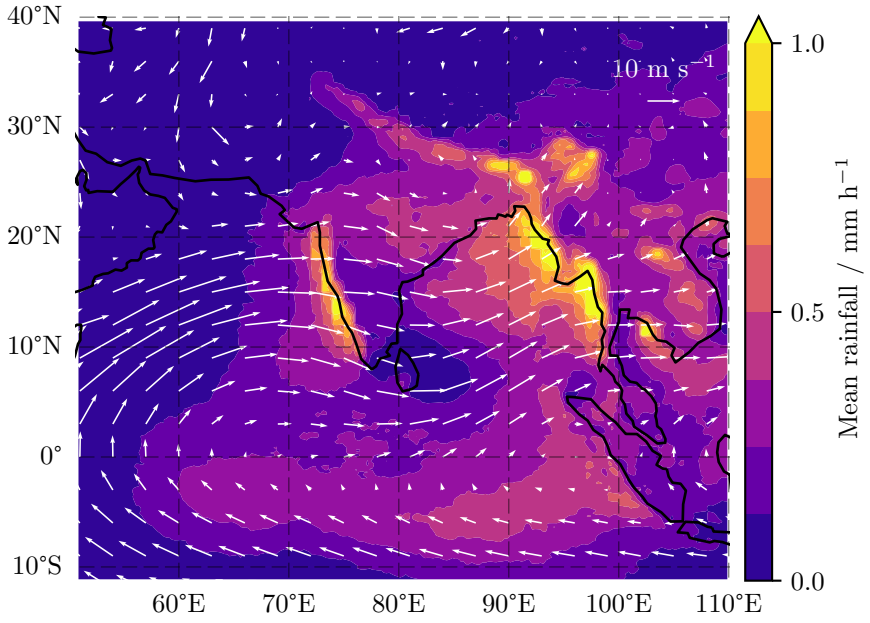

FIGURE : Climatological mean TRMM 3B42 rainfall and ERA-Interim 850 hPa wind (June-September 1998-2015)

Xie *et al.* (2006) showed how imposing narrow bands of diabatic heating upstream of the Myanmar coast and other mesoscale mountain ranges in the tropics improved the representation of monsoon rainfall by intensifying the hydrological cycle which in turn induced a lower tropospheric cyclonic circulation around India.

A climatology of retrievals from the precipitation radar on the TRMM satellite shows a rainfall maximum on the windward slopes of the Western Ghats, around 500m above sea level (Shrestha *et al.*, 2015). There is also a secondary peak over the sea, a few kilometres from the coast. The majority of rain is convective. This is in contrast to the tendency, in the tropics, for precipitation maxima to be in large regions of stratiform rainfall that develop as a result of extreme convective events (Romatschke and Houze Jr, 2011; Shrestha *et al.*, 2015). The rainfall on the windward slopes results primarily from a high frequency of weak convective events, which do not develop large stratiform regions. The most intense rainfall (>4 mm h^{-1}) is primarily observed offshore, where the precipitation columns are also deeper than over the mountain slopes.

Prevailing theories to explain offshore rainfall upstream of the Western Ghats do not include the offshore propagation of rainfall. This is perhaps understandable given the mean environment of strong monsoon westerlies over the Arabian Sea and that, to the author's knowledge, observational experiments over the eastern Arabian Sea have only

documented quasi-stationary or east to south-eastward moving storms (Roadcap and Rao, 1993). Grossman and Durran (1984) hypothesised that deceleration of the monsoon flow due to the blocking effects of the mountains could provide enough gentle lifting of potentially unstable air for deep convection to initiate over the sea. Smith (1985) argues, partly based on previous work (Smith and Lin, 1982, 1983) that Grossman and Durran (1984) chose to ignore the effects of background wind shear, the boundary layer, the Coriolis force, and latent heating in their theoretical model, all of which could be more important in bringing about deep convection over the sea. Using a two-dimensional, compressible moist cloud model, Ogura and Yoshizaki (1988) bypass some of the limitations in these previous studies and find that including the effects of vertical shear gives a more accurate representation of the estimated rainfall amounts, and including the sensible and latent heat fluxes from the ocean correctly places the deep convection over the sea, and not over the coast during times of offshore convection. More recently, another modelling study (Zhang and Smith, 2018) finds that the occurrence of offshore rainfall is controlled by incoming Convective Available Potential Energy (CAPE), the entrainment of mid-tropospheric dry air in the monsoon westerlies over the Arabian Sea, and the latent heat flux and Sea Surface Temperatures (SSTs) of the Arabian Sea. They say offshore convection is not triggered by the Western Ghats. Based on observations from the INCOMPASS field campaign, Fletcher *et al.* (2018) also find that offshore convection is only weakly associated with orographic blocking by the Western Ghats, secondarily associated with SSTs, and primarily with mid-tropospheric humidity.

To fully explain the rainfall upstream of the Western Ghats will require considering temporal and spatial variability on a range of scales. Non-periodic Monsoon IntraSeasonal Oscillations (MISOs), which take 30-60 days to propagate north-eastward from the Indian Ocean, dominate intraseasonal variability in the Indian monsoon, so much so that the number that occur each year can influence the interannual variability (e.g. Annamalai and Sperber, 2005). Hoyos and Webster (2007) show that the northward propagating cyclonic circulations of MISOs drive moist air towards the Western Ghats, which considerably enhances the upstream rainfall. The location of the rainfall maximum varies between the windward slopes and offshore, on timescales upwards of a few days. Whether convection occurs primarily over land or offshore at a certain time could be influenced by a number of factors, including mid-level dry intrusions, Arabian sea surface temperatures and sensible and latent heat fluxes, and circulation factors such as the strength and depth of the monsoon westerlies and

wind shear (Grossman and Durran, 1984; Smith, 1985; Ogura and Yoshizaki, 1988; Fletcher *et al.*, 2018; Zhang and Smith, 2018).

In the tropics, diurnal rainfall often moves offshore from coastlines (e.g. Yang and Slingo, 2001). This can result from a number of different mechanisms, such as land-sea breezes (Houze *et al.*, 1981), gravity waves generated by convection (e.g. Yang and Slingo, 2001; Mapes *et al.*, 2003; Love *et al.*, 2011), cold gravity currents that form under developed convection, and advection by the background wind flow. In the modelling studies of Smith and Lin (1983); Grossman and Durran (1984); Ogura and Yoshizaki (1988); Zhang and Smith (2018) diurnal effects were not considered, in part because the diurnal cycle has been found to be small compared to other high rainfall regions in the tropics (e.g. Romatschke *et al.*, 2010).

This chapter examines rainfall propagation upstream of the Western Ghats. This begins with a comparison of the propagation in model simulations and satellite rainfall retrievals. The main aim of the work, though, is to understand the role of rainfall propagation in determining the distribution of rainfall upstream of the Western Ghats. This involves characterising, to some extent, the nature of the rainfall propagation and its relationship to local and large-scale intraseasonal variability and to the diurnal cycle. From this some hypotheses to explain the climatology and intraseasonal variability in the rainfall propagation are proposed.

§ 6.2 describes the model simulations, observational data sets, and methodologies. In the Results section (§ 6.3), § 6.3.1 compares, in 2 case-study periods, convection-permitting and parametrised simulation representations of rainfall in the Western Ghats region with observations, § 6.3.2 uses climatological data sets to characterise rainfall propagation, and the environment in which it does so, upstream of the Western Ghats, and § 6.3.3 then looks at how variability in the direction of rainfall propagation is linked to large-scale intraseasonal variability. Finally, § 6.4 provides a summary of the results.

6.2 Methods

In this chapter, the MetUM 2011 2.2E and 8P and 2012 2.2E and 10P simulations, ERA-Interim reanalysis, CMORPH satellite rainfall retrievals, and radiosonde datasets are used

here (Chapter 3). In addition, the TRMM 3B40RT satellite rainfall retrieval product (Huffman *et al.*, 2007), which uses only merged (i.e multi-satellite) microwave estimates, has been used to compare diurnal cycles of rainfall, as there is potential for a systematic bias in rainfall propagation in CMORPH as result of the use of infrared data in its retrieval algorithm, which could conceivably overestimate precipitation from cold anvil clouds.

CMORPH was chosen as the primary observational dataset for estimates of rainfall estimate in this study because of its relatively high spatial and temporal grid-spacing (8 km and 0.5 hourly). Another commonly used product is The Tropical Rainfall Measuring Mission (TRMM) Multisatellite Precipitation Analysis (TMPA)-3B42 (version 7) rainfall product (Huffman *et al.*, 2007), which also includes, in addition to multi-satellite microwave and infrared rainfall retrievals, rainfall estimates from the precipitation radar on the TRMM satellite, but the 3-hourly 0.25x0.25 km grid spacings were thought to be unfavourably coarse in the context of this study.

6.2.1 Space-time spectral analysis

The method used here decomposes CMORPH rainfall data into wavenumber and frequency components for eastward and westward propagation (Hayashi, 1982), in a 5° wide region west of and running perpendicular to the Western Ghats ('FFT region' in Figure). Before further processing, the data are lowpass filtered in time and space, close to the respective spatial and temporal Nyquist frequencies to avoid aliasing. For each latitude within the 5° wide domain, following the method of Wheeler and Kiladis (1999), the data are split into 96 (48 hours) or 480 timestep (10 days) overlapping segments, which each have 68 longitudinal points. For each segment the mean and linear trend are removed in time using a linear least-squares fit and a Blackman filter applied to taper the edges to zero. The complex Fast Fourier Transforms (FFTs) are then taken in longitude and then time, to obtain the space-time frequency spectrum of that segment. The CMORPH data have an 8km and 30 minute resolution, and with the chosen 68 and 96 spatial and temporal sample lengths, the frequency domain resolution (Fs/N where Fs is the sampling rate, and N is the sample length) is ∼0.19/100km (19km wavelength) and 0.5/day (12 hour period). For the 480 segment lengths, the frequency domain resolution is 0.1/day (2.4 hour period). The 96 length segment FFTs have been used where assessments of the time domain variability are important, and the 480 segment length FFTs have been used where higher frequency

domain resolution is more important. To composite a subset of the segments, the time means of the segment's spectral power are taken for each latitude, which are then summed.

6.2.2 Defining periods with the most offshore or onshore storm propagation

In order to define periods with the most offshore or onshore propagation, a time-series of the fraction of offshore propagation to all propagation is constructed from 2-day or 7-day means of the CMORPH frequency-wavenumber spectrum in the 5° wide FFT region (dashed box in Figure), for the years 1998-2015. The power of negative wavenumbers (offshore propagation) over the total power gives the fraction of offshore propagation. Periods outside the upper and lower 25th percentile of the fraction are defined as 'offshore' and 'onshore' periods. Composites of 2-day 'offshore' and 'onshore' periods are used everywhere other than § 6.3.3 which looks at large-scale intraseasonal variability and uses 7-day period composites, to give a clear display of the relationship of 'offshore' and 'onshore' periods to variability on

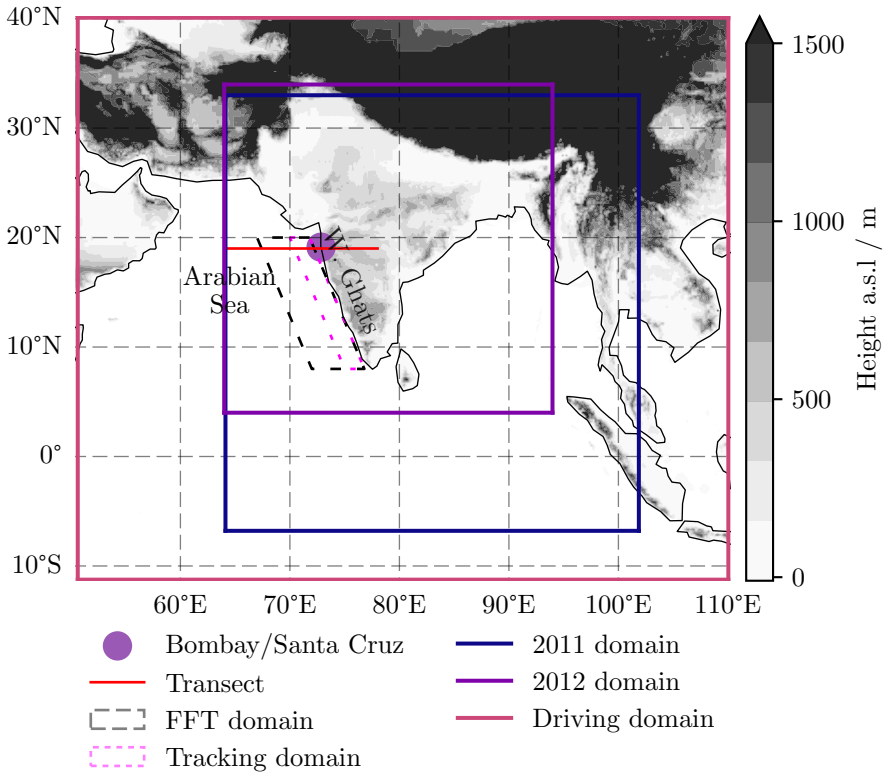

FIGURE : MetUM model simulation domains, regions where storm tracking and wavenumber-frequency spectrum processing (FFT) have been applied to CMORPH data, transect at 19°N, and the location of the Bombay / Santa Cruz radiosonde station. Shading shows orographic height (m).

those timescales. As will be explained in more detail in § 6.3.3, only the years 2001-2014 are used in that section, to exclude years with strong El Niño (1998, 2015) or La Niña (1999, 2000) effects.

6.2.3 Storm tracking

Storm tracks were obtained from the CMORPH and MetUM model output rainfall (after coarse-graining to the CMORPH grid) using the alogrithm developed by Thorwald Stein (University of Reading) and described in Stein *et al.* (2014). Storm clusters are identified at each timestep as contiguous grid cells passing a certain threshold requirement. A precipitation threshold of 1 mm h^{-1} was used here, as in Stein *et al.* (2014). To track the propagation of storms, a velocity field is calculated by cross correlation of images at times t_{i-1} and t_i. The velocity field is used to advect the storms at time t_{i-1}, before calculating their areal overlap with storms at time t_i The amount of areal overlap is used to determine if they are the same storm, if a storm has newly initiated, if a storm has dissipated or if there are split initiations from a parent storm or storms have merged. Storm speeds are calculated from the between timestep difference in the storm centre point.

6.2.4 Tropical modes

The relationship of rainfall propagation to tropical wave modes is examined using the algorithm of Roundy (2012), which projects interpolated NOAA Earth Systems Research Laboratory OLR retrievals (Liebmann and Smith, 1996) onto equatorial wave patterns. The algorithm produces a gridded time series of coherent structures that are within the zonal wavenumber-frequency domains of major tropical wave modes, such as the Madden-Julian Oscillation (MJO).

6.3 Results

6.3.1 2011 and 2012 case-study periods: Bias in convection-permitting and parametrised convection simulations

In the two case-study periods, there is significant disparity between modelled and observed rainfall propagation, both upstream of the Western Ghats and over the Indian monsoon region in general. This is first examined for rainfall upstream of the Western Ghats, in longitude-time sections of rainfall and wind profiles where the section crosses the coast. Storm tracking results are then used to examine the spatial patterns of propagation over the Indian monsoon region in general.

6.3.1.1 Rainfall hovmöllers and wind profiles

Figures and show, for 18 August to 7 September 2011, and 25 June to 15 July 2012 respectively, rainfall Hovmöllers along a meridional transect at 19°N which crosses the Western Ghats and the concurrent time evolution of westerly wind profiles (ERA-Interim) at a similar latitude near the coast (Figure). In CMORPH, much of the time the rainfall propagates westward or offshore (Figure (a), Figure (a)). In the '2.2E' 2.2km convection-permitting simulations, there is a consistent pattern of rainfall moving eastward (or onshore) with speeds of ∼10 m s^{-1} (Figure (b), (b)). In the simulations with parametrised convection the '8P' 8km 2011 simulation exhibits mostly no propagation and some onshore propagation (Figure (c)), while the '10P' 10km 2012 simulation does show one instance of rainfall propagating offshore, in better agreement with CMORPH (Figure (c)).

The CMORPH rainfall Hovmöller for the 2011 period (Figure (a)) shows variability in the location and propagation speed and direction of rainfall. In the first half of the 2011 period, from 18-26 August 2011 (lighter shaded period), rainfall propagates westward at speeds of ∼10 m s^{-1}, and begins and is mostly over land. After 26 August, there is an apparent mix of onshore and offshore propagation. Around 27-28 August 2011 there are features propagating offshore from a rainfall maximum close to the coast, with a range of possible speeds (∼5-15 m s^{-1}). Later, from ∼1 September 2011 (in the darker shaded period), offshore rainfall at ∼100km along transect moves slowly eastward towards the coast (to ∼400km along transect on 3 September, with a speed of <5 m s^{-1}), and then there is a

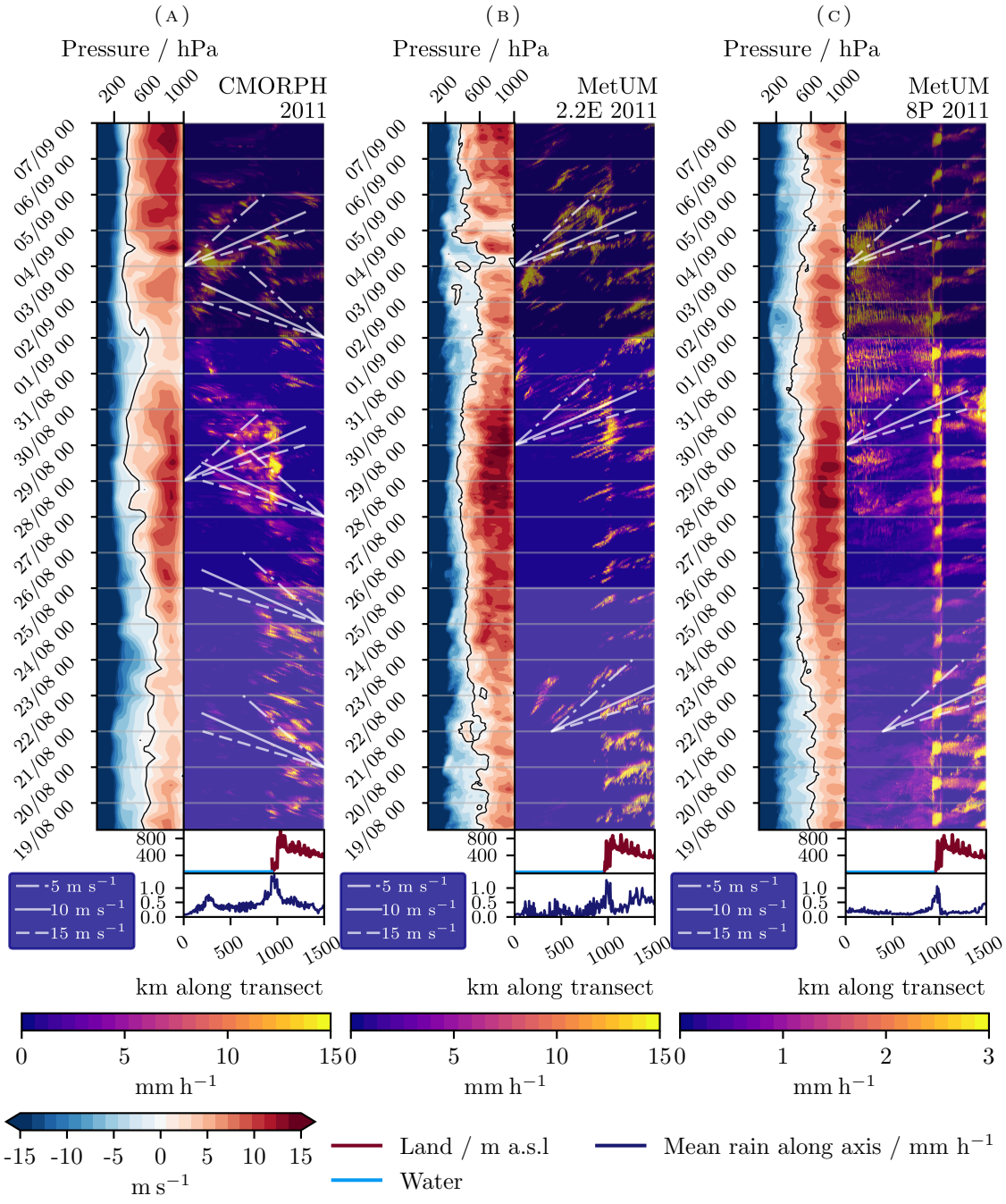

FIGURE : Observed and modelled time-longitude rainfall sections along 19°N transect (1° meridional width) and westerly wind time-pressure sections at nearest model grid point to Bombay/Santa Cruz radiosonde station, for 18 August to 7 September 2011. (a) shows CMORPH rainfall and the ERA-Interim westerly wind section. (b) is from the 2.2E simulation and (c) is from the 8P simulation. In each panel, the filled contours in the top right subfigure show the rainfall Hovmöller and to their left is the westerly wind section. Lines on the rainfall Hovmöllers show some propagation speeds. The bottom 2 line plots in each panel show the topography and mean rainfall for the period along the transect. Light shading in the rainfall transects indicates periods with clear offshore propagation, and dark shading indicate periods with less clear offshore propagation (where there may also be onshore propagation). Figure shows the location of the transect and Bombay/Santa Cruz radiosonde station.

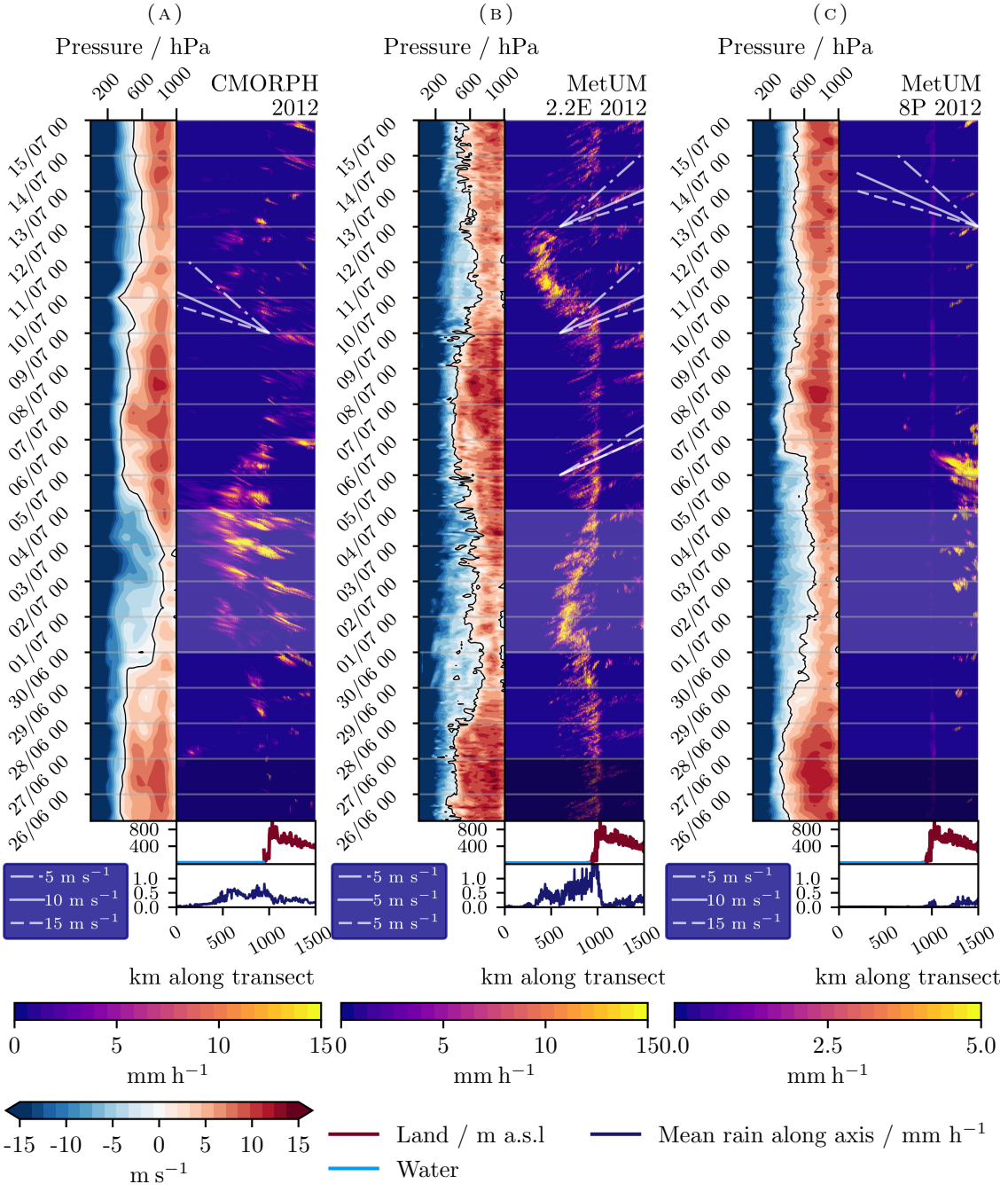

FIGURE : As Figure , but for 25 June to 15 July 2012. (a) shows CMORPH rainfall and ERA-Interim westerly winds. (b) is from the 2.2E simulation and (c) is from the 10P simulation.

rainfall maximum close to the coast on 3 September. This pattern, after 1 September, is formed from smaller-scale events which show offshore rainfall propagation with speeds of 5-15 m s^{-1}.

The biases in rainfall propagation in the convection-permitting simulations, from these rainfall Hovmöller are clearest for rainfall propagation at speeds of 10-15 m s^{-1}. When rainfall propagates offshore at these speeds in CMORPH, rainfall propagates onshore at similar speeds in the simulations. For slower rainfall propagation, there is some agreement between CMORPH and the 2011 2.2E simulation for the <5 m s^{-1} onshore propagation of rainfall in the later, dark shaded period (Figure (a),(b)).

In the observations, there is a relationship between the temporal variations in the westerly wind profile near the coast and in the rainfall propagation along this transect. The CMORPH rainfall transects and ERA-Interim winds (Figure (a) and Figure (a)) indicate that, in this region, weaker and/or shallower low-level westerly monsoon flow and deeper easterlies above are related to offshore rainfall propagation and stronger and/or deeper westerlies are related to onshore propagation. In the 2011 period, deeper easterlies and weaker and shallower westerlies (18-27 August and 30 August to 1 September 2011), correspond to periods of clearer offshore propagation. Conversely, when the monsoon westerlies are strongest and deepest, from 27-30 August and from 1-5 September 2011, there is an apparent mixture of offshore and onshore propagation. In the 2012 period, the westerly monsoon winds weaken and substantially shallow in height from 29 June-04 July, which is also when, perhaps lagged by 1-2 days, the rainfall markedly increases and shows clear offshore propagation. This relationship is examined in a climatological sense in § 6.3.2.

The differences in rainfall propagation between the observations and the simulations could be due to a bias in the representation of the strength and depth of the monsoon westerlies and of the easterlies above. The mean wind profile at Bombay/Santa Cruz for the 2011 period (Figure (a)), shows that the the 2.2E convection-permitting simulation does have stronger westerlies from near the surface to ∼425 hPa, compared to radiosonde soundings, MetUM analysis, ERA-Interim and the 8P parametrised simulation. In the 2012 period (Figure (b)), unlike in the 2011 period, the radiosonde profile shows substantially weaker westerlies than the MetUM analysis and ERA-Interim. There are also some quite large differences between the radiosonde and analysis/reanalysis southerly wind profiles, between ∼600-300 hPa in the 2011 period (Figure (a)) and between ∼850-625 hPa in the 2012

period (Figure (b)). The differences makes it difficult to make any firm conclusion about a systematic bias in the 2012 2.2E westerly profile because it is comparable to, or weaker than ERA-Interim above ∼825 hPa. From the surface to ∼825 hPa, there is a similar bias in both the 2011 and 2012 periods, however, where the 2.2E westerlies are ∼3 m s^{-1} stronger than the radiosondes and analysis/reanalysis. Whether such a wind bias could be a major factor in the differences in rainfall propagation is unclear.

6.3.1.2 Storm Tracking

The pattern, in the Hovmöller rainfall transects (Figure &), of mostly offshore (or westward) rainfall propagation in CMORPH, and onshore propagation in the 2.2E convection-permitting simulations is widespread, as illustrated by Figure , which shows the number of times that tracked storms move eastward and westward in the 2011 and 2012 2.2E simulations and in the matching periods in CMORPH. In both the 2011 and 2012 convection-permitting simulations, there is a pattern of predominantly eastward moving storms in the eastern Arabian Sea, in the equatorial Indian Ocean, and over much of India (Figure (b) &(f)), with a peak close to or over the Western Ghats. Much fewer storms move westward (Figure (a) &(e)). In CMORPH, by contrast, there are relatively very few storms moving eastward over the domain (Figure (d),(h)), compared to the number of storms moving westward (Figure (c) &(g)).

6.3.2 Climatology

In the 2011 and 2012 case-study periods in § 6.3.1, there is a discrepancy between CMORPH and the convection-permitting simulations for rainfall propagating at speeds of ∼10-15 m s^{-1}. This motivates the rest of the work presented in this chapter, which characterises the climatological nature of the rainfall propagation in CMORPH, using storm tracking and wavenumber-frequency spectral analysis, and an examination of the diurnal cycle. It is also possible that the discrepancy between the simulations and observations is due to a bias in CMORPH, and this is addressed this by use of the TRMM microwave only product in the diurnal cycle section § 6.3.2.3. Throughout this section some hypotheses are also outlined, based on the climatological observations, to explain the rainfall propagation.

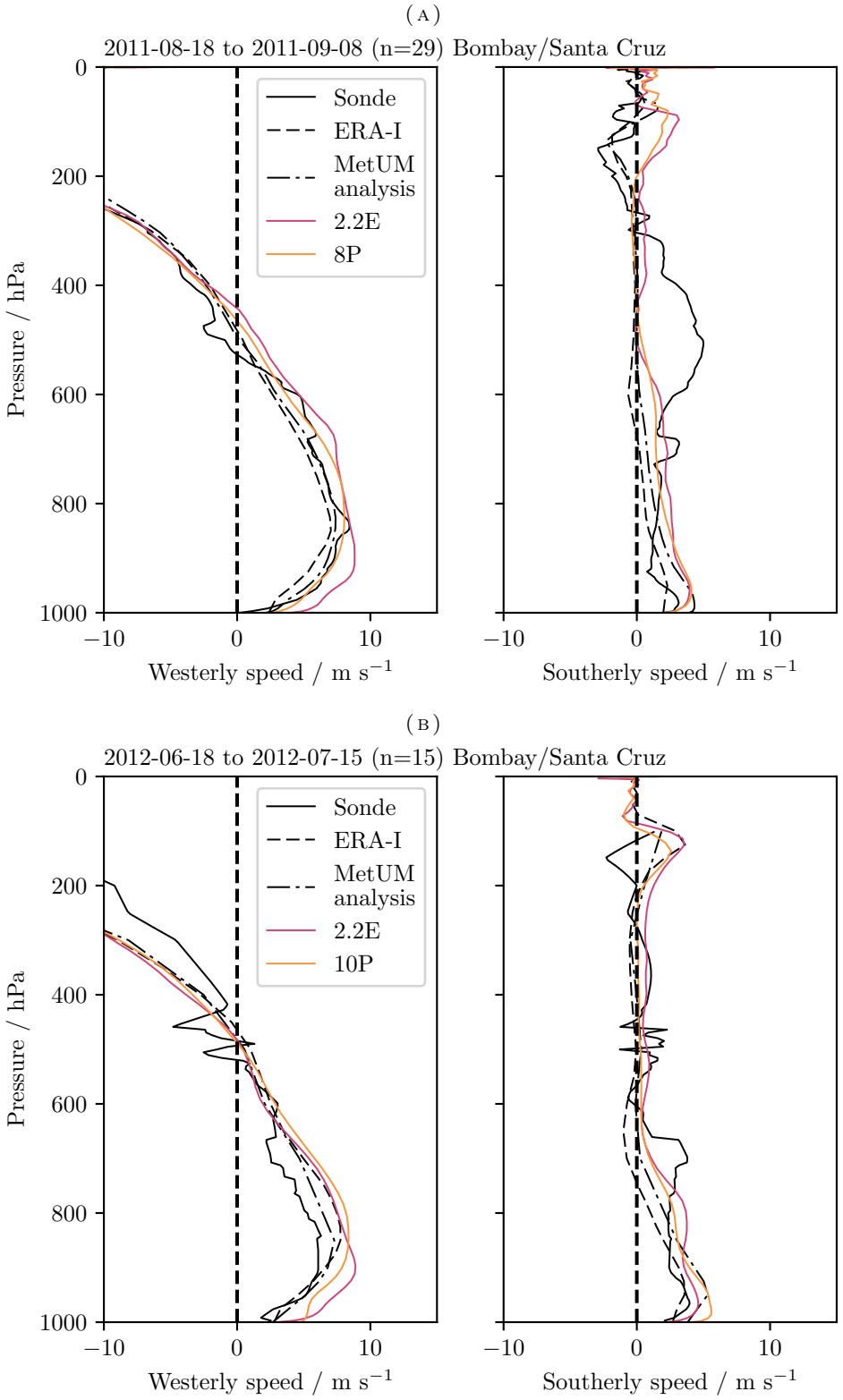

FIGURE : Mean model, analysis, reanalysis and radiosonde westerly and southerly wind profiles at Bombay/Santa Cruz (or the nearest model grid-point to it) for (a) the 2011 simulated period and (b) for June 18 to July 15 in the 2012 simulated period. The wind profiles obtained from model output are averaged from the wind profiles at timesteps nearest to the radiosonde sounding times. 'n' is the number of radiosonde soundings. Figure shows the location of Bombay / Santa Cruz.

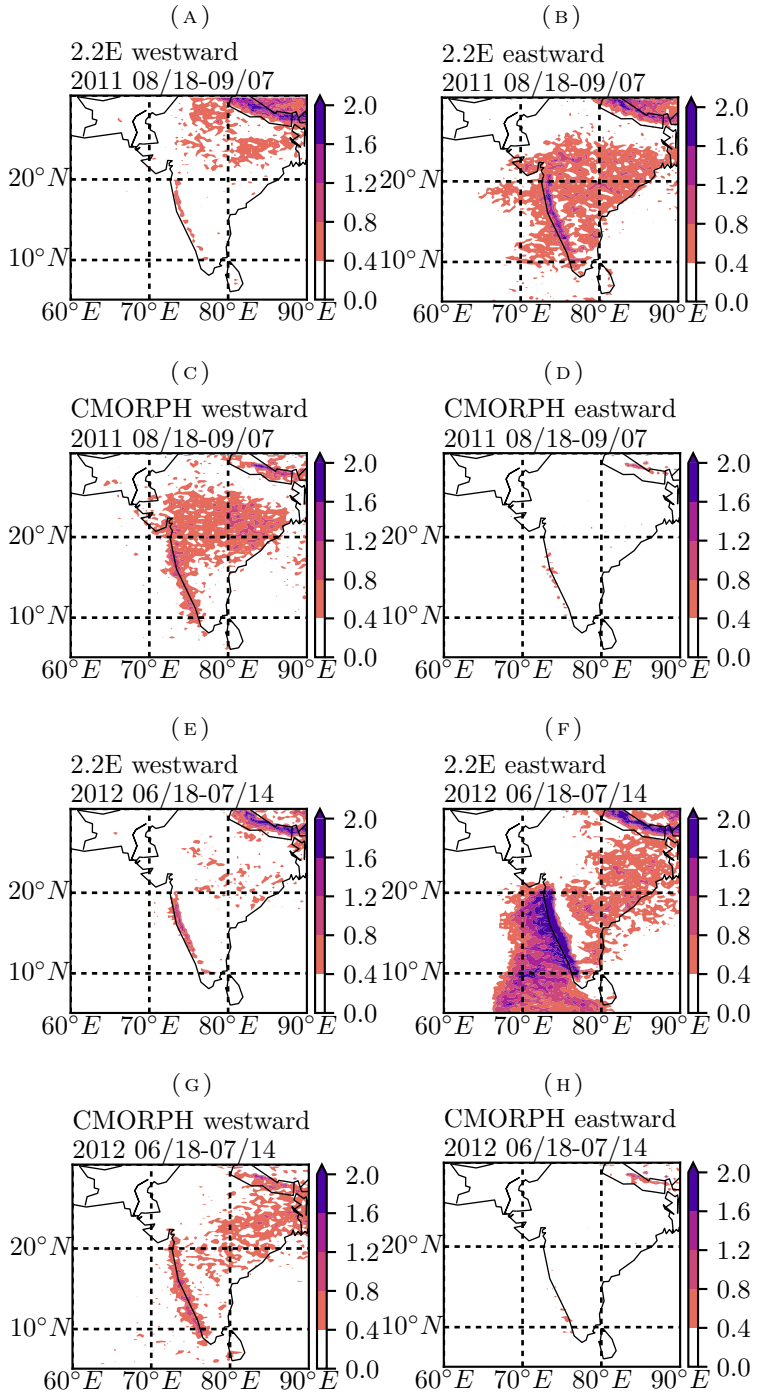

FIGURE : The average number of storms in the 2.2E MetUM simulations and CMORPH, in ∼24km grid boxes, which propagate westward or eastward. (a) and (b) are for westward and eastward propagation respectively, from the 2.2E simulation for 18 August to 7 September 2011. (c) and (d) show westward and eastward propagation respectively, from the same 2011 period in CMORPH. Likewise, (e) and (f) are for westward and eastward propagation respectively from the 2.2E simulation, for 18 June to 14 July 2012, and (g) and (h) are for westward and eastward propagation for the same 2012 period in CMORPH. The zonal storm propagation directions are determined by storm tracking, which is described in § 6.2.3). The 2.2km model and 8km CMORPH storm tracking counts have been coarse-grained, by area-weighted averaging, to the Driving simulation grid-spacing of ∼24km.

6.3.2.1 Mean storm propagation characteristics

It is useful to first consider the contribution of propagating rainfall to the total rainfall upstream of the Western Ghats. Figure shows, from storm tracking applied to the CMORPH climatology, the relative amounts of rainfall that come from storms moving at certain velocities, in a 5° wide polygon upstream of the Western Ghats (Figure). Rainfall upstream of the Western Ghats comes mostly from stationary storms, or storms that move offshore at speeds of up to 15 m s^{-1}. The major axis of the distribution is aligned towards WSW, which is consistent with storms moving offshore approximately perpendicular to the coast. Contributions to rainfall upstream of the Western Ghats come almost equally from storms that are close to stationary (1.0 on normalised scale), storms that move westward at 2-6 m s^{-1} (1.0), storms moving southward or SSW at speeds of 2-6 m s^{-1} ($\sim$0.5 southward + $\sim$0.5 SSW), and storms moving westward at speeds >6 m s^{-1} ($\sim$0.7 at 6-11 m s^{-1} + $\sim$0.3 at 11-15 m s^{-1}).

A pertinent question is how much the histogram of offshore propagating storm speeds is composed of storms that initiate near the coast as opposed to storms that initiate away from the coast. Figure shows a large majority of offshore storms that rain heavily away from the coast initiate in situ. This is true both for storms (Figure) above the 90^{th} and 50^{th} percentiles of storm rainfall amounts between 500 and 750 km along transect (Figure (a) & (b), respectively) It also shows that, where the storm tracking finds a chain of parent and child storms (where a storm splits from another), a large majority of the first parent storms also initiate well offshore, but the peak is closer to shore. There is a local minimum between the offshore peaks, and a much smaller peak over the coast. It may be that, through other processes such as gravity waves, convection that initiates near the coast causes parcels of convection to propagate offshore, but the tracked storms in CMORPH do not show a large number of storms propagating offshore for long distances from near the coast. In conclusion, offshore propagation of rainfall does not appear to be significantly caused by the movement of individual storms from land to sea. Instead, it is influenced by the offshore movement of storms which have initiated over the sea.

The speeds of tracked storms in Figure show a near east-west orientation to the propagation, which motivates an analysis of the zonal wavenumber-frequency spectrum of rainfall upstream of the Western Ghats. Figure shows the zonal frequency-wavenumber log(power)

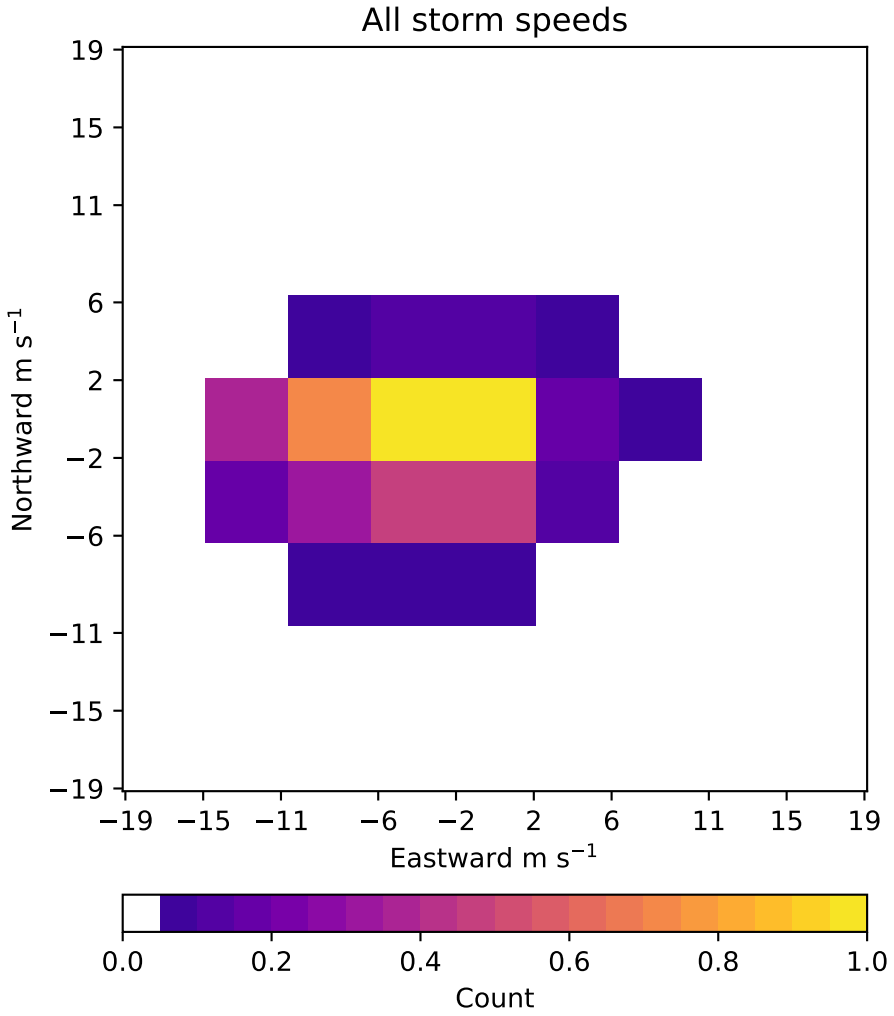

FIGURE : Normalised histogram of climatological mean storm rainfall amounts from tracked storm areas in CMORPH moving at certain velocities. The mean rainfall amounts in the histogram are normalised to a fraction of the highest mean rainfall amount in the histogram. The tracked storms are from June through September 2000-2015 and the 'tracking' domain in Figure .

spectrum of CMORPH rainfall within a 5° wide domain running perpendicular to the Western Ghats, over the sea (Figure). The power spectrum peaks for both offshore and onshore propagation are centred on zero wavenumber and frequency. There is more power in the negative, offshore wavenumbers than onshore power at these lower wavenumbers and frequencies (consistent with the case study patterns of rainfall propagation CMORPH shows in Figure (a) & (a)). At frequencies $<$ ∼2/day, the peak in the power spectrum for negative wavenumbers (offshore propagation) is at 0.11/100km (the lowest resolved wavenumber), at a range of speeds from $<$5 m s^{-1} to ∼15 m s^{-1}. At frequencies $>$∼2/day (period $<$∼12 hours), there is a peak in the negative wavenumber propagation at speeds of

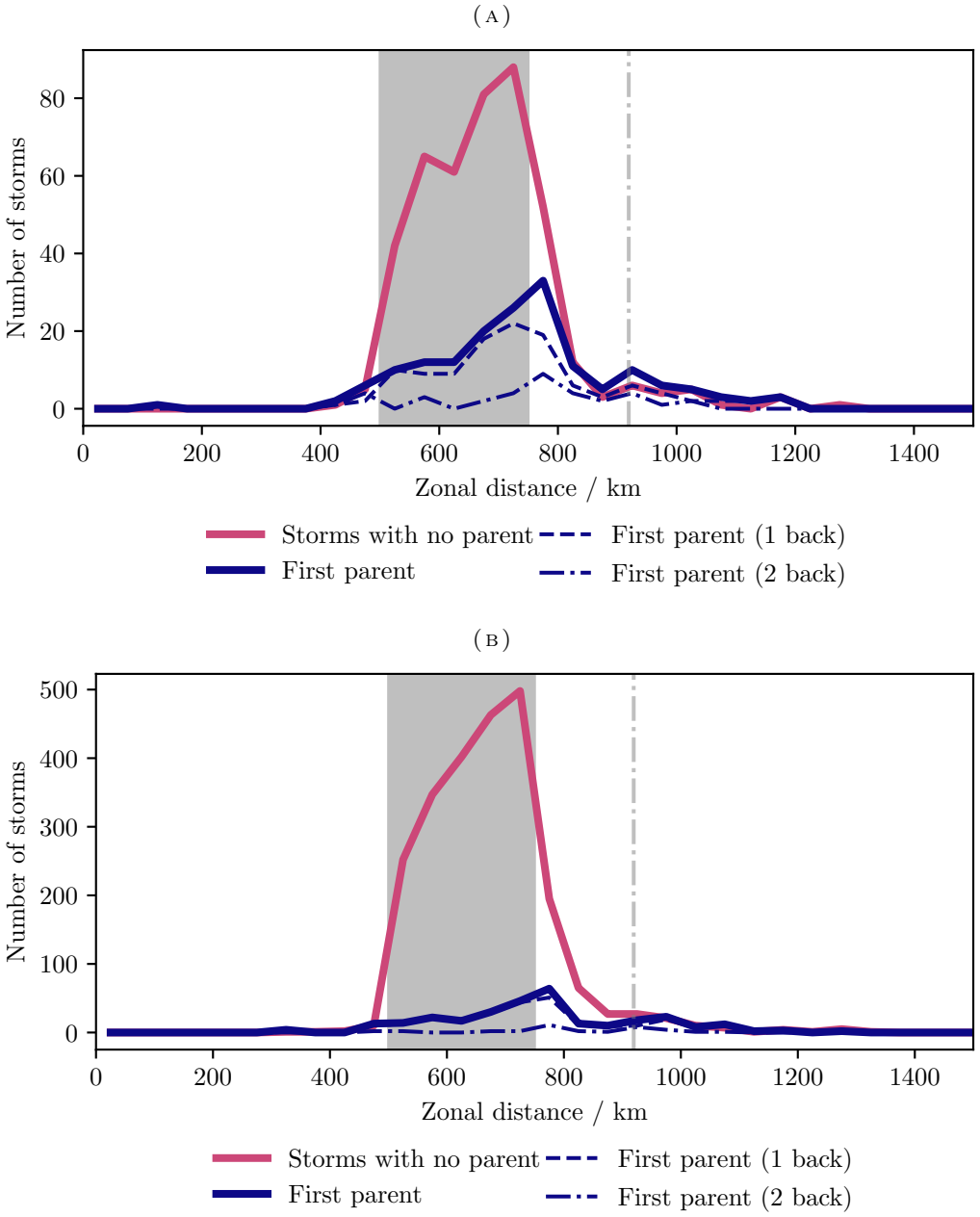

FIGURE : Distance along 19°N transect (Figure) where high offshore rainfall storms, or their first 'parent' storm, are first identified in CMORPH by storm tracking. The storms, when they are between 500 and 750 km along transect (the shaded region) have rainfall amounts, higher than the local (a) 90^{th} and (b) 50^{th} percentiles. Where the high rainfall storm is the 'child' of a previously formed storm or storms the initiation point of the first 'parent' is taken to be the initiation point. The storm tracking identifies a storm as a child storm (a storm which form from a split initiation) where it is not the largest of multiple storms at time t_i which overlap with one storm advected from time t_{i-1} (§ 6.2.3). '1 back' refers to where the first parent storm is the previous storm and '2 back' refer to where the first parent storm is the parent of the previous storm. The tracked storms are from June through September 2000-2015 and the 'tracking' domain in Figure .

10-15 m s^{-1} for all higher frequencies. The linear relationship of frequency to wavenumber for these peak values would be consistent with hydrostatic long gravity waves modes where the speed is non-dispersive and given by $c = N/m$ or $\omega = Nk/m$.

6.3.2.2 The climatological co-variability of wind and rainfall propagation

In the case-study periods the westerly winds and storm propagation characteristics show co-variability. To examine the relationship of winds and rainfall in the climatology, periods with relatively high amounts of offshore or onshore propagation upstream of the Western Ghats are defined (the way these periods are selected is described in § 6.2.2). The relationship

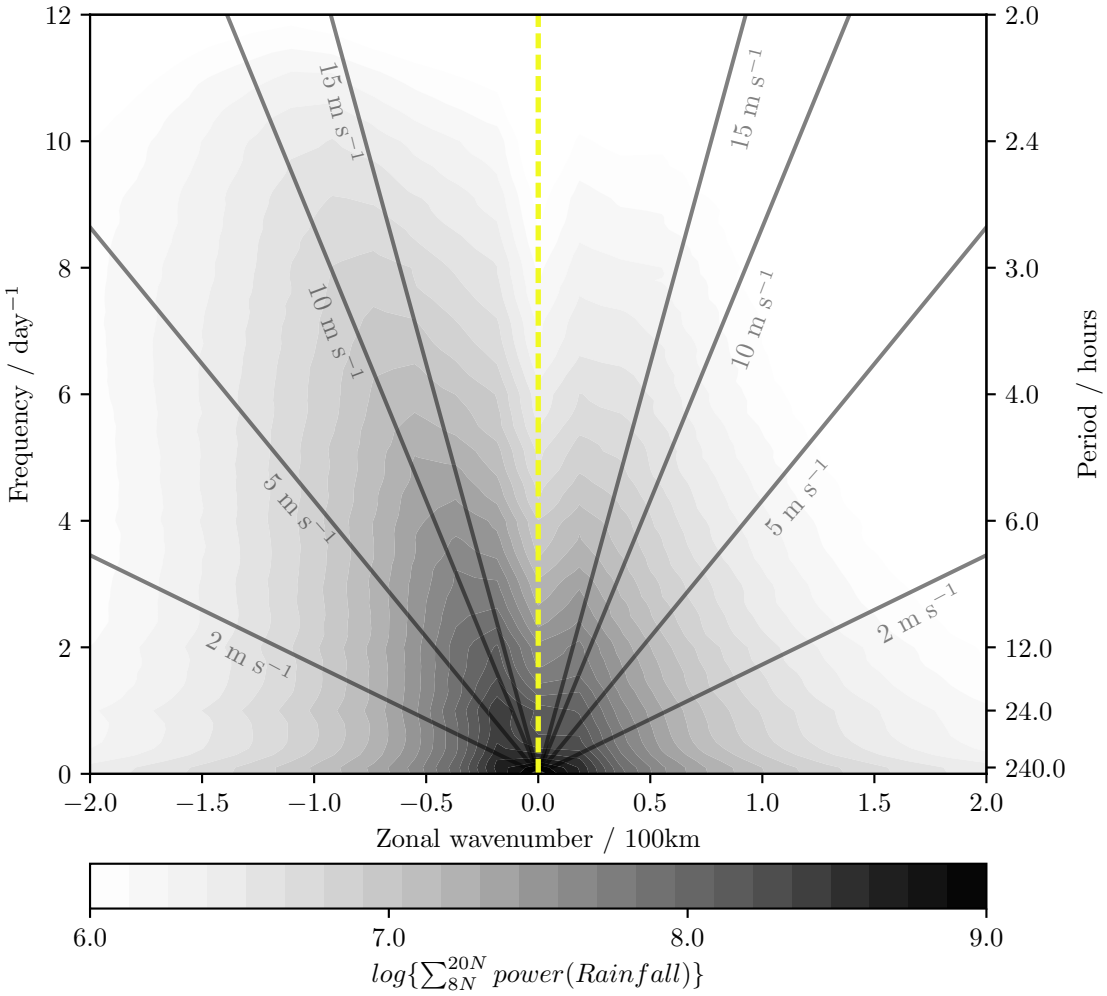

FIGURE : Time-mean zonal (summed between 8°N and 20°N) wavenumber-frequency power spectrum (base-10 logarithm) of CMORPH rainfall in the eastern Arabian Sea FFT domain in Figure for June through September in the years 1998-2015. The solid black lines show 2, 5, 10 and 15 m s^{-1} onshore and offshore propagation speeds.

of wind profile to rainfall propagation speeds for these periods (Figure) suggests that the winds play a significant role in the rainfall propagation. The peak propagation velocity in the offshore periods is westward at 2-6 m s^{-1} (Figure (a)) and in the onshore periods is close to stationary (Figure (b)). The higher number of onshore moving storms in the onshore periods is largest between 2-11 m s^{-1} eastward propagation (Figure (c)).

Comparing the mean radiosonde wind profiles at Bombay/Santa Cruz for the offshore and onshore periods (Figure (e)), in the onshore periods there is a stronger westward component to the wind at all heights. As a result, the height at which the low-level westerlies transition to easterlies above is lower in the offshore periods, at around 600 hPa compared to 400 hPa for the onshore periods. The boxes in the westerly wind profile plot show the pressures where the wind speed is the same as the peak in zonal storm propagation speed, which is 2 to 6 m s^{-1} in offshore periods, and close to 0 m s^{-1} in onshore periods. In both sets of periods, the lowest possible steering height for these peak propagation speeds, from these profiles is $\sim$500 hPa, while the upper limit is higher in the offshore periods at $\sim$350 hPa, compared to $\sim$375 hPa in the onshore periods. Comparing the wind profiles with offshore and onshore period storm propagation speeds, the differences in the peak propagation velocity, and the differences in onshore propagation that appear likely to be a result of variability in the winds affecting the distribution of storm propagation speeds.

The histogram for all storm propagation upstream of the Western Ghats in Figure shows that there is a lot more offshore propagation than onshore propagation. The offshore and onshore periods (Figure (a),(b)) both also have more offshore than onshore propagation. The overall amount of storm activity is lower in the onshore periods, but in both cases about half the number of storms that move westward at 2-6 m s^{-1} move westward at 11-15 m s^{-1} (Figure (c)). That the relative distributions of offshore storm propagation speeds in the offshore and onshore periods are similar, but the overall amount of storm activity in the offshore periods is higher, suggests that variability in the distribution of offshore propagation speeds is determined primarily by the same factors that control whether convection across the region upstream of the Western Ghats is generally enhanced or suppressed.

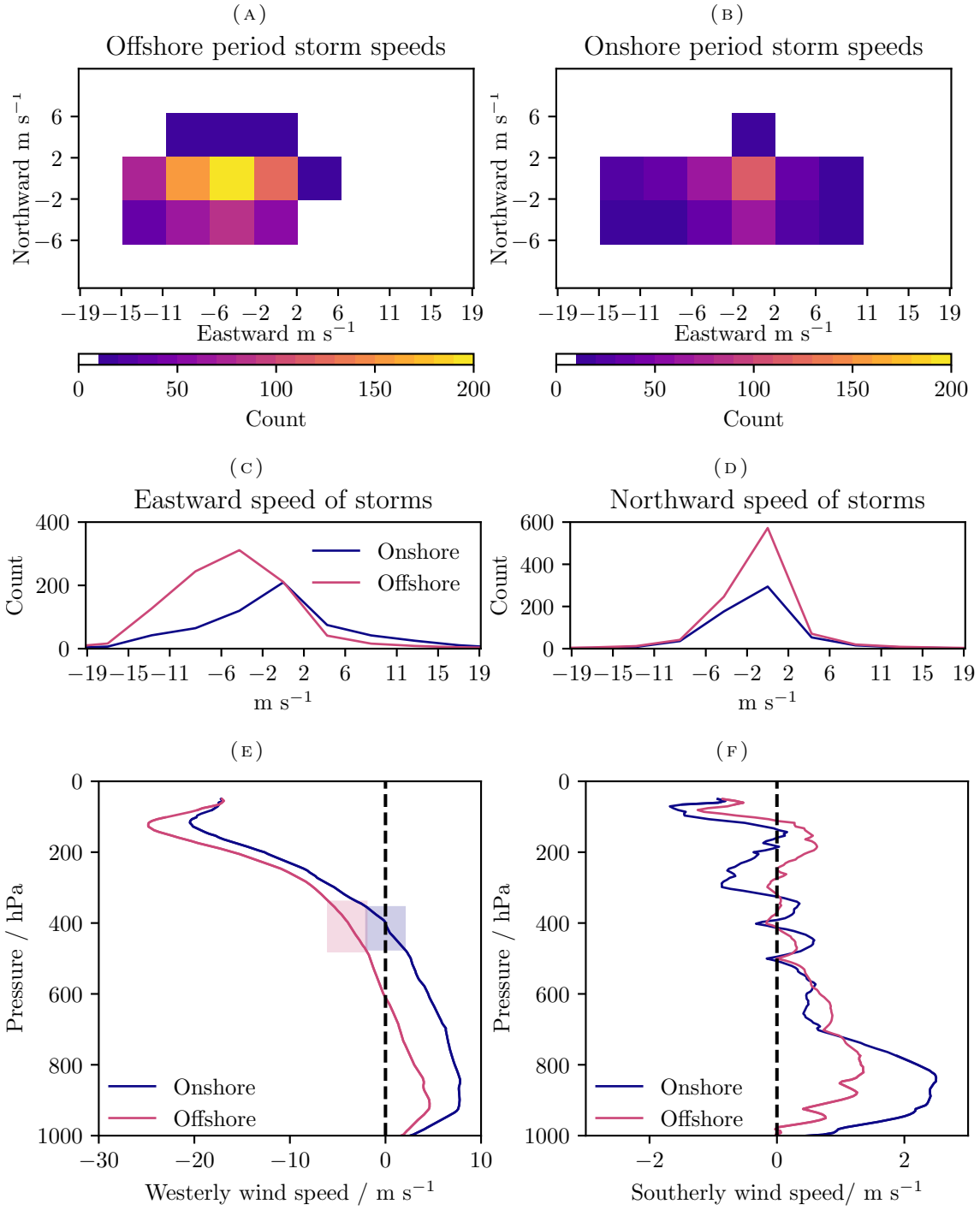

FIGURE : 'Offshore' and 'onshore' period mean CMORPH tracked storm speeds (in the storm tracking domain in Figure) and mean radiosonde wind profiles at Bombay / Santa Cruz. (a) and (b) show the number of storms moving at different velocities in, respectively, the offshore and onshore periods. (c) and (d) show the number of offshore and onshore period storms moving, respectively at different zonal and meridional speeds. (e) and (f) show, respectively, the mean zonal and meridional wind components at Bombay / Santa Cruz for the offshore and onshore periods. 'Offshore' and 'onshore' periods have relatively high amounts of westward or eastward rainfall propagation, respectively (§ 6.2.2). The boxes in (e) show where the westerly wind speed matches the peak in (c), the zonal storm propagation speed distribution.

6.3.2.3 Diurnal cycle of rainfall

For the offshore and onshore periods, Figure shows the mean diurnal cycle of CMORPH rainfall along the 19°N Western Ghats transect (Figure). The CMORPH rainfall retrievals are only able to provide rainfall estimates at 30 minute intervals by using infrared geostationary satellite information to propagate rainfall patterns between less-frequent microwave rainfall estimates from polar orbiting satellites. Although infrared data are only used to propagate patterns between microwave rainfall estimates, it is possible that they are too sensitive to anvil clouds in the upper troposphere which here may be propagating in the upper-level easterly winds, potentially in a significantly different direction to the rain producing part of the storm. To address this, the mean diurnal cycles for the offshore and onshore periods are also shown as estimated from the multi-satellite TRMM microwave-only product (Figure (c),(d)).

The mean offshore and onshore period diurnal cycles, from both the CMORPH and TRMM-microwave rainfall retrievals, show a general similarity, over land, coast and sea, to diurnal cycles in other tropical coastal regions (e.g. Kikuchi and Wang, 2008).

- Over the continent, there is a rainfall minimum in the morning and early afternoon and a maximum in the late afternoon and night-time.
- Over the sea, the pattern is the opposite to that over the continent, with a rainfall maximum in the morning and afternoon and a minimum in the night-time.
- Near the coast, there are late night/morning and afternoon peaks, with the morning peak situated more over the sea, and the afternoon peak more over land. As also commonly observed in other tropical coastal regions (e.g. Kikuchi and Wang, 2008), rainfall propagates offshore from the seaward morning peak, and inland from the landward afternoon/evening peak.

The mean rainfall along the transect shows that the near-coastal rainfall peaks result in the highest rainfall upstream of the Western Ghats being near the coast. In the TRMM-microwave diurnal cycles the peak is further offshore than in CMORPH. Previous studies have differed in finding that the rainfall peak near the coast is either over the sea or over the slopes, so it is noted that the actual location of the peak near the coast may differ somewhat

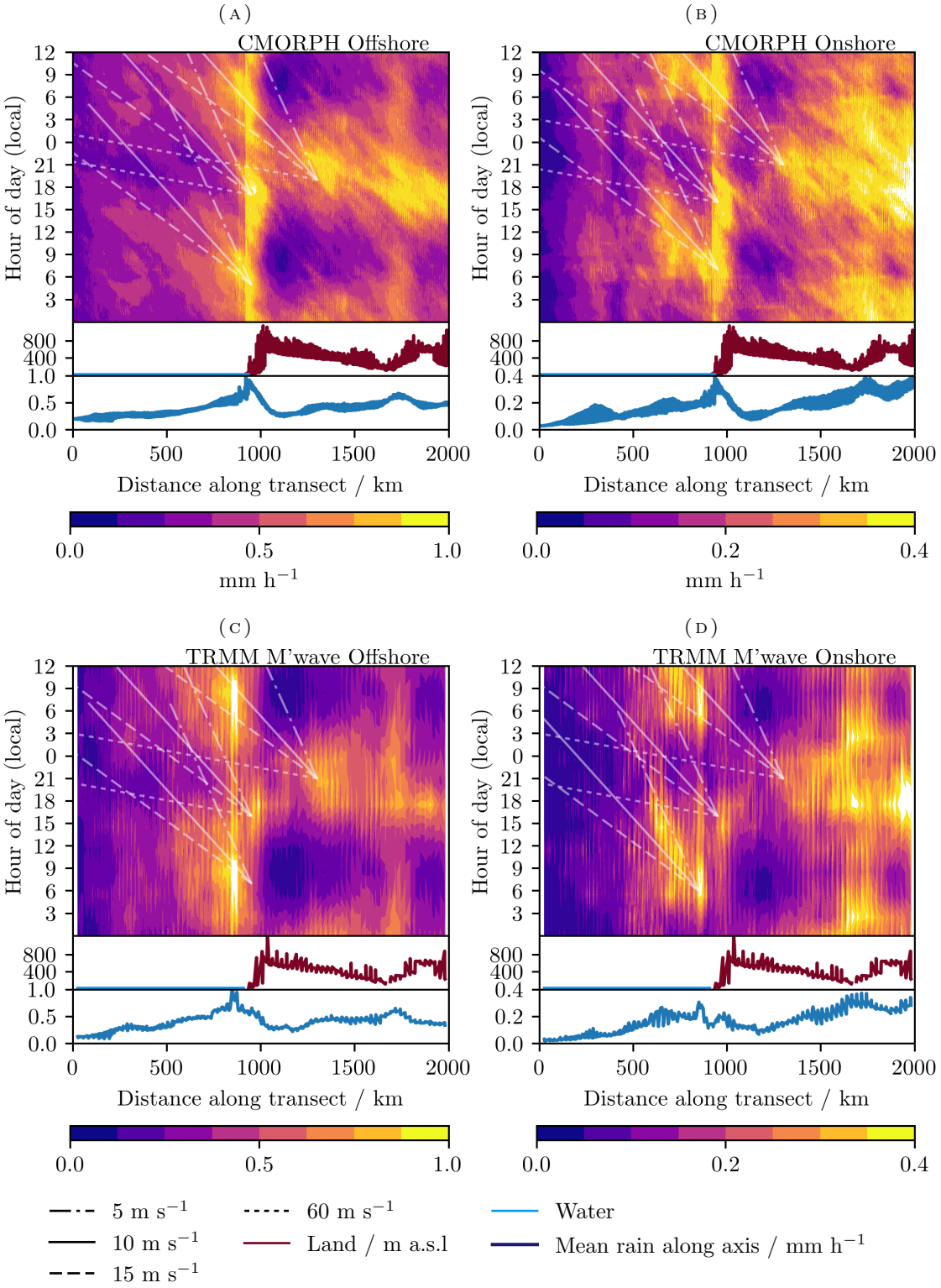

FIGURE : Mean diurnal cycle composites of CMORPH rainfall along 19°N transect (1° meridional width) for (a) offshore and (b) onshore periods, and of TRMM-microwave rainfall (c) offshore and (d) onshore periods. The line plots in each panel show the topography and mean rainfall along the transect. Lines on the rainfall Hovmöllers show some propagation speeds. The way offshore and onshore periods are selected is described in § 6.2.2. Figure shows the location of the transect.

from what is shown here. As expected from the storm speed histograms in Figure , there is more rainfall overall in the offshore periods, and this is the case along the entire transect. Relatively, however, in the onshore periods the mean coastal rainfall peak is about the same magnitude as the peak in the continental rainfall, whereas in the offshore periods the coastal rainfall peak is higher than the continental rainfall peak ($\sim$1 mm h^{-1} to $\sim$0.6 mm h^{-1}).

The mean rainfall amount over the sea generally decreases with distance from the coast, but there are local peaks. In both sets of periods, there is a local rainfall peak, over the sea, at $\sim$300km along transect, which could be a result of an SST gradient. In the onshore periods, there is also a local peak over the sea at $\sim$600km along transect. This onshore period peak potentially relates to the concept of gentle lifting as a mechanism for the initiation of deep offshore convection originally proposed by Grossman and Durran (1984), which would require sufficiently strong monsoon westerlies and would also coincide with suppressed convection near the coast, an environment which is consistent with that of the onshore periods in relation to the offshore periods.

Both the offshore and onshore period diurnal cycles indicate offshore propagation at a range of possible speeds, from 5-15 m s^{-1}, from near the coast. There is some difference in the pattern of morning and night-time rainfall though. In both the offshore and the onshore periods, rainfall is seen to propagate offshore from the near-coastal morning peak. The pattern differs in that, while there is also offshore propagation of similar rainfall magnitudes during the night in the offshore periods, the night-time rainfall over the sea is markedly lower than the morning rainfall in the onshore periods. Offshore propagation at speeds of 10-15 m s^{-1}, from night-time and morning near-coastal convection in the tropics has been shown to be consistent with a destabilising effect of convectively generated gravity waves (e.g. Love *et al.*, 2011). Offshore propagation at speeds of $\sim$5 m s^{-1} could also result from gravity waves, but is more consistent with a shallower wave generated by land breezes converging with the mean flow (Yang and Slingo, 2001). The monsoon westerlies are weaker in the offshore periods, making it more likely that land breezes will develop during the night, which could help to explain the differing patterns of night-time and morning offshore rainfall propagation.

Over land, there is possible propagation both eastward inland from the late afternoon/evening coastal rainfall peak and also westward towards the coast from the night-time continental rainfall. The contours in between the continental afternoon peak, and the near-coastal

morning peak, in both the offshore and onshore periods, indicate westward propagation towards the coast at speeds of 10-15 m s^{-1} between them. In the opposite direction, there is a propagation inland from the landside coastal peak in the latter part of the day at similar speeds.

Gravity waves may also act to suppress rainfall in the evening over the sea. First internal mode gravity waves, which can be generated by a deep convective heating profile, and travel at speeds of ∼50-60 m s^{-1}, can suppress convection (Marsham and Parker, 2006; Love *et al.*, 2011), where the passage of their downwelling wavefront has a stabilising effect. While the rainfall over the sea is at a minimum in both the offshore and onshore periods, the timings differ. In the offshore periods, a ∼60 m s^{-1} propagation speed joins the afternoon and early evening part of the landside coastal peak (∼1500-2000LST) and rainfall minima over the sea (∼1900-2200LST and at ∼400km and ∼750km along transect). The rainfall minima over the sea in the offshore periods are, however, earlier than the continental rainfall maximum. In the onshore periods, the rainfall minima at about the same locations persist for much longer (until ∼0600LST), which could perhaps be due to differences in the characteristics of gravity waves generated by the near-coastal and continental convection and/or differences in the onshore period environment over the sea.

This sections has examined climatological wind and rainfall differences between periods with relatively high amounts of offshore rainfall propagation and relatively high amounts of onshore rainfall propagation. These offshore and onshore periods correspond to 2 distinct regimes. In periods with the most offshore propagation there are more storms and rainfall upstream of the Western Ghats and the monsoon westerlies are weaker and transition to easterlies at a lower level (Figure). The different wind profiles correspond to a different distribution of storm propagation speeds, with the peak at 2-6 m s^{-1} westward in the offshore periods, and at -2 to 2 m s−1 westward in the onshore periods. In both the offshore and onshore period regimes, there is offshore phase propagation of both rainfall enhancement and suppression in the diurnal cycle, consistent with the effects of gravity waves. In the next section, the relationships between wind and rainfall identified in the offshore and onshore period regimes are examined in the context of larger-scale intraseasonal variability.

6.3.3 Links between Western Ghats rainfall propagation and larger-scale variability

A large part of the intraseasonal variability in the Indian summer monsoon comes in the form of Boreal Summer Intraseasonal Oscillations (BSISOs). The majority of the time, BSISO interrelated convection and circulation anomalies propagate northward over India and, at the same time, eastward near the equator and over India (Lawrence and Webster, 2001). This gives a characteristic WNW-ESE slopes to the anomalies. Modelling studies have found that intraseasonal oscillations are better represented in coupled ocean-atmosphere models compared to atmosphere-only models because of a better representation of feedbacks between SST and convection (e.g. Ratnam *et al.*, 2009; Sharmila *et al.*, 2013).

Figures & show the spatial patterns of onshore minus offshore period 850 hPa wind, precipitation and Sea Surface Temperature (SST), at a range of lagged periods from the onshore and offshore periods, for 2001 to 2014. The years 2001 to 2014 were used, instead of 1998 to 2014, because when data from 1998 (a 'very strong' El Niño year), was included, any pattern of intraseasonal variability in the SST was dominated, over the equatorial central and west Pacific, by the related seasonal pattern in the SST differences. Consequently, all years with 'very strong' El Niño (1998, 2015) or La Niña (1999, 2000) have been excluded. 7-day periods outside the upper and lower 25th percentile of the ratio of offshore to onshore propagation power in the wavenumber-frequency domain form the 0-day offshore and onshore periods respectively and the positive and negative lag composites are composed of the subsequent 7-day periods each side of the upper and lower percentile periods.

There is a north-south dipole in the rainfall differences between the onshore and offshore periods (0-days lag in Figure), with more rainfall to the north in the onshore periods (in a band from the north Bay of Bengal to the west Pacific), and more rainfall to the south in the offshore periods (in a band from the Arabian Sea across southeast Asia and the maritime continent into the equatorial west Pacific). The 0-days lag wind differences at 850 hPa — stronger westerlies in the onshore periods — are greatest where they bisect the dipole in the rainfall differences, and are collocated, between ∼90-130°E, with a band of cooler SSTs (Figure).

The changing rainfall differences with lag (Figure) show a reversing dipole on a ∼7-14-day time period. In the ∼14-days lag periods there is, opposite to the 0-days lag periods, more

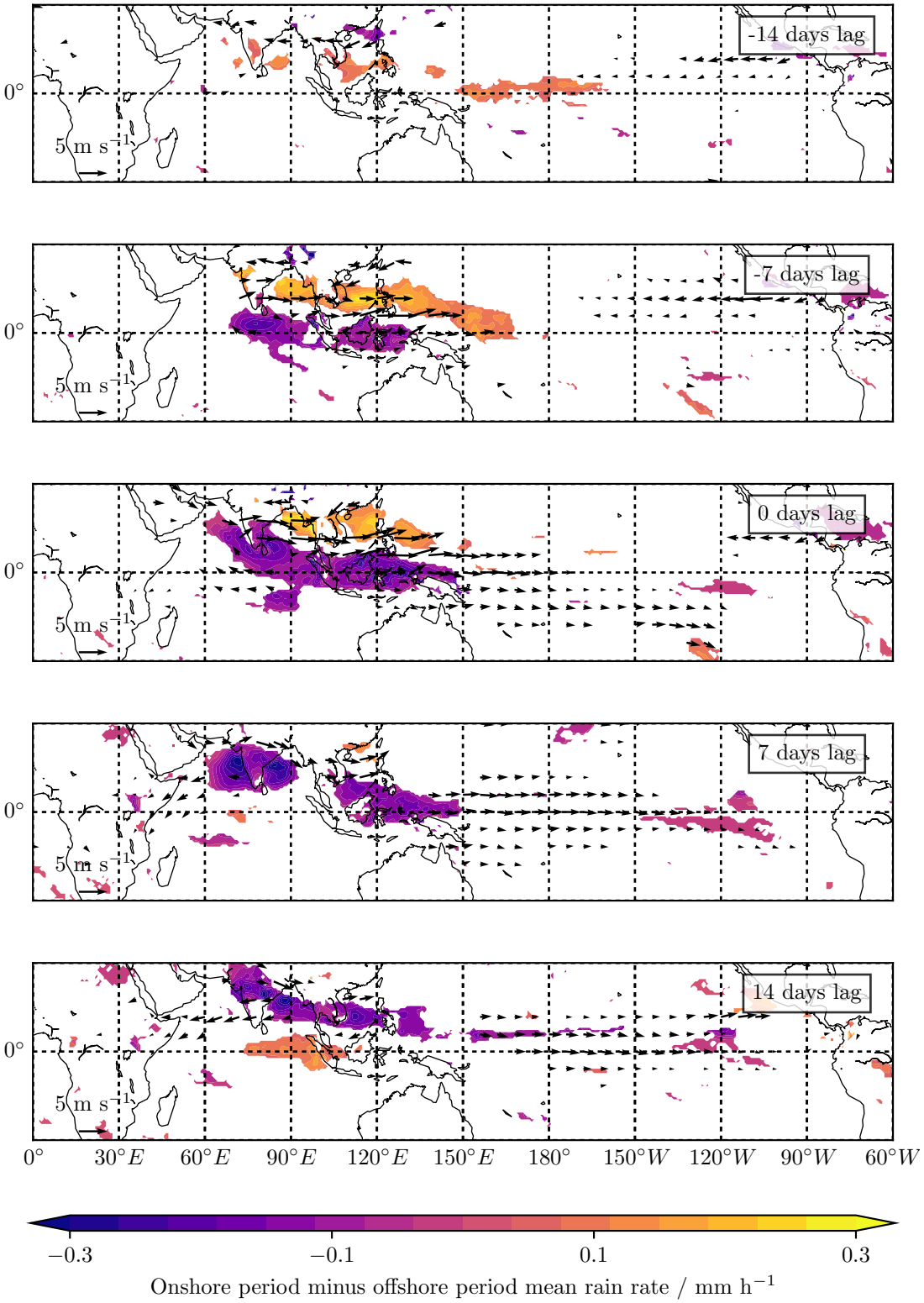

FIGURE : Lagged composites of onshore minus offshore period ERA-Interim rain rate and 850 hPa wind (arrows show difference), for 2001 to 2014. Only statistically significant differences are shown, where significance is above the 99% confidence interval, as determined by the Mann-Whitney U test. The time-lagged composites either side of 0 days lag are composites of 7-day periods lagged by increments of 7 days from the onshore and offshore periods. The rain rate is converted from 3-hourly accumulated precipitation. The way offshore and onshore periods are selected is described in § 6.2.2.

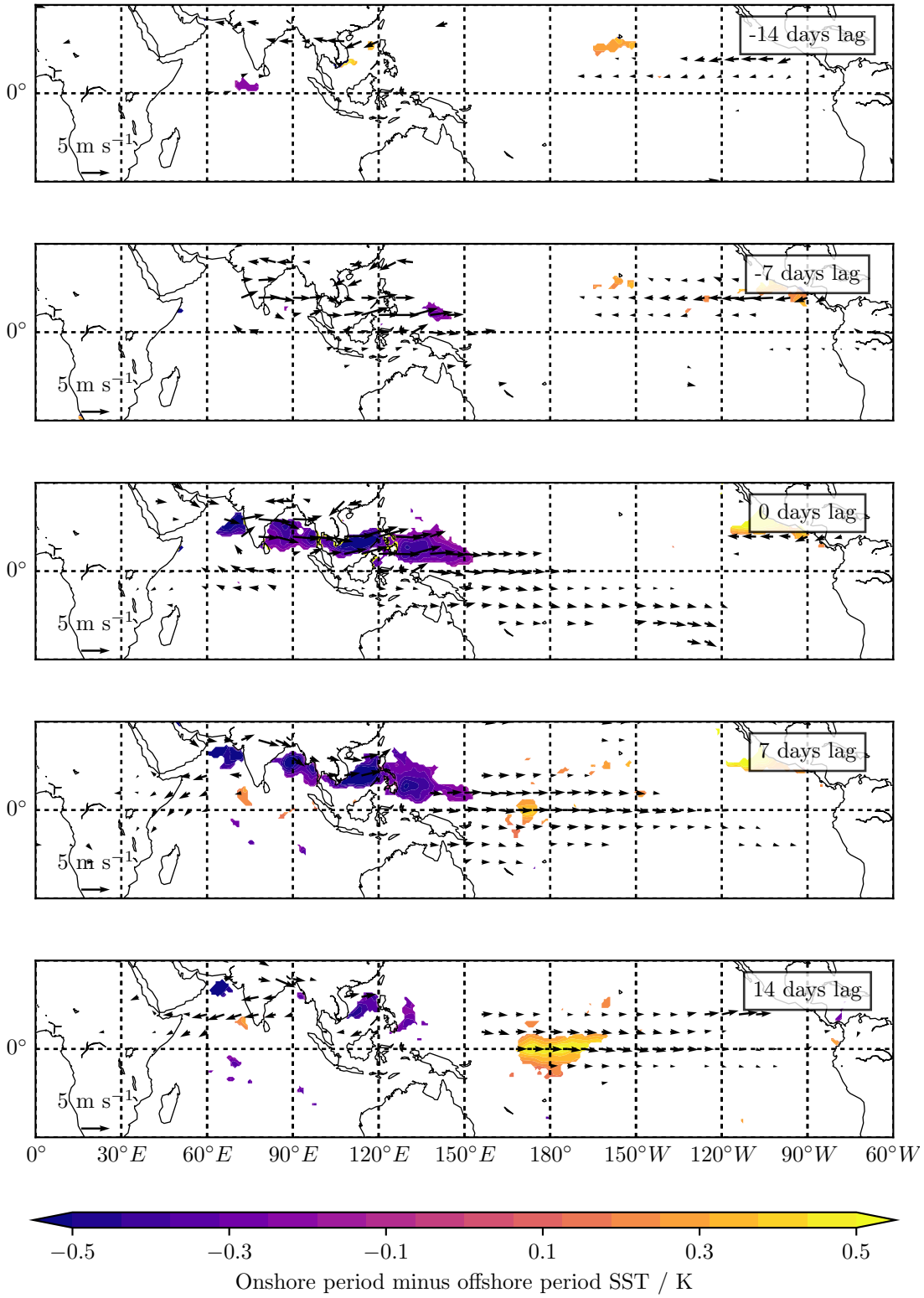

FIGURE : As Figure but for sea surface temperature and 850 hPa wind (arrows show difference).

onshore period rainfall to the south (over south India and the equatorial Indian Ocean), and less to the north (over the south China Sea). At -7-days lag, the dipole in the rainfall differences has reversed. From 0 to 14 days lag, the dipole again reverses. Between all of the lag periods, both positive and negative rainfall differences move northward with time.

There is a band of cooler SSTs in onshore periods over south Asia (Figure), at 0 and 7-days lag, which extends eastward from the western Arabian Sea, across the Bay of Bengal, South China Sea, and extends into the west Pacific. The largest 850 hPa onshore minus offshore period wind differences, which are in a band between ∼90-130°E, are spatially correlated with this band of cooler SSTs. In the east equatorial Pacific, there are warmer onshore period SSTs at negative and 0-day lag periods, and in the central equatorial Pacific there are warmers SSTs at positive lags. At -14 and -7 days lag the warmer east Pacific SSTs are spatially correlated with stronger 850 hPa easterlies there, and at +7 and +14 days the warmer central Pacific SSTs are spatially correlated with weaker easterlies.

If the offshore and onshore period differences in convection, circulation, and SST (Figure &) are related to BSISOs, then it is reasonable to expect that the periods are related to the propagation of equatorial waves (Wang and Xie, 1997; Lawrence and Webster, 2001). Figure shows offshore and onshore period lagged mean OLR anomalies, in a box covering Indian monsoon longitudes and south Indian latitudes, for the wavenumber-frequency domains of major tropical modes. The MJO anomalies relative to the offshore periods are the largest with a negative peak at +1 day (consistent with the 0-day lag rainfall differences in Figure) and a positive peak +21 days lag. There is also a smaller positive peak at -19 days giving the offshore period MJO anomalies a period of 20 days throughout the range of lags. In the 10 days before and after the offshore period 0 lag, the oscillations in the Kelvin and Rossby wave anomalies are both at close to double the frequency of the MJO anomaly oscillation and are near zero at +1 day lag. The smallest anomalies, but still apparently with some relationship to the offshore periods, are in the mixed Rossby-gravity wave anomalies, which oscillate throughout the lag range with a variable frequency.

Relative to the onshore periods, the MJO OLR anomalies, offset by 3-4 days show a reversed pattern compared to the onshore periods. There is a positive MJO OLR anomaly peak at +4 days lag, and a negative peak at -17 days lag, giving a similar period to the MJO anomalies in the offshore periods. Any coherent signal in the mixed Rossby-gravity anomalies is difficult to discern, as in the offshore periods. However, the relationships of the negative

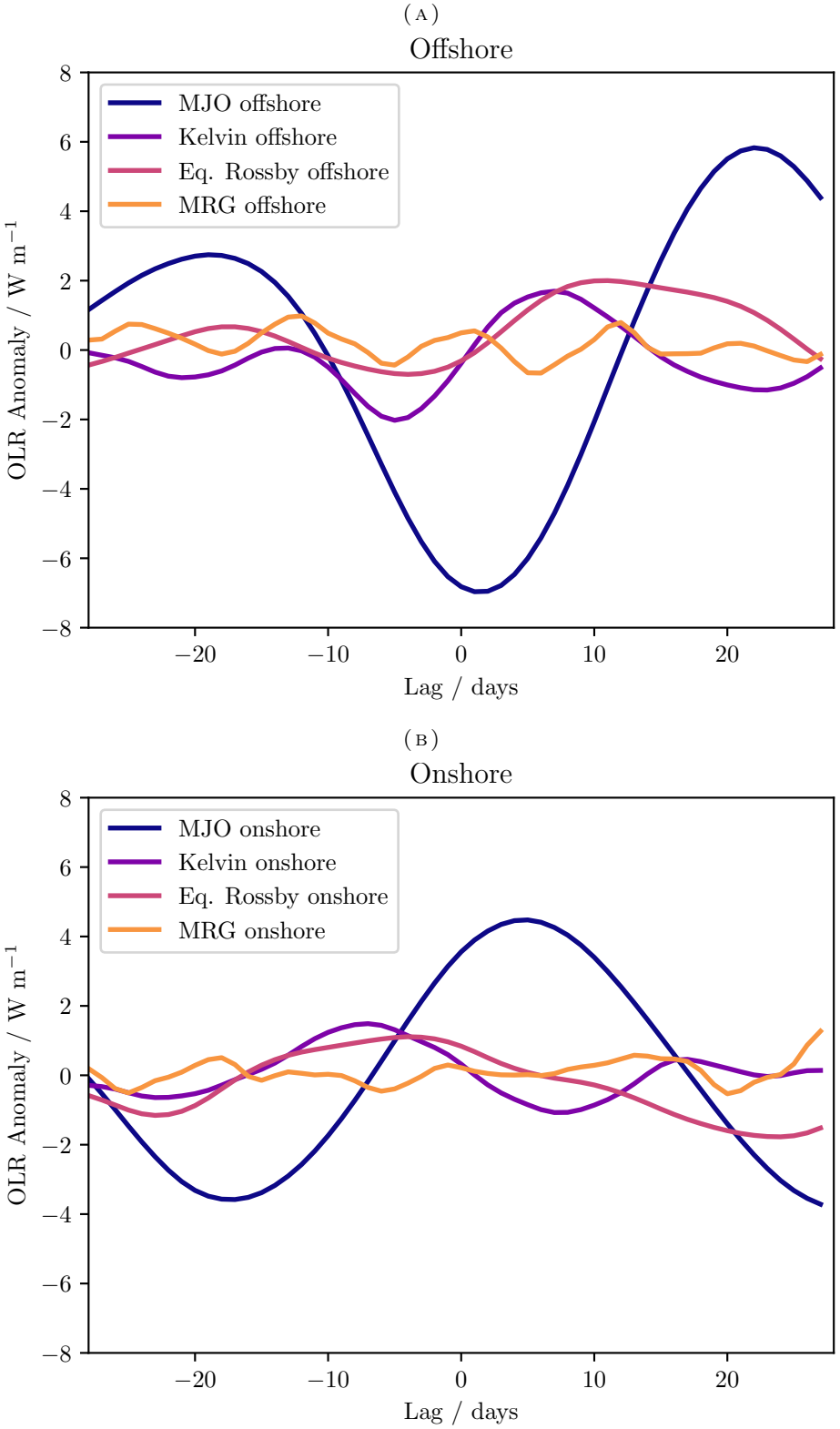

FIGURE : Projected mean OLR anomalies for 5-17.5N, 60-100E (Figure), at lagged days around the (a) offshore and (b) onshore periods, for the zonal wave-number frequency bands of major tropical modes. MRG stands for Mixed Rossby-Gravity. The algorithm used to calculate the OLR anomalies is described in § 6.2.4. The way offshore and onshore periods are selected is described in § 6.2.2.

MJO anomaly peaks in the onshore (-17 days lag) and offshore (+1 days lag) periods to the respective equatorial Rossby and Kelvin wave oscillations is very similar. Considering that there is a high correlation between the number of offshore and onshore periods in each year (ρ=0.96), this relationship between the offshore and onshore period wave OLR anomalies is consistent with the onshore periods relating to a later phase of the BSISO.

Taken together, the panels of Figure indicate that the onshore and offshore periods are strongly related to the prevailing MJO state, and much less strongly related to other equatorial modes, with Kelvin and Equatorial Rossby wave modes perhaps playing secondary roles to the MJO. This observation confirms that the onshore and offshore modes identified in this chapter are coherent modes of activity related to larger-scale dynamics.

6.4 Conclusions

This chapter presents novel findings on the nature of rainfall propagation upstream of the Western Ghats. Previous works have considered how rainfall can form at different times over both the coastal seas and windward slopes of the Western Ghats (Smith and Lin, 1982, 1983; Smith, 1985; Grossman and Durran, 1984; Ogura and Yoshizaki, 1988; Zhang and Smith, 2018; Fletcher *et al.*, 2018), but have not considered the role of propagating rainfall in the high rainfall region upstream of the Western Ghats.

Tracked storms in a climatology of CMORPH satellite rainfall retrievals show that more rainfall comes from storms that propagate offshore than from near stationary storms. Storms propagating offshore at speeds between 6 and 15 m s^{-1} contribute as much rainfall as storms propagating offshore at speeds of 2-6 m s^{-1} The wavenumber-frequency spectrum and diurnal cycle of rainfall also show significant offshore propagation of rainfall and provide evidence of the influence of gravity waves propagating from land to sea. The behaviour is significantly modulated by large-scale intraseasonal oscillations.

Comparing periods with relatively high and low amounts of offshore propagation (determined from Fourier analysis) shows 2 distinct regimes, called "offshore" and "onshore" periods here. The onshore and offshore periods are seen to be part of a larger-scale variability, lasting on timescales of at least 4 weeks. The variability, in wind, rainfall and SST, is distinctly similar to the variability associated with Boreal Summer IntraSeasonal Oscillations (BSISOs)

which are significantly determined by large-scale circulation anomalies associated with intraseasonal waves (Figure & &). The storm tracking results indicate that in both the offshore and the onshore periods, there is a fairly broad distribution of storm propagation speeds of +/- 10-15 m s^{-1} about the mean. In periods with the most offshore propagation the peak in propagation speed is 2-6 m s^{-1} westward. In periods with the most onshore propagation, the peak in propagation speed is between 2 m s^{-1} westward and 2 m s^{-1} eastward. Storms move onshore at speeds up to 10 m s^{-1} in these onshore periods, but there is still more offshore than onshore propagation. In both the offshore and the onshore periods storms propagate offshore at speeds of up to 15 m s^{-1}.

The wind profile, as measure by radiosonde soundings at Bombay/Santa Cruz varies coherently between the offshore and onshore regimes. The monsoon westerlies, are stronger and deeper in the onshore periods compared to the offshore periods This means that the modal value of tracked storm speeds in each regime is similar to the regime mean wind speed at 500-400 hPa.

Rainfall over both the windward slopes of the Western Ghats and over the sea are significantly modulated by the diurnal cycle. There are distinct diurnal cycles of rainfall near the coast, over the coastal sea, and over the continent, which are similar to those found in other tropical coastal regions (e.g. Kikuchi and Wang, 2008). Inland, away from the coast, rainfall peaks at 1800 LST and is at a minimum at 0900 LST. There is a significant minimum in rainfall in the lee of the Ghats (extending over 200 km). Near the coast there is a night-time and morning rainfall peak (0000-0900 LST in the offshore periods and 0600-0900LST in the onshore periods) and an afternoon/early evening peak (1200-2000LST). The earlier peak is close to or just over the sea, and the later peak is further inland, on the windward slopes of the Western Ghats. The locations and times of the near-coastal diurnal peaks are consistent with the effects of thermally driven orographic flows on moist convection (Kirshbaum *et al.*, 2018). There appears to be a fast deep wave of suppression emanating from the early afternoon Ghats/continental convection which suppresses convection over the sea. This moves at a speed consistent with the deepest tropospheric gravity wave mode (60 m s^{-1}), and is too fast to be explained by the propagation of individual storms (e.g. Love *et al.*, 2011). There are offshore phase propagations from the near-coastal night-time and morning rainfall peak, with speeds of 2 to 15 m s^{-1} in both regimes, consistent with shallower slower gravity waves, and the tracked storm speeds.

What causes the offshore propagation of rainfall patterns? There is evidence both of propagating storms and of gravity waves modulating the envelope of convection. Offshore propagation is related to the offshore movement of individual, tracked storms (Figure . However, the initiation of these storms is mostly over the sea, and so is not directly controlled by the diurnal cycle of heating over land. Instead, the diurnal cycle of heating over land causes various gravity wave response to propagate over the sea and modulate the occurrence of rainfall there.

This work was originally motivated by an apparent systematic discrepancy in storm propagation between model simulations and CMORPH. The convection-permitting simulations have storms consistently propagating to the east or onshore. Storm tracking shows this bias pattern is widespread, both upstream of the Western Ghats, and over much of India. The cause of the model bias in the rainfall propagation is not yet clear, nor are the implications of this for modelling the Indian monsoon. The work here shows evidence that the observed rainfall propagation is due to storm advection and convectively-generated gravity waves, and also perhaps land breezes when the monsoon westerlies are not too strong. It seems unlikely that the propagation bias results from errors in representing the effect of land breezes because the propagation bias is widespread over much of India. It also seems unlikely that the consistent pattern of onshore propagation at 10-15 m s $^{-1}$ is due to storm advection because the model wind speeds simply are not fast enough (Figure & &). The model bias in storm propagation could also result from errors in where deep convection develops and/or the depth to which it develops, and also potentially from errors in the representation of gravity waves and their effects on convection.

It is possible that the rainfall propagation bias could impact on larger-scales. Two key questions are:

- How might the rainfall propagation bias affect the mean rainfall upstream of the Western Ghats?
- How might the rainfall propagation bias affect the interaction of the rainfall upstream of the Western Ghats with intraseasonal oscillations? The offshore and onshore regimes identified here are distinctly similar to, respectively, active and break phases of BSISO events. Given the interaction of the propagating anomalies in circulation and convection that make up these events, it may be that improving the model response of

rainfall propagation characteristics during a BSISO event could improve the representation of the propagating anomalies. Intraseasonal oscillations have a large effect on the interannual variability of the Indian monsoon, so improved representation of BSISO events is an important goal for improved modelling of the Indian monsoon on a wide range of timescales.

The work here has focused on the role of rainfall propagation in determining the spatial and temporal distribution of rainfall upstream of the Western Ghats. An important question not addressed here is why rainfall at different times forms preferentially offshore or over the Western Ghats. Recent modelling (Zhang and Smith, 2018) and observational studies (Fletcher *et al.*, 2018), both find that Arabian Sea SSTs and mid tropospheric humidity play a significant role in determining the type and location of convection. The finding that warm Arabian Sea SSTs encourage rainfall to form offshore is consistent with the climatological analysis here (Figure). With regard to midtropospheric humidity, in the Fletcher *et al.* (2018) study, a midtropospheric dry intrusion over the Arabian Sea is found to greatly influence the offshore rainfall and the thermodynamics of the monsoon flow.

Both Zhang and Smith (2018) and Fletcher *et al.* (2018) look at case study periods, which raises the question of how consistent these results are with the climatology. In the particular case examined in Fletcher *et al.* (2018) the switch from offshore rainfall to coastal rainfall was governed by the passage of an active phase of a BSISO. When the rainfall is focused offshore, the monsoon westerlies are relatively weak, and when the rainfall is focused over the coast, the westerlies are relatively strong. Furthermore, there is evidence, in their offshore phase, of offshore propagation, and in their coastal phase, of eastward propagation in the Bay of Bengal (Figure). Clearly, there is some consistency between the regimes identified here and the regimes identified in Fletcher *et al.* (2018). A complete understanding of the processes that govern these rainfall regimes will need to consider the roles of local SST anomalies and dry intrusions, the influence of the diurnal cycle on offshore convection through gravity wave effects, the influence of the wind profile on storm propagation, and the role of BSISOs.

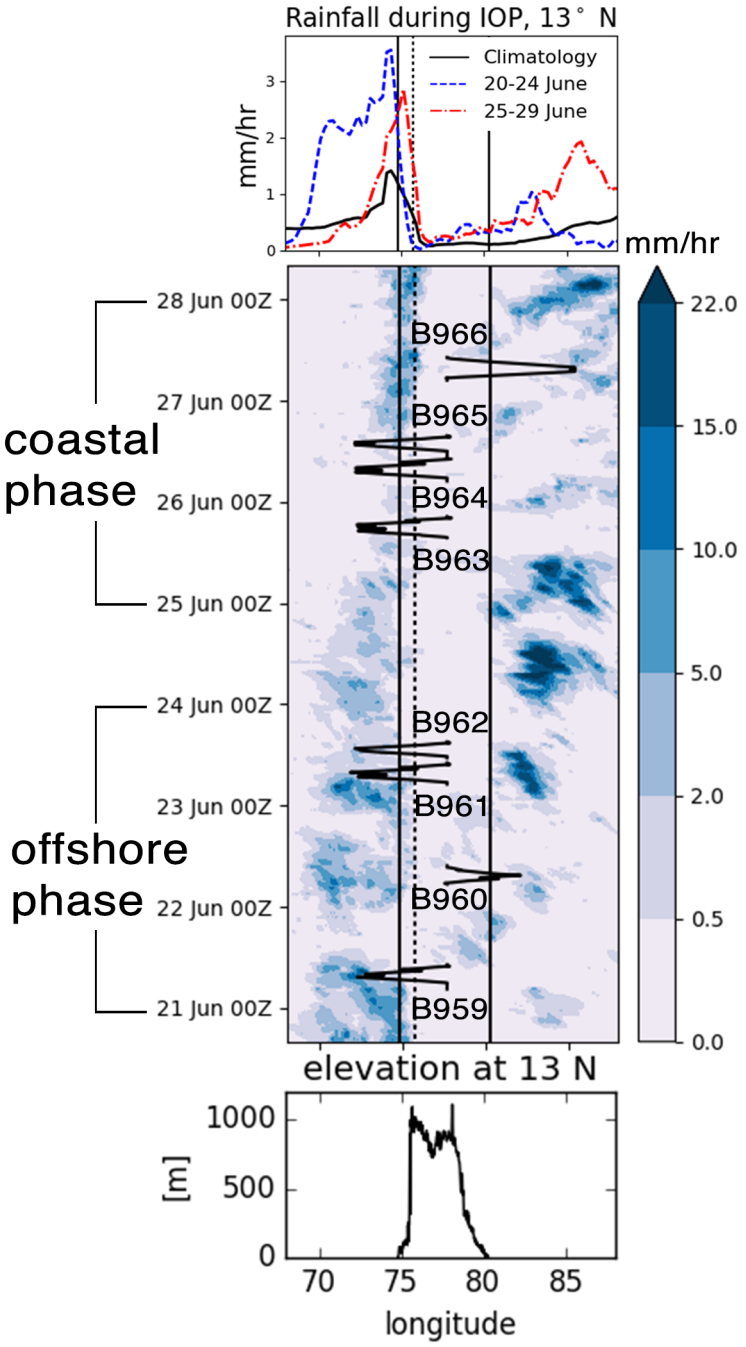

FIGURE : Top: mean rainfall from 12-13°N from TRMM 3B42 over the time periods in 2016 indicated in the legend. Centre: Time-longitude section of IMERG rainfall (mm h^{-1}) averaged over 12-14°N during the 2016 INCOMPASS campaign intense observation period. Flight paths are overlaid in black. Note the non-linear colourbar. Bottom: elevation profile at 13°N. Solid black vertical lines on the top two panels indicate the coasts; dashed line indicates the peak of the Western Ghats. Reproduced from Fletcher *et al.* (2018), which also has further information on the INCOMPASS field campaign.

Chapter 7

Conclusions

The aim of this thesis is to better understand some of the various roles and interactions of moist convection within the highly complex Indian summer monsoon system. Key issues addressed here are an incomplete knowledge of processes that determine the spatial and temporal evolution and variability of the monsoon onset (Chapter 4), systematic model biases in the representation of the mean large-scale monsoon (Chapter 5), and the role of rainfall propagation in one of the highest regions of monsoon rainfall, upstream of the Western Ghats mountain range on the west coast of India (Chapter 6).

In this chapter, following a review of the main results of the thesis in §7.1, §7.2 will consider possible further work that could build on the work presented in this thesis.

7.1 Review of results

The work looking at the monsoon onset in a climatology of radiosonde data (Chapter 4) presented work originally published in Parker *et al.* (2016), and extended the analysis.

Parker *et al.* (2016) studied the role of mid-level dry air in determining the 6 week long northwestward progression of the onset of the rainy season, proposing that the onset of deep convection happens from the south because that is where a wedge of pre-onset mid-level dry air is thinnest. The dry layer is eroded from the south, as moisture advection into the subcontinent increases as the monsoon circulation strengthens, and it is moistened from

below by cumulus and congestus clouds, allowing the limit of deep convection to move to the north.

There are two main objectives of the work further to the analysis originally presented in Parker *et al.* (2016):

- Document in more detail the relationship of the dynamics of the onset to the thermodynamic changes central to the hypothesis of mid-level dry air as a control on the progression of the onset.
- Test the hypothesis that in years where the onset is considered late, there is a drier mid-level layer.

The dynamical fields show that the progress of the northern limit of the onset towards the northwest is closely accompanied by large-scale changes in the circulation. Moving towards the northwest with the northern limit as the onset progresses, is the boundary between upper-level and mid-level baroclinic westerlies to the north and easterlies to the south, and the boundary between low-level and mid-level northwesterlies to the north and the monsoon trough circulation to the south. At Nagpur, in central India, these circulation changes are closely related in time. For about a week before the onset, mid-level winds with an easterly component indicate the passage of the boundary between the northwesterly flow and the monsoon trough circulation. This is closely related, on the timescale of a few days, to a transition away from the persistent mid-level northwesterlies, and also the final seasonal transition from upper-level westerlies to easterlies. A few days later, the upper-level winds transition from southerly to northerly indicating the rapid seasonal change to the summertime deep meridional overturning circulation.

In Parker *et al.* (2016), it is proposed that the onset occurs at a certain location once the mid-level dry layer has been sufficiently eroded, which is suggested to come about through convective moistening. The circulation changes at Nagpur that take place about a week before the onset are also closely related in time to a marked increase in the subcloud θ_e, due to an in crease in moisture content, and an increase in mid-level relative humidity. The dynamical changes mean that the northwesterly flow of mid-level dry air becomes much less prominent while, at the same time, the subcloud and mid-level thermodynamical changes indicate a transition to a profile consistent with adjustment by convective moistening.

The similarities among the timings of the dynamic and thermodynamic changes certainly highlight how the onset involves interactions between moist convection and major transitions in the circulation on timescales ranging from a few days to weeks and months. At the same time, this makes it difficult to establish to what extent the weakening of the mid-level northwesterlies and convective moistening might control the onset.

The work that examines the interannual variability of the onset also shows there is further scope to understand the roles of moist convection, the large-scale circulation, and mid-level dry air in the onset. Years with an early onset, compared to years with a late onset, show a pattern of drier mid-levels and moister low-levels. As such, the results point towards pre-onset low-level moisture content being a significant factor in the interannual variability, and also that the low-level moisture content is negatively correlated with mid-level moisture. Although dry mid-level air apparently does not control the interannual variability, it may still play a significant role in inhibiting the onset. The erosion of the mid-levels, by some combination of circulation changes and convective moistening may still be a significant driver of the onset. A thorough examination of what causes this pattern may reveal dominant processes that modulate the onset, and also how these processes relate to the erosion of the mid-level dry air. Interannual variability in the pre-onset shallow meridional circulation is one possible factor.

In Chapter 5, the role of convective parametrisation in generating typical systematic model biases in the Indian monsoon, is examined using convection-permitting simulations which capture the large-scale Indian monsoon circulation, and run for 3 weeks. The large domain, duration and resolution allows a novel insight into how the effects of small-scale, short-timescale processes can influence biases in larger-scale processes, such as the mean monsoon circulation. The suite of simulations is comprised of convection-permitting and parametrised simulations at a range of grid-spacings, which allows for a number of comparisons to be made. Overall, Chapter 5 shows how the continental dry bias, equatorial Indian Ocean wet bias and too weak low-level monsoon circulation in the MetUM, which is similar to many other models (Sperber *et al.*, 2013) are related to each other and result from biases in convective parametrisation.

In general, the convection-permitting simulations rain more over the subcontinent, which comes from more intense convection, and give a better diurnal cycle, with rainfall over land peaking in the late afternoon. The increased diabatic heating from higher rainfall increases

the temperature gradient between land and sea, which in turn increases the circulation and advection of moisture into the subcontinent. The later diurnal peak in rainfall reduces cloud cover earlier in the day, when insolation peaks, leads to greater surface solar shortwave heating. In the convection-permitting simulations, higher sensible and lower latent surface heat fluxes indicate a drier surface, which is due to the more intense rainfall, which results in more rainfall penetrating the vegetation and reaching the surface where it can be lost through run-off and penetration into the soil, rather than being re-evaporated from the vegetation.

The higher sensible heat fluxes at the surface also enhance the land-sea temperature gradient, which again enhances the onshore flow. However, the latent heating is an order of magnitude larger than the sensible heating, and so is likely the dominant process in determining the circulation differences between the convection-permitting and parametrised simulations.

The improved diurnal cycle in the convection-permitting simulations is also found to improve the diurnal cycle of the land-sea pressure gradient, consistent with Marsham *et al.* (2013), which found that later latent heating over land in the convection-permitting simulations caused the subsequent increase in the land-sea pressure gradient to be greater. This is because, the land-sea pressure gradient grows in the late afternoon and night-time when the low-level monsoon flow becomes decoupled from the boundary layer as the drag effect of boundary layer convection is at a minimum.

Rainfall over the Western Equatorial Indian Ocean (WEIO) is also found to be important in determining the land-sea pressure gradient. The 2.2km convection-permitting simulation has higher inflow into the subcontinent than both the 8km convection-permitting and 8km parametrised simulations. Coarser grid-spacings in the convection-permitting simulations increase the rainfall amount in the WEIO, with the 2.2km simulation giving the mean closest to the satellite observations, while the parametrised simulations give a similar rainfall magnitude to the 4E simulation over the WEIO. Small differences in the profiles of specific humidity within the flow differences over the Arabian Sea show that the increased circulation does not hold more moisture. However, the limited domain of the simulations does not fully contain the main part of the cross-equatorial and Somali jet flow, which may impede a correct representation of the changes to the circulation, and hence its moisture content.

The convection-permitting simulations give a good representation of the speed of propagation of a low-pressure system from the Bay of Bengal to the northwest, whereas in the parametrised simulations, it moves too fast. This results in a bias in the depth of the monsoon trough low over northern India. Further simulations would be required to determine if this bias in the parametrised simulations might be systematic, which could alter the representation of the large-scale circulation.

Previous work looking at how an altered representation of convection affects other aspects of the monsoon, such as the circulation, have primarily tested sensitivity to differences in the convective parametrisation scheme (e.g. Bush *et al.*, 2015). While the convection-permitting simulations have their own, sometimes substantial biases, they give a fundamentally different representation of convection to models with convective parametrisation. Previous studies have shown, using continental-scale simulations run over many days, how an explicit representation of convection can improve the large-scale representation of the West African monsoon (Marsham *et al.*, 2013; Birch *et al.*, 2014). The work here has followed on from this, and applied a similar framework to the study of the Indian monsoon. Simulations with small enough grid-spacings to sensibly allow the convective parametrisation scheme to be switched off are, compared to models with parametrised convection, well known to produce more rainfall (which is too intense compared to the observations), which is also more intense, and to have an improved diurnal cycle of continental rainfall (Weisman *et al.*, 1997; Guichard *et al.*, 2004; Dirmeyer *et al.*, 2012; Holloway *et al.*, 2012b). These rainfall differences, in the case of the Indian monsoon, are shown here to alter the low-level circulation and associated moisture transport into India, and to alter the land surface characteristics.

Systematic model biases inhibit our ability to assess the response of the Indian monsoon to predictable slow-varying boundary forcings, such as SST (Shukla, 1998). In turn, efforts to understand how unpredictable the Indian monsoon is, because of internal chaotic processes, are hampered by the lack of ability to represent the response to the predictable forcings (e.g. Palmer, 1994; Sperber *et al.*, 2000). While this work has shown a number of ways in which typical convective parametrisation biases alter other aspects of the modelled Indian monsoon, biases in parametrisations of convection have not, to date, been easily reduced. The results suggest, however, that convective parametrisations which better represent the diurnal cycle of moist convection and the amount and intensity distribution of rainfall, will

be necessary to improved our ability to predict, and also to better understand the Indian monsoon and its interactions within the global Earth system.

Chapter 6 examines rainfall propagation over the Western Ghats and eastern Arabian Sea. The thin band of rainfall over the windward slopes of the mountains and over the coastal sea are, after the rainfall upstream of the mountains of Myanmar over the Bay of Bengal, the second highest within the Indian Summer monsoon. The existing literature concerning deep convection over the eastern Arabian Sea (Smith and Lin, 1982, 1983; Smith, 1985; Grossman and Durran, 1984; Ogura and Yoshizaki, 1988; Roadcap and Rao, 1993; Zhang and Smith, 2018; Fletcher *et al.*, 2018), does not consider offshore propagation of rainfall over the eastern Arabian Sea.

This study has shown evidence that there is a dominant pattern of offshore rainfall propagation upstream of the Western Ghats, and that a number of mechanisms are responsible, namely storm advection by the mean winds, and the destabilising effects of gravity waves resulting from convection. Two regimes are identified, based on variability in the rainfall propagation, which have distinct large-scale circulation, rainfall and SST patterns that relate to different phases of Boreal Summer IntraSeasonal Oscillations (BSISOs). Furthermore, in an assessment of the performance of convection-permitting and convection simulations in two case-study periods, the simulations and satellite rainfall retrievals show quite different patterns of rainfall propagation, with a consistent pattern of rainfall propagating onshore, or eastward in the model simulations, when rainfall is propagating offshore in the observations.

Storm tracking of rainfall, in a climatology of satellite rainfall, shows that most offshore rainfall events are stationary, or move offshore at speeds of 2-6 m s^{-1} and that there is always a relatively significant amount of offshore storm propagation up to speeds of 15 m s^{-1}, even in periods with more onshore rainfall propagation. The distribution of zonal storm propagation speeds varies, between periods with more offshore and onshore propagation, with the zonal wind profile, indicating a role for storm advection The storm tracking also shows that the rainfall over the sea comes predominantly from storms that initiate over the sea away from the coast, indicating the importance of offshore waves in the propagation. Reanalysis and radiosonde wind profiles show that, in periods identified as having more offshore propagation, the monsoon westerlies at the coast are weaker and transition to upper-level easterlies at a lower height. Weaker, shallower westerlies mean that more storms can be advected offshore, at speeds of less than 6 m s^{-1}. Conversely,

in onshore periods, stronger and deeper westerlies, advect more storms onshore than in the offshore periods, although the maximum in the distribution of storm speeds is close to 0 m s^{-1}, and there is still more offshore propagation than onshore propagation. The destabilising effect of offshore propagating gravity waves resulting from the diurnal cycle of convection (e.g. Yang and Slingo, 2001; Love *et al.*, 2011) is proposed as a key mechanism for offshore propagation. The diurnal cycles of rainfall in the offshore and onshore periods show westward phase propagations, at speeds of 10-15 m s^{-1}, from the late afternoon and evening inland continental rainfall peak towards the night-time and morning rainfall peak over the sea, close to the coast, and also offshore from this morning peak, consistent with the characteristic speeds of rainfall propagation resulting from the effects of gravity waves generated by convection.

While the climatological mean nature of the work here that characterises the environment in which rainfall propagation occurs, based on the selection of offshore and onshore periods, establishes that offshore propagation of rainfall should be considered important to the distribution of rainfall upstream of the Western Ghats and shows some evidence for the importance of certain processes, it cannot examine the detailed mechanics of the processes that determine the rainfall characteristics of individual events. Given the compositing of a large number of time periods, it cannot establish the relative importance of certain factors, such as mid-level dry air, Arabian Sea sea surface temperatures, and the circulation.

The Indian monsoon remains one of the major biases in global models (e.g. Sperber *et al.*, 2013). The representation of convection is a dominant source of error in global models (Jung *et al.*, 2010; Sherwood *et al.*, 2014), primarily as a result of errors in the representation of fast convective processes (Murphy *et al.*, 2004; Rodwell and Palmer, 2007). This motivates the work presented in this thesis, which aims to better understand the relationships between the fast, small-scale process of moist convection and the large-scale monsoon system. The work here has addressed this on different scales, in the climatology of the onset, in the upscale effects of the representation of convection on the larger-scale monsoon, and in the mesoscale, the climatological characteristics of storms in the Western Ghats region and their relationship to the large-scale intraseasonal variability. The work has shown how well both convection-permitting and parametrised convection simulations relate to observations on both the large-scale and mesoscale, and highlighted some ways in which models likely need to improve, if they are to improve their representation of the Indian monsoon.

Together the chapters demonstrate a range of mechanisms for coupling between the convective-scale storms and their rainfall to the large-scale monsoon, both atmospheric and via the land surface. Capturing these mechanism is shown to be a challenge, even where convection is treated explicitly in 2.2 km simulations. The work shows the importance of capturing cloud entrainment and detrainment, the diurnal cycle of convection, the amount and intensity of rainfall, the Bowen ratio and surface fluxes, and convective couplings with mesoscale features such as gravity waves. The work raises a number of new avenues for further research, which are now outlined in §7.2.

7.2 Further work

For much of the further work considered here, the INCOMPASS project is particularly relevant (Willetts *et al.*, 2017b). It incorporates a programme of high-resolution convection-permitting simulations, detailed land surface modelling, investment in eddy covariance flux towers in India and in May to mid-July 2016, there was an intensive ground-based observation campaign, which included an increased frequency of radiosonde launches at a number of stations in India, a period of 3-hourly radiosonde launches at a station close to Lucknow and an aircraft campaign, which included a number of flights during the onset of the monsoon along similar northwest to southeast lines as the radiosonde sections shown here, and also a number of flights traversing the Indian peninsula, crossing the Western Ghats into the Arabian Sea.

7.2.1 Onset

Proposed ideas for further work are based around two main uncertainties the work here has raised:

- The roles of the changing circulation and convective moistening in the erosion of the mid-level dry layer
- The causes of the pattern of moister low-levels above drier mid-levels over India in years with an earlier onset

Separating the influence of the changing circulation and convective moistening on the erosion of the dry layer is very difficult using observations alone. Work is already underway in developing a highly idealised theoretical model of the dynamics of the onset, which incorporates the large-scale dynamics, land-surface forcing, convective moistening, and elements of the unique Indian orography (Recchia, PhD, Leeds, expected 2020). Any further work would greatly benefit from modelling studies, in particular where certain processes can be modified. The assessment of Menon *et al.* (2018), that the Met Office GloSea5 seasonal forecast model effectively captures the mid-level dry layer and the northwestward progress of the onset, suggests that this is feasible with state-of-the-art models which parametrise convection. Model simulations that, for example, trace detrained air from the evaporation of cloud could be used to investigate the hypothesised roles of mid-level dry air and low-level moistening related to SMCs. Testing model sensitivities to the effects of moistening the dry layer by convection could be undertaken by, for example, reducing how much detrained moisture in the convection scheme is allowed to affect water values, or relaxing the free-troposphere moisture back to drier values. There are also some high-resolution convection-permitting simulation data that could be of benefit. The 2012 simulations used in Chapter 6 include convection-permitting and parametrised convection simulations, and model the onset from 15 May to 15 July, so intercomparison between the observations and the different simulations could be made to, like in Chapter 5, assess any biases in both the convection-permitting and parametrised simulations, and use the differences between them to understand how the difference in their representation of convection alters their representation of the progression of the onset. Simulations performed as part of the INCOMPASS project also provide a suite of convection-permitting and parametrised convection simulations that simulate the onset of 2016.

The evolution of the onset could provide a useful test case to aid in the development of convective parametrisation and land surface schemes. Dry air suppresses convection via entrainment, and detrainment from clouds moistens the atmosphere. In representing the full range of development of moist convective clouds, parametrised convection schemes need to adequately represent the effects of entrainment and detrainment. Cloud characteristics, such as their size (e.g. Stirling and Stratton, 2012), affect the entrainment and detrainment. Cloud size, in turn, has been found to be controlled by the variability of moist static energy in the boundary layer (Grabowski *et al.*, 2006; Khairoutdinov and Randall, 2006). Parker *et al.* (2016) say that increasing soil moisture, which happens ahead of and behind the

onset of deep convection, feeds moisture to the boundary layer; Because the Bowen ratio is reduced, dry entrainment in the boundary layer reduces, and the boundary layer θ_e increases (Betts and Ball, 1995). The ability of models to represent the progression of the onset of deep convection therefore likely depends on their ability to represent the effects of entrainment, detrainment and soil moisture variability. The interactions between the evolving convection and mid-level dry air that take place as the onset progresses thus provide a good test for convective parametrisation and land surface schemes, and may provide new information on how entrainment and detrainment rates vary depending on the environment and cloud characteristics.

In the interannual variability of the onset, an understanding of the pre-onset pattern, when years with an earlier onset are compared to years with a later onset, of drier mid-level above moister low-levels, again would benefit from future work towards separating the influence of the circulation and convective moistening on the progress of the onset. This is complicated by the spatial and temporal complexity of the onset, where many factors may lead to an early or late onset at a certain location in a certain year. The effect of the shallow meridional circulation on interannual variations in moisture patterns over India is an obvious first step. Further to that, how might this affect the erosion of the mid-level dry layer during the onset? In this regard, other pertinent methods for defining the interannual variability of the onset and the shallow meridional circulation could be explored.

7.2.2 Convection-permitting compared to parametrised simulations

How does the limited domain affect the circulation differences? This is most prominently highlighted by the difference in the flow from the equatorial Indian Ocean north towards India, between the 2.2km convection-permitting simulation and the higher grid-spacing convection-permitting and parametrised simulations. In larger-domain simulations which extend far enough to the west to capture the full cross-equatorial and Arabian Sea flow, it is conceivable that instead of enhanced northward flow in the 2.2E simulation, there would be a strengthening of the main monsoon circulation concentrated in the jet winds close to east Africa and the westerly winds over the Arabian Sea, which may also be moister.

How does the representation of convection affect the water budget in the simulation? The convection-permitting simulations rain more than the parametrised convection simulations.

However, any work looking at this with the simulations used here is complicated by the version of the MetUM that was used not conserving water for simulations with smaller grid-spacings. What differences result from the convection-permitting simulations having, for example, a deeper monsoon trough enhancing moisture flux convergence, or a wetter inflow profile as a result of lighter oceanic rainfall to the west. There is very excessive rainfall in the first 3 days of the convection-permitting simulations, when the rainfall amounts spin down as the atmosphere adjusts from that of the parametrised convection analysis. Further model tests could reinitialise free-running convection-permitting and parametrised convection simulation wit h the evolved state of the simulations with the other treatment of convection, to test whether the spin-down reoccurs.

Is there a systematic bias in the propagation of low-pressure systems in parametrised simulations? The low-pressure system in the 2011 simulations propagates too fast to the northwest in the parametrised simulations, but is better captured by the convection-permitting simulations. It is not clear, from this one set of simulations, whether there might be a similar systematic bias, which could be addressed through a more thorough assessment of the representation of low-pressure systems in simulations with parametrised convection. This could use already available model output, such as from the operational MetUM global model and reanalysis, which could be compared with an automated feature tracking algorithm (e.g. Hunt and Parker, 2016).

Fletcher *et al.* (2017) find that monsoon depressions interact with mid-level dry intrusions 30-40% of the time, which affects their rainfall characteristics and inhibits their northwestward progression. Sensitivity tests, where parameters such as free-troposphere moisture are artificially perturbed, could be done with convection-permitting and parametrised simulations, on a number of identified or idealised low-pressure system events, to compare the effects of a drier free troposphere when convection is resolved or parametrised.

The work did not compare the surface fluxes from the simulations with observations. As well as reanalysis, the INCOMPASS campaign is providing new measurements from installed and upgraded eddy covariance flux towers, from which heat fluxes can be estimated, which would provide a useful inter-comparison between the free-running simulations, analysis and observations.

7.2.3 Western Ghats and eastern Arabian Sea rainfall

The discrepancy in rainfall propagation between the 2.2 km convection-permitting simulations and the satellite rainfall retrievals would benefit from further validation. One concern is that the method used in CMORPH, where rainfall estimates from microwave retrievals are propagated using infrared estimates, could be falsely showing westward rainfall propagation where the infrared estimates pick up upper troposphere clouds moving in the mean easterly flow that are not part of the main precipitating storm, which could be moving westward. Although there is similar offshore propagation of rainfall in the diurnal cycles of the CMORPH and the TRMM microwave product, which has a good physical connection to the rain-rate, the work did not examine the non-diurnal propagation of rainfall. As part of the INCOMPASS project, data from the IMD radar network will become available to the participating institutions. A similar analysis of the statistics of storm propagation as the one presented here could be done using radar data, as well as work looking at the 3-d structure of storms.

Do the model biases in rainfall over the eastern Arabian Sea and Western Ghats have an affect on larger-scales, such as in the circulation? Xie *et al.* (2006) showed how imposing narrow bands of diabatic heating just upstream of the Myanmar mountain ranges, and other similar "mesoscale" mountain ranges in the tropics induced a cyclonic circulation over India, but they did not describe any experiments where they performed a similar test for the Western Ghats heating. Simulations could be run with imposed diabatic heating patterns created from those of the simulations and observations, where there is more rainfall well upstream of the Ghats in the simulations.

In considering the relationship of the intraseasonal variability to the ratio of offshore to onshore propagation, the work shows evidence that it relates to 30-60 day intraseasonal variability, which has been identified as the dominant mode of intraseasonal variability (e.g. Annamalai *et al.*, 1999). In further work, considering the rainfall variability in the Western Ghats coastal region to its environment, an Empirical Orthogonal Analysis may uncover other statistically significant relationships which may assist in understanding what influence certain factors, such as the winds or mid-level dry air for example, have on the rainfall characteristics.

7.2.3.1 Final remarks

This thesis has shed some new light on this critically important meteorological system. Datasets and models already available should enable further progress in the years to come.

References

Agriculture Census Division. 2015. All india report on agriculture census 2010-11. Technical report, Department of Agriculture, Cooperation and Farmer's Welfare, Ministry of Agriculture and Farmer's Welfare, Government of India.

Ananthakrishnan R, Acharya U, Ramakrishnan A. 1967. On the criteria for declaring the onset of the southwest monsoon over kerala. *Forecasting Manual. FMU Report No. IV-18.1* **52**: 1620–1639.

Anderson DLT. 1976. The Low-Level Jet as a Western Boundary Current. *Monthly Weather Review* **104**: 907–921, doi: 10.1175/1520-0493(1976)104<0907:TLLJAA>2.0.CO;2. 00074.

Annamalai H, Slingo JM. 2001. Active / break cycles: diagnosis of the intraseasonal variability of the Asian Summer Monsoon. *Climate Dynamics* **18**: 85–102, doi: 10.1007/s003820100161. 00202.

Annamalai H, Slingo JM, Sperber KR, Hodges K. 1999. The Mean Evolution and Variability of the Asian Summer Monsoon: Comparison of ECMWF and NCEP–NCAR Reanalyses. *Monthly Weather Review* **127**(6): 1157–1186, doi: 10.1175/1520-0493(1999)127<1157:TMEAVO>2.0.CO;2.

Annamalai H, Sperber K. 2005. Regional Heat Sources and the Active and Break Phases of Boreal Summer Intraseasonal (30-50 Day) Variability*. *Journal of the atmospheric ...* **62**: 2726–2748, doi: 10.1175/JAS3504.1. 00000.

Arakawa A, Schubert WH. 1974. Interaction of a Cumulus Cloud Ensemble with the Large-Scale Environment, Part I. *Journal of the Atmospheric Sciences* **31**: 674–701, doi: 10.1175/1520-0469(1974)031<0674:IOACCE>2.0.CO;2. 02178.

Bannon PR. 1982. On the Dynamics of the East African Jet. III: Arabian Sea Branch. *Journal of the Atmospheric Sciences* **39**: 2267–2278, doi: 10.1175/1520-0469(1982)039<2267:OTDOTE>2.0.CO;2. 00020.

Basu BK. 2007. Diurnal Variation in Precipitation over India during the Summer Monsoon Season: Observed and Model Predicted. *Monthly Weather Review* **135**: 2155–2167, doi: 10.1175/MWR3355.1.

Bessafi M, Wheeler MC. 2006. Modulation of south Indian Ocean tropical cyclones by the madden–julian oscillation and convectively coupled equatorial waves. *Monthly Weather Review* **134**(2): 638–656.

Best MJ, Pryor M, Clark DB, Rooney GG, Essery RLH, Ménard CB, Edwards JM, Hendry MA, Porson A, Gedney N, Mercado LM, Sitch S, Blyth E, Boucher O, Cox PM, Grimmond CSB, Harding RJ. 2011. The Joint UK Land Environment Simulator (JULES), model description – Part 1: Energy and water fluxes. *Geosci. Model Dev.* **4**: 677–699, doi: 10.5194/gmd-4-677-2011, URL `http://www.geosci-model-dev.net/4/677/2011/`.

Betts AK, Ball J. 1995. The fife surface diurnal cycle climate. *Journal of Geophysical Research: Atmospheres* **100**(D12): 25 679–25 693.

Betts AK, Jakob C. 2002. Evaluation of the diurnal cycle of precipitation, surface thermodynamics, and surface fluxes in the ECMWF model using LBA data. *Journal of Geophysical Research: Atmospheres* **107**: LBA 12–1, doi: 10.1029/2001JD000427.

Birch CE, Marsham JH, Parker DJ, Taylor CM. 2014. The scale dependence and structure of convergence fields preceding the initiation of deep convection. *Geophysical Research Letters* **41**: 2014GL060 493, doi: 10.1002/2014GL060493. 00000.

Birch CE, Roberts MJ, Garcia-Carreras L, Ackerley D, Reeder MJ, Lock AP, Schiemann R. 2015. Sea-breeze dynamics and convection initiation: The influence of convective parameterization in weather and climate model biases. *Journal of Climate* **28**(20): 8093–8108.

Blanford HF. 1884. On the connexion of the himalaya snowfall with dry winds and seasons of drought in india. *Proceedings of the Royal Society of London* **37**(232-234): 3–22.

Bollasina M, Nigam S. 2009. Indian Ocean SST, evaporation, and precipitation during the South Asian summer monsoon in IPCC-AR4 coupled simulations. *Climate Dynamics* **33**: 1017–1032, doi: 10.1007/s00382-008-0477-4. 00033.

Bollasina M, Nigam S. 2011. The summertime "heat" low over Pakistan/northwestern India: evolution and origin. *Climate Dynamics* **37**: 957–970, doi: 10.1007/s00382-010-0879-y. 00012.

Bollasina MA, Ming Y. 2013. The general circulation model precipitation bias over the southwestern equatorial Indian Ocean and its implications for simulating the South Asian monsoon. *Climate Dynamics* **40**: 823–838, doi: 10.1007/s00382-012-1347-7. 00006.

Boos WR. 2015. A review of recent progress on tibet's role in the south asian monsoon. *CLIVAR Exch* **19**: 23–27.

Boos WR, Emanuel KA. 2008. Wind–evaporation feedback and abrupt seasonal transitions of weak, axisymmetric hadley circulations. *Journal of the Atmospheric Sciences* **65**(7): 2194–2214.

Boos WR, Emanuel KA. 2009. Annual intensification of the somali jet in a quasi-equilibrium framework: Observational composites. *Quarterly Journal of the Royal Meteorological Society* **135**(639): 319–335.

Boos WR, Hurley JV. 2013. Thermodynamic Bias in the Multimodel Mean Boreal Summer Monsoon*. *Journal of Climate* **26**: 2279–2287, doi: 10.1175/JCLI-D-12-00493.1. 00000.

Boos WR, Kuang Z. 2010. Dominant control of the South Asian monsoon by orographic insulation versus plateau heating. *Nature* **463**: 218–222, doi: 10.1038/nature08707, URL `http://www.nature.com/nature/journal/v463/n7278/abs/nature08707.html`. 00122.

Bordoni S, Schneider T. 2008. Monsoons as eddy-mediated regime transitions of the tropical overturning circulation. *Nature Geoscience* **1**: 515–519, doi: 10.1038/ngeo248. 00037.

Branković Č, Palmer TN. 2000. Seasonal skill and predictability of ecmwf provost ensembles. *Quarterly Journal of the Royal Meteorological Society* **126**(567): 2035–2067.

Bryan GH, Wyngaard JC, Fritsch JM. 2003a. Resolution Requirements for the Simulation of Deep Moist Convection. *Monthly Weather Review* **131**: 2394–2416, doi: 10.1175/1520-0493(2003)131<2394:RRFTSO>2.0.CO;2. 00347.

Bryan GH, Wyngaard JC, Fritsch JM. 2003b. Resolution requirements for the simulation of deep moist convection. *Monthly Weather Review* **131**(10): 2394–2416.

Bush SJ, Turner AG, Woolnough SJ, Martin GM, Klingaman NP. 2015. The effect of increased convective entrainment on asian monsoon biases in the metum general circulation model. *Quarterly Journal of the Royal Meteorological Society* **141**(686): 311–326, doi: 10.1002/qj.2371.

Bushell AC, Butchart N, Derbyshire SH, Jackson DR, Shutts GJ, Vosper SB, Webster S. 2015. Parameterized Gravity Wave Momentum Fluxes from Sources Related to Convection and Large-Scale Precipitation Processes in a Global Atmosphere Model. *Journal of the Atmospheric Sciences* **72**: 4349–4371, doi: 10.1175/JAS-D-15-0022.1.

Chakraborty A, Nanjundiah RS, Srinivasan J. 2006. Theoretical aspects of the onset of Indian summer monsoon from perturbed orography simulations in a GCM. *Annales Geophysicae* **24**: 2075–2089, doi: 10.5194/angeo-24-2075-2006, URL `http://repository.ias.ac.in/79945/`. 00019.

Chao WC, Chen B. 2001. The origin of monsoons. *Journal of the Atmospheric Sciences* **58**(22): 3497–3507.

Charney J, Shukla J. 1981. Predictability of monsoons. *Monsoon dynamics* **99109**.

Charney JG. 1969. A further note on large-scale motions in the tropics. *Journal of the Atmospheric Sciences* **26**(1): 182–185.

Charney JG, Eliassen A. 1964. On the Growth of the Hurricane Depression. *Journal of the Atmospheric Sciences* **21**: 68–75, doi: 10.1175/1520-0469(1964)021<0068:OTGOTH>2.0.CO;2. 00689.

Chaudhuri S, Das D, Goswami S, Das S. 2016. Long-range forecast of all india summer monsoon rainfall using adaptive neuro-fuzzy inference system: skill comparison with cfsv2 model simulation and real-time forecast for the year 2015. *Climate dynamics* **47**(9-10): 3319–3333.

Chen TC, Yoon JH. 2000. Some remarks on the westward propagation of the monsoon depression. *Tellus A* **52**: 487–499, doi: 10.1034/j.1600-0870.2000.01127.x, URL `http://tellusa.net/index.php/tellusa/article/view/12282`. 00011.

Christensen JH, Hewitson B, Busuioc A, Chen A, Gao X, Held R, Jones R, Kolli RK, Kwon W, Laprise R, *et al.* 2007. Regional climate projections. In: *Climate Change, 2007: The Physical Science Basis. Contribution of Working group I to the Fourth Assessment Report of the Intergovernmental Panel on Climate Change, University Press, Cambridge, Chapter 11*, pp. 847–940.

Cullen M. 1993. The Unified Forecast Climate Model. *Meteorological Magazine* **122**: 81–94. WOS:A1993LG31800001.

Davies L, Plant RS, Derbyshire SH. 2013. Departures from convective equilibrium with a rapidly varying surface forcing. *Quarterly Journal of the Royal Meteorological Society* **139**: 1731–1746, doi: 10.1002/qj.2065. 00001.

Davies T, Cullen MJP, Malcolm AJ, Mawson MH, Staniforth A, White AA, Wood N. 2005. A new dynamical core for the Met Office's global and regional modelling of the atmosphere. *Quarterly Journal of the Royal Meteorological Society* **131**: 1759–1782, doi: 10.1256/qj.04.101.

Dee DP, Uppala SM, Simmons aJ, Berrisford P, Poli P, Kobayashi S, Andrae U, Balmaseda Ma, Balsamo G, Bauer P, Bechtold P, Beljaars aCM, van de Berg L, Bidlot J, Bormann N, Delsol C, Dragani R, Fuentes M, Geer aJ, Haimberger L, Healy SB, Hersbach H, Hólm EV, Isaksen L, Kållberg P, Köhler M, Matricardi M, McNally aP, Monge-Sanz BM, Morcrette JJ, Park BK, Peubey C, de Rosnay P, Tavolato C, Thépaut JN, Vitart F. 2011. The ERA-Interim reanalysis: configuration and performance of the data assimilation system. *Quarterly Journal of the Royal Meteorological Society* **137**: 553–597, doi: 10.1002/qj.828. 01699.

Derbyshire S, Beau I, Bechtold P, Grandpeix JY, Piriou JM, Redelsperger JL, Soares P. 2004. Sensitivity of moist convection to environmental humidity. *Quarterly Journal of the Royal Meteorological Society* **130**(604): 3055–3079.

Dirmeyer PA, Cash BA, Iii JLK, Jung T, Marx L, Satoh M, Stan C, Tomita H, Towers P, Wedi N, Achuthavarier D, Adams JM, Altshuler EL, Huang B, Jin EK, Manganello J. 2012. Simulating the diurnal cycle of rainfall in global climate models: resolution versus parameterization. *Climate Dynamics* **39**: 399–418, doi: 10.1007/s00382-011-1127-9.

Done J, Davis CA, Weisman M. 2004. The next generation of NWP: explicit forecasts of convection using the weather research and forecasting (WRF) model. *Atmospheric Science Letters* **5**: 110–117, doi: 10.1002/asl.72. 00187.

Donlon CJ, Martin M, Stark J, Roberts-Jones J, Fiedler E, Wimmer W. 2012. The Operational Sea Surface Temperature and Sea Ice Analysis (OSTIA) system. *Remote Sensing of Environment* **116**: 140–158, doi: 10.1016/j.rse.2010.10.017, URL `http://www.sciencedirect.com/science/article/pii/S0034425711002197`. 00094.

Durre I, Vose RS, Wuertz DB. 2006. Overview of the integrated global radiosonde archive. *Journal of Climate* **19**: 53–68.

Emanuel KA. 1995. On thermally direct circulations in moist atmospheres. *Journal of the atmospheric sciences* **52**: 1529–1534.

Emanuel KA, David Neelin J, Bretherton CS. 1994. On large-scale circulations in convecting atmospheres. *Quarterly Journal of the Royal Meteorological Society* **120**: 1111–1143, doi: 10.1002/qj.49712051902. 00463.

Essery R, Best M, Cox P. 2001. MOSES 2.2 Technical Documentation. Technical report, {Hadley Centre Technical Note, URL `http://www.metoffice.gov.uk/media/pdf/9/j/HCTN_30.pdf`.

Fasullo J. 2004. A stratified diagnosis of the indian monsoon—eurasian snow cover relationship. *Journal of climate* **17**(5): 1110–1122.

Fieux M, Stommel H. 1977. Onset of the Southwest Monsoon over the Arabian Sea from Marine Reports of Surface Winds: Structure and Variability. *Monthly Weather Review* **105**(2): 231–236, doi: 10.1175/1520-0493(1977)105<0231:OOTSMO>2.0.CO;2.

Findlater J. 1969. A major low-level air current near the Indian ocean during the northern summer. *Quarterly Journal of the Royal Meteorological Society* **95**(404): 362–380.

Findlater J. 1971. *Mean monthly airflow at low levels over the western Indian ocean.* 116, HM Stationery Office.

Findlater J. 1977. Observational aspects of the low-level cross-equatorial jet stream of the western Indian Ocean. *pure and applied geophysics* **115**: 1251–1262, doi: 10.1007/BF00874408. 00061.

Fitzpatrick RGJ, Parker DJ, Willetts PD. 2016. Assessing the level of spatial homogeneity of the agronomic Indian monsoon onset. *Geophysical Research Letters* **43**: 2016GL070 711, doi: 10.1002/2016GL070711.

Flatau MK, Flatau PJ, Rudnick D. 2001. The Dynamics of Double Monsoon Onsets. *Journal of Climate* **14**(21): 4130–4146, doi: 10.1175/1520-0442(2001)014<4130:TDODMO>2.0.CO;2.

Flatau MK, Flatau PJ, Schmidt J, Kiladis GN. 2003. Delayed onset of the 2002 Indian monsoon. *Geophysical Research Letters* **30**(14): 1768, doi: 10.1029/2003GL017434.

Fletcher J, Hunt K, Parker D. 2017. The interaction of indian monsoon depressions with northwesterly dry intrusions. In: *EGU General Assembly Conference Abstracts*, vol. 19. p. 3524.

Fletcher JK, Parker DJ, Turner AG, Menon A, Martin GM, Birch CE, Mitra AK, Mrudula G, Hunt KM, Taylor CM, *et al.* 2018. The dynamic and thermodynamic structure of the monsoon over southern india: New observations from the incompass iop. *Quarterly Journal of the Royal Meteorological Society* .

Flohn H. 1957. Large-scale aspects of the "summer monsoon" in south and east asia. *J. Meteor. Soc. Japan* **75**(180186): 6.

Flohn H. 1960. Recent investigations on the mechanism of the "summer monsoon" of southern and eastern asia. In: *Proc. Symp. Monsoon of the World*. pp. 75–88.

Flohn H. 1968. *Contributions to a meteorology of the Tibetan Highlands*. Department of Atmospheric Science, Colorado State University Fort Collins, Colorado, URL `http://digitool.library.colostate.edu/exlibris/dtl/d3_1/apache_media/L2V4bGlicmlzL2R0bC9kM18xL2FwYWNoZV9tZWRpYS8yMDQw.pdf`. 00232.

Gadgil S. 2003. The Indian Monsoon and Its Variability. *Annual Review of Earth and Planetary Sciences* **31**: 429–467, doi: 10.1146/annurev.earth.31.100901.141251. 00229.

Gadgil S, Rajeevan M, Nanjundiah R. 2005. Monsoon prediction - Why yet another failure? *Current Science* **88**: 1389–1400, URL `http://eprints.iisc.ernet.in/3309/`.

Gadgil S, Srinivasan J, Nanjundiah RS, Krishna Kumar K, Munot AA, Rupa Kumar K. 2002. On forecasting the Indian summer monsoon: the intriguing season of 2002. *Current*

Science **83**: 394–403, URL http://cs-test.ias.ac.in/cs/Downloads/article_35447.pdf.

Gadgil S, Vinayachandran PN, Francis PA. 2003. Droughts of the Indian summer monsoon: Role of clouds over the Indian Ocean. *Current Science* **85**: 1713–1719, URL http://www.ias.ac.in/currsci/dec252003/contents.htm.

Ghosh S, Das D, Kao SC, Ganguly AR. 2012. Lack of uniform trends but increasing spatial variability in observed Indian rainfall extremes. *Nature Climate Change* **2**(2): 86–91, doi: 10.1038/nclimate1327, URL http://www.nature.com/nclimate/journal/v2/n2/full/nclimate1327.html.

Gill AE. 1980. Some simple solutions for heat-induced tropical circulation. *Quarterly Journal of the Royal Meteorological Society* **106**(449): 447–462, doi: 10.1002/qj.49710644905.

Goessling H, Reick C. 2011. What do moisture recycling estimates tell us? exploring the extreme case of non-evaporating continents. *Hydrology and Earth System Sciences* **15**: 3217–3235.

Goswami BN, Ajaya Mohan RS. 2001. Intraseasonal oscillations and interannual variability of the Indian summer monsoon. *Journal of Climate* **14**: 1180–1198, URL http://repository.ias.ac.in/23787/.

Goswami BN, Ajayamohan RS, Xavier PK, Sengupta D. 2003. Clustering of synoptic activity by Indian summer monsoon intraseasonal oscillations. *Geophysical Research Letters* **30**: n/a–n/a, doi: 10.1029/2002GL016734. 00106.

Goswami BN, Venugopal V, Sengupta D, Madhusoodanan MS, Xavier PK. 2006. Increasing Trend of Extreme Rain Events Over India in a Warming Environment. *Science* **314**: 1442–1445, doi: 10.1126/science.1132027, URL http://www.sciencemag.org/content/314/5804/1442. 00464 PMID: 17138899.

Grabowski W, Bechtold P, Cheng A, Forbes R, Halliwell C, Khairoutdinov M, Lang S, Nasuno T, Petch J, Tao WK, *et al.* 2006. Daytime convective development over land: A model intercomparison based on lba observations. *Quarterly Journal of the Royal Meteorological Society* **132**(615): 317–344.

Gregory D, Rowntree PR. 1990. A Mass Flux Convection Scheme with Representation of Cloud Ensemble Characteristics and Stability-Dependent Closure. *Monthly Weather Review* **118**: 1483–1506, doi: 10.1175/1520-0493(1990)118<1483:AMFCSW>2.0.CO;2.

Grossman RL, Durran DR. 1984. Interaction of Low-Level Flow with the Western Ghat Mountains and Offshore Convection in the Summer Monsoon. *Monthly Weather Review* **112**: 652–672, doi: 10.1175/1520-0493(1984)112<0652:IOLLFW>2.0.CO;2.

Guichard F, Petch J, Redelsperger JL, Bechtold P, Chaboureau JP, Cheinet S, Grabowski W, Grenier H, Jones C, Köhler M, Piriou JM, Tailleux R, Tomasini M. 2004. Modelling the diurnal cycle of deep precipitating convection over land with cloud-resolving models and single-column models. *Quarterly Journal of the Royal Meteorological Society* **130**: 3139–3172, doi: 10.1256/qj.03.145. 00127.

Halley E. 1686. An Historical Account of the Trade Winds, and Monsoons, Observable in the Seas between and Near the Tropicks, with an Attempt to Assign the Phisical Cause of the Said Winds, By E. Halley. *Philosophical Transactions of the Royal Society of London* **16**: 153–168, doi: 10.1098/rstl.1686.0026. 00000.

Hayashi Y. 1982. Space-Time Spectral Analysis and its Applications to Atmospheric Waves. *Journal of the Meteorological Society of Japan. Ser. II* **60**: 156–171.

He H, McGinnis JW, Song Z, Yanai M. 1987. Onset of the asian summer monsoon in 1979 and the effect of the tibetan plateau. *Monthly Weather Review* **115**(9): 1966–1995.

Holloway CE, Neelin JD. 2009. Moisture vertical structure, column water vapor, and tropical deep convection. *Journal of the Atmospheric Sciences* **66**(6): 1665–1683.

Holloway CE, Woolnough SJ, Lister GMS. 2012a. The Effects of Explicit versus Parameterized Convection on the MJO in a Large-Domain High-Resolution Tropical Case Study. Part I: Characterization of Large-Scale Organization and Propagation*. *Journal of the Atmospheric Sciences* **70**: 1342–1369, doi: 10.1175/JAS-D-12-0227.1. 00000.

Holloway CE, Woolnough SJ, Lister GMS. 2012b. Precipitation distributions for explicit versus parametrized convection in a large-domain high-resolution tropical case study. *Quarterly Journal of the Royal Meteorological Society* **138**: 1692–1708, doi: 10.1002/qj.1903. 00014.

Holton JR. 1992. An introduction to dynamic meteorology Academic Press. *San Diego* .

Hoskins BJ, Rodwell MJ. 1995. A Model of the Asian Summer Monsoon. Part I: The Global Scale. *Journal of the Atmospheric Sciences* **52**: 1329–1340, doi: 10.1175/1520-0469(1995)052<1329:AMOTAS>2.0.CO;2. 00150.

Houze RA, Geotis SG, Marks FD, West AK. 1981. Winter Monsoon Convection in the Vicinity of North Borneo. Part I: Structure and Time Variation of the Clouds and Precipitation. *Monthly Weather Review* **109**: 1595–1614, doi: 10.1175/1520-0493(1981)109<1595:WMCITV>2.0.CO;2.

Houze RA, Rasmussen KL, Zuluaga MD, Brodzik SR. 2015. The variable nature of convection in the tropics and subtropics: A legacy of 16 years of the Tropical Rainfall Measuring Mission satellite. *Reviews of Geophysics* **53**: 2015RG000 488, doi: 10.1002/2015RG000488.

Hoyos CD, Webster PJ. 2007. The Role of Intraseasonal Variability in the Nature of Asian Monsoon Precipitation. *Journal of Climate* **20**: 4402–4424, doi: 10.1175/JCLI4252.1.

Huffman GJ, Bolvin DT, Nelkin EJ, Wolff DB, Adler RF, Gu G, Hong Y, Bowman KP, Stocker EF. 2007. The TRMM Multisatellite Precipitation Analysis (TMPA): Quasi-Global, Multiyear, Combined-Sensor Precipitation Estimates at Fine Scales. *Journal of Hydrometeorology* **8**: 38–55, doi: 10.1175/JHM560.1.

Hunt KM, Parker DJ. 2016. The movement of Indian monsoon depressions by interaction with image vortices near the himalayan wall. *Quarterly Journal of the Royal Meteorological Society* **142**(698): 2224–2229.

Johnson SJ, Levine RC, Turner AG, Martin GM, Woolnough SJ, Schiemann R, Mizielinski MS, Roberts MJ, Vidale PL, Demory ME, *et al.* 2016. The resolution sensitivity of the south asian monsoon and indo-pacific in a global 0.35 agcm. *Climate Dynamics* **46**(3-4): 807–831.

Joseph S, Sahai A, Sharmila S, Abhilash S, Borah N, Chattopadhyay R, Pillai P, Rajeevan M, Kumar A. 2015. North indian heavy rainfall event during june 2013: diagnostics and extended range prediction. *Climate Dynamics* **44**(7-8): 2049–2065.

Joshi MK, Kucharski F. 2017. Impact of Interdecadal Pacific Oscillation on Indian summer monsoon rainfall: an assessment from CMIP5 climate models. *Climate Dynamics* **48**(7-8): 2375–2391, doi: 10.1007/s00382-016-3210-8.

Joyce RJ, Janowiak JE, Arkin PA, Xie P. 2004. CMORPH: A method that produces global precipitation estimates from passive microwave and infrared data at high spatial and temporal resolution. *Journal of Hydrometeorology* **5**: 487–503, doi: 10.1175/1525-7541(2004)005\%3C0487:CAMTPG\%3E2.0.CO;2.

Jung T, Balsamo G, Bechtold P, Beljaars ACM, Köhler M, Miller MJ, Morcrette JJ, Orr A, Rodwell MJ, Tompkins AM. 2010. The ECMWF model climate: recent progress through improved physical parametrizations. *Quarterly Journal of the Royal Meteorological Society* **136**: 1145–1160, doi: 10.1002/qj.634. 00041.

Karmacharya J, Levine RC, Jones R, Moufouma-Okia W, New M. 2015. Sensitivity of systematic biases in South Asian summer monsoon simulations to regional climate model domain size and implications for downscaled regional process studies. *Climate Dynamics* : 1–19doi: 10.1007/s00382-015-2565-6.

Kawamura R, Fukuta Y, Ueda H, Matsuura T, Iizuka S. 2002. A mechanism of the onset of the australian summer monsoon. *Journal of Geophysical Research: Atmospheres* **107**(D14).

Keshavamurty RN, Awade ST. 1970. On the maintenance of the mean monsoon trough over north india. *Monthly Weather Review* **98**(4): 315–320, doi: 10.1175/1520-0493(1970)098<0315:OTMOTM>2.3.CO;2.

Khairoutdinov M, Randall D. 2006. High-resolution simulation of shallow-to-deep convection transition over land. *Journal of the atmospheric sciences* **63**(12): 3421–3436.

Khole M, Devi SS. 2012. MONSOON SEASON (June to September 2011). *Mausam* **63**: 511–528, URL `http://metnet.imd.gov.in/mausamdocs/36331.pdf`. WOS:000307484200017.

Kikuchi K, Wang B. 2008. Diurnal Precipitation Regimes in the Global Tropics. *Journal of Climate* **21**: 2680–2696, doi: 10.1175/2007JCLI2051.1.

Kirshbaum D, Adler B, Kalthoff N, Barthlott C, Serafin S. 2018. Moist orographic convection: Physical mechanisms and links to surface-exchange processes. *Atmosphere* **9**(3): 80.

Koteswaram P. 1958. The easterly jet stream in the tropics. *Tellus* **10**(1): 43–57.

Kripalani R, Oh J, Kulkarni A, Sabade S, Chaudhari H. 2007. South asian summer monsoon precipitation variability: coupled climate model simulations and projections under ipcc ar4. *Theoretical and Applied Climatology* **90**(3): 133–159.

Krishnamurti T, Ardanuy P. 1980. The 10 to 20-day westward propagating mode and "breaks in the monsoons". *Tellus* **32**(1): 15–26.

Krishnamurti T, Simon A, Thomas A, Mishra A, Sikka D, Niyogi D, Chakraborty A, Li L. 2012. Modeling of forecast sensitivity on the march of monsoon isochrones from kerala to new delhi: the first 25 days. *Journal of the Atmospheric Sciences* **69**(8): 2465–2487.

Krishnamurti TN. 1971. Tropical East-West Circulations During the Northern Summer. *Journal of the Atmospheric Sciences* **28**(8): 1342–1347, doi: 10.1175/1520-0469(1971)028<1342:TEWCDT>2.0.CO;2.

Krishnamurti TN, Bhalme HN. 1976. Oscillations of a Monsoon System. Part I. Observational Aspects. *Journal of the Atmospheric Sciences* **33**: 1937–1954, doi: 10.1175/1520-0469(1976)033<1937:OOAMSP>2.0.CO;2. 00448.

Kumar KK, Rajagopalan B, Cane MA. 1999. On the Weakening Relationship Between the Indian Monsoon and ENSO. *Science* **284**(5423): 2156–2159, doi: 10.1126/science.284.5423.2156, URL `http://science.sciencemag.org/content/284/5423/2156`.

Kuo HL. 1965. On Formation and Intensification of Tropical Cyclones Through Latent Heat Release by Cumulus Convection. *Journal of the Atmospheric Sciences* **22**: 40–63, doi: 10.1175/1520-0469(1965)022<0040:OFAIOT>2.0.CO;2. 00859.

Lau K, Peng L. 1990. Origin of low frequency (intraseasonal) oscillations in the tropical atmosphere. part iii: Monsoon dynamics. *Journal of the Atmospheric Sciences* **47**(12): 1443–1462.

Lawrence DM, Webster PJ. 2001. Interannual variations of the intraseasonal oscillation in the south asian summer monsoon region. *Journal of climate* **14**(13): 2910–2922.

Liebmann B, Smith CA. 1996. Description of a complete (interpolated) outgoing longwave radiation dataset. *Bulletin of the American Meteorological Society* **77**(6): 1275–1277.

Lock AP, Brown AR, Bush MR, Martin GM, Smith RNB. 2000. A New Boundary Layer Mixing Scheme. Part I: Scheme Description and Single-Column Model Tests. *Monthly*

Weather Review **128**: 3187–3199, doi: 10.1175/1520-0493(2000)128<3187:ANBLMS>2.0.CO;2.

Lorenz EN. 1963. Deterministic nonperiodic flow. *Journal of the atmospheric sciences* **20**(2): 130–141.

Lorenz EN. 1969. Atmospheric Predictability as Revealed by Naturally Occurring Analogues. *Journal of the Atmospheric Sciences* **26**: 636–646, doi: 10.1175/1520-0469(1969)26<636:APARBN>2.0.CO;2.

Loschnigg J, Meehl GA, Webster PJ, Arblaster JM, Compo GP. 2003. The Asian Monsoon, the Tropospheric Biennial Oscillation, and the Indian Ocean Zonal Mode in the NCAR CSM. *Journal of Climate* **16**(11): 1617–1642, doi: 10.1175/1520-0442(2003)016<1617:TAMTTB>2.0.CO;2.

Love BS, Matthews AJ, Lister GMS. 2011. The diurnal cycle of precipitation over the Maritime Continent in a high-resolution atmospheric model. *Quarterly Journal of the Royal Meteorological Society* **137**: 934–947, doi: 10.1002/qj.809.

Lucas-Picher P, Christensen JH, Saeed F, Kumar P, Asharaf S, Ahrens B, Wiltshire AJ, Jacob D, Hagemann S. 2011. Can Regional Climate Models Represent the Indian Monsoon? *Journal of Hydrometeorology* **12**: 849–868, doi: 10.1175/2011JHM1327.1.

Ma D, Boos W, Kuang Z. 2014. Effects of orography and surface heat fluxes on the south asian summer monsoon. *Journal of Climate* **27**(17): 6647–6659.

Madden RA. 1986. Seasonal Variations of the 40-50 Day Oscillation in the Tropics. *Journal of the Atmospheric Sciences* **43**(24): 3138–3158, doi: 10.1175/1520-0469(1986)043<3138:SVOTDO>2.0.CO;2.

Maini P, Basu S. 2016. Economic impact of the agro meteorological advisory services of ministry of earth sciences—a review. *Mausam* **67**(1): 297–310.

Maloney E, Hartmann D. 2001. The sensitivity of intraseasonal variability in the NCAR CCM3 to changes in convective parameterization. *Journal of climate* : 2015–2034doi: 10.1175/1520-0442(2001)014, URL `<2015:TSOIVI>2.0.CO;2`. 00153.

Mapes BE, Warner TT, Xu M. 2003. Diurnal Patterns of Rainfall in Northwestern South America. Part III: Diurnal Gravity Waves and Nocturnal Convection Offshore. *Monthly*

Weather Review **131**: 830–844, doi: 10.1175/1520-0493(2003)131<0830:DPORIN>2.0.CO;2.

Markowski P, Richardson Y. 2011. *Mesoscale meteorology in midlatitudes*, vol. 2. John Wiley & Sons.

Marsham J, Parker D. 2006. Secondary initiation of multiple bands of cumulonimbus over southern britain. ii: Dynamics of secondary initiation. *Quarterly Journal of the Royal Meteorological Society: A journal of the atmospheric sciences, applied meteorology and physical oceanography* **132**(617): 1053–1072.

Marsham JH, Dixon NS, Garcia-Carreras L, Lister GMS, Parker DJ, Knippertz P, Birch CE. 2013. The role of moist convection in the West African monsoon system: Insights from continental-scale convection-permitting simulations. *Geophysical Research Letters* **40**: 1843–1849, doi: 10.1002/grl.50347.

Marteau R, Moron V, Philippon N. 2009. Spatial coherence of monsoon onset over western and central sahel (1950–2000). *Journal of Climate* **22**(5): 1313–1324.

Martin GM, Milton SF, Senior CA, Brooks ME, Ineson S, Reichler T, Kim J. 2010. Analysis and Reduction of Systematic Errors through a Seamless Approach to Modeling Weather and Climate. *Journal of Climate* **23**: 5933–5957, doi: 10.1175/2010JCLI3541.1. 00039.

McCollum JR, Ferraro RR. 2003. Next generation of noaa/nesdis tmi, ssm/i, and amsr-e microwave land rainfall algorithms. *Journal of Geophysical Research: Atmospheres* **108**(D8).

Meehl GA, Covey C, Taylor KE, Delworth T, Stouffer RJ, Latif M, McAvaney B, Mitchell JF. 2007. The wcrp cmip3 multimodel dataset: A new era in climate change research. *Bulletin of the American Meteorological Society* **88**(9): 1383–1394.

Mega T, Ushio T, Kubota T, Kachi M, Aonashi K, Shige S. 2014. Gauge adjusted global satellite mapping of precipitation (GSMaP_gauge). In: *General Assembly and Scientific Symposium (URSI GASS), 2014 XXXIth URSI*. pp. 1–4, doi: 10.1109/URSIGASS.2014.6929683.

Menon A, Turner A, Martin G, MacLachlan C. 2018. Modelling the moistening of the free troposphere during the northwestward progression of indian monsoon onset. *Quarterly Journal of the Royal Meteorological Society* **144**(713): 1152–1168.

Molnar P, Boos WR, Battisti DS. 2010. Orographic Controls on Climate and Paleoclimate of Asia: Thermal and Mechanical Roles for the Tibetan Plateau. *Annual Review of Earth and Planetary Sciences* **38**: 77–102, doi: 10.1146/annurev-earth-040809-152456. 00092.

Moron V, Robertson AW. 2014. Interannual variability of Indian summer monsoon rainfall onset date at local scale. *International Journal of Climatology* **34**(4): 1050–1061.

Murphy JM, Sexton DMH, Barnett DN, Jones GS, Webb MJ, Collins M, Stainforth DA. 2004. Quantification of modelling uncertainties in a large ensemble of climate change simulations. *Nature* **430**: 768–772, doi: 10.1038/nature02771, URL `http://www.nature.com/nature/journal/v430/n7001/abs/nature02771.html`. 00957.

Nie J, Boos WR, Kuang Z. 2010. Observational evaluation of a convective quasi-equilibrium view of monsoons. *Journal of Climate* **23**(16): 4416–4428.

Numaguti A. 1995. Dynamics and energy balance of the hadley circulation and the tropical precipitation zones. part ii: Sensitivity to meridional sst distribution. *Journal of the atmospheric sciences* **52**(8): 1128–1141.

Ogura Y, Yoshizaki M. 1988. Numerical Study of OrograPhic-Convective Precipitation over the Eastern Arabian Sea and the Ghat Mountains during the Summer Monsoon. *Journal of the Atmospheric Sciences* **45**: 2097–2122, doi: 10.1175/1520-0469(1988)045<2097:NSOOCP>2.0.CO;2. 00042.

Pai D, Bhan S. 2015. Monsoon 2014: a report (imd met. monograph no: Esso/imd/synoptic met/01-2015/17). *India Meteorological Department, National Climate Center, Pune, India* .

Palmer T. 1994. Chaos and predictability in forecasting the monsoons. *PROCEEDINGS-INDIAN NATIONAL SCIENCE ACADEMY PART A* **60**: 57–57.

Palmer TN, Anderson DL. 1994. The prospects for seasonal forecasting—a review paper. *Quarterly Journal of the Royal Meteorological Society* **120**(518): 755–793.

Parker DJ, Willetts P, Birch C, Turner AG, Marsham JH, Taylor CM, Kolusu S, Martin GM. 2016. The interaction of moist convection and mid-level dry air in the advance of the onset of the indian monsoon. *Quarterly Journal of the Royal Meteorological Society* **142**: 2256–2272.

Parthasarathy B. 1995. Monthly and seasonal rainfall series for all india, homogeneous regions and meteorological subdivisions: 1871-1994. *Indian Institute of Tropical meteorology Research Report* .

Parthasarathy B, Kumar KR, Munot A. 1993. Homogeneous indian monsoon rainfall: variability and prediction. *Proceedings of the Indian Academy of Sciences-Earth and Planetary Sciences* **102**(1): 121–155.

Petch JC, Brown AR, Gray MEB. 2002. The impact of horizontal resolution on the simulations of convective development over land. *Quarterly Journal of the Royal Meteorological Society* **128**: 2031–2044, doi: 10.1256/003590002320603511.

Prakash S, Mitra AK, Momin IM, Pai D, Rajagopal E, Basu S. 2015a. Comparison of tmpa-3b42 versions 6 and 7 precipitation products with gauge-based data over india for the southwest monsoon period. *Journal of Hydrometeorology* **16**(1): 346–362, doi: 10.1002/joc.4446.

Prakash S, Mitra AK, Rajagopal EN, Pai DS. 2015b. Assessment of TRMM-based TMPA-3b42 and GSMaP precipitation products over India for the peak southwest monsoon season. *International Journal of Climatology* : n/a–n/adoi: 10.1002/joc.4446.

Prakash S, Sathiyamoorthy V, Mahesh C, Gairola RM. 2014. An evaluation of high-resolution multisatellite rainfall products over the Indian monsoon region. *International Journal of Remote Sensing* **35**: 3018–3035, doi: 10.1080/01431161.2014.894661.

Raghavan K. 1973. Tibetan anticyclone and tropical easterly jet. *pure and applied geophysics* **110**, doi: 10.1007/BF00876576. 00009.

Rajeevan M, Bhate J, Kale J, Lal B. 2006. High resolution daily gridded rainfall data for the indian region: Analysis of break and active. *Current Science* **91**(3): 296–306.

Raju P, Mohanty U, Bhatla R. 2005. Onset characteristics of the southwest monsoon over india. *International journal of climatology* **25**(2): 167–182.

Ramage CS. 1971. *Monsoon meteorology (international geophysics series; v. 15)*. Academic Press.

Randall D, Khairoutdinov M, Arakawa A, Grabowski W. 2003. Breaking the Cloud Parameterization Deadlock. *Bulletin of the American Meteorological Society* **84**: 1547–1564, doi: 10.1175/BAMS-84-11-1547. 00406.

Rao MS. 1966. Equations for global monsoons and toroidal circulations in the σ-coordinate system. *pure and applied geophysics* **65**(1): 196–215, doi: 10.1007/BF00874967.

Ratnam JV, Giorgi F, Kaginalkar A, Cozzini S. 2009. Simulation of the indian monsoon using the regcm3–roms regional coupled model. *Climate Dynamics* **33**(1): 119–139.

Recchia L. ???? Dynamics of the indian monsoon. `https://physicalsciences.leeds.ac.uk/pgr/1050/lucy-recchia`. Accessed: 2019-07-05.

Roadcap JR, Rao GV. 1993. An Analytical Study of the Dependence of Orientation and Propagation of the Arabian Sea Convection Bands on Wind Shear, Static Stability, and Preexisting Convection. *Monthly Weather Review* **121**: 1656–1670, doi: 10.1175/1520-0493(1993)121<1656:AASOTD>2.0.CO;2.

Roberts NM, Lean HW. 2008. Scale-Selective Verification of Rainfall Accumulations from High-Resolution Forecasts of Convective Events. *Monthly Weather Review* **136**: 78–97, doi: 10.1175/2007MWR2123.1. 00219.

Rodell M, Velicogna I, Famiglietti JS. 2009. Satellite-based estimates of groundwater depletion in india. *Nature* **460**(7258): 999.

Rodwell MJ, Hoskins BJ. 1995. A Model of the Asian Summer Monsoon.Part II: Cross-Equatorial Flow and PV Behavior. *Journal of the Atmospheric Sciences* **52**: 1341–1356, doi: 10.1175/1520-0469(1995)052<1341:AMOTAS>2.0.CO;2. 00065.

Rodwell MJ, Hoskins BJ. 1996. Monsoons and the dynamics of deserts. *Quarterly Journal of the Royal Meteorological Society* **122**(534): 1385–1404, doi: 10.1002/qj.49712253408.

Rodwell MJ, Palmer TN. 2007. Using numerical weather prediction to assess climate models. *Quarterly Journal of the Royal Meteorological Society* **133**: 129–146, doi: 10.1002/qj.23.

Romatschke U, Houze Jr RA. 2011. Characteristics of precipitating convective systems in the south asian monsoon. *Journal of Hydrometeorology* **12**(1): 3–26.

Romatschke U, Medina S, Houze Ra. 2010. Regional, Seasonal, and Diurnal Variations of Extreme Convection in the South Asian Region. *Journal of Climate* **23**: 419–439, doi: 10.1175/2009JCLI3140.1. 00039.

Romero R, Doswell CA, Riosalido R. 2001. Observations and Fine-Grid Simulations of a Convective Outbreak in Northeastern Spain: Importance of Diurnal Forcing and Convective Cold Pools. *Monthly Weather Review* **129**: 2157–2182, doi: 10.1175/1520-0493(2001)129<2157:OAFGSO>2.0.CO;2. 00034.

Roundy PE. 2012. Tracking and prediction of large-scale organized tropical convection by spectrally focused two-step space–time eof analysis. *Quarterly Journal of the Royal Meteorological Society* **138**(665): 919–931.

Rupa Kumar K, Sahai AK, Krishna Kumar K, Patwardhan SK, Mishra PK, Revadekar JV, Kamala K, Pant GB. 2006. High-resolution climate change scenarios for India for the 21st century. *Current Science* **90**: 334–345, URL `http://cs-test.ias.ac.in/cs/Downloads/article_39716.pdf`.

Sabeerali C, Ramu Dandi A, Dhakate A, Salunke K, Mahapatra S, Rao SA. 2013. Simulation of boreal summer intraseasonal oscillations in the latest cmip5 coupled gcms. *Journal of Geophysical Research: Atmospheres* **118**(10): 4401–4420.

Saji NH, Goswami BN, Vinayachandran PN, Yamagata T. 1999. A dipole mode in the tropical Indian Ocean. *Nature* **401**: 360–363, doi: 10.1038/43854, URL `http://www.nature.com/nature/journal/v401/n6751/abs/401360a0.html`. 01946.

Sankar-Rao M. 1970. On global monsoons — further results. *Tellus* **22**(6): 648–654, doi: 10.3402/tellusa.v22i6.10265.

Sato T, Miura H, Satoh M, Takayabu YN, Wang Y. 2009. Diurnal Cycle of Precipitation in the Tropics Simulated in a Global Cloud-Resolving Model. *Journal of Climate* **22**: 4809–4826, doi: 10.1175/2009JCLI2890.1.

Sawyer J. 1947. The structure of the intertropical front over nw india during the sw monsoon. *Quarterly Journal of the Royal Meteorological Society* **73**(317-318): 346–369.

Schneider T, Bordoni S. 2008. Eddy-mediated regime transitions in the seasonal cycle of a hadley circulation and implications for monsoon dynamics. *Journal of the Atmospheric Sciences* **65**: 915–934.

Senan R, Orsolini YJ, Weisheimer A, Vitart F, Balsamo G, Stockdale TN, Dutra E, Doblas-Reyes FJ, Basang D. 2016. Impact of springtime himalayan–tibetan plateau snowpack on the onset of the Indian summer monsoon in coupled seasonal forecasts. *Climate Dynamics* **47**(9-10): 2709–2725.

Sharmila S, Pillai P, Joseph S, Roxy M, Krishna R, Chattopadhyay R, Abhilash S, Sahai A, Goswami B. 2013. Role of ocean–atmosphere interaction on northward propagation of indian summer monsoon intra-seasonal oscillations (miso). *Climate dynamics* **41**(5-6): 1651–1669.

Sherwood SC, Bony S, Dufresne JL. 2014. Spread in model climate sensitivity traced to atmospheric convective mixing. *Nature* **505**: 37–42, doi: 10.1038/nature12829, URL `http://www.nature.com/nature/journal/v505/n7481/full/nature12829.html`. 00023.

Shrestha D, Deshar R, Nakamura K. 2015. Characteristics of summer precipitation around the western ghats and the myanmar west coast. *International Journal of Atmospheric Sciences* **2015**.

Shukla J. 1998. Predictability in the midst of chaos: A scientific basis for climate forecasting. *science* **282**(5389): 728–731.

Shukla J, Paolino DA. 1983. The southern oscillation and long-range forecasting of the summer monsoon rainfall over india. *Monthly Weather Review* **111**(9): 1830–1837.

Sikka DR, Gadgil S. 1980. On the maximum cloud zone and the ITCZ over Indian , longitudes during the southwest monsoon. *Monthly Weather Review* **108**: 1840–1853, doi: 10.1175/1520-0493(1980)108\%3C1840:OTMCZA\%3E2.0.CO;2, URL `http://journals.ametsoc.org/toc/mwre/108/11`. 00506.

Simpson GC. 1921. The South-West monsoon. *Quarterly Journal of the Royal Meteorological Society* **47**: 151–171, doi: 10.1002/qj.49704719901. 00065.

Slingo J, Spencer H, Hoskins B, Berrisford P, Black E. 2005. The meteorology of the western Indian ocean, and the influence of the east african highlands. *Philosophical Transactions of the Royal Society of London A: Mathematical, Physical and Engineering Sciences* **363**(1826): 25–42.

Smith R, Lin Y. 1983. Orographic rain on the western Ghats. In: *Proc. First Sino-American Workshop on Mountain Meteorology*. pp. 71–94.

Smith RB. 1985. Comment on "Interaction of Low-Level Flow with the Western Ghat Mountains and Offshore Convection in the Summer Monsoon". *Monthly Weather Review* **113**: 2176–2177, doi: 10.1175/1520-0493(1985)113<2176:COOLLF>2.0.CO;2.

Smith RB, Lin YL. 1982. The addition of heat to a stratified airstream with application to the dynamics of orographic rain. *Quarterly Journal of the Royal Meteorological Society* **108**: 353–378, doi: 10.1002/qj.49710845605.

Speer MS, Leslie LM. 2002. The prediction of two cases of severe convection: implications for forecast guidance. *Meteorology and Atmospheric Physics* **80**: 165–175, doi: 10.1007/s007030200023. 00011.

Sperber KR, Annamalai H. 2008. Coupled model simulations of boreal summer intraseasonal (30–50 day) variability, part 1: Systematic errors and caution on use of metrics. *Climate Dynamics* **31**(2-3): 345–372.

Sperber KR, Annamalai H. 2014. The use of fractional accumulated precipitation for the evaluation of the annual cycle of monsoons. *Climate dynamics* **43**(12): 3219–3244.

Sperber KR, Annamalai H, Kang IS, Kitoh A, Moise A, Turner A, Wang B, Zhou T. 2013. The Asian summer monsoon: an intercomparison of CMIP5 vs. CMIP3 simulations of the late 20^{th} century. *Climate Dynamics* **41**: 2711–2744, doi: 10.1007/s00382-012-1607-6.

Sperber KR, Slingo JM, Annamalai H. 2000. Predictability and the relationship between subseasonal and interannual variability during the Asian summer monsoon. *Quarterly Journal of the Royal Meteorological Society* **126**: 2545–2574, doi: 10.1002/qj.49712656810.

Stein THM, Hogan RJ, Hanley KE, Nicol JC, Lean HW, Plant RS, Clark PA, Halliwell CE. 2014. The Three-Dimensional Morphology of Simulated and Observed Convective Storms over Southern England. *Monthly Weather Review* **142**: 3264–3283, doi: 10.1175/MWR-D-13-00372.1.

Stephens GL, L'Ecuyer T, Forbes R, Gettlemen A, Golaz JC, Bodas-Salcedo A, Suzuki K, Gabriel P, Haynes J. 2010. Dreary state of precipitation in global models. *Journal of Geophysical Research: Atmospheres* **115**: D24 211, doi: 10.1029/2010JD014532.

Stirling A, Stratton R. 2012. Entrainment processes in the diurnal cycle of deep convection over land. *Quarterly Journal of the Royal Meteorological Society* **138**(666): 1135–1149.

Trenberth KE, Stepaniak DP, Caron JM. 2000. The global monsoon as seen through the divergent atmospheric circulation. *Journal of Climate* **13**(22): 3969–3993.

Turner A, Inness P, Slingo J. 2005. The role of the basic state in the enso–monsoon relationship and implications for predictability. *Quarterly Journal of the Royal Meteorological Society* **131**(607): 781–804.

Turner AG, Annamalai H. 2012. Climate change and the South Asian summer monsoon. *Nature Climate Change* **2**: 587–595, doi: 10.1038/nclimate1495, URL `http://www.nature.com/nclimate/journal/v2/n8/full/nclimate1495.html`. 00072.

Turner AG, Slingo JM. 2011. Using idealized snow forcing to test teleconnections with the Indian summer monsoon in the hadley centre gcm. *Climate dynamics* **36**(9-10): 1717–1735.

UK Meteorological Office. 2015. Met office (2012): Met Office Integrated Data Archive System (MIDAS) Land and Marine Surface Stations Data (1853-current). NCAS British Atmospheric Data Centre.

Vecchi GA, Harrison DE. 2004. Interannual Indian rainfall variability and indian Ocean sea surface temperature anomalies. In: *Geophysical Monograph Series*, vol. 147, Wang C, Xie SP, Carton JA (eds), American Geophysical Union, ISBN 0-87590-412-2, pp. 247–259, URL `http://www.agu.org/books/gm/v147/147GM14/147GM14.shtml`. 00000.

Venkateswarlu B, Rao V. 2013. Climate change and its impact on Indian agriculture. In: *Climate Change Modeling, Mitigation, and Adaptation*, pp. 419–453.

Walker G. 1924. Correlations in seasonal variations of weather. i. a further study of world weather. *Mem. Indian Meteorol. Dep.* **24**: 275–332.

Walters DN, Williams KD, Boutle IA, Bushell AC, Edwards JM, Field PR, Lock AP, Morcrette CJ, Stratton RA, Wilkinson JM, Willett MR, Bellouin N, Bodas-Salcedo A, Brooks ME, Copsey D, Earnshaw PD, Hardiman SC, Harris CM, Levine RC, MacLachlan C, Manners JC, Martin GM, Milton SF, Palmer MD, Roberts MJ, Rodríguez JM, Tennant WJ, Vidale PL. 2014. The Met Office Unified Model Global Atmosphere 4.0 and JULES Global Land 4.0 configurations. *Geosci. Model Dev.* **7**: 361–386, doi: 10.5194/gmd-7-361-2014, URL `http://www.geosci-model-dev.net/7/361/2014/`.

Wang B, Xie X. 1997. A model for the boreal summer intraseasonal oscillation. *Journal of the Atmospheric Sciences* **54**(1): 72–86.

Wang Y, Sen OL, Wang B. 2003. A highly resolved regional climate model (iprc-regcm) and its simulation of the 1998 severe precipitation event over china. part i: Model description and verification of simulation. *Journal of Climate* **16**(11): 1721–1738.

Webster P, Toma VE, Kim HM. 2011. Were the 2010 pakistan floods predictable? *Geophysical research letters* **38**(4).

Webster PJ. 1983. Mechanisms of Monsoon Low-Frequency Variability: Surface Hydrological Effects. *Journal of the Atmospheric Sciences* **40**: 2110–2124, doi: 10.1175/1520-0469(1983)040<2110:MOMLFV>2.0.CO;2. 00219.

Webster PJ, Chou LC. 1980. Seasonal Structure of a Simple Monsoon System. *Journal of the Atmospheric Sciences* **37**: 354–367, doi: 10.1175/1520-0469(1980)037<0354:SSOASM>2.0.CO;2.

Webster PJ, Magana VO, Palmer TN, Shukla J, Tomas RA, Yanai M, Yasunari T. 1998. Monsoons : Processes , predictability , and the prospects for prediction 2 . Description of the Monsoons. *Journal of Geophysical Research* **103**: 14 451–14 510, doi: 10.1029/97JC02719. 00000.

Webster S, Uddstrom M, Oliver H, Vosper S. 2008. A high-resolution modelling case study of a severe weather event over new zealand. *Atmospheric Science Letters* **9**(3): 119–128.

Weisman ML, Skamarock WC, Klemp JB. 1997. The Resolution Dependence of Explicitly Modeled Convective Systems. *Monthly Weather Review* **125**: 527–548, doi: 10.1175/1520-0493(1997)125<0527:TRDOEM>2.0.CO;2, URL <0527:TRDOEM>2.0.CO;2. 00316.

Wheeler M, Kiladis GN. 1999. Convectively Coupled Equatorial Waves: Analysis of Clouds and Temperature in the Waveissue–Frequency Domain. *Journal of the Atmospheric Sciences* **56**: 374–399, doi: 10.1175/1520-0469(1999)056<0374:CCEWAO>2.0.CO;2.

Willetts PD, Marsham JH, Birch CE, Parker DJ, Webster S, Petch J. 2017a. Moist convection and its upscale effects in simulations of the Indian monsoon with explicit and parametrized convection. *Quarterly Journal of the Royal Meteorological Society* **143**(703): 1073–1085, doi: 10.1002/qj.2991.

Willetts PD, Turner AG, Martin GM, Mrudula G, Hunt KM, Parker DJ, Taylor CM, Birch CE, Mitra AK, Heming JT, *et al.* 2017b. The 2015 indian summer monsoon onset–phenomena, forecasting and research flight planning. *Weather* **72**(6): 168–175.

Wilson DR, Ballard SP. 1999. A microphysically based precipitation scheme for the UK meteorological office unified model. *Quarterly Journal of the Royal Meteorological Society* **125**: 1607–1636, doi: 10.1002/qj.49712555707.

Woolnough SJ, Slingo JM, Hoskins BJ. 2004. The Diurnal Cycle of Convection and Atmospheric Tides in an Aquaplanet GCM. *Journal of the Atmospheric Sciences* **61**: 2559–2573, doi: 10.1175/JAS3290.1.

Wu G, Liu Y, He B, Bao Q, Duan A, Jin FF. 2012. Thermal Controls on the Asian Summer Monsoon. *Scientific Reports* **2**, doi: 10.1038/srep00404, URL `http://www.nature.com/srep/2012/120511/srep00404/full/srep00404.html?WT.ec_id=SREP-20120515`. 00047.

Wu G, Liu Y, Zhang Q, Duan A, Wang T, Wan R, Liu X, Li W, Wang Z, Liang X. 2007. The influence of mechanical and thermal forcing by the tibetan plateau on asian climate. *Journal of Hydrometeorology* **8**(4): 770–789.

Xie P, Joyce R, Sun F, Wu S, Yarosh Y, Yoo S. 2013. A Reprocessed and Bias-Corrected High-Resolution Satellite Derived Precipitation Record Covering the Entire TRMM/GPM Era. In: *AGU Fall Meeting Abstracts*, vol. 32. p. 03, URL `http://adsabs.harvard.edu/abs/2013AGUFM.H32B..03X`.

Xie SP, Xu H, Saji NH, Wang Y, Liu WT. 2006. Role of Narrow Mountains in Large-Scale Organization of Asian Monsoon Convection*. *Journal of Climate* **19**: 3420–3429, doi: 10.1175/JCLI3777.1. 00000.

Xin-Xin Z, Xun-Qiang BI, Xiang-Hui K. 2015. Observed diurnal cycle of summer precipitation over South Asia and East Asia based on CMORPH and TRMM satellite data. *Atmospheric and Oceanic Science Letters* **8**: 101, URL `http://159.226.119.58/aosl/CN/article/downloadArticleFile.do?attachType=PDF&id=553`.

Yanai M, Esbensen S, Chu JH. 1973. Determination of Bulk Properties of Tropical Cloud Clusters from Large-Scale Heat and Moisture Budgets. *Journal of the Atmospheric Sciences* **30**: 611–627, doi: 10.1175/1520-0469(1973)030<0611:DOBPOT>2.0.CO;2. 01039.

Yanai M, Li C, Song Z. 1992. Seasonal heating of the tibetan plateau and its effects on the evolution of the asian summer monsoon. *Journal of the Meteorological Society of Japan. Ser. II* **70**(1B): 319–351.

Yanai M, Wu GX. 2006. Effects of the tibetan plateau. In: *The Asian Monsoon*, Springer, pp. 513–549, doi: 10.1007/3-540-37722-0_13.pdf. 00097.

Yang GY, Slingo J. 2001. The Diurnal Cycle in the Tropics. *Monthly Weather Review* **129**: 784–801, doi: 10.1175/1520-0493(2001)129<0784:TDCITT>2.0.CO;2. 00441.

Yasunari T. 1979. Cloudiness fluctuations associated with the northern hemisphere summer monsoon. *Journal of the Meteorological Society of Japan. Ser. II* **57**(3): 227–242.

Yasunari T. 1980. A quasi-stationary appearance of 30–40 day period in the cloudiness fluctuation during summer monsoon over India. *Journal of the Meteorological Society of Japan* **58**(3): 225–229.

Yasunari T. 1990. Impact of Indian monsoon on the coupled atmosphere/ocean system in the tropical pacific. *Meteorology and Atmospheric Physics* **44**(1-4): 29–41, doi: 10.1007/BF01026809.

Ye D. 1981. Some Characteristics of the Summer Circulation Over the Qinghai-Xizang (Tibet) Plateau and Its Neighborhood. *Bulletin of the American Meteorological Society* **62**: 14–19, doi: 10.1175/1520-0477(1981)062<0014:SCOTSC>2.0.CO;2. 00105.

Yeh T, Lo S, Chu P. 1957. The wind structure and heat balance in the lower troposphere over tibetan plateau and its surrounding. *Acta Meteorol. Sin* **28**: 108–121.

Yoon JH, Chen TC. 2005. Water vapor budget of the Indian monsoon depression. *Tellus A* **57**: 770–782, doi: 10.1111/j.1600-0870.2005.00145.x. 00020.

Zhai J, Boos WR. 2017. The drying tendency of shallow meridional circulations in monsoons. *Quarterly Journal of the Royal Meteorological Society* **143**(708): 2655–2664.

Zhang C, Nolan DS, Thorncroft CD, Nguyen H. 2008. Shallow meridional circulations in the tropical atmosphere. *Journal of Climate* **21**(14): 3453–3470.

Zhang F, Snyder C, Rotunno R. 2003. Effects of Moist Convection on Mesoscale Predictability. *Journal of the Atmospheric Sciences* **60**: 1173–1185, doi: 10.1175/1520-0469(2003)060<1173:EOMCOM>2.0.CO;2. 00171.

Zhang G, Smith RB. 2018. Numerical study of physical processes controlling summer precipitation over the western ghats region. *Journal of Climate* **31**(8): 3099–3115.

Zhou T, Wu B, Wang B. 2009. How well do atmospheric general circulation models capture the leading modes of the interannual variability of the asian–australian monsoon? *Journal of Climate* **22**(5): 1159–1173.